Development of highly porous carbon and ceramic materials

Aoki, Yasuyuki

Award date:
1993

Awarding institution:
University of Bath

DEVELOPMENT OF

HIGHLY POROUS CARBON AND CERAMIC MATERIALS

Submitted by Yasuyuki Aoki

for the degree of PhD

of the University of Bath

1993

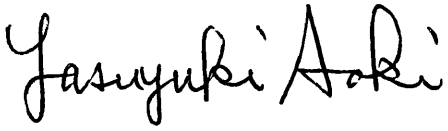

Yasuyuki Aoki

ProQuest LLC
789 East Eisenhower Parkway
P.O. Box 1346
Ann Arbor, MI 48106-1346

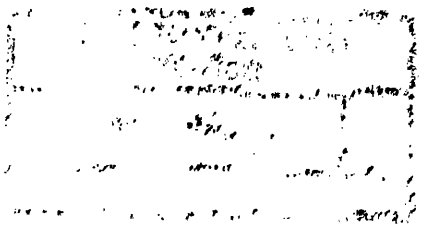

ACKNOWLEDGMENTS

I would like to thank Professor Brian McEnaney for his help throughout this research project, and the staff and technicians of the School of Materials Science, the University of Bath for their assistance.

I would like to express my gratitude to my company, Oji Paper Co., Ltd. for giving me this valuable opportunity to carry out this research.

I am very grateful to my wife for her support and to my son for his encouragement.

ABSTRACT

The objectives of this thesis were to develop new methods for manufacturing highly porous and low-density carbon and ceramic materials by simple methods using low-cost precursors, which can exhibit high corrosion resistance and high-temperature performance with advantageous porous microstructure.

Various types of porous carbon materials were manufactured using different techniques. These materials included porous carbons fabricated by paper making technology, foamed resin based carbons, resin powder based porous carbons and carbon bonded carbon fibre composites. Then, these different forms of porous carbon preforms were converted into lightweight and low-density ceramics by two main fabrication routes.

In the first route, porous carbon-ceramic composites were manufactured by infiltration of a mixture of silica sol-gels and a resin carbon source into porous carbon preforms. The silica was subsequently converted into SiC or Si_3N_4 by carbothermal reduction or nitridation, respectively. Furthermore, boron oxide glass was impregnated in addition to SiC. However, the porous carbon-ceramic composites from this fabrication method exhibited poor high-temperature performance due to low oxidation resistance.

In the second route, porous carbon preforms were directly converted into porous SiC materials by a reaction bonding technique with silicon vapour infiltration. The ceramics produced by this route were proved to have high potentiality as lightweight and low-density materials at elevated temperatures and corrosive atmospheres, with modified mechanical properties.

Structural and morphological characterizations of the porous materials were carried out using optical and electron microscopy, diffraction and spectroscopic techniques. Mechanical properties were also measured including flexural, tensile and compressive strength, and elastic modulus at room and elevated temperatures, and the results of mechanical properties were analyzed in relation to density/porosity values. Furthermore, corrosion resistance at high temperatures in air was evaluated.

DEVELOPMENT OF

HIGHLY POROUS CARBON AND CERAMIC MATERIALS

CONTENTS

CHAPTER I INTRODUCTION AND OVERVIEW OF THE THESIS

I-1 Introduction

There is an increasing demand for strong, tough materials in many engineering applications, especially at high temperatures and in corrosive environments. In particular, the development of porous, low-density and lightweight materials has attracted interest with advances in aerospace and other high technology industries. Applications of low density materials for these industries include thermal insulation, high temperature gas and liquid metal filtration, and advanced electrodes. Examples of such applications include the thermal protection system of space shuttles, particulate filters in hot gas and molten-metal filtration, and electrodes for flow electrolysis.

The properties and characteristics which are required for the materials are thermal stability, low density, chemical purity, low thermal expansion, thermal stress and shock resistance, corrosion resistance, etc. For such applications, carbon and ceramic materials which have highly porous microstructures have great potential.

Hitherto, the principal drive for these developments has been from defence and aerospace industries, where cost has been secondary to performance. For general engineering applications, there is a strong need for high-performance as well as low-cost materials, and it is to this need that the present project is addressed.

The objectives of the project are to develop new methods for manufacturing highly porous and low-density carbon and ceramic materials, which exhibit high corrosion resistance and high-temperature performance. The materials were manufactured from silicon carbide, silicon nitride and carbon by simple methods starting from low-cost precursors.

Ceramic materials have strong chemical bonds of a covalent or ionic character. As a result, they have high intrinsic strength at high temperatures, hardness, chemical inertness, corrosion resistance and relatively low density. However, ceramic materials are generally brittle, and their failure strain, fracture energy and fracture toughness are low; thus they usually fail in a catastrophic manner.

Non-oxide silicon ceramics such as silicon carbide (SiC) and silicon nitride (Si_3N_4) are attractive materials for high-temperature engineering applications because of their good thermo-physical and thermo-mechanical properties and their resistance to corrosion, erosion, abrasion and wear damage. As a result, there has been extensive development of monolithic ceramic components based upon these materials. The principal disadvantage of the monolithic ceramics is also their inherent brittleness. (Komeya - 1988, Iseki - 1988)

On the other hand, carbon and graphite materials have various unique characteristics that other ceramic materials do not have. These characteristics include

low density, excellent thermal stability in non-oxidizing atmospheres, strength which increases with temperature, thermal shock resistance, corrosion resistance, and high thermal- and electrical-conductivity. Carbon materials have two major disadvantages: they are easily oxidized at temperatures as low as 400-500° C in air, and their mechanical properties are relatively poor compared with other engineering materials.

Therefore, it can be said that both carbon and ceramic materials are attractive candidates as structural materials for high-temperatures and corrosion resistance. In addition, heterogeneous hybrid materials, which are made from carbon and other ceramics that have different characteristics from carbon, may have the potential to modify and improve the inferior properties of carbon materials. As a result, highly advanced composite materials can be manufactured to achieve properties which are superior to those of the separate components. For example, ceramic coatings used to protect carbon and graphite materials against oxidation can be regarded as a class of heterogeneous hybrid materials consisting of carbon and ceramics, that is, carbon-ceramic composites.

Of particular interest to this study are low-density and lightweight porous carbon and ceramic materials. Porous low-density materials can be roughly classified into fibrous and cellular forms, with the latter sub-classified into open-cell and closed-cell forms. It is

possible to produce open-cell lightweight ceramics by infiltration methods using highly porous open-cell preforms as starting materials, such as porous carbons and polymer foams. A wide range of infiltrating methods and materials have been used in this application, e.g., liquid and vapour phase infiltration, and chemical vapour infiltration (CVI) (as infiltration techniques), and materials including oxides, carbides, nitrides, borides and refractory metals. (Sherman - 1991)

I-2 Overview of the project

In this project, porous and lightweight ceramics were fabricated by two main routes starting from different forms of open-cell porous carbon preforms. These forms include porous carbons fabricated by paper making technology, foamed resin based carbons, resin powder based porous carbon pellets and porous carbon-carbon composites.

In the first route, porous carbon-ceramic composites were manufactured by infiltration of a mixture of silica sol-gels and a resin carbon source into porous carbon preforms. The silica was subsequently converted into SiC or Si_3N_4 by carbothermal reduction or nitridation in an argon or nitrogen atmosphere to generate porous carbon-SiC or Si_3N_4 composites, respectively. Furthermore, the porous carbon-SiC composites were impregnated with boron oxide glass in order to improve oxidation resistance.

In the second route, porous carbon preforms were directly converted into porous SiC materials by a reaction bonding technique by silicon vapour infiltration.

There has been some work on porous cellular ceramic products using polymer foam based preforms, but mainly using infiltration of a fine slurry of ceramic powder or chemical vapour infiltration method. Such methods have some process limitations or they are expensive and time-consuming. (Sherman - 1991) There are no industrial products of this type available based upon liquid infiltration of sol-gel systems or a vapour phase reaction bonding technique using porous carbon preforms as low-cost precursors. Thus, the concepts of formation of porous and lightweight ceramics, as proposed in this project, are innovative. The fabrication methods developed in the project are simple and low-cost so that this class of materials would be expected to find a wide variety of general industrial applications.

The silicon based non-oxide ceramics, SiC and Si_3N_4, in the first route were formed by carbothermal reduction, and a combination of carbothermal reduction and nitridation of sol-gel silica in the presence of a resin carbon source. Although these processes are well-known methods for production of the ceramics in various forms and with various starting materials, the application into ceramic coatings has been less commom. (Castro - 1990)

In the second route, silicon carbide was produced by reaction bonding of silicon vapour with carbon. Reaction bonding techniques are well-established methods that convert a porous green body into a dense ceramic form. Thus, there are many fundamental studies concerning the conversion of carbon into dense SiC by liquid or vapour silicon infiltration. (Popper - 1960)

There are basic studies on the reactivity of different carbons and silicon liquid. (Fitzer - 1983) However, the mechanism of heterogeneous reaction between solid carbon and vapour phase silicon is so complicated that it is not fully understood.

The corrosion behaviour of the ceramics was measured by assessment of the oxidation resistance in flowing air at temperatures up to 1200° C. At the same time, any structural and chemical changes resulting from oxidation were also studied.

The mechanical properties of porous low-density materials strongly depend on their microstructural forms. Therefore, it is essential to develop an understanding of the relationship between mechanical properties and microstructure in order to design effective products. However, the factors influencing the mechanical properties of porous ceramics are not well-understood and this question also was addressed in this project.

The structure of this thesis is as follows. A literature survey on porous materials is presented in Chapter II. The structure, mechanical behaviour,

application fields, fabrication methods and properties of low-density, porous carbon and ceramic materials are described in Chapter II-1. Chapter II-2 summarizes the properties of the solid materials from which they are made: that is, carbon, non-oxide ceramics and carbon-ceramic hybrids. In Chapter II-3, the preparation system for non-oxide silicon ceramics via carbothermal reduction of sol-gel silica is described, and the reaction bonding technique to produce SiC from carbon with silicon is summarized. Chapter III describes the experimental methods used. Chapter IV presents results and discussion of physical properties and characteristics of porous forms of carbon materials which are prepared from various fabrication techniques. Chapter V describes the results of the study of porous carbon-ceramic composites prepared by infiltration of non-oxide silicon ceramics via carbothermal reduction of sol-gel silica into porous carbons. In Chapter VI, the results obtained from the studies of the porous ceramic materials formed by reaction bonding between various types of porous carbon preforms and infiltrated silicon are presented and discussed. Comparative studies of various types of porous carbon and ceramic materials are presented and discussed in Chapter VII. The thesis concludes with a list of the main conclusion to emerge for the work and suggestions for future work in Chapter VIII.

CHAPTER II REVIEW OF THE LITERATURE

II-1 Porous carbon and ceramic materials

II-1.1 Introduction

A common form for structural materials in nature consists of an inter-connected network of struts or plates, that is a cellular structure which is highly porous and lightweight, but yet possesses attractive mechanical properties. (Gibson - 1988) For example, wood has been used for long time as a structural material because its low density combined with relatively high strength are based on its cellular microstructure. The cellular forms of natural products, such as bones, coral, sponge and cork, are also well known. However, with the exception of wood, these lightweight and low-density materials have not been extensively exploited for structural applications until recently.

Considering man-made porous materials, two typical structures been developed; honeycombs and foams. The simplest form of honeycomb is a two-dimensional array of polygons which pack to fill a plane area, similar to the hexagonal cells of bees. The structure of foams consists of polyhedral cells which pack in three-dimensions to fill space. Almost any material can be made into a porous structure for example polymers, metals, glasses, ceramics, and even composites. However, only synthesized polymer foams have been widely available commercially for thermal insulation, cushioning, padding and packaging materials. (Gibson -

1988) Figure II-1-1 (p.12) and II-1-2 (p.13) show the microstructures for some examples of porous natural and man-made cellular materials, respectively.

The properties and characteristics of porous materials, e.g., low-density, low thermal conductivity, low modulus, low strengths and large compressive strains, find a wide range of applications which are not satisfied by fully dense solids. The low-density structure enables the design of light and stiff structural components such as sandwich panels and large portable structures. The low thermal conductivity permits various kinds of thermal insulation. The low stiffness enables porous materials for cushioning and packaging applications, and low strength and large compressive strains make them attractive for energy-absorbing applications.

Despite these usuful properties, porous low-density materials have not been extensively developed for general structural applications until recently. This limited development is due to two main reasons. First, scepticism about the mechanical reliability of these materials because of a lack of understanding of the relationship between mechanical behaviour and microstructure. Second, fabrication methods are limited so that the optimum structural advantage of the materials cannot always be obtained.

In this Chapter II-1, the literature regarding porous lightweight materials is reviewed, especially concerning their structure, the relationships between

microstructure and mechanical behaviour, application fields, and fabrication methods, and with particular emphasis on porous carbon and ceramic materials.

II-1.2 Structure of porous materials

The properties and characteristics of porous materials are strongly dependent on their microstructure. The following are examples of properties which are critical for mechanical and other characteristics; the fraction of pore space, pore size, pore shape, the connectivity of the solids and of the pore space, and the geometric form.

The most important property of a porous material is its relative density, ρ/ρ_s; that is the apparent density of the porous material, ρ, divided by that of the solid from which the porous material is made, ρ_s. The fraction of pore space in the material is its porosity, p which is $(1-\rho/\rho_s)$. Clearly, the porosity of materials decreases in proportion to increases in relative density. At $\rho/\rho_s \sim 0.4$ there exists a transition point from an efficient porous structure to one that is better thought of as a solid containing isolated pores. Therefore, in this thesis, materials with relative densities of less than 0.4 are considered as materials with an efficient porous structure.

Lightweight and porous materials, in general, can be categorized into two main classes; fibrous and cellular forms, depending on their microstructure. (Hagiwara - 1988) Fibrous materials, such as paper, felt, cotton

wool and the thermal protection tiles of the U.S. Space Shuttles are generally constituted of randomly orientated fibres which are bonded strongly to each other to form entangled three-dimensional networks. (Figure II-1-3, p.14) On the other hand, cellular materials consist of an arrangement of comparatively homogeneous hollow cells. Moreover, cellular materials can be further sub-classified into open-cell and closed-cell structures, depending on whether the faces of the cells are empty or covered by thin membranes. (Figure II-1-4, p.14)

In addition, porous materials can also be classified into isotropic systems, that have structures and properties with no directionality, and anisotropic systems that have structures which are axisymmetric or orthotropic and properties which reflect this structure. When pores are even slightly elongated or flattened into one direction, the properties of the materials exhibit a strong dependence on direction.

In order to exploit porous low-density materials efficiently, it is essential to comprehend various properties and characteristics, including the mechanical and thermal properties, in relation to the geometric microstructure, as well as the intrinsic properties of the materials of which the solids are made. Thus, theoretical studies of relationships between the mechanical behaviour and the microstructure of porous materials, both cellular and fibrous materials, are presented in the next section.

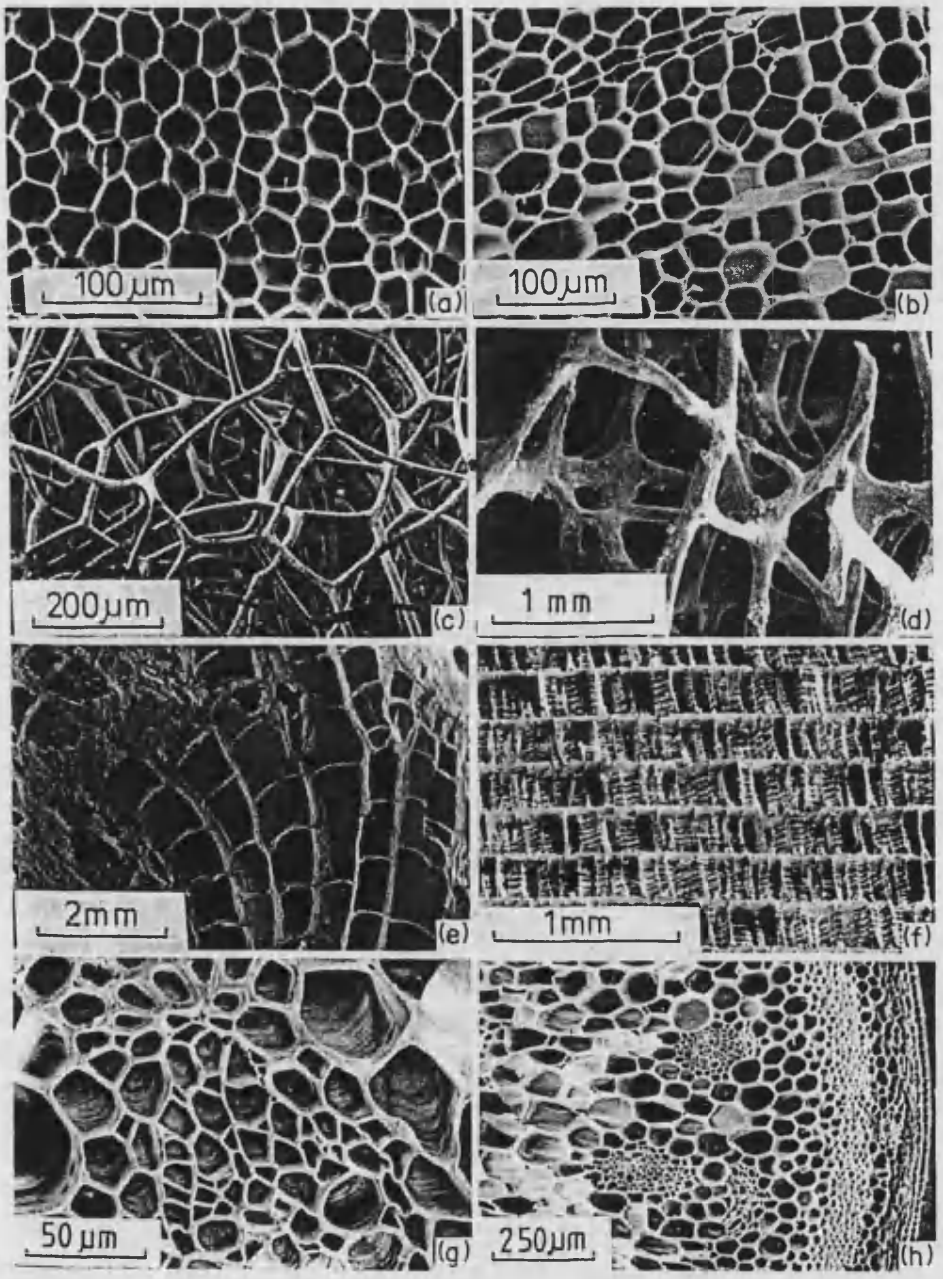

Figure II-1-1 Natural cellular materials: (a) cork, (b) balsa, (c) sponge, (d) cancellous bone, (e) coral, (f) cuttlefish bone, (g) iris leaf, (h) stalk of a plant (from Gibson - 1988)

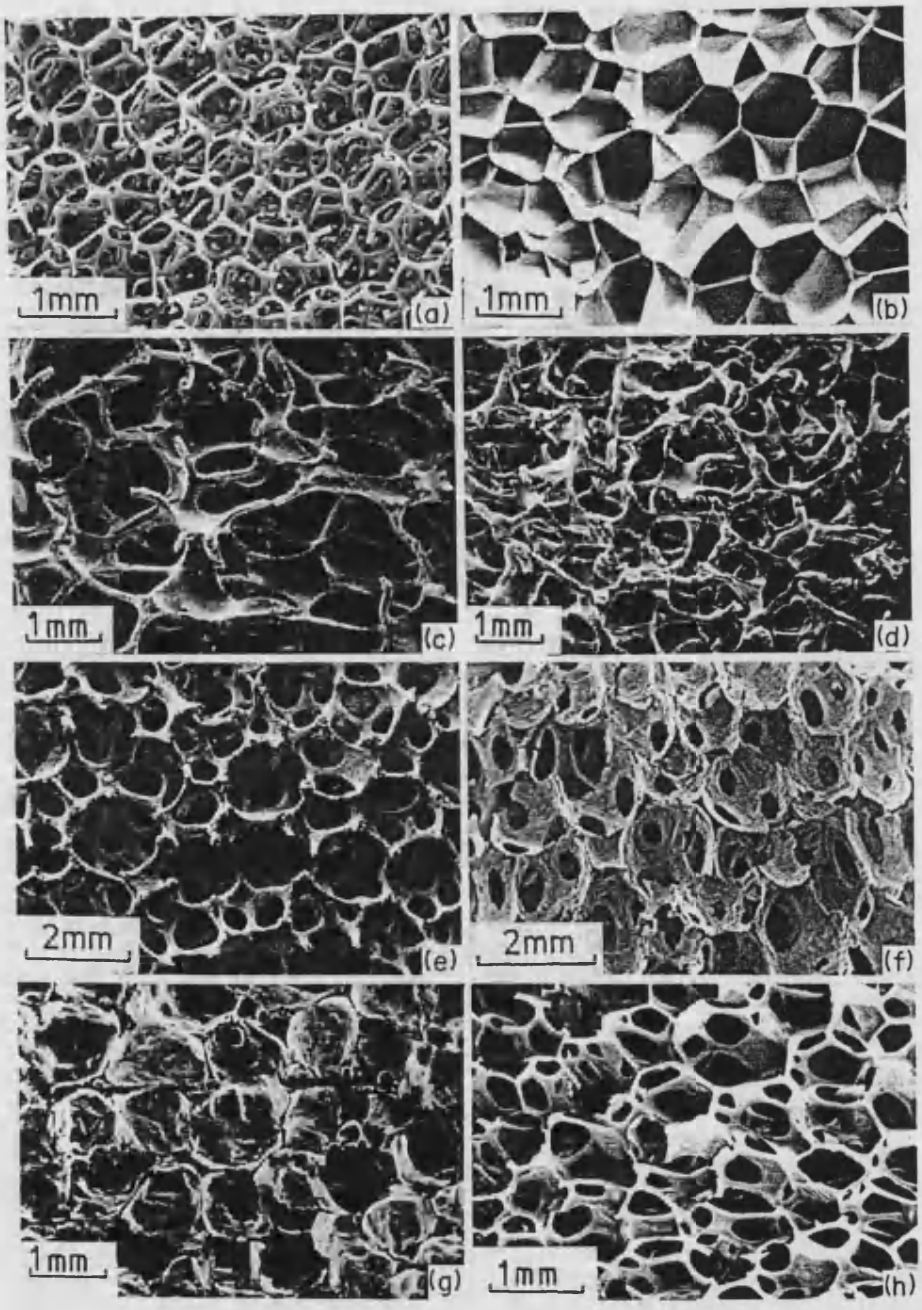

Figure II-1-2 Man-made cellular materials: (a) polyurethane, (b) polyethylene, (c) nickel, (d) copper, (e) zirconia, (f) mullite, (g) glass, (h) polyether (from Gibson - 1988)

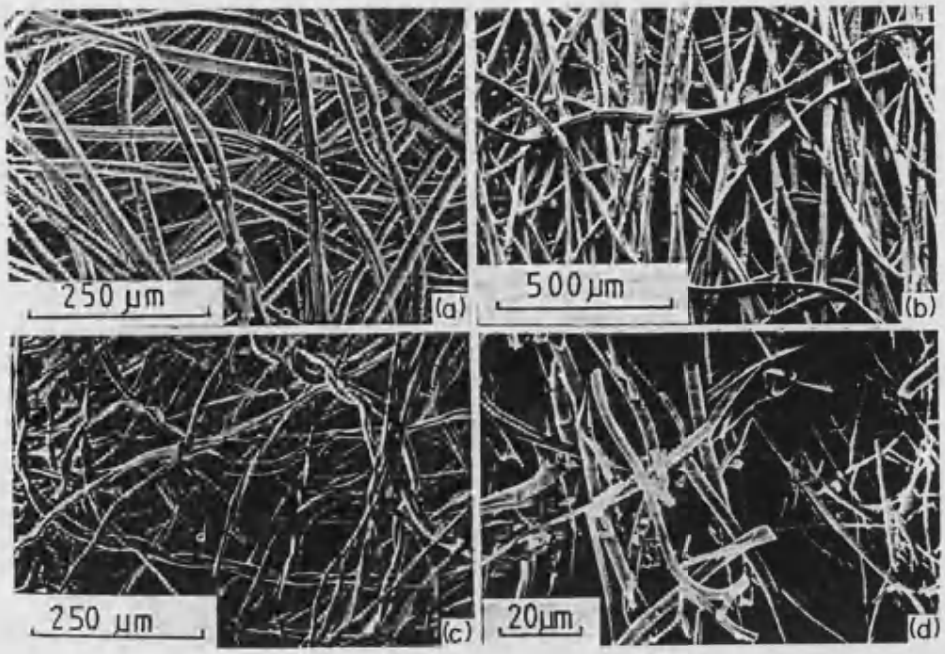

Figure II-1-3 Fibrous materials: (a) felt, (b) paper, (c) cotton wool, (d) space shuttle tile (from Gibson - 1988)

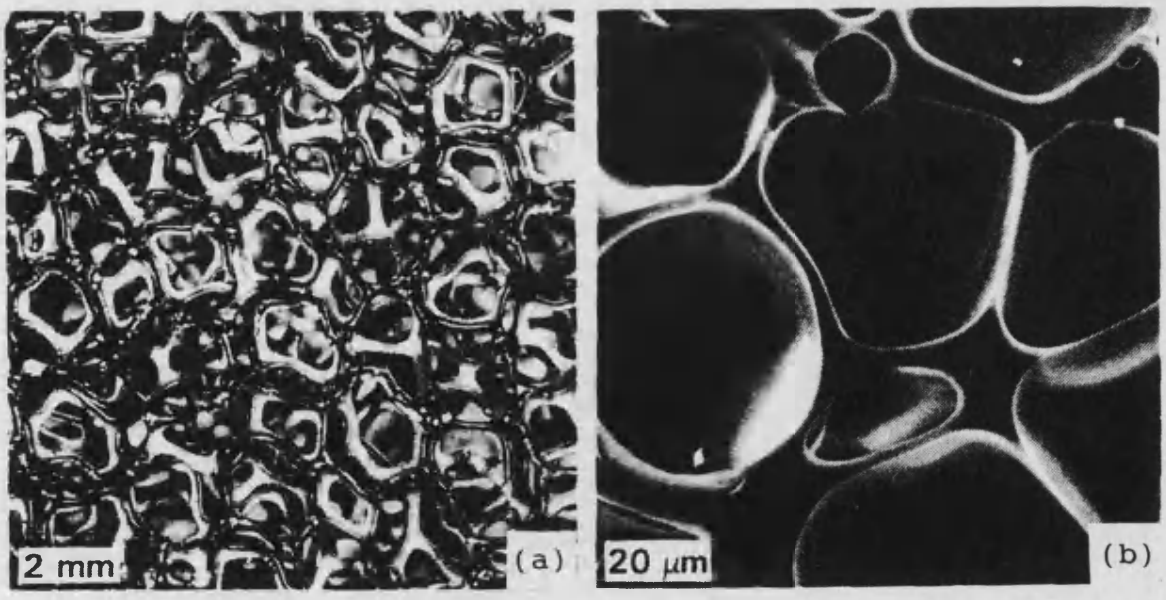

Figure II-1-4 Cell structure: (a) open cell, (b) closed cell (from Hagiwara - 1988)

II-1.3 Microstructure and mechanical behaviour

There have been extensive theoretical studies of the micromechanical behaviour of both cellular and fibrous porous materials. The theoretical equations which have been derived from previous work are compared with the mechanical behaviour of the porous carbons and ceramics produced in this project in later chapters. Therefore, the previous work is reviewed briefly in this section.

II-1.3.1 Mechanical behaviour of cellular materials

Ashby, Gibson and co-workers have developed a comprehensive set of theoretical relationships for the mechanical properties of cellular materials using a simple model by a combination of beam theory applied to honeycomb structures and scaling laws. (Gibson - 1982, Ashby - 1983, Maiti - 1984(a), 1984(b))

A typical compressive stress-strain curve for cellular materials, shown in Figure II-1-5 (p.16), has three distinct regions of behaviour; linear elasticity, collapse and densification. (Ashby - 1983) Figure II-1-6 (p.17) shows schematic compressive stress-strain curves for an elastomeric, elastic-plastic and a brittle cellular material. Each of the three distinct regions is connected with the mechanism for the deformation of the cell; the elastic region is induced by bending in the cell unit; cell collapse is caused by elastic buckling (e.g., rubbers), plastic yielding (e.g., metals) or brittle crushing (e.g., ceramics), which depend on the nature of material. Densification is caused by crushing together the cell struts.

The tensile stress-strain curves of each kind of these cellular solids are shown schematically in Figure II-1-7 (p.17). The initial linear elasticity is also caused by bending in the cell unit. Regarding mechanical behaviour of brittle cellular ceramic materials, they also show an initial elastic regime. However, in the case of compressive stress response, after reaching at a critical stress at which the cell walls begins to fracture, the stress-strain curve becomes irregular though roughly horizontal. This collapse continues approximately at a constant stress until the cell's struts have fractured and collapsed, and then touch each other. Further deformation is similar to a densification process, where the stress increases steeply. (Maiti - 1984(a)) On the other hand, in the case of tensile stress response, brittle ceramics exhibit linear elasticity until the point where a crack propagates catastrophically to give fast brittle fracture.

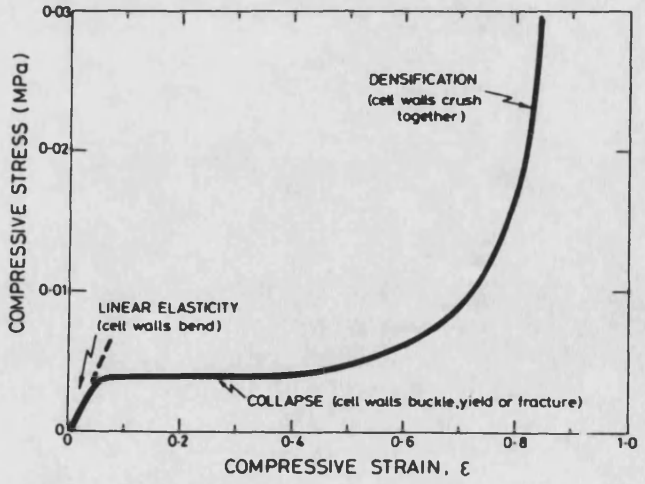

Figure II-1-5 Typical shape of the stress-strain curve for a foam (from Ashby - 1983)

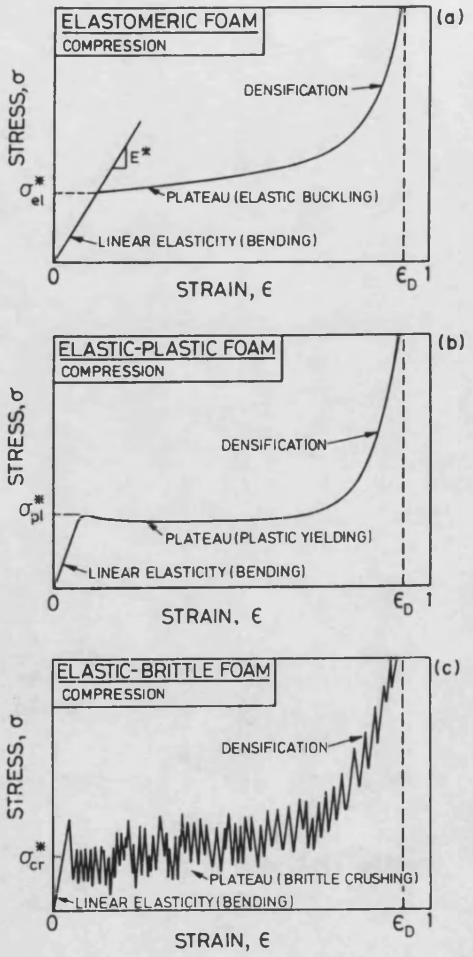

Figure II-1-6 Schematic compressive stress-strain curves for foams:

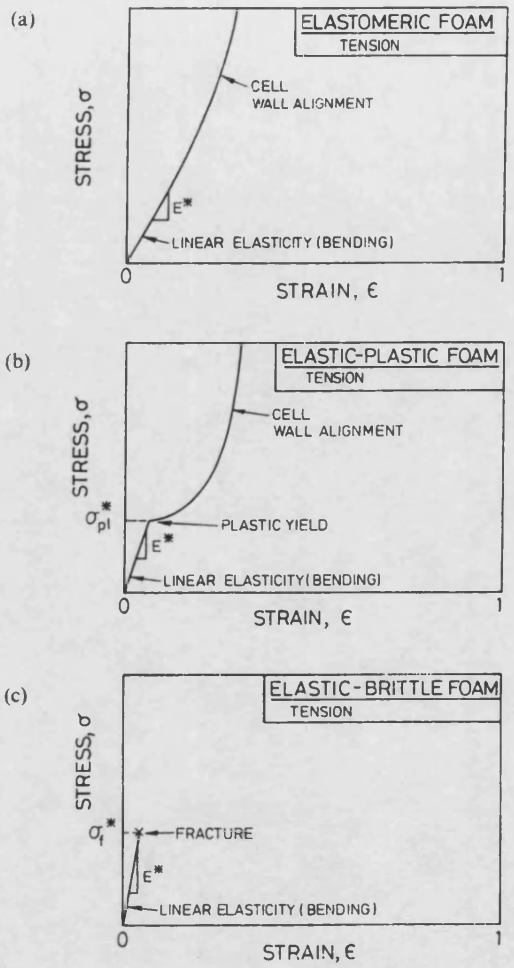

Figure II-1-7 Schematic tensile stress-strain curves for foams:

(a) elastic foam, (b) elastic-plastic foam, (c) elastic-brittle foam (from Gibson - 1988)

(1) Isotropic structure materials

The micro-mechanical unit cell, used by Ashby et al., is shown in Figure II-1-8 (p.24) which consists of a cubic array of cell struts with a square cross section, of width t and length l. In this idealized geometrical unit cell model for isotropic and open-cell materials, relationships between the mechanical properties of the material and its relative density, the properties of the struts and cell geometry can be found.

The relative density of the cell, the most salient feature of porous materials (ρ/ρ_s) can be related to the cell strut dimension (t) and the cell size (l). At low relative densities this is given by:

$$\rho/\rho_s \propto (t/l)^2 \qquad (1)$$

For most applications of cellular materials, failure results from compressive stress. Thus, first of all, the compressive behaviour, in particular of open-cell brittle materials, is discussed in the following section.

- linear elasticity

The elastic properties can be characterized by the linear elastic bending of the beam loaded at its mid-point in the unit cell. (Figure II-1-9, p.24) The bending deflection of the cell δ produced by a force F is proportional to Fl^3/E_sI according to standard beam theory, where E_s is Young's modulus of the cell strut material, and I is the second moment of the area. For open-cell materials, the stress σ is proportional to

F/l^2, the strain ε to δ/l, and the second moment I to t^4. Therefore, Young's modulus of the cellular material (E) is:

$$E = \sigma/\varepsilon \propto E_s (t/l)^4 \qquad (2)$$

The combination of Eqs. (1) and (2) gives:

$$E/E_s = C_1 (\rho/\rho_s)^2 \qquad (3)$$

where C_1 is a constant that depends on the geometry of the micromechanical model.

The theory for the shear modulus (G) is very similar because, in this case, shear deformation also causes simple bending of the cell and it gives:

$$G = \tau/\gamma \propto E_s (t/l)^4 \qquad (4)$$

therefore

$$G/E_s = C_2 (\rho/\rho_s)^2 \qquad (5)$$

where C_2 is also a geometric constant.

It was suggested by Ashby et al. that $C_1 = 1$ and $C_2 = 3/8$ on the basis of a comparison with experimental data for a wide range of materials and density.

- brittle crushing

Brittle ceramic materials collapse mainly by a brittle crushing mechanism in compression. If the modulus of rupture of the cell strut material is σ_f, a cell will then fail (Figure II-1-10, p.24) when the moment acting on it exceeds:

$$M_f = (1/6)\,\sigma_f t^3 \qquad (6)$$

The moment M_f due to the force F is proportional to Fl, and the stress to F/l^2. Combining these results gives the crushing strength of the solid:

$$\sigma_c/\sigma_f = C_3\,(\rho/\rho_s)^{3/2} \qquad (7)$$

where C_3 is a geometric constant, and the limited experimental data suggested $C_3 = 0.65$.

In the case of structural applications, e.g., the core structure of sandwich panels, porous materials are often subjected to tensile stress as well as compressive stress. Thus, a consideration of mechanical behaviour for tensile stress, based on the results developed in the previous section, is discussed in the following section.

- linear elasticity

The moduli of open cell materials in tension are also determined by a cell edge bending mechanism, thus, they can be given by equations (3) and (5).

- fracture strength

Regarding brittle materials, which contain defects such as cracks or flaws, the stress concentration induced by them will fracture cell walls locally, propagate the cracks and lead to sudden fracture (Figure II-1-11, p.25).

However, since brittle cellular ceramic materials deform linear-elastically under a tensile stress up to

fracture, tensile strength (σ_t) of cellular materials has been also modeled in relation to their relative density.

$$\sigma_t/\sigma_f = C_4 (\rho/\rho_s)^{3/2} \cdot (a/l)^{-1/2} \qquad (8)$$

where a is a critical crack length. The equation is valid only for $a>1$, otherwise there is no crack and then the tensile strength is the same as the crushing strength. ($\sigma_t=\sigma_c$) C_4 is a geometric constant, and the experimental data of brittle polymeric foams suggested that C_4 is 0.65. Unlike all the other properties, fracture strength depends on the cell size.

(2) Anisotropic structure materials

The theoretical analysis for mechanical behaviour of isotropic open-cell materials was described in the previous section. However, porous materials are, in practice, often anisotropic, and, therefore, their mechanical properties are also anisotropic. Most man-made synthetic porous materials are anisotropic due to their fabrication methods. Natural porous materials, like wood and bones, are almost always anisotropic.

Hence, an analysis of anisotropy in axisymmetric porous structures, developed by the same researchers (Gibson - 1988), is briefly presented in this section. The anisotropy is characterized by a single value of R (anisotropic ratio, the ratio of the largest cell dimension to the smallest). The various properties are strongly dependent on R. Therefore, in order to obtain

optimum performance from the porous structure, its anisotropy should be considered in detail. Figure II-1-12 (p.25) shows an idealized open-cell unit that illustrates an axisymmetric structure.

- linear elasticity

A load in the X_3 direction is carried out by the four beams of length l. The force F on each beam is proportional to Fl^3/E_sI. The strain ε_3 is related to the displacement δ_3 by $\varepsilon_3 = \delta_3/h$. Combining these results gives Young's modulus E_3;

$$E_3 = \sigma_3/\varepsilon_3 = CE_sIh/l^5 = CE_s(t/l)^4\cdot(h/l) \qquad (9)$$

where C is a constant of proportionality.

On the other hand, a load in the X_1 direction is carried out by two beams of length l and two beams of length h. The deflection δ_1 must be equal in both sets of beams, thus, the load carried by shorter beams is proportional to E_sI/h^3, and the other to E_sI/l^3. The total force is $\delta_1 hl$, and the strain $\varepsilon_1 = \delta_1/l$. Thus, Young's modulus E_1 is:

$$\begin{aligned} E_1 = \sigma_1/\varepsilon_1 &= (CE_sI/2h)\cdot(1/l^3+1/h^3) \\ &= (CE_s/2)\cdot(t/l)^4\cdot(l/h)\cdot(1+(l/h)^3) \end{aligned} \qquad (10)$$

The combination of the equation (9) and (10), and anisotropy ratio, R = h/l, gives the Young's modulus anisotropic ratio:

$$E_3/E_1 = 2R^2/(1+(1/R)^3) \qquad (11)$$

- brittle crushing

Brittle collapse of anisotropic structures is analyzed in a similar way as isotropic structures. A cell fails when the fracture moment M_f is exceeded. For loading in the X_3 direction, four beams of length l collapse. The moment M_f due to the force F is proportional to Fl, and the force F to $\sigma_3 l^2$. Combining these results gives the crushing strength $(\sigma_c)_3$:

$$(\sigma_c)_3 = CM_f / l^3 \qquad (12)$$

where C is a constant of proportionality.

For loading in the X_3 direction, two beams of length l and two of length t collapse. The first pair support a force proportional to M_f/l, while the other pair support a force proportional to M_f/h. The total force is $\sigma_1 lh$, giving:

$$(\sigma_c)_1 = (CM_f / 2lh) \cdot (1/l + 1/h) \qquad (13)$$

The combination of the equation (12) and (13), and anisotropy ratio, R = h/l, gives the brittle crushing strength anisotropy ratio:

$$(\sigma_c)_3 / (\sigma_c)_1 = 2R / (1 + (1/R)) \qquad (14)$$

In conclusion, Table II-1-1 (p.30) shows a summary of these theoretical equations for cellular brittle materials, derived by Ashby, Gibson et al. (Gibson - 1988)

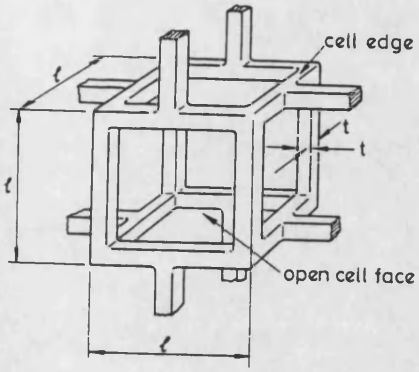

Figure II-1-8 A cubic model for an open-cell foam

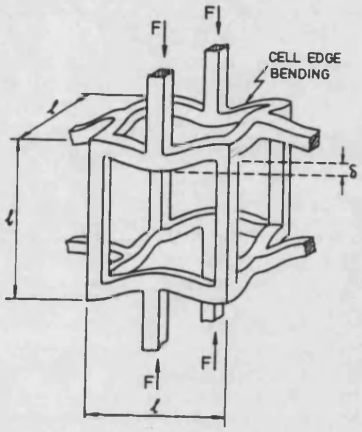

Figure II-1-9 Cell edge bending during linear elastic deformation

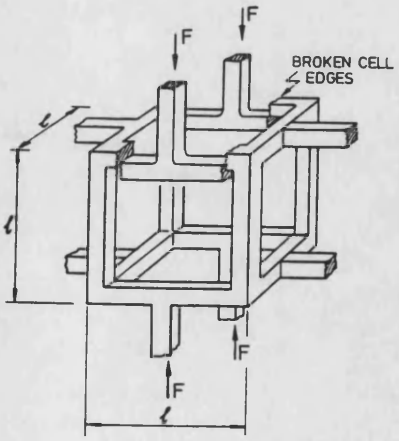

Figure II-1-10 Cell wall fracture during crashing of a brittle open-cell foam (from Gibson - 1988)

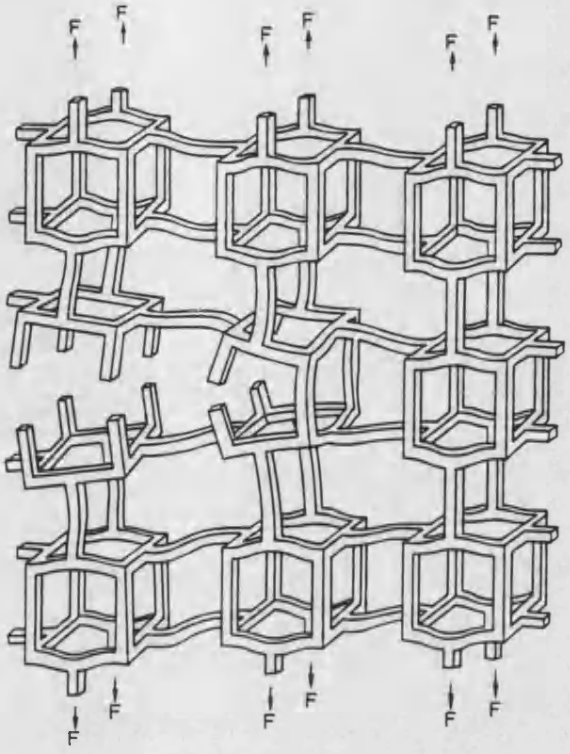

Figure II-1-11 Propagation of a crack through a brittle open-cell foam

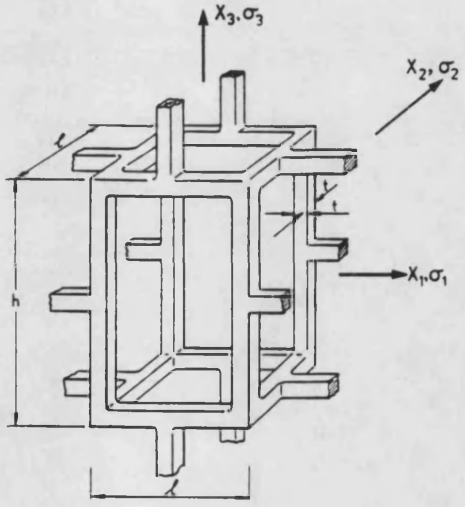

Figure II-1-12 An axisymmetric unit cell with R = 1.5 (from Gibson - 1988)

II-3.2 Mechanical behaviour of fibrous materials

A micromechanical model for low-density fibrous ceramic bodies which were used for the thermal protection of the American Space Shuttle was studied by Green et al. to investigate the fibre properties and their special distribution in relation to the mechanical properties. They found that mechanical properties such as the elastic moduli, fracture toughness and strength are dependent on the fibre spacing. (Green - 1982)

In their study, the geometry of fibres can be simulated by an orthotropic network of fibres. Although the fibres have a variety of orientations about an axis, in this model, the orthogonal fibres are joined at the nodes of the network. (Figure II-1-13, p.29)

The Shuttle tile material LI-900 (Figure II-1-14, p.29), the amorphous silica fibre based tile, has a preferred orientation such that more fibres are aligned in one plane than in the third direction, which is typical for these fibrous materials. For a transversely isotropic material such as LI-900, the fibre spacing, D, could be assumed to be;

$$D_1 = D_2 < D_3 \tag{15}$$

Then, the density of the fibrous material (ρ) is given approximately by;

$$\rho = \pi r^2 \rho_f \left[(1/D_3^2) + (2/D_2^2) \right] \tag{16}$$

where r is the average fibre radius and ρ_f is the true density of the fibres. Young's moduli in the weak and strong directions (E_3 and E_2) were considered to depend on the area fraction of fibres aligned in those directions;

$$E_3 = \pi r^2 E_f / (D_3)^2 , \quad E_2 = \pi r^2 E_f / (D_2)^2 \qquad (17)$$

where E_f is Young's modulus of the fibres.

These equations can be rewritten as

$$E_3/E_2 = (D_2/D_3)^2 \qquad (18)$$

Whereas the critical stress intensity factors for the weak (K_{C3}) and strong (K_{C2}) directions can be related to the fibre radius, r, and the strength, σ_{fb};

$$K_{c3} = \sigma_{fb} \pi r^2 (\pi/2 D_3^3)^{1/2}, \quad K_{c2} = \sigma_{fb} \pi r^2 (\pi/2 D_2^3)^{1/2} \qquad (19)$$

Therefore, the ratio of the critical stress intensity factors can be also expressed in the relation to the degree of preferred orientation of fibre;

$$K_{c3}/K_{c2} = (D_2/D_3)^{3/2} \qquad (20)$$

Table II-1-2 (p.30) shows a summary of these theoretical equations for the mechanical behaviour of low-density fibrous ceramic bodies used for the thermal protection of the American Space Shuttle, studied by Green and co-workers. (Green - 1982)

In another approach, Wei and Robinson (Wei - 1985) proposed a simple model for carbon bonded carbon fibre

insulation materials as shown in Figure II-1-15 (p.29). The basic assumption that fibres lay in planes perpendicular to the moulding direction, neglects carbon binder because fracture was observed to occur only in fibres and not in binders. From this simple model, σ_f, the apparent compressive stress that fractures the fibre can be expressed as:

$$\sigma_f = (128/3\pi^3) \cdot \sigma_c \cdot (\rho/\rho_f)^3 \qquad (21)$$

Therefore, Equation (21) suggests that the compressive strength of the material, σ_f, is proportional to the cube of the bulk density and that compressive strength increases with increasing bending strength of the carbon fibre, σ_c.

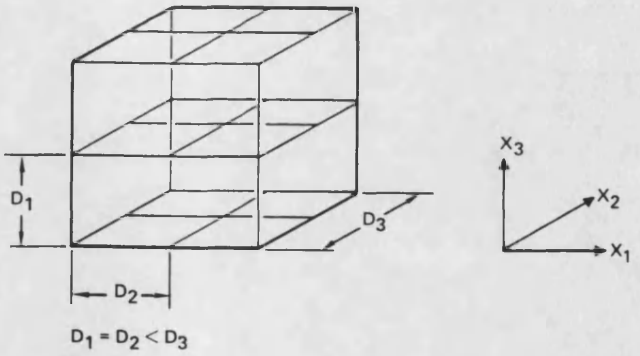

Figure II-1-13 Fibre model for low-density fibrous ceramics (from Green - 1982)

Figure II-1-14 Microstructure of low-density fibrous ceramic tile material (LI-900) (from Green - 1982)

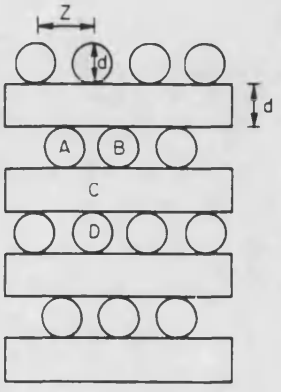

Figure II-1-15 Idealized fibre model for carbon bonded carbon fibre composites (from Wei - 1985)

Properties	Theoretical equations
Isotropic material	
Young's modulus	$E/E_s = C_1 (\rho/\rho_s)^2$
Shear modulus	$G/E_s = C_2 (\rho/\rho_s)^2$
Crushing strength	$\sigma_c/\sigma_f = C_3 (\rho/\rho_s)^{3/2}$
Tensile strength	$\sigma_t/\sigma_f = C_4 (\rho/\rho_s)^{3/2} (a/l)^{-1/2}$
Anisotropic material	
Young's modulus	$E_3/E_1 = 2R^2/(1+(1/R)^3)$
Crushing strength	$(\sigma_c)_3/(\sigma_c)_1 = 2R/(1+(1/R))$

Table II-1-1 Summary of theoretical equations for cellular brittle material (from Gibson - 1988)

Properties	Theoretical equations
Young's modulus	$E_3 = \pi r^2 E_f/(D_3)^2$ $E_2 = \pi r^2 E_f/(D_2)^2$ $E_3/E_2 = (D_2/D_3)^2$
Critical stress intensity factor	$K_{C3} = \sigma_{fb} \pi r^2 (\pi/2D_3^3)^{1/2}$ $K_{C2} = \sigma_{fb} \pi r^2 (\pi/2D_2^3)^{1/2}$ $K_{C3}/K_{C2} = (D_2/D_3)^{3/2}$

Table II-1-2 Summary of theoretical equations for low-density fibrous ceramics (from Green - 1982)

II-1.4 Porous carbon materials

II-1.4.1 Introduction

Carbon and graphite materials have various unique characteristics that other ceramic materials do not have. These include low density, excellent thermal stability combined with higher strength at temperatures over 1000° C than at ambient temperature, outstanding thermal shock resistance, corrosion resistance against molten metals, slag, and chemical reagents, and high thermal- and electrical-conductivity. However, carbon materials have two major disadvantages; poor oxidation resistance in air at high temperatures and relatively low mechanical strength. Owing to their unique combination of diverse properties, carbon and graphite materials have been used in many engineering applications.

To describe the properties and applications of conventional engineering carbon and graphite materials is outside the scope of this review. Instead the emphasis here is on the wide range of porous carbon materials which have been developed. For example, these include foamed resin-based carbons (Sherman - 1991, Sylwester - 1987, 1989), reticulated vitreous carbons (Wang - 1981, Blaedel - 1980, Strohl - 1979), porous carbons produced by paper-making technology (Oji - 1985, 1986, 1989, 1991, Toray - 1988, Tokai - 1990), porous carbon fibre composites (Kureha - 1984, Wei - 1985, Shui - 1991). There are other kinds of porous carbons, such as carbon/graphite felt (Oren - 1983,

Lestrade - 1981) and graphite cloth (Zur - 1981) which have been mainly employed as electrode materials for various electrochemical applications, and extruded or moulded porous carbon and graphite particle solids.

II-1.4.2 Application fields

Porous carbon materials have unique properties and characteristics which have led to their use in a wide variety of application fields including the following.

(1) Electrode materials

Carbon and graphite materials have been widely used as electrode materials because of their good electrical and thermal conductivity, low thermal expansion, and good corrosion resistance. In particular, porous forms of carbon are suitable electrode materials for heavy metal removal from industrial effluents and for phosphoric acid fuel cells.

Porous carbon materials have been used as an electrode material for flow electrolysis. (Sioda - 1982) In particular, electrodeposition on porous carbon electrodes is a promising method to remove toxic heavy metals from industrial effluents resulting from processes such as electroplating and other industrial metal processing operations. (Agarwal - 1984)

Also, phosphoric acid fuel cells have shown promise recently as a new generation system with low pollution and high efficiency. In this application, electrodes with high porosity and high surface area are required for electrolyte flow and electrochemical reaction. The electrodes of this cell must also have

high chemical and thermal stability because they are immersed in phosphoric acid and exposed to an electrochemical reaction at over 200° C for periods of thousands of hours. Highly porous carbon materials which are homogeneous and chemically inert are particularly suitable for this application, as demonstrated recently. (Oji -1990)

(2) Heat sink materials

The requirement for heat dissipation from electronic devices has increased recently with the rapid increase of packing density and power of microelectronics. Porous heat sink materials have attractions for this application since they permit cooling by both convection and conduction. In addition, they also allow cooling by the flow of a cooling fluid through the pores in the materials. Carbon does not have any oxide on its surface and also enhances cooling by radiation because of its black colour. Hence, porous carbon materials are good candidates for heat sink materials.

(3) High temperature insulators and filters

The most common application of porous materials is thermal insulation, because of their low thermal conductivity. Therefore, porous carbons find application as heat insulators for extremely high temperatures due to their low thermal conductivity, good thermal stability, excellent thermal shock resistance, and their low coefficient of thermal expansion. For example, carbon bonded carbon fibre

materials were developed as insulators for radioisotopic heat generators used aboard space probes. (Wei - 1985)

Also, porous carbons allow particulate removal from hot gases or liquid metal filtration in a number of industrial processes. Hence, it is expected that porous carbon materials can be applied to extremely high-temperature and corrosion resistant filters due to their excellent thermal stability and chemically inertness. However, their application fields are limited to non-oxidising environments because carbon is easily oxidized at temperatures from 400-500° C in air.

(4) Precursors for hybrid materials

In addition to these applications, porous carbon materials can be considered as desirable precursors for hybrid materials of carbon and ceramics because they have a porous structure that is suitable for impregnation with ceramic, glass or metal materials.

II-1.4.3 Fabrication methods and their properties

Properties and characteristics of porous carbons can be varied in a wide range by choice of raw materials, fabrication methods and manufacturing processes. In this section, typical examples of porous carbon materials are reviewed in brief and their properties are compared.

(1) Foamed resin-based carbons

Foamed carbon can be prepared from carbonization of

polymeric foams in a carefully controlled environment. Polymeric foams are generally manufactured by introducing gas bubbles into the liquid monomer or hot polymer, allowing the bubbles to grow and stabilize, and then solidifying the foamed polymer by cross-linking or cooling. As a result, a wide variety of polymers such as thermoplastics, thermosets and elastomers are used to make foams. Among them, phenolic resin foams, are suitable precursors for foamed carbon due to their high carbon yield. Phenolic foams are dominantly produced by the acid catalyzed reaction of a resol resin with added blowing agent and surfactant. (Papa - 1973)

Therefore, carbon foams with a wide range of properties and characteristics can be obtained via high temperature pyrolysis of phenolic resin foams prepared by controlled foaming conditions. Carbon foams, formed in this way, are a form of glassy carbon (vitreous carbon) and are called reticulated vitreous carbon, RVC.

Sylwester and co-workers prepared foamed carbon by carbonization of polyacrylonitrile (PAN) foams. (Sylwester - 1987) Carbon foams had low densities, and had full open-porosity and high surface area which were translated from the initial PAN foam morphology. Moreover, carbonized foams were filled with non-conductive polymer or resin to provide porous three-dimensional electrically-conducting reticulated carbon structures. (Sylwester - 1989) Sherman et al. used

foamed carbon, which appears to be prepared from foamed resin, as a precursor for refractory ceramic foams through chemical vapor deposition. (Sherman - 1991)

(2) Reticulated vitreous carbons

Reticulated vitreous carbon (RVC) has been developed as a very useful and versatile electrode material. (Wang - 1981) RVC has a cellular structure with open pores giving it useful electrochemical, hydrodynamic and structural properties, such as chemical inertness, thermal and electrical conductivity, and high surface area with self supporting rigidity. (Wang - 1981) An enlarged view of RVC is shown in Figure II-1-16 (p.40) and physical properties of standard RVC are presented in Table II-1-3.

Table II-1-3 Physical properties of standard reticulated vitreous carbon

Bulk density (g/cm^3)	0.048
Void volume (%)	97
Specific resistivity (ohm m $x10^{-2}$)	0.47-0.69
Tensile strength (MPa)	0.3-1.2

(3) Porous carbons produced by paper-making technology

Porous carbon materials have been developed by utilizing a combination of paper making technology and a novel carbonization method. These materials have not only a low density and a highly porous structure, but they also have higher uniformity, strength and chemical

inertness than other kinds of porous carbon materials. In addition, the process is applicable for mass production at lower cost. (Oji - 1990)

The typical manufacturing process for preparing the porous carbon materials is summarized as follows:

A mixture of chopped carbon fibres, are made to form a sheet by utilizing paper manufacturing technology. The sheets consist of randomly oriented and well tangled short fibres. Then, the sheet is impregnated with a resin to produce a prepreg sheet, next these prepreg sheets are laminated and hot-pressed. After this process, the composite is carefully carbonized and graphitized in an inert atmosphere.

This material can be considered as a porous carbon bonded carbon fibre composite, because it is made from carbon fibres which are bonded with carbon matrix. However, it is possible to prepare a homogeneous carbon structure without any distinction between fibre and matrix by choosing special kinds of fibres and regulating the manufacturing process. Therefore, it is possible to adjust widely the properties of the porous carbon materials, such as density, strength, modulus, porosity, and degree of graphitization.

Table II-1-4 describes the typical properties of porous carbon material produced by Oji Paper. This material is employed for this project as a main precursor for conversion into ceramic materials.

Table II-1-4 Physical properties of porous carbon material by paper-making technology

Bulk density (g/cm^3)	0.50
Porosity (%)	70
Electrical resistivity (mohm cm)	50
Thermal conductivity (W/(mK))	0.035
Flexural strength (MPa)	15
Young's modulus (GPa)	3.7

(4) Porous carbon bonded carbon fibre composites

Porous carbon-carbon composites in the form of short carbon fibres bonded with carbon matrix, have been developed mainly for electrode materials or heat insulation. (Kureha - 1984, Shui - 1991, Wei -1985)

Porous carbon-carbon composites, or more precisely, carbon matrix bonded short carbon fibres, were fabricated in a method which is considerably different from that used to make conventional dense carbon-carbon composites. They are typically fabricated by moulding from slurries containing short carbon fibres and binders including resins, pitches and polymers.

These porous carbon-carbon composites have high surface area, low electrical resistivity, and good mechanical properties, and a polished section of a porous carbon-carbon composite is shown in Figure II-1-17 (p.40). By controlling the fibre length, it is possible to vary the properties of these materials in a wide range. (Table II-1-5)

Table II-1-5 Physical properties of porous carbon bonded carbon fibre composites
((a) Shui - 1991, (b) Kureha - 1984)

Fibre length (μm)	50[a]	100[a]	200[a]	400[a]	100-600[b]
Apparent density (g/cm^3)	0.66	0.62	0.43	0.29	0.65
Porosity (%)	58.8	61.3	73.3	81.8	61
Electrical resistance (mohm cm)					
longitudinal	51	66	102	230	-
transverse	32	41	60	104	16
Mechanical strength (MPa)					
compressive	6.9	4.8	1.8	0.55	-
flexural	-	-	-	-	17
Surface area (cm^2/cm^3)	1030	968	670	455	

(5) Other types of porous carbon

Other types of porous carbon materials include fibrous carbon and graphite, and extruded or moulded porous carbon and graphite particle solids which have been used in many industrial fields. For example, fibrous carbons including carbon/graphite felt (Oren - 1983, Lestrade - 1981) and graphite cloth (Zur - 1981) have been employed for electrode materials for flow electrolysis systems.

Extruded or moulded porous carbon and graphite particle solids usually suffer from one serious drawback. Their porosity is too low for applications such as filtration and insulation. (porosity is usually less than ca. 50%) These methods are mainly used to produce a green body for a reaction-sintering to ceramic materials.

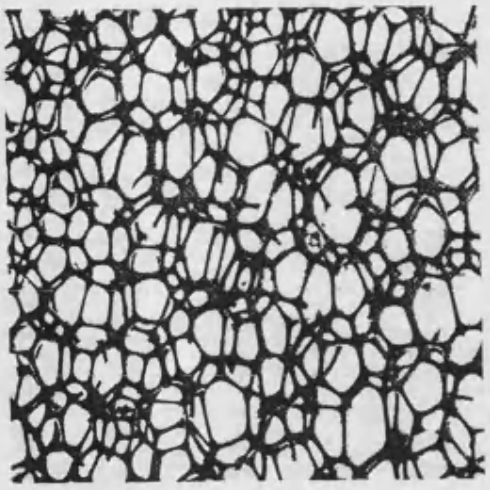

Figure II-1-16 Enlarged view of reticulated vitreous carbon (from Wang - 1981)

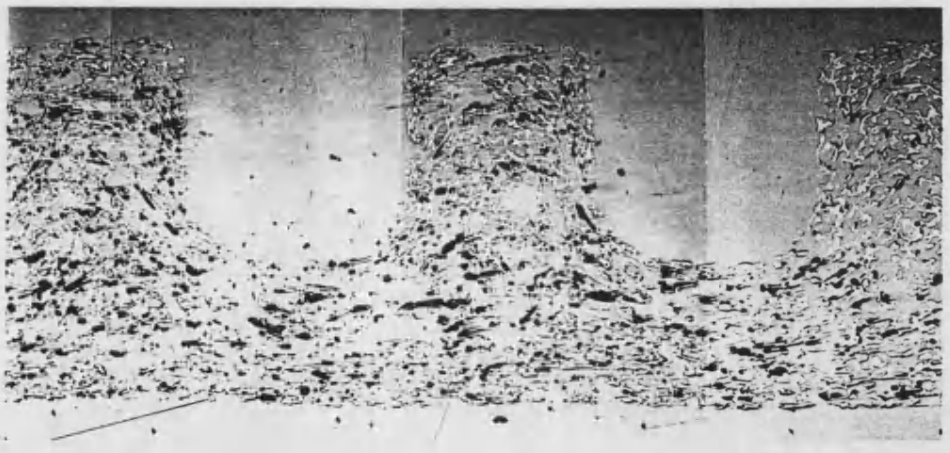

Figure II-1-17 Polished section of porous carbon-carbon composites (from Kureha - 1990)

II-1.5 Porous ceramic materials

II-1.5.1 Introduction

The potential applications for high-performance, low-cost ceramic materials can be diverse, and can be extended to a wide range of industrial fields. In particular, porous, lightweight and low-density ceramic materials will have varied uses as insulators and filters where extremely high temperatures and severe corrosive environments are applied. They may be also applied as structural materials where weight-saving is also critical, e.g., as core components of sandwich structures. Table II-1-6 (p.45) lists examples of components and potential industrial applications for porous ceramic materials, excluding defence and aerospace industries.

II-1.5.2 Application fieilds

(1) Thermal insulation at high temperatures

Fibrous ceramic materials have been used as a thermal protection system of re-entry vehicles. For example, the U.S. Space Shuttles have used silica tiles which are made from very high porosity amorphous silica fibers (1-4 μm in diameter, 0.32cm long) bonded with a slurry binder and sintered into blocks. The tiles are coated with borosilicate glass to provide the proper thermal properties and water resistance, and in high-temperature locations they are coated black by the addition of silicon tetraboride to faciliate radiation. The silica tile has 93% porosity and thus a low thermal conductivity, 0.017-0.052 W/mK. As a result, the

performance of the tiles has been successfully demonstrated by a series of flights of the Space Shuttles. (Korb - 1981, Schramm - 1981, Buckley - 1981, Leiser - 1981) Figure II-1-18 (p.45) illustrates basic insulation material concept for the Space Shuttle.

In addition to applications in aerospace and defence industries, porous and lightweight ceramics can also be expected to be used as thermal insulators in a wide range of general industrial fields as shown in Table II-1-6.

(2) Hot gas particulate filters

Highly efficient particulate removal from hot gas streams is important in a number of industrial processes from the advanced fossil-fuel processing technology (e.g., fluidized-bed combustion, coal gasification), to high-temperature industrial processes (e.g., metal production, plasma processing, and energy recovery) and waste incineration processes. Various types of porous ceramic materials have been studied for this application and they have proved to be highly efficient for collection of small particles. Detailed discussions of the application of porous ceramics as hot gas filters have been given by Alvin (1991), Zievers (1991) and Sheppard (1991).

(3) Molten metal filtration

Porous ceramic materials have been used widely for molten metal filtration, because ceramics, in general, exhibit high-temperature stability and corrosion

resistant properties in contact with a variety of molten metals, which can contain such reactive elements as aluminium, titanium, hafnium, and carbon. As a result, ceramic filters can significantly improve productivity and quality of products during manufacture of castings by removing slag, dross and nonmetallic inclusions. It was found that ceramic filters reduced scrap rate by 40 %, salvage rate by 30%, and increased yield by 10%. (Sheppard - 1991)

(4) Ceramic membranes for separation technologies

A wide range of membranes for separation have attracted attention recently as a result of increasing requirements for effective separation techniques in various industries. In particular, ceramic membranes have many advantages over conventional polymeric and metallic membranes in high-temperature applications and those which require chemically inertness, corrosion resistance, and abrasion resistance. However, ceramic membranes have not been exploited extensively due to their high costs and scepticism about control of pore size distribution. Nonetheless, recent developments including sol-gel processing have enabled ceramic membranes with uniform pore size distribution to be produced at low cost. Therefore, potential applications of these membranes extend to very diverse fields, including food processing, pharmaceutical production, petro-chemical production, gas separation, waste processing and other chemical processes. (Chan - 1991)

(5) Structural sandwich panels

Structural materials composed of two stiff, strong skins separated by a lightweight core are known as sandwich panels. The core materials act to separate the skins, increasing the moment of inertia of the panel, with little increase in weight, producing an efficient structure for resisting bending and buckling loads. Usually, lightweight cellular materials are used for the core. They are preferred because of low thermal conductivity in addition to low weight. The sandwich panels are often used in applications where weight-saving is important such as aircraft, portable structures and sports equipment. Modern aerospace sandwich components are made almost exclusively with honeycomb cores and fibre-composite faces bonded together with advanced adhesives. This technology is being transferred to the construction industry where the main use is in building panels. The foam core gives excellent thermal insulation while the faces provide the structural stiffness and strength of the panels. The reduced weight of sandwich construction is also useful in applications where the component must be lifted or moved into another place. Consequently, the weight of sandwich panels is minimized by appropriate optimization. Applications where porous ceramics are expected to be useful are lightweight core materials for panels, beams, tiles and decking where high temperatures and severe circumstances are required such as fire protection or abrasive environments.

Engineering System	Example Components	Potential Markets
Heat Recovery[1]	tubes, supports	Re-melting(steel,Al,glass)
Incineration	particle filters	
Separation / Filtration	filters, membranes	PF and combined
Chemical Processes	refractories, filters, catalyst supports	
Structural Applications[2]	beams, panels, tiles, decking	Fire protection abrasive environments

1) for thermal insulation; 2) in cellular sandwich structures

Table II-1-6 Examples of components and potential industrial markets for porous ceramics

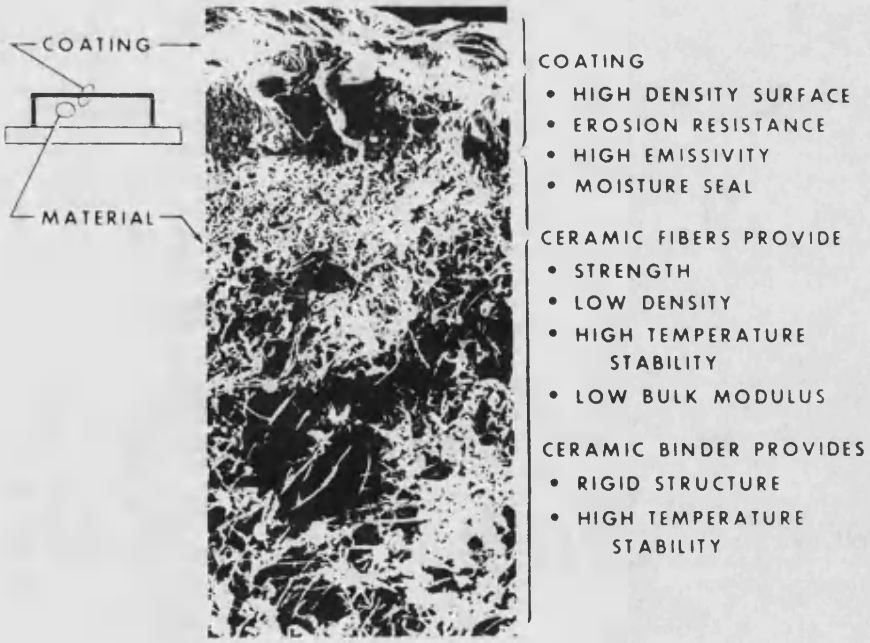

Figure II-1-18 Basic surface insulation material concept for the Space Shuttle (from Buckley - 1981)

II-1.5.3 Fabrication methods and properties

Although relatively a wide range and a large number of application fields of porous ceramic materials have been reported, very little has been published on fabrication methods for the porous ceramics, apart from conventional firing fabrication methods from ceramic powders. Details of fabrication of some materials have been published and can be divided into (1) cellular ceramic materials and (2) fibrous ceramic materials. These materials are reviewed in the following sections.

(1) Cellular ceramic materials

There are several techniques for fabricating low-density porous cellular ceramics where a foamed polymer or carbon is infiltrated by a ceramic slurry or by chemical vapour infiltration. Commercially available porous cellular ceramics from several companies seemed to be produced using these infiltration methods, because these materials have a structure consisting of cells separated by struts: e.g., open-cell alumina from Astro Met Associates, Cincinnati, OH. and HiTech Ceramics, Alfred, N.Y. (Hagiwara - 1987), porous mullite from Morgan Thermic, G.B. (Maiti -1984(a)), porous zirconia (Ashby - 1986), and various refractory ceramic foams from Ultramet Corporation (Sherman - 1991).

In the first process, porous ceramics are produced by dipping the polymer foams in to a slurry containing an appropriate binder and ceramic phases, followed by a pressureless sintering process at elevated

temperatures. A ceramic foam replica of the original foam can be gained after burning out the polymer. However, there are some restrictions in this slurry infiltration technique. The impregnation of slurries into the preforms is limited by the filtering action of the preform and this also has limitations on the thickness of the specimens that can be infiltrated. Furthermore, it poses strict limits on the particle size distributions tolerated in the slurries. Hence, there is serious scepticism about the ability to produce high performance porous ceramics using this route.

The second process is infiltration of porous carbon preform skeletons, prepared from the pyrolysis of polymeric foam in a carefully controlled carbonization process, with refractory materials using chemical vapour infiltration (CVI) / chemical vapour deposition(CVD) techniques. Figure II-1-19 (p.51) shows an artist's conception of infiltrated / sheathed foam structure and individual coated foam ligaments. A scanning electron micrograph of CVI-infiltrated foam is presented in Figure II-1-20. A fractured surface of open-cell alumina is shown in Figure II-1-21.

Ultramet Corporation (Sherman - 1991) reported that the mechanical properties for CVD/CVI deposited porous ceramics were usually 1 to 2 orders of magnitude higher than slurry-cast materials due to their small grain size and the low impurities in the deposited refractory. However, this chemical vapour infiltration

method is expensive and slow. This is because in order to attain a uniform deposition rate throughout the material, the temperature must be low so that the reaction takes place in the chemical control regime. Therefore, chemical vapour infiltration is a time-consuming route that requires weeks or even months.

(2) Fibrous ceramic materials

In the early 1970's, silica and mullite (aluminum silicate) fibre based ceramics were chosen as the most promising candidates for heat-shield tiles on the Space Shuttle. The silica and mullite fibre tiles were fabricated by using slightly different techniques. The silica was made by dispersing silica fibres in water and casting, by gravity or centrifugal force, onto a screen. The resulting unbonded felt was dried, and fired, followed by impregnation with a binder solution. In the case of mullite fibre, the fibres and microsphere fillers were dispersed in a binder solution and the impregnated felt was vacuum-cast onto a screen. These materials were fired at 1260-1370° C. Typical properties of silica and mullite reusable surface insulation evaluated in the early 1970's are shown in Table II-1-7 (p.49). (Buckley - 1981)

As a result of further technical development, the U.S. Space Shuttle, Columbia used silica tiles which were made from very high porosity amorphous silica fibres (1-4 μm in diameter, 0.32cm long) bonded with a slurry and sintered into blocks. (Korb - 1981)

	Silica	Mullite
Density (kg/m^3)	240	192-240
Tensile strength ($N/m^2 \times 10^5$)		
Longitudinal	4.8	5.9-6.6
Transverse	1.0	1.9-1.5
Compressive strength ($N/m^2 \times 10^5$)		
Longitudinal	10	6.5-15
Transverse	2.8	2.9-4.3
Tensile modulus ($N/m^2 \times 10^7$)		
Longitudinal	41	29-39
Transverse	4.1	6.3-13
Tensile strain to Failure (%)	0.09	0.23-0.17
Thermal expansion coefficient ($m/mK \times 10^6$)	0.5	5.0
Specific heat (cal/gK)	0.24	0.25

Table II-1-7 Typical properties of silica and mullite reusable surface insulation (Buckley - 1981)

(3) Other porous ceramic materials

In addition to cellular and fibrous ceramics, there are also some other methods for preparing porous silicon carbide ceramics, such as recrystallization of SiC, reaction-sintering technique, and carbothermal reduction of rice hulls.

Highly porous self-bonded silicon carbide materials were prepared by recrystallizing silicon carbide at very high temperatures. (Van Der Beck - 1957)

Popper and Davis prepared porous forms of reaction-bonded silicon carbide with a dense surface. (Popper - 1961) A mixture of 94 wt% of SiC particles (320 mesh) and 6 wt% of graphite powder was pressed, and silicided

to produce a non-porous product of silicon carbide and silicon, containing about 50% silicon. Then, this solid was heated to 2000° C in a carbonaceous atmosphere. The specimen was covered with dense SiC on the surface, whereas much of the silicon was driven out and well-bonded porous SiC was produced inside.

It is well-known that rice hulls, which consist mostly of silica (15-20 wt%) and some organics, produce silicon carbide when they are heated at temperature above 1500° C via carbothermal reduction of silica. Accordingly, Komatsu et al. prepared porous SiC ceramics from rice hulls using a hot-pressing method. (Komatsu - 1990) Thus, the rice hulls were chopped into 50-100 mesh in size and carbonized at 500° C in a nitrogen atmosphere, followed by impregnation of Fe(II) as a reaction catalyst. Then the excess carbon content in the rice hull chars was burned off at 296° C for various times. After grinding (-7 μm), the rice hull chars were hot-pressed at above 1700° C to produce a porous SiC form. The bulk density and porosity of SiC compact after removal of residual carbon in the hot-pressed material varied from 0.67 to 1.9 g/cm^3 and 78 to 40 vol%, respectively, depending on the residual carbon content in the rice hulls.

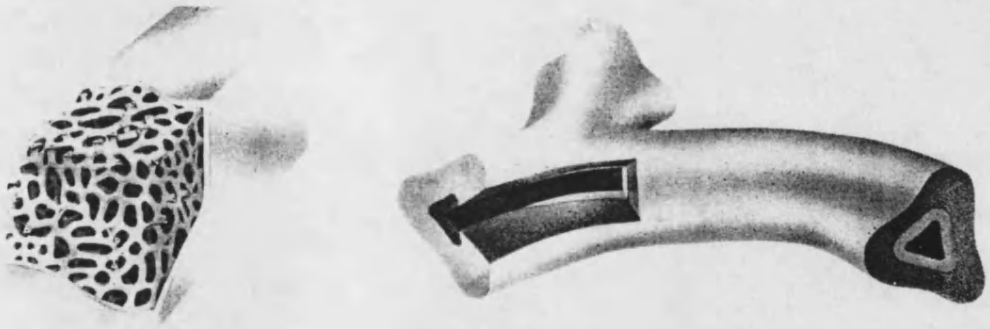

Figure II-1-19 Artist's conception of (a) infiltrated and sheathed foam structure, and (b) an individual coated foam ligaments (from Sherman - 1991)

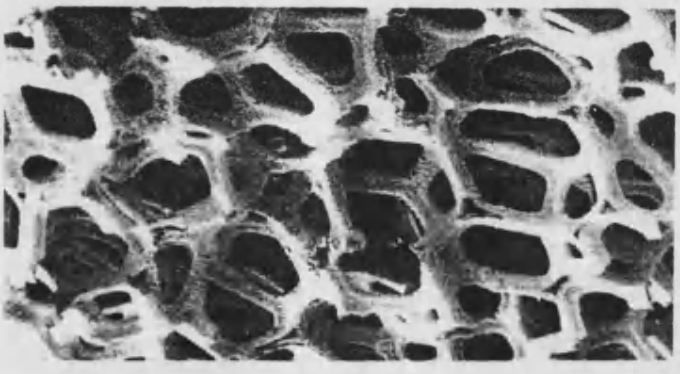

Figure II-1-20 SEM of the structure of CVI-infiltrated foam material (from Sherman - 1991)

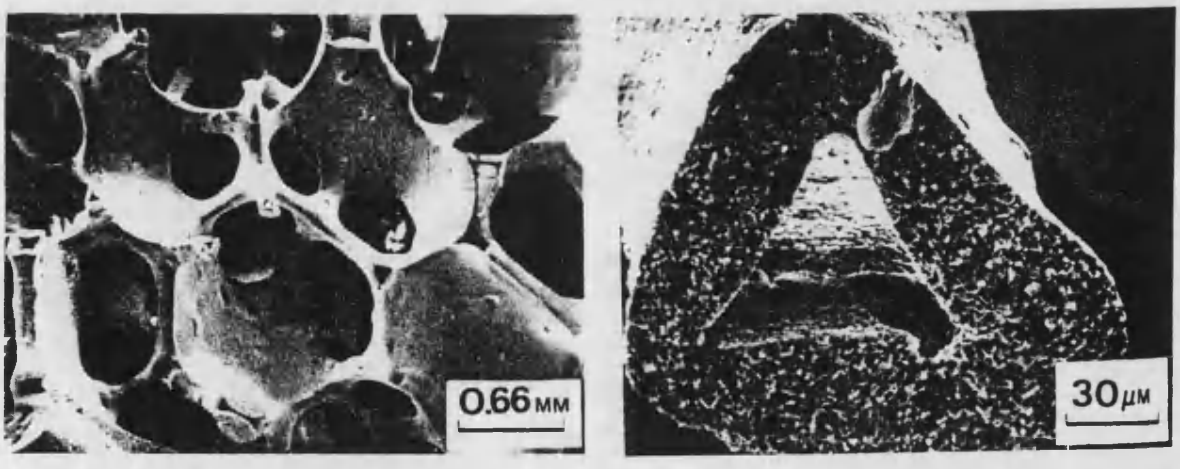

Figure II-1-21 Fracture surface of a commercially available open-cell alumina (from Hagiwara - 1987)

II-2 Material properties and production processes of carbon and ceramics

II-2.1 Introduction

The properties and characteristics of porous materials are determined by two separate sets of parameters. One is the geometric structure of porous solids, that is described in Chapter II-1, including the size and shape of the pores, the shape anisotropy, the degree to which the solids are open or closed, and the apparent density and porosity. The other set of parameters is the intrinsic nature of the materials of which the porous solids are made. The crucial material properties include the solid density, the yield strength, the fracture strength, the elastic modulus, the thermal conductivity, the thermal expansion coefficient, the specific heat, and the electrical conductivity.

Therefore, Chapter II-2 describes material properties of carbon and ceramics, which are essential for the understanding and analysis of mechanical and thermal behaviour for porous carbon and ceramic materials. In addition, preparation methods and densification processes of silicon carbide and silicon nitride are also summarized concisely. Furthermore, heterogeneous hybrid materials consisting of carbon and ceramics, more briefly carbon-ceramic composites, are also discussed.

II-2.2 Carbon

A wide variety of carbon and graphite products have found diverse industrial applications owing to their unique combinations of properties that other ceramic materials do not have.

II-2.2.1 Structure of carbon and graphite

The unique combination of properties of carbon and graphite materials is strongly related to the nature of their crystal structure. In graphite, carbon atoms are arranged in layers, in which each carbon atom is strongly bonded with three others by single or double bondings to form an hexagonal array. Bonding between the layer planes is by much weaker van der Waal's forces. The carbon-carbon bond length in the layers is 0.142 nm and the distance between the layers is typically 0.335 nm. Graphite is known to have two types of crystal structure: hexagonal and rhombohedral. (Figure II-2-1, p.56) The dimension of layer planes along any axis direction can vary considerably, and layer planes are combined together to form larger units.

The size of crystallite, which varies from 1 to 100 nm, contributes strongly to properties and characteristics of carbon and graphite.

The nature of the carbon precursor molecules, in general, determines the size and form of crystallite structure. For instance, carbons resulting from heat-treatment up to 1300° C of polynuclear aromatic hydrocarbons can have a well-ordered structure that can begin recrystallization at temperatures above 1500° C to

give highly graphitized structure. On the other hand, carbons resulting from carbonization of a phenolic resin have a random structure which is inherited from the highly cross-linked thermosetting polymer. This material has a glass-like structure and is well known as vitreous carbon. The further heat-treatment can give only negligible change in structure. Franklin called the former and the latter type of carbons graphitizing carbon (soft carbon) and non-graphitizing carbon (hard carbon), respectively. (Franklin - 1951) The structural models of Franklin are presented in Figure II-2-2 (p.56).

Therefore, it is possible to provide a very wide variety of crystallite structure in carbon and graphite materials according to their precursors and their thermal history. As a result, the properties and characteristics of carbon and graphite products, which are greatly influenced by the crystallite structure, permit a wide range of grades to be produced for selected applications.

II-2.2.2 Fabrication methods and properties

Carbon and graphite materials can exhibit a wide variety of properties and characteristics due to the range of compositions used for carbon precursor materials and the diversity of subsequent fabrication processes. These properties and characteristics are deliberately sought to achieve optimum performance for particular applications.

It is also important that the property values of carbon and graphite materials, which are often used at high temperatures, can be varied in different temperature ranges. For example, as temperature rises, strength increases and conductivity decreases.

Meanwhile, material anisotropy is another significant factor affecting their properties. The flexural strength of a material produced from flake graphite by extrusion may be two times greater when tested along its length than when tested on a transverse sample. In contrast, materials produced from amorphous precursors by moulding would be nearly isotropic.

Table II-2-1 presents some typical property values of representative carbon and graphite materials.

	Electro-graphite	Glassy carbon	Resin-impregnated carbon graphite
Bulk density (g/cm^3)	1.5-1.8	1.45-1.55	1.85
Flexural strength (MPa)	10-30	60-120	100
Compressive strength (MPa)	20-50		200
Young's modulus (GPa)	7-15	25-30	20
Coefficient of thermal expansion (10^{-6}/° C)	1-3	2-3	5
Thermal conductivity (cal/cm sec ° C)	0.3-0.4	0.01-0.035	0.07
Electrical resistivity (10^{-6} ohm cm)	6-12	35-50	45

Table II-2-1 Physical properties of typical carbon and graphite materials at 20° C.

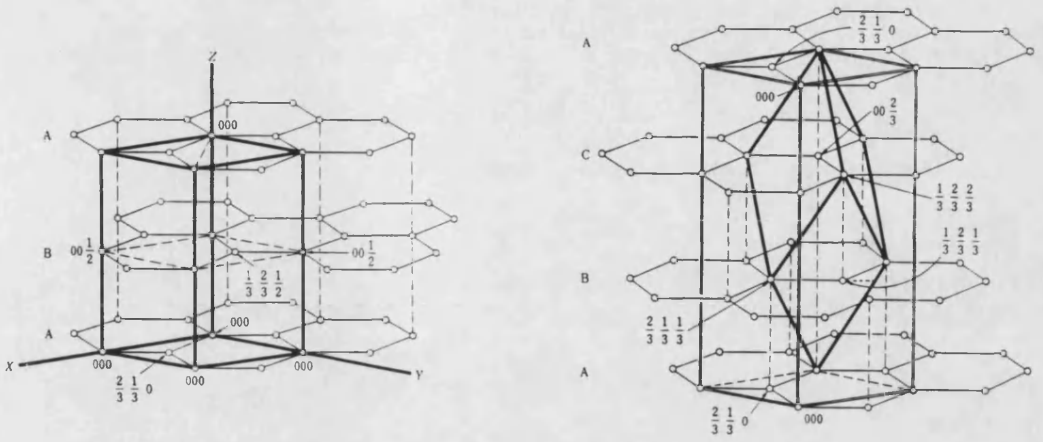

(a) Hexagonal (b) Rhombohedral

Figure II-2-1 Crystal structures of graphite

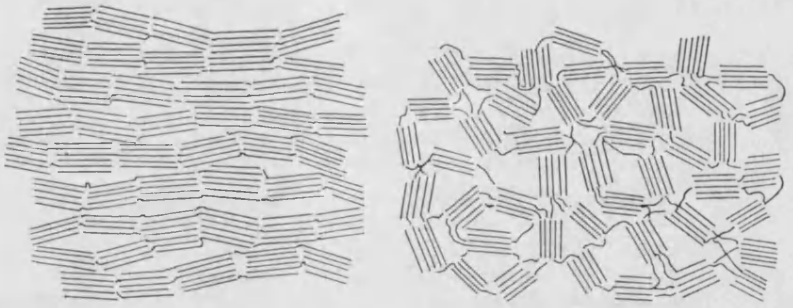

(a) Graphitizing carbon (b) Non-graphitizing carbon

Figure II-2-2 The structural model for carbons (Franklin - 1951)

II-2.3 Ceramics

Non-oxide ceramic materials, such as carbides, nitrides, borides and halides, have been intensively developed as high-temperature structural materials because of their high potentiality in engineering applications. (Hampshire - 1986, Riley - 1983) Compared with conventional materials like metals, metallic alloys and oxide ceramics, non-oxide ceramics have generally higher intrinsic strength at elevated temperatures, better oxidation and corrosion resistance, and also have lower density. These ceramics generally exhibit better properties above ca. 1000° C except in one respect, that is their inherent brittleness. Therefore, there have been many research programs dedicated to the possible substitution of metals by ceramics, especially in high-temperature applications such as components for gas-turbine and diesel engines. As a result, dramatic advances in the materials have been achieved and ceramics have gained a place in a wide variety of structural engineering applications.

In particular, silicon carbide and silicon nitride have been main targets for developing high-temperature structural materials due to their high strength, good oxidation resistance, and excellent wear resistance. (Komeya - 1988, Iseki - 1988) SiC has higher thermal expansion than Si_3N_4 and higher thermal conductivity. Intrinsic strength of SiC is lower than that of Si_3N_4, however sintering additives to Si_3N_4 reduce its creep

resistance to the same as that of SiC. Furthermore, recently ceramic alloys based on combinations of silicon nitride with alumina and other oxides, sialons (Si-Al-O-N), have widened interest in these ceramics. (Jack - 1986, Mitomo - 1988) Table II-2-2 shows basic characteristics of ceramics including SiC and Si_3N_4 in contrast with sialon, SiO_2 and graphite.

	SiC	Si_3N_4	SiAlON	SiO_2	Graphite
Density ρ (g/cm³)	3.1-3.2	3.1-3.2	3.2	2.6	1.5-1.8
Bend strength σ (MPa) 20℃	450-600	550-1200	600-1000	5	10-30
Young's modulus E (GPa) 20℃	420	300	300	100	7-15
Hardness (Vickers) (Kg/mm²)	3000	2000	1725	500	-
Thermal expansion α ($\times 10^{-6}$/℃)	4.3	3.2	3.2	0.5-1	1-3
Thermal conductivity λ (W/mK)	50-85	20	20-25	2.1	120-200
Maximum temperature for use (℃)	1500	1400	1500	1000	450

Table II-2-2

Basic characteristics of various ceramics

II-2.3.1 Silicon carbide, SiC

Silicon carbide was first prepared in laboratory experiments in the mid-1800s using carbothermal reduction of silica. Since then, SiC has been used mainly as grinding, cutting and abrasive materials due to its hardness, and also as refractory brick materials because of its thermal stability over a wide range of temperatures. However its excellent physical and chemical properties at high-temperatures had not been fully utilized as a structural material because of difficulty in sintering.

In recent years, thanks to the development in sintering processes to obtain high-density materials, dense silicon carbide materials which have excellent mechanical strength at elevated temperatures and good thermal shock resistance, have become increasingly important as engineering materials under conditions of extreme thermal and mechanical stress. Silicon carbide, therefore, has been intensively developed as a suitable substitute for high temperature metal alloys. Si_3N_4 based materials were extensively studied at the early stages, but it was eventually realized that SiC has many valuable features and can be produced to very precise specifications.

Consequently, commercial application fields of SiC based materials can be expected to spread further and wider in accordance with the expansion of new advanced engineering applications, especially where high temperatures and corrosive environments are found.

(1) Properties

Silicon carbide is the only compound formed in the C-Si phase diagram, and this can be present up to its peritectic decomposition temperature of 2830° C.

The molecular structure of silicon carbide consists of tetrahedrally co-ordinated C and Si atoms, the bonding between which is ca. 90% covalent. These tetrahedra can be stacked to give a cubic structure (β-SiC), or a multiplicity of hexagonal or rhombohedral structures (α-SiC). The β-form is usually regarded as metastable with respect to the α-form. Heating SiC to temperatures over 2100° C normally leads ultimately to the formation of the α-phase.

As shown in Table II-2-2 (p.58), very strong inter-atomic bonding between Si and C causes a high value for Young's modulus, and low thermal expansion, in addition C and Si diffusion coefficients are very low which is believed to be responsible for the difficulties in sintering silicon carbide powder to high density. The high thermal conductivity, associated with the low thermal expansion, contributes to the exceptionally good thermal shock resistance. Highly pure silicon carbide exhibits excellent oxidation resistance because of formation of a protective thin layer of a glassy or partly crystallized silica film on the surface. The diffusion of molecular oxygen through this layer determines the kinetics of the oxidation reaction.

(2) Production routes

Silicon carbide is produced using a number of methods

and from various raw materials, which determine the physical and chemical characteristics.

The most conventional and commercial production method is reaction of a mixture of silica and carbon (the Acheson process).

$$SiO_2(s) + 3C(s) \longrightarrow SiC(s) + 2CO(g) \quad (1)$$

SiC is also produced by gas-phase reaction processes, such as, between silanes, alkyl silanes, or silicon halides, and hydrocarbon. Typical reactions are:

$$2SiH_4(g) + C_2H_4(g) \longrightarrow 2SiC(s) + 6H_2(g) \quad (2)$$

$$SiCl_4(g) + CH_4(g) \longrightarrow SiC(s) + 4HCl(g) \quad (3)$$

The decomposition of gaseous or volatile compounds of silicon and carbon, on a small scale, is another gas-phase reaction to deposit SiC on a suitable hot substrate. This process, typically shown by the following equation, is known as chemical vapour deposition (CVD), and it has been studied extensively in the formation of SiC coatings to protect carbon materials against oxidation degradation. (Christin - 1980, Naslain -1981)

$$CH_3SiCl_3(g) \longrightarrow SiC(s) + 3HCl(g) \quad (4)$$

Silicon carbide can be obtained by high-temperature crystallization from a carbon-rich silicon melt that is supersaturated with respect to SiC. (Shaffer -1987)

$$Si(l) + C(s) \longrightarrow SiC(s) \quad (5)$$

This reaction established the fundamentals of a reaction bonding technique for bonding fine-grain silicon carbide powders.

The sintering of silicon carbide is very difficult, and so it is important to prepare the carbide with small particle size, high purity and homogeneity in order to obtain a high sinterability. Accordingly new synthetic routes based on chemical methods, such as sol-gel methods (Kuramoto-1983, Wei - 1984) and polymer pyrolysis (Rice - 1983, Wynne -1984), have attracted wide interest recently because, since the reactants are mixed at a molecular or atomic level, the products may be highly pure and homogeneous.

(3) Densification of silicon carbide

There are several methods to produce high-density silicon carbides for structural applications, and the processing routes used to fabricate dense SiC ceramics are almost similar to those of Si_3N_4 described in the next section: reaction-bonded silicon carbide (RBSC), chemical vapour deposited silicon carbide (CVDSC), hot-pressed silicon carbide (HPSC) and sintered silicon carbide (SSC).

It is well known that powders of higher purity and with uniform particle size distributions, show a higher rate of densification. Thus, the preparation of silicon carbide powders has an important bearing on sintering. However, in general, pure silicon carbide powders cannot be sintered without sintering aids due to low values for the C and Si diffusion coefficients.

The boron-carbon system (Prochazka - 1974) and the aluminum-carbon (Bocker - 1979) system are well known as sintering aids for the pressureless sintering of SiC. In 1973, Prochazka et al. successfully sintered a submicron β-phase SiC powder to near theoretical density without applied pressure using sintering aids of boron and carbon. (Prochazka - 1973) Moreover, it has been found that combinations of aluminum, boron and carbon are more effective for sintering of SiC. (Iseki - 1983) It was originally believed that sintering aids favourably influence the free surface and grain-boundary energies, coupled possibly with enhancement of atomic diffusion rates. However, the mechanisms of the sintering aids are not yet clearly understood.

II-2.3.2 Silicon nitride, Si_3N_4

Silicon nitride can maintain excellent mechanical strength and creep resistance at high temperatures, and has good resistance to thermal shock, and strong wear and corrosion resistance. Hence, in recent years, considerable research efforts have been devoted to development of silicon nitride ceramics. As a result, these materials have established a wide range of commercial applications, such as engine components, metallurgical and chemical plant components, wear-resistant parts, heat-jigs and cutting tools, etc. (Komeya - 1988)

(1) Properties

Silicon nitride has two types of hexagonal crystal structures, α- and β-phase, both of which can be regarded as consisting of interleaved corrugated sheets of 8- and 12- membered rings of silicon and nitrogen atoms. The α-structure contains a degree of strain and it is believed that a stabilizing factor is required. Solution or evaporation of α-phase allows the reconstructive α-β phase transformation to occur. (Jack -1983)

The silicon-nitrogen bonding in Si_3N_4 has approximately 30% ionic character, hence the preponderant strong covalent interatomic bonding gives excellent thermal stability combined with good mechanical properties over a wide range of temperatures.

Silicon nitride does not melt under normal pressure, but it starts to decompose at 1882 °C under 1 atm of nitrogen into nitrogen and liquid silicon. The dissociation rate become appreciable at ca. 1500 °C, and above this temperature silicon nitride is effectively unstable under vacuum, or in the presence of silicon vapour or nitrogen sinks.

(2) Production routes

Silicon nitride powders can be obtained in a number of ways, which result in a wide variety of microstructures and associated properties. There are four main routes: silicon direct nitriding, silica reduction, vapour phase reaction and a pyrolysis

method, and three different raw materials: metallic silicon, oxide and halide.

The most common and simplest method is the direct nitridation of silicon powder at temperatures over 1200° C.

$$3Si(s) + 2N_2(g) \longrightarrow Si_3N_4(s) \quad (6)$$

The carbothermal reduction of silica in nitrogen atmosphere is an alternative route.

$$3SiO_2(s) + 6C(s) + 2N_2(g) \longrightarrow Si_3N_4(s) + 6CO(g) \quad (7)$$

Silicon nitride, produced in the simultaneous carbothermal reduction and nitridation, is of high purity and of much finer particle size, and predominantly consists of α-phase. Therefore, silicon nitride produced by carbothermal reduction can sinter more rapidly and at lower temperatures and pressures than silicon nitride produced by direct nitridation. In addition to these advantages, the raw materials for this route are available at low cost, and this process is suitable for a large-scale production.

Silicon nitride with relatively high purity can also be synthesized by a vapour phase reaction such as between SiH_4 and N_2, and $SiCl_4$ and NH_3 or a mixture of NH_3 and H_2.

$$3SiCl_4(g) + 16NH_3(g) \longrightarrow Si_3N_4(s) + 12NH_4Cl(g) \quad (8)$$

The alternative route is the decomposition of organometallic imides, which has received considerably

attention recently because high-purity ceramic products with high-surface area can be produced homogeneously since the Si and N atoms are mixed at the molecular level.

$$3Si(NH)_2(s) \text{ ---> } Si_3N_4(s) + 2NH_3(g) \qquad (9)$$

The fabrication method, thus, is very important to determine the physical and chemical characteristics on which the sinterability of silicon nitride strongly depends.

(3) Densification of silicon nitride

The densification of silicon nitride powder compacts is very difficult due to the strong covalent bonding between silicon and nitrogen, furthermore silicon nitride begins to decompose by volatilization of nitrogen at temperatures around 1900° C. Therefore, additions of sintering aids, usually metal oxides, are thus generally required and several methods which result in a variety of microstructures and associated properties have been developed in order to produce high densification forms by using different sintering processes. These include reaction-bonded silicon nitride (RBSN), hot-pressed silicon nitride (HPSN), post-sintered reaction-bonded silicon nitride (PSRBSN), and sintered silicon nitride (SSN). (Katz - 1983)

The liquid-phase sintering process with sintering additives, metal oxides such as MgO and Y_2O_3, singly or in combination, and together with Al_2O_3, has

contributed to progress in densification of the ceramics. In the case of magnesium oxide (MgO), oxynitride liquid phase is formed on the surface of silicon nitride particle in the temperature range of 1000-1400° C. Above this temperature, α-Si_3N_4 begins to transform to β-form by a solution-precipitation mechanism in a liquid phase. The $\alpha \rightarrow \beta$ transformation is completed by 1700 °C, and on cooling the liquid solidifies as a magnesium silicon oxynitride glass. (Sun - 1986)

This viscous phase is responsible for the deterioration of mechanical properties and oxidation at high temperatures. Therefore, it is of considerable interest to form silicon nitride ceramics with a minimum or none of the metal oxide sintering aids, however this has not been successful yet.

II-2.4 Carbon-ceramic hybrid materials

Carbon-ceramic hybrid materials, which consist of a combination of carbon and other ceramic materials that have different characteristics from carbon, seem to have potential to modify and improve the inferior properties of carbons: low oxidation resistance and mechanical properties. Thus, heterogeneous hybrid materials consisting of carbon and ceramics, have been intensively developed in order to achieve properties superior to those of the components.

Since a variety of methods, techniques, systems and materials have been developed for carbon-ceramic hybrid materials, it is difficult to classify them simply. However, carbon-ceramic hybrids can be categorized conveniently according to the system used: (1) carbon materials impregnated or coated with ceramics, (2) composites of ceramics and carbon, and others. The main objectives of these systems are generally associated with oxidation inhibition and/or improvement of mechanical properties. On the other hand, carbon fibre reinforced ceramics (ceramic matrix composites: CMC) can be considered as one category of carbon-ceramic hybrids, however their main aim is improvement of brittleness of ceramics by reinforcement of high strength and modulus carbon fibres.

II-2.4.1 Carbon materials impregnated or coated with ceramics

In order to protect externally carbon and graphite materials against oxidation with protective ceramic or

glass coatings, a number of methods, techniques, systems and materials have been employed. In general, an impregnation of carbon materials with inorganic salts, mainly boron oxide and phosphates, is reported to be an effective system for oxidation inhibition for the intermediate temperature ranges up to ca. 1000° C. (McKee - 1991) For higher temperatures and thermocycling applications, oxidation protective ceramic coatings, especially SiC coatings, have been developed using various methods including chemical vapour deposition (CVD), pack cementation technique, the Silmor process, sol-gel method, etc. (Castro - 1991) The main problem with the coating system is the low thermal expansion coefficient of carbons in comparison with that of potential refractory inhibitors. There are some comprehensive reviews concerned with oxidation inhibition of carbon materials by protective coatings. (McKee - 1991, Ehrburger - 1990, Sheehan - 1989, Strife - 1988)

II-2.4.2 Composites of ceramics and carbon

Carbon and graphite materials are well known as good refractory materials in a non-oxidizing environment. Therefore, ceramic dispersed carbon composites (CDC Composites) have been investigated in order to take advantages of the refractoriers of carbon materials in metallurgical application. (Ishibashi - 1983,1984) One fabrication method is the hot-pressing sintering method (CDC-HP) that utilizes boron compounds as sintering aids under hot pressing. The other is the

pressureless sintering method (CDC-NP) that uses sinterable carbon powder derived from the raw coke by mechanical and chemical treatment. (Kobayashi - 1988)

The composites which were prepared in CDC-HP method, exhibited remarkable oxidation resistance in air at 800° C because of a thin layer of boron oxide formed on the surface of the composite at the initial stage of oxidation. Furthermore, the addition of some carbide ceramic compounds such as TiC, NbC, and TaC as a third component increased their strength and thermal shock resistance. (Kobayashi - 1988)

Carbon-SiC or carbon-SiC-B_4C composites, fabricated in CDC-NP method, showed good mechanical properties and oxidation resistance. (Ogawa - 1988) Particularly the addition of boron carbide into the composites has contributed significantly to improvement of their properties. The addition of boron compounds enhanced the graphitization of the ground coke which itself gives a hard carbon. Moreover, when they are oxidized, a protective borosilicate glass layer seemed to form on the surface of the composites. This protective thin layer is thought to make a great contribution to the improvement of oxidation resistance.

II-2.4.3 Other methods

Polymer pyrolysis method to produce ceramics has also been studied for application to production of carbon-ceramic composites. Polycarbosilane, as the precursor of silicon carbide, was impregnated into cellulose

paper or a cloth of novolac fibres. After being cured, the composites were heat-treated at temperature up to 1400° C to give carbon-SiC composites. (Hasegawa - 1985) Similarly, fabrication of SiC-carbon composites was studied by pyrolysis of a mixture of carbosilane polymer and pitch. (Kawamura - 1991) In like manner, carbon-Si_3N_4 composites were also prepared by using the polymer pyrolysis method. The composite were produced by moulding carbon materials with polysilazane, $(SiH_2NH)n$, and heat-treated. (Tonen - 1991)

A sol-gel technique is an alternative method to produce carbon-ceramic composites. Tanaka reported carbon-SiC composites prepared by a sol-gel method by using TEOS and phenolic resin as raw materials. On the other hand, SiC dispersed carbon composites were prepared by the combination of sol-gel method and subsequent pressureless sintering process. (Kim - 1991)

Highly exothermic reactions can become self-sustaining and propagate through the reactant mixture in the form of a combustion wave. As the combustion wave advances, the reactants are converted to the products. The use of this technique to prepare materials has been called the self-propagating high temperature synthesis (SHS) method. It is well known that the reaction between carbon and silicon is very exothermic, as a result, carbon-SiC composites were fabricated by the self-propagating high temperature synthesis (SHS). (Yamamoto - 1990)

II-3 Non-oxide ceramics via reduction of sol-gel silica

II-3.1 Introduction

The sol-gel processing for the preparation of inorganic ceramic and glass materials has been extensively exploited for achieving higher purity and homogeneity and lower processing temperatures, compared with traditional glass melting or ceramic powder processes. Especially the silica sol-gel process has been the most intensively studied. As a result, its complicated reaction mechanisms and the effects of various factors have been firmly established.

In addition to conventional sol-gel processes for production of glass or oxide-ceramics, the use of sol-gel routes to prepare non-oxide ceramics has received considerable attention recently. One of the important driving forces to develop the technique is the lowering of the sintering temperature and the increase of the sinterability due to preparing submicrometer sized powders with high surface areas. For instance, highly sinterable SiC powder was synthesized by carbothermal reduction of silica prepared from sol-gel process. (Kuramoto - 1983, Wei - 1984) Furthermore, the combination of carbothermal reduction and nitridation of sol-gel SiO_2 is known as one of the best ways to produce a high purity and controlled size of Si_3N_4. (Szweda - 1981, Zhang -1984)

Consequently, Chapter II-3 summarizes the principal features of sol-gel processes, and then focuses on the

carbothermal reductions of sol-gel silica, which is an attractive route to non-oxide silicon ceramics.

II-3.2 The basis of silica sol-gel process

Sol-gel processes are basically the synthesis of an inorganic network by a chemical reaction in solution at low temperature. The most obvious features of this reaction, the transition from a liquid form (solution or colloidal solution) into a solid (di- or multiphasic gel) led to the expression "sol-gel process". (Schmidt - 1989)

Although there exist a large number of precursors for sol-gel processes, metal alkoxides have been most commonly used as suitable starting materials because firstly they are a convenient source of inorganic monomers, and secondly there is the possibility to control the rate of reaction by regulating chemical conditions.

A silica sol-gel process from alkoxide precursors is reviewed in this section in order to comprehend the principal features of the sol-gel process. The sol-gel process for preparing silica requires many different steps, and the properties of final product are strongly dependent on the conditions of each step.

A silica sol, in the form of a low viscosity liquid, may be prepared from a mixture of alkoxides and water, a gel may then be formed, by addition of a catalyst, by formation of an interconnected 3-dimensional network by simultaneous hydrolysis (1), and polycondensation (2)

and (3), resulting in Si-O-Si (siloxane) linkages. During this gelation step, the viscosity of sol sharply increases when the gelation point is reached, then a porous solid may be formed at last.

$$\equiv Si\text{-}OR + H_2O \quad ---> \quad \equiv Si\text{-}OH + ROH \qquad (1)$$

$$\equiv Si\text{-}OR + \equiv Si\text{-}OH \quad ---> \quad \equiv Si\text{-}O\text{-}Si\equiv + ROH \qquad (2)$$

$$\equiv Si\text{-}OH + \equiv Si\text{-}OH \quad ---> \quad \equiv Si\text{-}O\text{-}Si\equiv + H_2O \qquad (3)$$

(1) : hydrolysis

(2) and (3) : condensation and polymerization

The chemical reactions that cause gelation continue long after the gel point, producing strengthening, stiffening, and shrinkage of the network. This step is called an aging process that develops sufficient strength to resist cracking during drying. (Scherer - 1989)

The liquid is then removed from the interconnected pore network of gel during drying process. A dried gel still contains a large concentration of chemisorbed hydroxyls on the surface of pores. Thermal treatment up to 800° C can remove the surface silanol (Si-OH) bonds, resulting in a chemically stable ultra-porous solid, a stabilized gel. Further heat treatment of a gel at high temperatures can result in the densification via viscous-phase sintering, where the number of pores and their connectivity reduce substantially.

The structure of a gel is largely established at the stage of gelation, and subsequent processes such as aging, drying, stabilization and densification are all

critically dependent on the gel structure. Therefore, it is essential to control the kinetics of the hydrolysis and condensation reactions that determine the structure of the gel. The parameters which influence the reaction mechanism, structure and properties are a wide range of variables including the type of precursors, solvents, reactant temperature, catalysts, pH, additives and pressure. (Orcel -1988)

The chemistry and science of each process of the silica sol-gel system have been established significantly. Nonetheless, understanding of the molecular reaction mechanisms and the thermodynamics and kinetics of sol-gel systems is meagre (Hench - 1990), and this is the one of the main obstacles to develop new applications.

II-3.3 Carbothermal reduction of silica

It is well known, as stated in Chapter II-2, that non-oxide ceramics, especially SiC and Si_3N_4, have desirable properties as high-temperature structural materials. However, the difficulty of sintering due to their strong covalently-bonds is the main problem to produce dense solid bodies. The non-oxide ceramic particles derived from carbothermal reduction of sol-gel silica are so pure, fine, and of such high surface area that they may be expected to sinter more rapidly and at lower temperature and pressure.

II-3.3.1 Silicon carbide via carbothermal reduction of silica

The carbothermal reduction of silica, shown in the equation (4), has been much researched in order to obtain SiC powders. This is the most conventional and commercial production method known as the Acheson process. This method generally produces silicon carbide of coarse particle size and of low surface area.

$$SiO_2(s) + 3C(s) \longrightarrow SiC(s) + 2CO(g) \qquad (4)$$

A more intimate mixing of reactants is made possible by using starting materials in the form of silica sol-gels and carbon mixture, compared with simple mixing of silica and carbon powders. Another advantage of this method is that sintering aids or other additives can be homogeneously incorporated with in the gel form. Consequently, SiC powder has been synthesized by carbothermal reduction of silica gels with carbon source, such as finely dived carbon or a soluble carbon source (e.g., sucrose in aqueous solution, or resin or pitch in organic solvents).

In the early 1980s, a number of patents were granted concerning SiC production from carbothermal reduction of silica. Asahi Glass (Asahi - 1983) achieved carbothermal reduction of silica gels derived from the hydrolysis of silicon alkoxide with finely divided carbon black. Asahi-Dow (Asahi-Dow - 1982) prepared reactant silica from ion-exchange of water glass. In addition, Central Glass (Kuramoto - 1983) developed highly sinterable SiC powders by incorporating boron,

as a sintering aid, homogeneously into the silica sol-gel.

Wei, Kennedy and Harris (Wei -1984) synthesized silicon carbide powders via carbothermal reduction of carbon doped silica gels prepared from both colloidal silica and silicon alkoxide. As a result, they reported that β-silicon carbide derived from colloidal silica had better sinterability than that from alkoxide because of small average particle sizes of < 0.1 μm and narrow particle size distribution of the powder, which depend on the particle size of silica and carbon and the composition of the reactants.

Harris and co-workers (Harris - 1984) observed SiC powders prepared from colloidal silica with petroleum pitch by using optical and electron microscopy. SiC powders consisted of spherical agglomerates and unattached particles of SiC. They concluded that the source of the agglomerates could be traced to the precursor mixtures and might be related to the colloidal nature of the mixture.

In addition to conventional silica sol-gel technique, White, Fox and co-workers (Fox - 1986, 1989, White - 1987) have exhibited the controlled pyrolysis of polymeric organosilicon gels for preparing high-purity and high-surface area SiC powders. Crosslinked gels, having the ideal formula $(RSiO_{1.5})_n$, were synthesized by hydrolysis and condensation of $RSiX_3$ compounds (R = alkyl, vinyl, allyl or phenyl ; X = alkoxide or

chloride). The gels were then decomposed to produce an intimate mixture of SiO_2 and carbon which were subsequently reacted to produce silicon carbide in almost the same manner described above as the carbothermal reduction of silica. The products were determined as a partially crystalline, partially amorphous mixture of β-SiC, SiO_2 and carbon.

Meanwhile, SiC can be synthesized by reaction between high surface area carbon with silicon monoxide, SiO, generated according to Equations (5) and (6).

$$Si(s) + SiO_2(s) \longrightarrow 2SiO(g) \qquad (5)$$

$$SiO(g) + 2C(s) \longrightarrow SiC(s) + CO(g) \qquad (6)$$

Hase and Suzuki (Hase - 1978(a)) reported that submicron β-SiC powders prepared by reaction between SiO and carbon black under reduced pressure at temperature from 1340 to 1570° C. The SiC powders could be then sintered to 95-96% densities with an addition of boron and carbon. (Hase - 1978(b)) Ledoux et al. (Ledoux - 1988) produced SiC materials with high surface area (60-400 m^2/g) by using this method, and investigated the materials for an application as catalyst supports.

The chemistry and thermodynamics of the carbothermal reduction of silica may seem to be a simple solid state reaction between silica and carbon, however it can involve complicated simultaneous gas-phase reactions.

The carbothermal reduction of silica, the Acheson process, can be expressed as a following Equation (4) that proceeds in the solid state:

$$SiO_2(s) + 3C(s) \longrightarrow SiC(s) + 2CO(g) \quad (4)$$

This reaction is highly endothermic and the free enthalpy is positive until 1600° C.

In addition to Equation (4), silicon monoxide can be generated mainly by the solid state reaction (7), and the reduction of silica by carbon monoxide also occurs by a gas-solid reaction (8).

$$SiO_2(s) + C(s) \longrightarrow SiO(g) + CO(g) \quad (7)$$

$$SiO_2(s) + CO(g) \longrightarrow SiO(g) + CO_2(g) \quad (8)$$

$$CO_2(g) + C(s) \longrightarrow 2CO(g) \quad (9)$$

Therefore SiC can be formed additionally by reductive reactions of gaseous SiO with carbon (6) or carbon monoxide via a gas-solid state or gas-phase (10).

$$SiO(g) + 2C(s) \longrightarrow SiC(s) + CO\ (g) \quad (6)$$

$$3CO(g) + SiO(g) \longrightarrow SiC(s) + 2CO_2(g) \quad (10)$$

Thus, carbothermal reduction of silica proceeds in a combination of various complicated solid state, gas-solid, gaseous phase reactions, and reactions may be greatly influenced by various experimental parameters.

II-3.3.2 Silicon nitride via carbothermal reduction and nitridation of silica

The carbothermal reduction and nitridation of silica, Equation (11), is an attractive route to produce high-

purity and fine particle size silicon nitride which consists of predominantlty α-phase.

$$3SiO_2(s) + 2N_2(g) + 6C(s) \text{ ---> } Si_3N_4(s) + 6CO(g) \quad (11)$$

This reaction can be achieved by using almost the same reactants of silica and carbon mixtures as those used for preparation of SiC, but heat-treated instead in a nitrogen atmosphere.

The starting silica-carbon mixtures, which are similar those described in SiC formation, can range from a mixture of fine silica and carbon particles (Bachelard - 1987) to carbon powders or soluble carbon sources in silica sol-gels. (Szweda - 1981, Ritsko - 1986) In addition, the products of partially combusted rice husks known as black ash, which consist of finely divided mixture of silica and carbon, can be used as a alternative starting materials for Si_3N_4 as well as SiC. (Lee - 1975, Reinoso - 1991)

The carbothermal reduction and nitridation of silica has been known for long time since the 19th century. However, the method was little utilized until recently because, firstly the complicated Si-C-O-N system in which many phases exist simultaneously including α- and β-silicon nitride, silicon oxynitride (Si_2N_2O), silicon carbide, silica and carbon, and secondly the difficulty to control the nature of the grain shape.

There is a boundary temperature between the formation of SiC and Si_3N_4 in the Si-C-O-N system. SiC forms above this boundary temperature and Si_3N_4 forms below

it as predicted by thermodynamic calculations. (Lee - 1977) This boundary temperature can vary depending on the nature of the reactants as well as the products. Several researchers reported different boundary temperatures ranging from 1400 to 1600° C. (Komeya - 1975, Lee - 1975,1977, Mori - 1983)

Siddiqi and Hendry reported diagrams, presented in Figure II-3-1, which show phase stability in the Si-C-O-N system as a function of temperature and oxygen partial pressure, calculated from existing thermodynamic data. (Siddiqi - 1985)

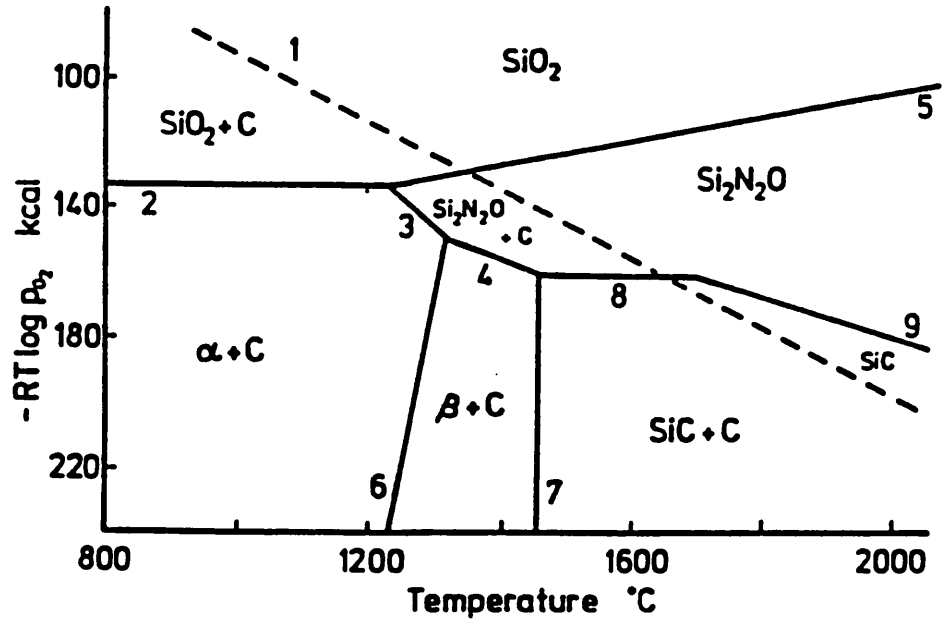

Figure II-3-1 Phase stability in the Si-C-O-N system (from Siddiqi - 1985)

In the temperature range shown in Figure II-3-1, the partial pressures of nitrogen and carbon monoxide make very little difference to the position of the phase boundary so that they can be taken as constant. Nonetheless, this diagram can be contradictory to the experimental facts in some respects. For example, the experimental results, reported previously, show that α-Si_3N_4 is the stable phase up to 1450-1500° C above which temperature SiC is formed, although the diagram predicts that β-Si_3N_4 is the stable phase at 1400° C and low partial pressure of oxygen. This inconsistency may be due to neglect of the partial pressure of silicon monoxide, SiO, which is a crucial intermediate in generating Si_3N_4.

The mechanism of formation of silicon nitride in the SiO_2-C-N_2 system, is generally believed to involve, firstly, the formation of SiO(g) by reduction of silica, and then SiO reacts with nitrogen to generate mainly α-Si_3N_4. (Lee - 1977, Szweda - 1981)

The reaction rate increases with increasing interfacial area of both reactants. (Blumenthal -1966) Therefore, silicon monoxide is likely to be mainly formed from the reduction of silica by carbon via solid-solid reaction:

$$SiO_2(s) + C(s) \longrightarrow SiO(g) + CO(g) \qquad (7)$$

Lee (Lee - 1976) suggested that the reduction of silica by carbon monoxide additionally takes place by a gas-solid reaction because a relatively rapid reaction

rate was observed:

$$SiO_2(s) + CO(g) \rightarrow SiO(g) + CO_2(g) \quad (8)$$

$$CO_2(g) + C(s) \rightarrow 2CO(g) \quad (9)$$

The final step in the formation of silicon nitride by nitridation of SiO is considered to be as:

$$3SiO(g) + 3C(s) + 2N_2(g) \rightarrow Si_3N_4(s) + 3CO(g) \quad (10)$$

Therefore, the overall reaction of carbothermal reduction and nitridation of silica can be expressed as Equation (11), as described already.

$$3SiO_2(s) + 2N_2(g) + 6C(s) \rightarrow Si_3N_4(s) + 6CO(g) \quad (11)$$

This reaction is endothermic with ΔH = 302.8 kcal/mol at 1700K. However, the value of its equilibrium constant is so small (e.g., 3.5 x 10^{-3} at 1700K) that it is difficult to advance the reaction in a closed system. As a result, it is essential to perform the reaction in nitrogen gas flow with the removal of evolved carbon monoxide out of the system.

Zhang and Cannon (Zhang - 1984) proposed a reaction mechanism in which heterogeneous nucleation occurs on either the SiO_2 or carbon surface only in the early stage, and then growth occurs via gas phase reaction on the surface of Si_3N_4 particles, as shown in the following equation (12).

$$3SiO(g) + 3CO(g) + 2N_2(g) \rightarrow Si_3N_4(s) + 3CO_2(g) \quad (12)$$

Komeya and Inoue (Komeya - 1975) reported that the reaction rate of silicon nitride was significantly increased with an increase in the C/SiO_2 ratio up to 20. In addition, they (Inoue - 1982) also showed that seeding with fine Si_3N_4 into the SiO_2-C mixture increased remarkably the reaction rate of Si_3N_4 and decreased the particle size. Toshiba has developed this technique to a commercial production method of silicon nitride powders (Toshiba - 1982, 1983), and their sinterability was proved to be excellent because of very low contamination of β-phase. (Mori - 1983, Pickup - 1986)

II-4 Reaction bonding of ceramics

II-4.1 Introduction

Reaction bonding technique, or reaction sintering, in ceramic technology is an important process by which a ceramic body can be formed from a powder compact by means of an in-situ chemical reaction. This technique can be defined as a process in which two or more components of the required compound react together during the sintering operation. (Popper - 1960, 1961) The advantage of reaction bonding is that only slight dimensional change occurs during the sintering process, thus the technique can be applied to the fabrication of complex and high-precision components shaped by conventional forming techniques such as die compaction, extrusion, injection moulding or slip casting. (Forrest - 1972)

This fabrication process is widely used in industrial production of ceramic materials such as tubes, rods or slabs. Especially, silicon carbide and silicon nitride ceramics are manufactured commercially on a large scale by reaction bonding due to its merits of slight volume change and economic performance.

In this Chapter II-4, the principles of forming a self-bonded silicon carbide by reaction bonding are described. Moreover, this technique is an effective method for conversion of a carbon form into silicon carbide while retaining the original structure of carbon form.

II-4.2 Reaction bonded silicon carbide

II-4.2.1 Reaction bonding process

Silicon carbide products can be prepared by a reaction bonding process in which molten silicon is drawn by capillary action into a porous compact body containing graphite and SiC powders. The liquid silicon, then reacts with the graphite to form SiC, as in the following formula (1), which bonds the original SiC grains.

$$C(s) + Si(l) \longrightarrow SiC(s) \qquad (1)$$

In general, a plastic body is formed using a mixture of silicon carbide powder, carbon or graphite, and a platicizer with additions of polymetric binder. The plastic body is pressed, extruded, injection-moulded or otherwise formed into a green body. The plasticizers are the burned off or converted into a porous char by pyrolysis. Silicon metal is then impregnated into the body where it reacts with the carbon to produce silicon carbide in situ, and a bonding is formed between the original and the newly formed carbide. Excess silicon is usually left to fill the residual pores, thus yielding a non porous body with a porosity below 0.1% and more than 8-10% free silicon. After siliciding, the excess silicon on the surface is removed by grit-blasting. The commercially available SiC materials, such as REFEL (UKAEA in the U.K.) and KT (Carborundum Co. of the U.S.), are typical examples produced by this method.

The green body must have sufficient porosity to accommodate the volume increase during the conversion of the graphite into silicon carbide. A theoretical green density, ρ, for a complete reaction can be calculated, as follows.

$$\rho = 3.21/(1+2.33x) \ /(g\ cm^{-3}) \qquad (2)$$

where x is the initial mass-fraction of carbon in the mixture. Nonetheless, in practice, bodies with theoretical green densities are difficult to impregnate with liquid silicon due to the formation of an impermeable skin of SiC. Hence, additional porosity is introduced to an overall density of 90-92% of the theoretical density, and residual porosity is filled with free silicon during the impregnation to give a pore free body. (Popper - 1961)

The impregnation process of molten silicon liquid requires temperatures in excess of 2000° C at atmospheric pressure, thus the reaction bonding of silicon carbide is usually carried out under vacuum at 1500-1700° C, however local temperatures may be higher due to the exothermic nature of the carbon-silicon reaction. (Popper - 1961)

II-4.2.2 Properties of reaction bonded silicon carbide

Typical values of physical properties for reaction bonded REFEL silicon carbide are presented in Table II-4-1. (Forrest - 1972) The high strength up to a temperature of ca. 1400° C combined with good oxidation

resistance and low thermal expansion coefficient allow this material to be used in applications at high temperatures and corrosive environments including nuclear fuel cladding materials, submersible pump shaft seals, high-temperature gas turbine components.

Table II-4-1 Physical properties of reaction bonded REFEL silicon carbide

Density (g/cm^3)	3.10 - 3.14
Porosity (%)	< 0.1
Bend strength (MPa)	400 - 600
Young's modulus (GPa)	420
Mean expansion coefficient ($10^{-6}/°C$)	4.4

Temperature dependences of bending strength for reaction bonded SiC (REFEL SiC), which were measured in air up to 1300° C and in argon up to 1750° C, are shown in Figures II-4-1 (p.89). (McLaren - 1972) No significant variations in strength with temperatures were observed below 1400° C, regardless of environmental atmospheres. Above the melting point of silicon (1420° C), a catastrophic decrease in strength was observed in argon, however the lower value of strength between 1420° C and 1600° C was not variant with temperature. From 1600° C to 1750° C, there was a slight increase in strength accompanied by textural change in the surface. At the same time, these workers showed that the toughness of the material increased with increase in temperature as a consequence of increased ductility of the free silicon phase. (McLaren - 1972)

The small variations of strength value between each experiment may be caused by differences in surface finish conditions. (Kennedy - 1973)

(a) in air

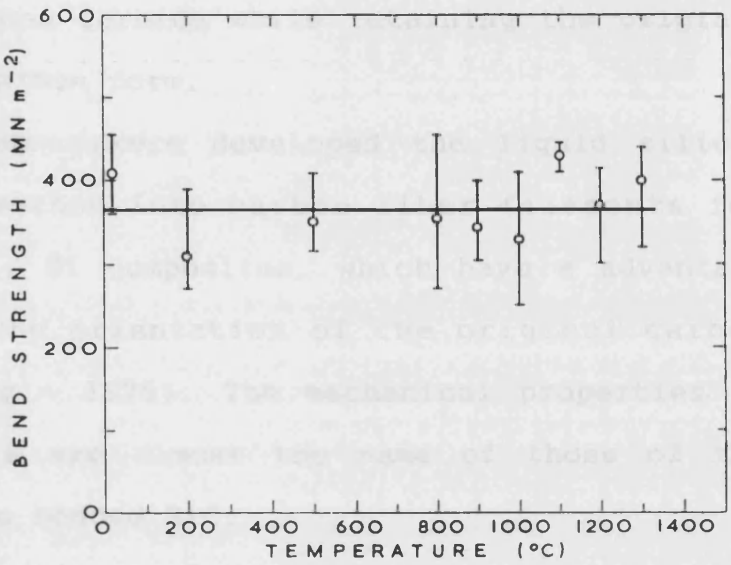

(b) in argon

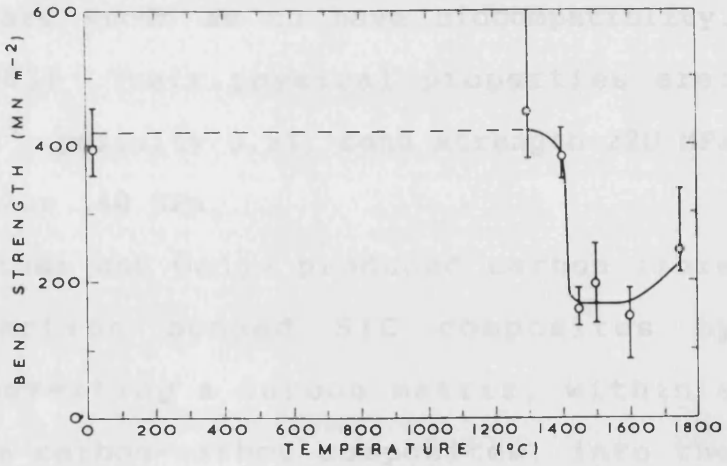

Figure II-4-1 Temperature dependences of bending strength for reaction-bonded SiC (a) in air, (b) in argon (from McLaren - 1972)

II-4.2.3 Conversion of carbon form into silicon carbide by reaction bonding

In addition to the conventional reaction bonding process for dense SiC from carbon/silicon carbide compacts with infiltrated silicon, this technique is used as an effective method for conversion of carbon form into silicon carbide while retaining the original structure of carbon form.

Hillig and co-workers developed the liquid silicon infiltration method into carbon fiber filaments for producing SiC / Si composites, which have a advantage of retaining the orientation of the original carbon fibers. (Hillig - 1975) The mechanical properties of these materials are almost the same of those of the normal reaction bonded SiC.

Partially reaction bonded SiC/graphite materials were developed for bio-implant materials because of both carbon and SiC are known as to have biocompatiblity. (Huttinger - 1983) Their physical properties are: density 2.6 g/cm^3, porosity 0.5%, bend strength 220 MPa and Young's modulus 140 GPa.

Meanwhile, Fitzer and Gadow produced carbon fibre reinforced reaction bonded SiC composites by selectively converting a carbon matrix, within a preformed porous carbon-carbon composites, into the carbide under conditions where the fibre reinforcement was only slightly attacked by the silicon melt. (Fitzer - 1986) Partly SiC-converted carbon-carbon composites showed quasi-plastic deformation with good oxidation resistance, while the samples completely converted into

SiC showed brittle fracture behaviour. The same researchers studied the reactivity of different carbons with liquid silicon, and they concluded the reactivity is strongly dependent on the porosity and the microstructure of the original carbon. However, there is no general agreement about the mechanisms of reaction of carbon with silicon. (Fitzer - 1983)

CHAPTER III EXPERIMENTAL METHODS

III-1 Design of the experimental programme

The experimental work of this thesis involves two main segments: (i) manufacture and (ii) characterization of a various form of porous carbon and ceramic materials.

III-1.1 Overview of the experimental programme

Various types of porous carbon materials with different characteristics were prepared using distinct fabrication techniques. These carbon materials were used as preforms for conversion into carbon-ceramic composites and ceramic materials. In the first route, porous carbon-ceramic composites were manufactured by infiltration of a mixture of sol-gel silica and a resin carbon source, which were subsequently converted into SiC or Si_3N_4 by carbothermal reduction or nitridation. In the second route, porous carbon preforms were directly converted into porous SiC materials by a reaction bonding technique with silicon vapour infiltration.

Bulk density and porosity were determined by the use of a water absorption method. Structural, morphological and surface characterizations of the materials were carried out using optical and electron microscopy, diffraction and spectroscopic techniques. Mechanical properties were measured, including flexural, compressive and tensile strength, and elastic modulus. The corrosion behaviour of the materials in air at high

temperatures was also studied to evaluate their high temperature performance.

A flowchart for the experimental programme which shows the main technological tasks and their inter-dependence is set out in Figure III-1-1.

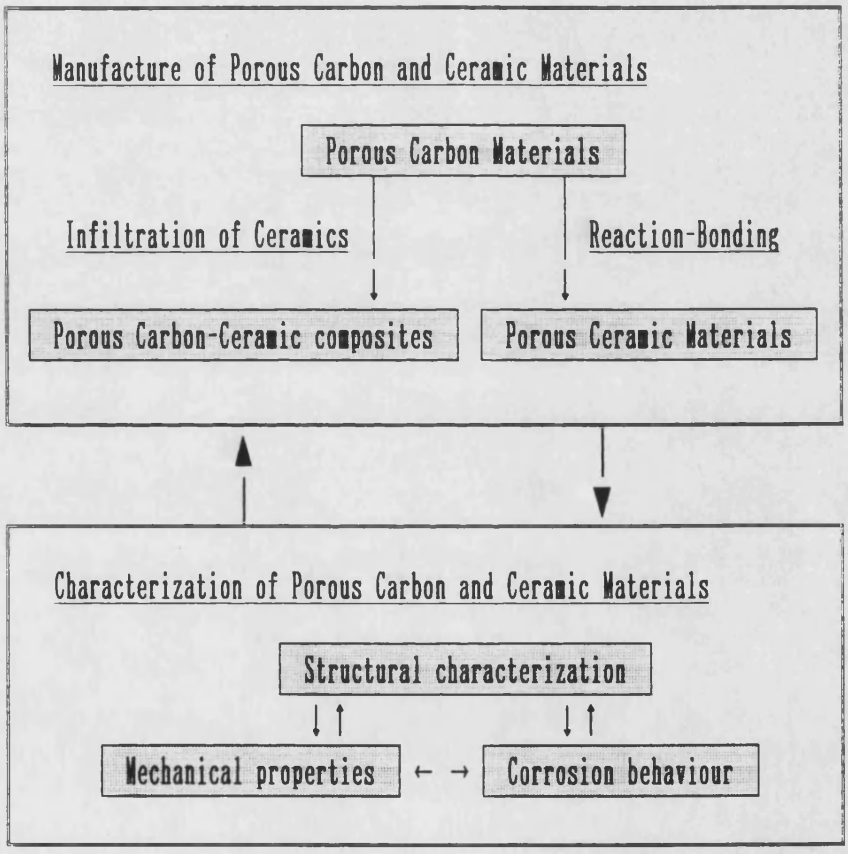

Figure III-1-1

The main technological experiments and their inter-dependence

III-1.2 Manufacture of porous carbon and ceramic materials

Various and different types of porous carbon materials, including porous carbons fabricated by paper making technology, foamed resin based carbons, resin powder compact based porous carbon pellets and porous carbon-carbon composites, were fabricated using different techniques as preforms for conversion into porous carbon-ceramic composites and ceramic materials. In the first route, porous carbon-ceramic composites based on the infiltration of silicon non-oxide ceramics from carbothermal reduction of sol-gel silica, were prepared starting from mainly porous carbons fabricated by paper making technology. In the second route, various porous carbon preforms were directly converted into SiC by a reaction bonding technique with infiltrated silicon vapour. The manufacturing routes for the production of porous carbon-ceramic composites and porous ceramic materials are outlined as a flow chart in Figure III-1-2.

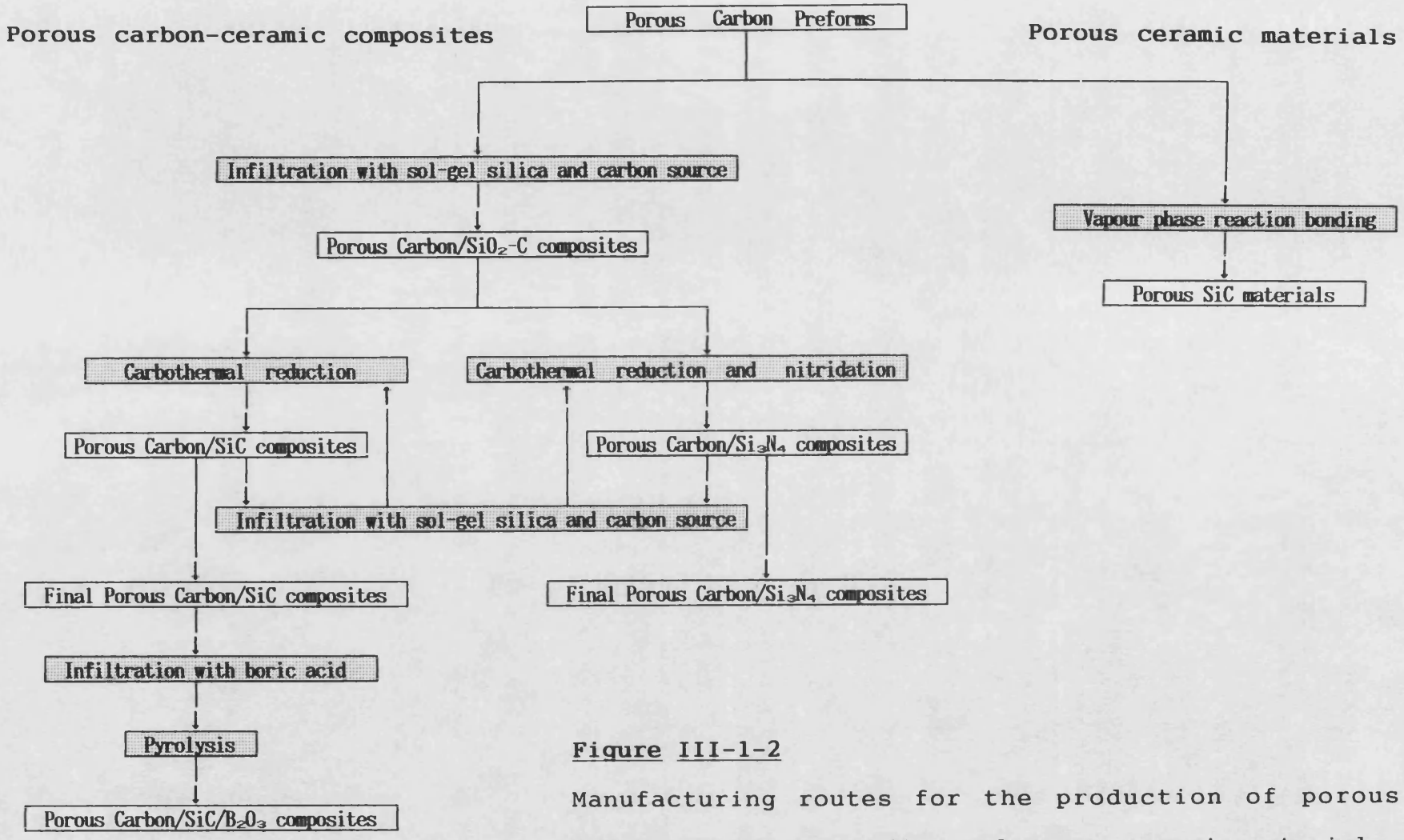

Figure III-1-2

Manufacturing routes for the production of porous carbon-ceramic composites and porous ceramic materials

III-1.2.1 Manufacture of porous carbon materials

The following porous carbon materials were prepared or obtained as preform materials for conversion into porous ceramic forms.

(1) Porous carbons fabricated by paper making technology

Randomly-orientated and short carbon fibre precursor sheets, prepared using paper making technology, were impregnated with phenolic resin and laminated by hot-pressing, followed by heat-treatment with a novel carbonization method.

(2) Foamed resin based carbons

Polymer foam preforms were impregnated with phenolic resin, and carbonized in a carefully controlled environment.

(3) Resin powder based porous carbon pellets

Phenolic resin powders were pressed with a moderate pressure into pellet forms, then carefully carbonized in inert atmosphere.

(4) Porous carbon-carbon composites

A slurry of short carbon fibres with a phenolic resin binder was cast into a mould and dried, followed by carbonization.

More detailed descriptions of the preparation of these materials are described in Chapter IV.

III-1.2.2 Manufacture of porous carbon-ceramic composites

Porous carbon-ceramic composites were fabricated starting with impregnation of a porous carbon preform with a mixture of silica sol-gel and resin carbon source. The synthesis of SiC was carried out by carbothermal reduction of silica with a carbon source in an argon atmosphere. The synthesis of Si_3N_4 was conducted using almost the same starting material but by carbothermal reduction and subsequent nitridation in a nitrogen atmosphere. In addition, the porous carbon-SiC composites were further impregnated with boron oxide glass (B_2O_3) in order to improve their oxidation resistance.

(1) Porous carbon-SiC composites

Silicon carbide was prepared by carbothermal reduction of sol-gel silica in the presence of a carbon source by heat treatment in an argon atmosphere up to 1350° C.

(2) Porous carbon-Si_3N_4 composites

Silicon nitride was prepared by a combination of carbothermal reduction and subsequent nitridation of sol-gel silica in the presence of a carbon source in a nitrogen atmosphere up to 1350° C.

(3) Porous carbon-SiC-B_2O_3 composites

The boron oxide was prepared by pyrolysis of orthoboric acid up to 700° C.

More detailed descriptions of the preparation of these materials are described in Chapter V.

III-1.2.3 Manufacture of porous ceramic materials

Various types of porous carbon preforms were directly converted into porous SiC materials in situ by a reaction bonding technique with infiltrated silicon vapour at temperatures from 1850° C to 2300° C.

More detailed descriptions of the preparation of these materials are described in Chapter VI.

III-1.3 Characterization of porous carbon and ceramic materials

Characterization of porous carbon and ceramic materials was conducted in order to investigate the influence of the processing parameters on the properties of the materials, their mechanical properties, and corrosion behaviour at high temperatures.

III-1.3.1 Structural characterization

Bulk density and porosity which are the most distinct and important structural features to determine their characteristics, were obtained by the use of a water absorption method. The structural, morphological and surface properties of the materials were characterized by using optical and electron microscopy, diffraction methods and spectroscopic techniques.

III-1.3.2 Mechanical properties of porous materials

The following mechanical properties of porous materials were measured at room temperature and at 800° C in air. The temperature of 800° C had been chosen

arbitrarily to represent a value in the likely upper temperature range of materials made from these ceramics.

- flexural strength (3 point bend test)
- compressive strength
- tensile strength (split cylinder test)
- elastic modulus

The factors influencing the mechanical properties of porous materials were studied in order to understand the relationship between mechanical properties and microstructure, and to apply theoretical analysis.

III-1.3.3 High temperature corrosion resistance

Corrosion behaviour of porous materials at high temperatures was measured by assessment of the oxidation resistance in flowing air at temperatures up to 1200° C. Any structural and chemical changes resulting from oxidation were also studied.

III-2 Experimental measurement techniques

A wide range of experimental techniques were applied for characterization of porous carbon and ceramic materials in order to investigate the structure of the materials, their mechanical properties, and high temperature performance.

III-2.1 Structural characterization

III-2.1.1 Density and porosity

Bulk density and apparent porosity of highly porous carbon and ceramic materials were obtained by the use of the boiling water absorption method as described in the American National Standard ASTM C 20-74.

In the case of foamed materials, bulk density was calculated from the weight and physical dimensions of specimens in air at room temperature.

III-2.1.2 Scanning electron microscopy (SEM)

Scanning electron microscopy (SEM) was conducted by using a JEOL JSM T330 scanning electron microscope, without any special preparation. The acceralated voltage was 15 kV, and the magnification is shown in each micrograph.

III-2.1.3 Optical microscopy

General microstructure of foamed specimens was examined by using a Wild Heebrugg M3Z optical microscope without any special preparation.

The optical micrographs of specimens were produced using polished samples. Samples were mounted in

Struers Epofix HQ epoxy resin in a vacuum, then left to cure over night in an autoclave at a pressure of 50 kgf/cm^2. The cured samples were polished by using a Motopol 12 auto plane polishing machine in the routine described in Table III-2-1 for carbon materials, or Table III-2-2 for ceramic materials.

The microstructure of the polished samples was studied using a Zeiss MC63 optical microscope. In the case of optically active specimens, such as graphitized carbon, polarized light microscopy with cross polarized light sources and a full wave quartz plate, was used to reveal their optical orientation.

In order to reveal the grain boundary of silicon carbide, polished samples were electro-chemically etched with 20% potassium hydroxide solution at 6.5 volts for 20 seconds by using Polectrol, an automatic etching machine.

III-2.1.4 X-ray diffraction analysis (XRD)

X-ray diffraction analysis was used to characterize the chemical structure of porous materials. A PW 1730/10 X-ray generator, PW 22/73 long fine focus 2 kW copper target X-ray tube (40kW, 20 mA) and PW 1820/00 computer controlled vertical diffractometer goniometer were used in this analysis. The X-ray diffraction spectrum was produced at a range of 2 theta = 10-80° and at a scan speed of 0.32° 2 theta/sec.

Table III-2-1
Polishing routine for porous carbon materials

Material	Porous carbon materials
Sectioning Technique	Diamond wheel saw cutting
Mounting Technique	Vacuum impregnation with epoxy resin Cure under pressure

Process	Surface	Abrasive size and type	Load per sample	Wheel speed	Head rotation	Process time
Planer Griding Stage	Paper	Silicon carbide 320 grid	5 lb	150	Complementary	Till plane (0.5 min)
Sample Integrity Stage	Pref tex	6 μm O/B Diamond	5 lb	240	Complementary	6 mins
	Texmet	1 μm O/B Diamond	5 lb	240	Complementary	4 mins
	Texmet	0.06 μm Colloidal silica	5 lb	100	Contradictory	5 mins
Final Polishing Stage	Master tex	0.06 μm Colloidal silica	2.5 lb	100	Contradictory	2 mins

Table III-2-2
Polishing routine for porous SiC materials

Material	Porous SiC materials
Sectioning Technique	Diamond wheel saw cutting
Mounting Technique	Vacuum impregnation with epoxy resin Cure under pressure

Process	Surface	Abrasive size and type	Load per sample	Wheel speed	Head rotation	Process time
Planer Griding Stage		Resin bonded diamond	5 lb	120	Contradictory	Till plane (3 min)
Sample Integrity Stage	Metlap 10	15 μm W/B Diamond	5 lb	120	Contradictory	3 mins
	Metlap 4	9 μm O/B Diamond	5 lb	minimum	Contradictory	5 mins
	Texmet	1 μm O/B Diamond	5 lb	240	Complementary	4 mins
	Texmet	0.06 μm Colloidal silica	5 lb	100	Contradictory	5 mins
Final Polishing Stage	Master tex	0.06 μm Colloidal silica	2.5 lb	100	Contradictory	2 mins

O/B = Oil based, W/B = Water based

III-2.2 Mechanical properties

The mechanical properties of porous carbon and ceramic materials were examined. These include flexural (3 point bend test), compressive, and tensile strength (split cylinder test), and elastic modulus at room temperature and 800° C in air. Specimens for the mechanical experiments were prepared with a diamond saw to the relevant dimensions. The surfaces were not normally polished after this initial cutting operation.

III-2.2.1 Flexural properties

The flexural tests were performed at room temperature and at 800 ° C in air, using Instron 1122 and 1195 with furnace, respectively, mechanical test machines being equipped with the 3-point bending test apparatus. The approximate dimensions were 3 x 7 x 60 mm for carbon specimens, or 3 x 7 x 40 mm for ceramic samples. A schematic illustration of the flexural test is shown in Figure III-2-1(a) (p.107). The specimens were placed on rollers of nominal diameter 6.3 mm. The crosshead speed was 0.5 mm/min and the span of 50 mm for carbons or 35 mm for ceramics was used, giving a span-to-depth ratio of approximate 17 or 12, respectively. The load and crosshead displacement were monitored, and the deflection of the specimens was assumed to be the crosshead displacement.

The flexural strength and modulus of elasticity were calculated from the following equations:

Flexural strength $\sigma = (3\ P\ L)/(2\ B\ D^2)$

Young's modulus $E = l^3/(4\ B\ D^3) \times (dP/dX)$

where P is the maximum load in N, L is the span in m, B is the width of specimen in m, D is the depth of specimen in m, and dP/dX is the slope of the linear region of the force-displacement curves in N/m.

III-2.2.2 Compressive properties

The compressive tests were performed at room temperature and at 800 °C in air using an Instron 1122 and 1195 with furnace, respectively, equipped with the compressive test apparatus. The approximate dimensions of plate and foamed specimens were 10 x 10 x 3 mm and 15 x 15 x 8 mm, respectively. A schematic illustration of the compressive test is shown in Figure III-2-1(b). The crosshead speed was 0.5 mm/min. The load and crosshead displacement were recorded, and the deflection of the specimens was assumed to be the crosshead displacement.

The compressive strength and Young's modulus were deduced from the following equations:

Compressive strength $\sigma = P / A$

Young's modulus $E = (dP/dX) \times (D/A)$

where P is the maximum load within the linear elastic region in N, A is the cross-sectional area in m^2, D is the depth of specimen in m, and dP/dX is the slope of the linear region of the force-displacement curves in N/m.

III-2.2.3 Tensile properties (Split cylinder test)

The tensile properties of pellet materials were determined by the split cylinder test using Instron 1122. A schematic illustration of split cylinder specimens is shown in Figure III-2-1(c). As the compression force is imposed, circumferential tensile stresses are induced in the material, these having maximum value at the central horizontal plane, and eventually fail and split at this plane. The approximate dimensions of specimens were 3 mm in thickness and 14 mm in diameter. The crosshead speed was 0.5 mm/min. The load and crosshead displacement were monitored, and the deflection of the specimens was assumed to be the crosshead displacement.

The tensile strength by the split cylinder test was calculated from the following equation:

$$\text{Tensile strength } \sigma = (2\ P)/(\pi\ L\ D)$$

where P is the maximum load in N, L is the cylinder length in m, and D is the diameter of specimen in m. The experimental details are described in the American National Standard ASTM C 496-86 or British Standard 1881; part 117, 1983.

III-2.3 High temperature corrosion resistance

Thermogravimetric analysis was conducted to investigate oxidation behaviour in air and to evaluate the ability of oxidation resistance of porous carbon and ceramic materials.

The changes in microstructure and morphology of composites during oxidation treatment were followed by observation using both the scanning electron microscope and the polarized optical microscope. In addition, the changes in formation of materials during oxidation were followed by analysis of Fourier transform infra-red spectroscopy.

III-2.3.1 Thermogravimetric analysis (TGA)

Thermogravimetric analysis was performed by using a thermobalance SETARAM DTA-92 where the samples were oxidized at a heating rate of 50° C/min up to 1200° C, and under flowing air at a constant flow rate of 1.5 liters/hour.

III-2.3.2 Fourier transform infra-red spectroscopy (FT-IR)

The surface changes of carbon-ceramic composites during oxidation at high air temperatures, were investigated by utilizing the infra-red dispersive reflection spectroscopy technique. The FT-IR Perkin-Elmer model 1720, equipped with the dispersive reflection accessory, was used to obtain the infra-red spectroscopy spectra. The measurements were observed in 20 scans with a resolution of 2 cm^{-1}.

(a) Flexural (3 point bend) test

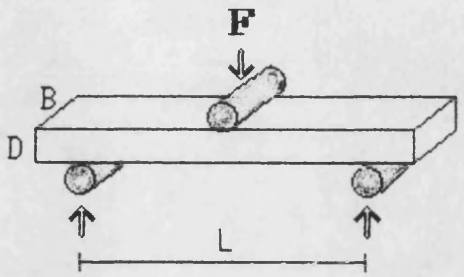

(b) Compressive test

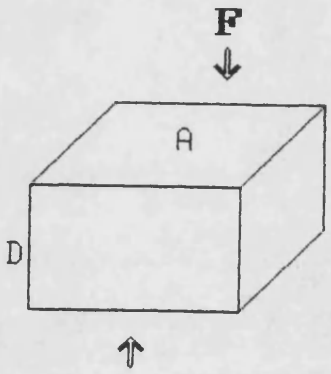

(c) Tensile (split cylinder) test

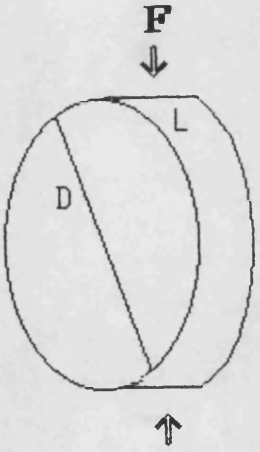

Figure III-2-1

Schematic illustration of mechanical tests

CHAPTER IV POROUS CARBON MATERIALS

IV-1 Introduction

Four distinctive types of porous carbon materials, including (i) porous carbons fabricated by paper making technology, (ii) foamed resin based carbons, (iii) resin powder based porous carbon pellets and (iv) carbon bonded carbon fibre composites, were manufactured using different techniques, and their structural features, mechanical behaviour and high temperature corrosion resistance were characterized. In particular, their mechanical properties were related to their geometrical structure and other material's properties.

IV-2 Porous carbons by paper manufacturing technology

IV-2.1 Manufacturing process

Porous carbon materials used in this experiment were produced by utilizing a combination of paper making technology and a novel carbonization method. The porous carbons were fabricated to follow the process of which Oji Paper Co., Ltd. in Japan holds the patents. (Oji - 1985, 1986, 1989, 1991) The manufacturing process is summarized below, and is also illustrated briefly in the following flowchart. (Figure IV-2-1, p. 143)

In the first step, a blended mixture of several kinds of chopped carbon fibre precursors of 0.5 - 5 mm in length and 20 - 40 μm in diameter, including polyacrylonitrile (PAN) fibres, rayon fibres, pitch fibres and wood pulps, were dissolved into water and

mixed well, to form a homogeneous slurry, then the water slurry was formed into a carbon fibre precursor sheet by utilizing a paper manufacturing process. In other words, low-density fibrous sheets that consist of short carbon fibre precursors randomly oriented in two dimensions (random in-plane) and well-tangled, were prepared by a standard paper making process. Fibre orientation in the sheet was only slightly distributed in the running direction of the paper making machine. The degree of preferred fibre orientation was related in a complex way to parameters of the papering process, e.g., the running speed of the machine, the viscoelastic properties of the slurry and the shape of the fibres.

Then, the fibrous sheet was impregnated with a resol type phenolic resin, occasionally with the addition of graphite particles, to produce a prepreg sheet, and next these prepreg sheets were unidirectionally laminated and hot-pressed at a pressure of 0.2 MPa at 155-170° C in air. After this process, the laminated material was stabilized in air, then carefully carbonized up to 1000° C by being heated at a rate of 125 ° C/hr in a nitrogen atmosphere, then graphitized up to 3000° C at a heating rate of 500 ° C/hr in an argon atmosphere, and finally held at 3000 ° C for 30 mins.

The properties of the porous carbon materials, such as density, porosity, strength, modulus and degree of graphitization, can be adjusted to meet specific requirements by choosing the kind of fibres and

regulating the manufacturing process. Porous carbon materials which were mainly employed in this experiment for preforms into ceramic materials had a density of ca. 0.5 g/cm^3 and a porosity of ca. 73%. In addition, in order to study the effect of density/porosity on mechanical properties, materials with densities and porosities in the range of ca. 0.4-0.6 g/cm^3 and ca. 76-65 %, respectively, were prepared by controlling compacting pressure at hot-pressing when laminating the prepreg sheets.

The schematic microstructure of porous carbon materials fabricated by paper manufacturing technology is illustrated in Figure IV-2-2 (p.143).

IV-2.2 Structural characterization

IV-2.2.1 Density and porosity

The physical properties of porous carbon materials fabricated by this method with different heat treatment temperatures are shown in Tables IV-2-1 and IV-2-2 (p.141). The bulk density and apparent porosity of both materials were ca. 0.5 g/cm^3 and more than 70%, respectively. The bulk density decreased slightly with increasing heat treatment temperature, while the apparent porosity increased on a small scale. Thus, heat treatment over 1000° C did not have a great influence on the density/porosity characteristics.

IV-2.2.2 Microscopic observation

(1) Scanning electron microscopy

Scanning electron micrographs for the surface and

fracture cross-section of porous carbons manufactured by the paper making process are presented in Figure IV-2-3 (p.144, 145) for the carbonized and Figure IV-2-4 (p.146, 147) for the graphitized carbon. It was revealed that carbonized fibres were bonded to each other by a resin-based carbon matrix. In this sense, this material can be considered a kind of carbon bonded carbon fibre composite (CBCF). The majority of the volume of the material consisted of the inter-connected open pores. The materials can be considered to consist of layers of random in-planar fibrous sheets, each one bonded to its neighbouring sheet by a relatively small number of bonding points. (Figures IV-2-3(b) and IV-2-4(b)) Heat treatment over 1000° C seems to have no significant effect on the morphology of the materials.

(2) Polarized optical microscopy

Polarized optical micrographs revealed only an obscure boundary between the fibre and the matrix after heat treatment at temperatures over 1000° C. (Figure IV-2-5, p.148) They fused into each other to form a coherent mass. Thus, the fibre and matrix seemed to be co-carbonized. Moreover, the micrographs after heat treatment at 3000° C showed a speckled mosaic appearance in a whole section of the materials. (Figure IV-2-6, p.149) Therefore, the carbon fibre and matrix became a highly graphitized structure in one body, presumably because pseudo-plastic deformation caused by the stress due to the dimensional change during heat treatment

processes enhanced the graphitization.

It was proved eventually by the observation of polished sections that this porous carbon cannot be regarded as a composite material because there is no distinction between the fibre and the matrix.

This graphitization behaviour is unique and different from the well-known phenomenon of stress graphitization of a hard carbon matrix in carbon-carbon composites. (Hishiyama - 1974, Kimura - 1975, Zaldivar - 1991)

Both co-carbonization of a phenolic resin with carbon fibres (Markovic - 1981) and the graphitization by plastic deformation (Fischbach - 1971) have been reported separately. However, the combination of these two effects has not been published yet. Therefore, a further detailed investigation is required for an understanding of precise graphitization mechanisms.

IV-2.2.3 X-ray diffraction analysis

X-ray diffraction profiles for porous carbons heat treated at 3000° C and 1000° C are presented in Figures IV-2-7 and IV-2-8 (p. 150), respectively. No other peaks but carbon were observed in either profile. Thus, the materials consisted exclusively of pure carbon. The (002) diffraction peak of the carbonized material is asymmetrical, which indicates the heterogeneity in the structure, part graphitized and part non-graphitized. Furthermore, it is noteworthy that the (002) diffraction peak became much sharper at a higher diffraction angle after heat treatment at 3000° C. This is another strong piece of evidence that the graphitic

structure developed greatly in the materials during heat treatment over 1000° C.

IV-2.2.4 Summary of structural features

The following conclusions concerning the structural features of porous carbons fabricated by paper making technology can be drawn from this study on the structure:

(i) The density of the materials was extremely low and the porosity was high, and the majority of the volume of the materials consisted of the inter-connected open pores.

(ii) The materials consisted of layers of random in-planar fibrous carbon sheet, bonded to its neighbouring sheet by a relatively small number of connecting points.

(iii) Carbonized fibres were bonded to each other by a resin based carbon matrix. However, they fused into each other to form a coherent carbon by co-carbonization mechanism.

(iv) The graphitic structure in the materials developed significantly at heat treatment temperatures between 1000 - 3000° C.

IV-2.3 Mechanical properties

The mechanical behaviour of porous carbons fabricated by the paper making process, including flexural and compressive properties, were determined at room temperature in air. A schematic designation of mechanical specimens is given in Figure IV-2-2 (p.

143). Flexural strength was measured in a XZ orientation which indicates that the length of sample was along the X direction (the running direction of a paper making machine), while the thickness (and also direction of crack propagation) was in the Z direction, i.e., the laminating direction. On the other hand, compressive strength was tested in the Z direction, the direction perpendicular to the laminating sheet.

Mechanical properties within the XY plane can be regarded to be roughly isotropic; however, there was a slight degree of preferred fibre orientation in the X direction, i.e., the paper running direction, which resulted in a minor mechanical anisotropy in the XY plane. Accordingly, critical mechanical anisotropy of the materials exists between the XY plane and ZX or ZY plane. This can be revealed by a comparison of flexural (XZ) with compressive (Z) properties.

IV-2.3.1 Effect of heat treatment temperature

It was found that the structure of the materials significantly changed at heat treatment temperatures between 1000° C - 3000° C. Hence, in order to investigate the influence of the graphitization by heat treatment on mechanical properties, both the specimens carbonized at 1000° C and graphitized at 3000° C were subjected to mechanical tests.

(1) Flexural properties

Experimental details of flexural tests are given in Chapter III-2.2.1. The results of the mechanical test

for porous carbon materials by paper making technology are shown in Tables IV-2-1 and IV-2-2, and also Figure IV-2-9 (p.151) shows schematic flexural stress-strain curves. Both the carbonized and graphitized samples failed in a brittle manner, with the stress-strain curves being linear until fracture. It was confirmed by visual observation that flexural failure was caused by tensile failure at the outer surface, and then the crack propagated catastrophically, giving fast brittle fracture. Flexural strength for both the samples was almost the same value about 13.5 MPa. However, the linear elastic region was to about 4.7% strain for the graphitized material, while it was only 2.4% strain for the carbonized specimen. Elastic modulus, thus decreased markedly due to the graphitization by heat treatment over 1000° C.

(2) Compressive properties

Experimental details of compressive tests are given in Chapter III-2.2.2. Figure IV-2-10 (p.151) shows schematic compressive stress-strain curves. Unlike flexural behaviour, compressive failure was considerably different in each specimen. Regarding the carbonized carbon, the stress-strain curve was linear to about 2% strain. However, from 2% to ca. 15% strain, the curve became irregular, and roughly horizontal. Over ca. 15% strain, the stress gradually increased. Consequently, the sample was crushed. Obviously, elastic deformation occurred up to 2% strain, after

which structural deformation occurred. To characterize the compressive strength of the carbonized specimen, the stress value at a plateau regime of roughly constant stress was defined as the compressive strength.

On the other hand, in the case of the graphitized carbon, the stress-strain curve was linear to about 2.5% strain, after which the curve changed to a gradual upward and practically linear trend. Above ca. 20% strain, the steepness of curve gradually increased. Similarly, elastic deformation occurred up to 2.5% strain, after which structural deformation occurred. Hence, the maximum stress in the initial linear elastic region was defined as the compressive strength of the graphitized sample.

The compressive strength values determined in the above manner are presented in Tables IV-2-1 and IV-2-2. Porous carbon, heat-treated at the lower temperature, exhibited much higher compressive strength and with higher elastic modulus. Whereas the graphitized specimen was deformed by relatively low stress with larger strain. Accordingly, the carbonized sample collapsed in a brittle crushing manner, while the graphitized carbon exhibited quasi-plastic deformation.

It may be supposed that shear deformation is possible on compressive loading of the graphite material, as a result of basal plane shear. Compressive failure of polygranular graphite is characterized by shear deformation (Brocklehurst - 1977)

(3) Comparison of flexural/compressive properties

It is obvious that, regardless of heat treatment temperature, the flexural strength and modulus in the XZ orientation were much greater than the compressive properties in the Z direction, because of the strong anisotropic structure resulting from the manufacturing process; fibrous layers were arranged parallel to the plane of the specimen surface.

It is well known that the mechanical properties of conventional bi-directional fibre composites are greater in the fibre directions than in the transverse direction and this reflects the anisotropy of mechanical properties of the fibre orientation. For example, for a bi-directional (in XY plane) carbon-carbon composite, Thomas and Walker (1986) showed tensile strength in the X or Y direction was 330 MPa, while strength in the Z direction was only 25 MPa. In particular, interlayer bonding of porous carbon materials was considerably weaker compared to intralayer bondings. Hence, failure in the Z direction would occur at much lower stress than in the X or Y direction because the latter failure is caused by the intralayer fracture, whereas the former failure occurs when the interlayer bonds fail.

In particular, the graphitized porous carbons showed much higher value for the ratio of flexural properties to compressive properties, which may reflect the degree of mechanical anisotropy. It was observed by microscopic observations that a fundamental geometrical

and structural change did not occur during heat treatment over 1000° C. Therefore, the noteworthy discrepancy of the flexural/compressive ratio due to the thermal treatment history may be attributed to a difference in the mechanical failure mechanism owing to the change in characteristics of carbon.

Porous carbons heat-treated at 1000° C collapsed in a brittle failure manner by both flexural and compressive stresses. However, the graphitized carbon heat-treated at 3000° C deformed in a brittle manner when loaded in bending, but there was some pseudo-plastic deformation in compression. This kind of collapse behaviour can be observed occasionally in porous rigid polymers. (Gibson -1988)

(4) Conclusion of effect of heat treatment temperature on mechanical properties

Porous carbons carbonized at 1000° C failed in a brittle manner under both flexural and compressive stresses. On the contrary, the graphitized carbons heat-treated at 3000° C deformed in a brittle manner under bending stress, but plastically in compression.

Heat-treatment over 1000° C did not modify the flexural strength values. However, the flexural modulus decreased significantly due to graphitization. On the other hand, porous carbons heat-treated at 1000° C showed much higher strength towards compressive stress, with higher elastic modulus than those of graphitized specimens.

Consequently, heat treatment temperatures over

1000° C, which results in graphitization of the porous carbons, has a significant effect on the mechanical properties of porous carbons by paper making technology.

IV-2.3.2 Effect of density/porosity

The mechanical properties of porous carbon specimens heat-treated at 2800° C which were prepared with densities and porosities in the range from 0.41 to 0.62 g/cm^3 and 76.2 to 64.5 %, respectively, were determined by flexural test in the XZ orientation and compressive test in the Z direction in order to investigate the influence of density/porosity on the mechanical behaviour. Particular interest is placed on the transformation of mechanical anisotropy due to the microstructural change. Density/porosity of porous carbons were varied by regulating the compacting rate in the laminating direction during the hot-pressing process.

Electron microscopic observation of cross-sections of various density/porosity carbon materials is shown in Figure IV-2-11 (p.152). As expected from the manufacturing process, interlayer dimension in the Z direction decreased significantly with increasing density. However, no significant change was observed in the XY plane orientation.

Data of mechanical properties of porous carbon materials with a wide range of densities/porosities are shown in Table IV-2-3 (p.142).

(1) Flexural properties

All specimens exhibited a brittle failure mode under flexural stress. The variation of flexural strength for the porous carbons with density is plotted in Figure IV-2-12 (p.153). It is apparent that the flexural strength value increased with increase of density; in other words, the strength decreased with increasing porosity.

In the same manner, the flexural modulus versus the density is plotted in Figure IV-2-13 (p.153). It is clear that the flexural modulus value also increased with density; that is to say, the modulus decreased with increasing porosity.

The increase in the flexural strength and modulus with increasing density can be considered to be caused most obviously by the reduction in porosity but also by increased linking bonds between interlayers associated with increasing compacting rate in the Z direction.

There have been some attempts to analyze the mechanical characteristics of porous materials by relating normalized mechanical properties with relative density. (Chapter II-1.3) Therefore, the normalized flexural strength (σ/σ_S) and modulus (E/E_S) are plotted against relative density (ρ/ρ_S), as shown in Figures IV-2-14 and IV-2-15 (p.154), respectively. The values for σ_S and E_S were chosen as 100 MPa and 20 GPa, respectively, which are typical values for graphites. The relative density was calculated from (1 - p/100), where p is a porosity in %.

The data were fitted to equation of the type $(X/X_S) = C(\rho/\rho_S)^n$, where n = 1, 2, 3, ···, X = σ or E, and C is constant. The following equations gave the best least squares fit to the data.

$$(\sigma/\sigma_S) = 1.48(\rho/\rho_S)^2 \quad (1)$$

$$(E/E_S) = 5.94(\rho/\rho_S)^3 \quad (2)$$

Hence, the flexural strength varied as the square of the density, while the modulus was proportional to the cube of the density.

(2) Compressive properties

All specimens exhibited almost the same compressive collapse behaviour as the graphitized porous carbons shown in Figure IV-2-10. The compressive strength of porous carbons increased with density as plotted in Figure IV-2-16 (p.155). Likewise, the compressive modulus increased with density as plotted in Figure IV-2-17. As with the flexural behaviour, the increase in the compressive strength with increasing density can be considered to be caused by decreases in porosity and increased linking bonds among interlayers.

The variations of normalized compressive strength (σ/σ_S) and modulus (E/E_S) with relative density (ρ/ρ_S) are plotted in Figures IV-2-18 and IV-2-19 (p.156), respectively. The values for σ_S and E_S were chosen as 200 MPa and 20 GPa, respectively, which are typical values for graphites.

The data were fitted to equation of the type $(X/X_S) = C(\rho/\rho_S)^n$, where n = 1, 2, 3, ···, X = σ or E, and C is constant. The following equations gave the best least squares fit to the data.

$$(\sigma/\sigma_S) = 0.45(\rho/\rho_S)^4 \quad (3)$$

$$(E/E_S) = 0.71(\rho/\rho_S)^5 \quad (4)$$

Therefore, the compressive strength varied as the fourth power of the density. Meanwhile, the modulus was proportional to the fifth power of the density.

Wei et al. (1985) proposed that the compressive strength of carbon bonded carbon fibre composites is proportional to the cube of the bulk density by using a simple fibre model. (Chapter II-3.2) A possible reason that the exponent was larger than previously proposed for CBCF is that carbon binder was neglected in the fibre model. Whereas, porous carbon materials by paper making technology contained a considerable amount of carbon binder which was used for strong bonding between fibres. Therefore, carbon matrix may have significant contribution to the improvement of mechanical properties.

(3) Mechanical anisotropy

It was revealed in the microscopic observations that there is a remarkable increase in interlayer bonds in the Z direction, without any significant morphological changes in the XY plane, with increasing density. (Figure IV-2-11) Therefore, it would be expected that this change in microstructure with density/porosity is

reflected in the anisotropy of mechanical properties.

The ratio of the flexural property values in the XZ direction to the compressive property values in the Z direction can be used as an indication of the mechanical anisotropy of the XY plane to the ZX or the ZY plane. As shown in Figures IV-2-20 for strength anisotropy and IV-2-21 for elastic modulus anisotropy, values of compressive properties increased more rapidly with the increase of density, than those of flexural properties. As a result, the mechanical anisotropy ratio decreased sharply with increasing density. This suggest that the compressive properties in the Z direction are more dependent on change of density/porosity, which is consistent with the observed changes of microstructure in the Z direction. This also follows by comparing Equations (1) - (4).

The anisotropy of porous materials can be conveniently expressed by the ratio of the largest space dimension to the smallest; this can be called the shape anisotropy ratio or fibre spacing ratio, as reviewed in Chapter II-1.3. (Ashby - 1988, Green - 1982)

Meanwhile, because the density of porous carbons was varied by controlling only the compacting rate in the Z direction during the hot-pressing process, fibre spacing ratio, $R = (D_Z/D_X)$ or (D_Z/D_Y), can be expressed in inverse proportion to the density, ρ:

$$R = (D_Z/D_X) \text{ or } (D_Z/D_Y) \propto (1/\rho) \quad (5)$$

The variations of mechanical anisotropies with density for porous carbons by paper making technology correspond well to the curves which are nearly in proportion to $(1/\rho)^2$ for both strength and modulus anisotropies as in the following equations. (Figure IV-2-20 and IV-2-21, p.157)

Strength anisotropy ratio:

$$(\sigma_{xz}/\sigma_z) = 1.17(1/\rho)^2 \quad (6)$$

Modulus anisotropy ratio:

$$(E_{xz}/E_z) = 24.94(1/\rho)^2 \quad (7)$$

Consequently, there is a decrease in mechanical anisotropy with increasing density. Mechanical anisotropies of the XY plane to the XZ or the XY plane are proportional to the square of the fibre spacing ratio of the Z direction to the X or Y direction.

Green et al. (1982) proposed that strength and modulus anisotropy of fibrous ceramic materials can be expressed in the relation to the fibre spacing ratio; modulus anisotropy is inverse proportional to the square of the fibre spacing ratio, and strength anisotropy is to the 3/2 power. (Chapter II-3.2) A possible reason that the exponent for strength anisotropy was slightly larger than previously proposed is that binder was neglected in the fibre model. Regarding porous carbon materials by paper making technology, the carbon binder cannot be neglected because

its
of significant contribution to the mechanical properties due to strong bonding between fibres.

(4) Conclusions of effect of density/porosity

Both flexural and compressive strength and modulus values were found to increase with density due to denser interlayer bonds. There was a sharp decrease in mechanical anisotropy with increasing density associated with the reduction of the fibre spacing in the Z direction. Strength and modulus anisotropies were almost proportionate to the inverse square of the density.

IV-2.3.3 Summary of mechanical properties

The following conclusions can be drawn from the study on the mechanical behaviour of porous carbon materials fabricated by paper manufacturing technology.

(i) Porous carbons carbonized at 1000° C failed in a brittle manner under flexural and compressive stresses. However, the graphitized carbons heat-treated at 3000° C deformed in a brittle manner under bending stress, but plastically in compression.

(ii) Heat-treatment over 1000° C did not modify the flexural strength values. However, the flexural modulus decreased significantly due to graphitization. On the other hand, porous carbons heat-treated at 1000° C showed much higher compressive strength with higher elastic modulus than those of graphitized specimens.

(iii) Heat treatment temperatures over 1000° C, which resulted in the graphitization of porous carbons,

consequently, showed a significant effect on the mechanical properties of porous carbons by paper making technology.

(iv) Both flexural and compressive strength and modulus values were found to increase with density due to denser interlayer bonds.

(v) Flexural strength varied as the square of the density. On the other hand, the modulus was proportional to the cube of the density.

(vi) Compressive strength varied as the fourth power of the density, while the modulus was proportional to the fifth power of the density.

(vii) There was a sharp decrease in mechanical anisotropy with increasing density. Both strength and modulus anisotropies were almost proportional to the inverse square of the bulk density.

IV-2.4 High-temperature corrosion behaviour

Unprotected carbon materials have generally very low oxidation resistance against air at high temperatures because oxidation reactions as described below, would occur.

$$C(s) + O_2(g) \longrightarrow CO_2(g) \quad (8)$$

$$C(s) + 1/2\ O_2(g) \longrightarrow CO(g) \quad (9)$$

Oxidation rates are considered to be influenced by various factors, including graphitization, porosity, active sites and impurities.

The graphite structure of the porous carbon materials

significantly developed at heat treatment temperatures between 1000° C - 3000° C. Hence, both specimens carbonized at 1000° C and graphitized at 3000° C were subjected to thermogravimetric analysis in flowing air up to 1200° C in order to determine the effect of the graphitization by heat treatment on oxidation behaviour. (Figure IV-2-22, p.158)

The carbonized porous carbon material reduced its weight by about 7% around 100-350° C, presumably due to evaporation of moisture because amorphous carbon can easily absorb a small amount of water from the atmosphere. The main oxidation of the carbon heat-treated at 1000° C began around 400° C, after which the weight of carbon was reduced steeply by rapid oxidation. On the other hand, oxidation of the graphitized porous carbon started as high as ca. 650° C, below which graphite was very stable against flowing hot-air. Accordingly, the graphitization has a great effect in enhancing oxidation resistance.

This result coincides with the fact that the oxidation rate of carbon derived from phenolic resin was observed to decrease according to the increase of heat treatment temperature, with the largest change between 1000 and 1400° C. (Chang - 1978)

Above ca. 1000° C, the rate of oxidation is almost the same for both carbons (ca. 4.5%/min). This is because at these temperatures the oxidation rate is controlled by diffusion of oxygen through a boundary layer of product gases (CO_2 + CO).

IV-3 Foamed resin based carbons

IV-3.1 Manufacturing process

The manufacturing process for foamed resin based carbon materials used in this work is summarized below, and is also illustrated briefly in the following flowchart, Figure IV-3-1 (p.160).

Commercially available polyurethane foams were used as low cost preforms which were converted into carbon foams. The foamed polymer preforms were impregnated with a resol phenolic resin (British Petroleum, Cellobond J2027L) solubilized in acetone. Then the foams were dried, and the resin was cured by heat-treatment at 160° C. Finally, the materials were carbonized up to 1200° C by heating at a rate of 120 °C/hr in a horizontal tube furnace in an atmosphere of flowing nitrogen to produce foamed carbon materials.

The foamed carbons were prepared with various densities by regulating the concentration of phenolic resin in acetone during the liquid impregnation process.

The carbon yield of polyurethane preform was under 3 %, while that of the phenolic resin was about 50%. Thus, the carbonized foam consisted of mainly the carbon derived from the phenolic resin.

IV-3.2 Structural characterization

IV-3.2.1 Density

The foamed carbons were prepared with varied densities in the range of 0.0245-0.0681 g/cm^3. Resin based carbons, in general, result in a glass-like

structure: glassy carbons, whose density was reported to be between 1.45-1.55 g/cm^3. Hence, porosities of foamed carbon materials are considered to be in the approximate range of 98-95 %. Consequently, the density of foamed carbons is extraordinary low and the porosity is high. This density/porosity range is almost the same as that of the reticulated vitreous carbons (RVC) employed for electrodes in flow electrolysis. (Wang - 1981)

IV-3.2.2 Microscopic observation

Optical micrographs and scanning electron micrographs of general microstructures for foamed carbons are presented in Figures IV-3-2 (p.161) and IV-3-3(p.162), respectively. The carbon foams had an inter-connected three-dimensional network of carbon. It is obvious from the micrographs that the material had an open-celled structure. The cells of foamed carbon were not a regular packing of identical units, but contained cells of different sizes and shapes with different connectivity. Nonetheless, this randomness can be considered to be a virtually symmetrical geometry in a macroscopic observation.

These microstructural features are basically inherited from the cell structure of polymer preforms. But some shape transformation may occur during resin impregnation and curing, and carbonization processes.

Figure IV-3-4 (p.163) shows microscopic observation of polished cross-sections of foamed carbons. The cell

struts are made of dense and homogeneous carbon, without any voids.

The general structural characterization of foamed carbons from these microscopic studies is as follows: the cell edge connectivity (the number of edges per vertex) was typically 4, and face connectivity (the number of faces per edge) was 3. Judging from these characteristics, a dodecahedral-like cell model can be assumed. (Anderson - 1992) However, it is difficult to standardize the cell structure because of limited information.

IV-3.2.3 X-ray diffraction analysis

X-ray diffraction profile of carbon foam is shown in Figure IV-3-5 (p.164). The diffraction peaks of carbon in the foam are very broad, so the foamed carbon was made of amorphous structure, and the size of graphite crystallite did not develop during heat-treatment. Therefore, as expected from its manufacturing process and the carbon precursor, glassy carbon (vitreous carbon) was formed in the materials.

IV-3.2.4 Summary of structural features

The structural features of foamed carbon can be summarized as follows:

(i) The density of the foamed carbons was extraordinary low and the porosity was high. The densities and porosities were in the range of 0.0245-0.0681 g/cm^3 and approximately 98-95 %, respectively.

(ii) The carbon foams had an inter-connected three-dimensional network and an open-celled structure.
(iii) The cell struts were made of dense and homogeneous carbon, without any voids.
(iv) The cell edge connectivity was typically 4, and face connectivity was 3.
(v) The foamed carbon was made of amorphous carbon structure.

IV-3.3 Mechanical properties

Mechanical properties of the carbon foams in the density range of 0.0245-0.0681 g/cm^3 were characterized by measurement of compressive test at room temperature. A schematic illustration of the compressive stress-strain curve for foamed carbons is given in Figure IV-3-6 (p.164). Elastic deformation occurred up to typically ca. 6 %, after which a structural deformation happened. Data of compressive strength and modulus of carbon foams is presented in Table IV-3-1 (p.159).

IV-3.3.1 Compressive properties

(1) Compressive strength

The variation of compressive strength with density is plotted in Figure IV-3-7 (p.165). It is obvious that compressive strength increases with density. In addition, the relative strength was determined as a function of relative density, and the data are shown in Figure IV-3-8 (p.166). The values for σ_s and ρ_s were chosen as 100MPa and 1.5 g/cm^3, respectively, values typical for glassy carbons. The figure shows that the

data could be expressed by

$$(\sigma/\sigma_s) = 0.12(\rho/\rho_s)^{3/2} \quad (10)$$

Therefore, this equation is in good agreement with the work of Gibson and Ashby on open-cell brittle materials. (Chapter II-1.3.1) However, there is a significant disagreement between the measured value of the geometric constant and that suggested by Gibson and Ashby (C=0.65).

It was shown before that the geometric constant is very sensitive to the microstructure (Hagiwara - 1987), and the constant is greatly influenced by selection of the value of σ_S and ρ_S.

(2) Compressive modulus

The variation of compressive modulus with density is plotted in Figure IV-3-9 (p.165). The compressive modulus value increased with density. The relative modulus was also determined as a function of relative density. (Figure IV-3-10, p.166) The values for E_S and ρ_S were chosen as 25GPa and 1.5 g/cm^3, respectively, values typical for glassy carbons. The data could be expressed by

$$(E/E_s) = 0.46(\rho/\rho_s)^2 \quad (11)$$

Hence, this equation is also in good agreement with the work of Gibson and Ashby on open-cell materials. However, again there is a significant disagreement between the measured value of the geometric constant and that suggested by Gibson and Ashby (C=1).

A possible reason that the geometric constant was less than previously suggested is that the selected strength and Young's modulus values, σ_s and E_s, are too small for the foamed carbon strut material. Nonetheless, this cannot explain such a big disagreement. Consequently, some geometric factors may be concerned with this significant disagreement of the constant because even a slight anisotropy plays a great influence on the mechanical properties.

Furthermore, it was suggested by Hagiwara et al. (1987) that the statistical nature of cell strut strength, which may be dependent on cell size or relevant density, could be an important effect. Therefore, further investigation may be required.

IV-3.3.2 Conclusion of mechanical properties

The normalized strength and modulus of the foamed carbons were determined as a function of relative density, as the following equations.

$$(\sigma/\sigma_s) = 0.12(\rho/\rho_s)^{3/2} \quad (10)$$

$$(E/E_s) = 0.46(\rho/\rho_s)^2 \quad (11)$$

The relative density exponents in both equations were in excellent agreement with the theoretical work by Gibson and Ashby on open-cell brittle materials. However, there is a significant disagreement between the measured value of the geometric constants and those suggested theoretically.

IV-3.4 High-temperature corrosion resistance

Oxidation behaviour of the carbon foams at high temperatures monitored by thermogravimetric analysis, is shown in Figure IV-3-11 (p.167). The weight of foamed carbon decreased by about 13% at temperatures around 100-350° C, probably owing to the evaporation of absorbed moisture. The main oxidation reaction started around 450° C, after which temperature carbon was steadily burned out. This low oxidation resistant behaviour, which is quite similar to that of the carbonized porous carbons by paper making technology, is typical for amorphous carbons.

IV-4 Resin carbon based porous carbon pellets

IV-4.1 Manufacturing process

Porous resin based carbon pellet samples were supplied by British Petroleum plc for this experiment. Figure IV-4-1 (p.168) shows the flowsheet for the fabrication route of porous carbon pellets. Phenolic resin powder of novolak type $(C_6H_5OHCH_2)_n$ (particle size up to 106 μm), pre-mixed with hexamine powder as an activator for polymerization, was placed in a cylindrical die, and cold-pressed to produce porous green resin pellets. The resin pellets were carbonized in an atmosphere of flowing nitrogen up to 800° C to produce porous carbon pellets of approximate dimensions 13mm in diameter and 3mm in thickness.

IV-4.2 Structural characterization

IV-4.2.1 Density and porosity

The bulk density and apparent porosity determined by a water absorption method are shown in Table IV-4-1 (p.168). The bulk density of the resin based porous carbons is 0.94 g/cm^3 and their apparent porosity is 44.4 %. Thus, their density is slightly higher and porosity is less than those of other types of porous carbons. However, this value appears to be nearly a maximum porosity that can be achieved by a powder pressing manufacturing route because it is above the porosity value (ca. 50%) where there is a transition point from a uniformly pore distributed structure to multi-modal pore distributed form. (McEnaney - 1990)

IV-4.2.2 Microscopic observation

Scanning electron micrographs and optical micrographs of polished section for the porous carbons are presented in Figures IV-4-2 and IV-4-3 (p.169, 170), respectively.

The majority of pore structure consisted of larger pores (ca. 100 μm in diameter) inter-connected three-dimensionally with smaller channel-like pores. Thus, the material had virtually an open-celled structure.

The larger pores have a globule-like appearance, Hence, the pore structure can be estimated as roughly equi-axed in shape, and the pores can be considered as an isotropically-distributed array of spheres.

IV-4.2.3 X-ray diffraction analysis

X-ray diffraction profile of the resin based porous carbon is shown in Figure IV-4-4 (p.171). The diffraction peaks of carbon are very broad, thus the carbon consisted of an amorphous structure.

IV-4.2.4 Summary of structural features

The structural features of the resin based porous carbon can be summarized to be as follows:

(i) The density (0.94 g/cm^3) was slightly higher and porosity (44.4 %) was less than those of other types of porous carbons.

(ii) The majority of pore structure consisted of larger pores (ca. 100 μm in diameter) inter-connected three-dimensionally with smaller channel-like pores. Thus, the material had virtually an open-celled structure.

(iii) The carbon consisted of an amorphous structure.

IV-4.3 Mechanical properties

The tensile strength of the porous carbon pellets was determined by the split cylinder test. The strength was 6.44 MPa, as shown in Table IV-4-1 (p.168).

IV-4.4 High temperature corrosion resistance

The oxidation behaviour of the porous carbon at high temperatures in air measured by thermogravimetric analysis, is shown in Figure IV-4-5 (p.171). The oxidation resistance was low and the behaviour is typical of amorphous carbons.

IV-5 Carbon bonded carbon fibre composites

IV-5.1 Manufacturing process

Carbon bonded carbon fibre (CBCF) composites in this work were supplied by Oak Ridge National Laboratory in the United States. The basic manufacturing process is briefly described below, and Figure IV-5-1 (p.173) shows the flowsheet for the fabrication route. (Wei - 1985)

Chopped rayon fibres were carbonized at 1350° C in an inert atmosphere. The carbon fibres with phenolic resin powders (novolak type) were slurried in water. Then, the fibre-resin-water slurry was vacuum moulded, followed by drying of the mould and simultaneous curing of the resin. Final carbonization was conducted by heating at a rate of about 300° C/hr to 1600° C and held for 3 hours in an argon atmosphere.

IV-5.2 Structural characterization

IV-5.2.1 Density and porosity

The bulk density and porosity, obtained by a water absorption method, are shown in Table IV-5-1 (p.172). The density and porosity were 0.347 g/cm^3 and 76.7%, respectively.

It was reported that the density and porosity of CBCF composites are principally dependent on the packing of fibres, which, in other words, is subject to fibre length and length distribution. Bulk density decreased with increasing fibre length. (Wei- 1985, Shui - 1990)

IV-5.2.2 Microscopic observation

Scanning electron micrographs and optical micrographs of polished sections for the CBCF composites, showing views of the perpendicular and parallel to the moulding direction are presented in Figures IV-5-2 and IV-5-3 (p.174-177).

It was revealed that the porous carbons consisted of short carbon fibres bonded together at their junctions by discrete, thin regions of the carbon matrix. And the vast majority of the volume was dominated by inter-connected open-pores.

The composites can be considered to be constituted of layers of planar random fibres because the fibres were preferably orientated in planes perpendicular to the thickness direction of the mould form.

These structural characteristics suggested that the CBCF composites have a lot of analogies with the porous carbons fabricated by the paper manufacturing process in their 2-D planar random microstructures.

IV-5.2.3 X-ray diffraction analysis

X-ray diffraction profile of the CBCF composites is shown in Figure IV-5-4 (p.178). The (002), (001) and (110) diffraction peaks of carbon are broad. However, they are slightly sharper than those of glassy carbons. Thus, the composites consisted of a mainly amorphous structure, and graphitization occurred in small regions. This is presumably stress graphitization at boundaries between the fibre and matrix, during the heat treatment up to 1600° C, which was also confirmed by polarized light microscopic observation.

IV-5.2.4 Summary of structural features

The structural characteristics of the carbon bonded carbon fibre composites can be concluded to be the following:

(i) The density and porosity were 0.347 g/cm^3 and 76.7%, respectively. The vast majority of the volume was dominated by inter-connected open-pores.

(ii) The composites consisted of short carbon fibres bonded together at their junctions by discrete, thin regions of the carbon matrix.

(iii) The fibres were preferably orientated in planes perpendicular to the thickness direction of the mould form.

(iv) The composites can be considered to be constituted of layers of planar random fibres.

(v) The composites were made of a mainly amorphous structure; however, stress graphitization occurred in small regions during the heat treatment.

IV-5.3 Mechanical properties

Mechanical properties of the CBCF composites including flexural and compressive strengths were determined at room temperature in air. A schematic designation of mechanical specimens is correspondent to that given in Figure IV-2-8. Flexural strength was measured in the XZ orientation. Meanwhile, compressive strength was tested in the Z direction; the direction perpendicular to the fibre array. Judging from its manufacturing process, mechanical properties within the

XY plane can be considered to be isotropic. The results of mechanical properties are presented in Table IV-5-1 (p.172).

The failure manner of the CBCF composites showed an analogy with that of the carbonized porous carbon by paper making technology, except with greater strain to failure. The composites thus failed in a brittle manner under both flexural and compressive stresses.

As with the porous carbons by the paper making process, failure in the Z direction occurred at much lower stress than in the X or Y direction because the latter failure is caused by the intralayer fracture, whereas the former failure occurs when the weak interlayer bonds fail.

Mechanical anisotropy (Flexural(XZ)/Compressive(Z)) of the composites was also determined. Strength and elastic modulus anisotropy ratios were 7.2 and 36.1, respectively.

IV-5.4 High temperature corrosion resistance

The oxidation behaviour of the CBCF composites at high temperatures in air measured by thermogravimetric analysis, is presented in Figure IV-5-5 (p.178). The composites showed high oxidation resistance up to about 600° C, below which they did not exhibit any weight decrease. This can be ascribed to high heat treatment temperature to 1600° C and stress graphitization of the matrix.

Physical properties of porous carbon prefroms by paper-manufacturing technology

Heat treatment temperature	3000℃
Bulk density ρ (g/cm^3)	0.512 ± 0.04
Porosity p (%)	73.3 ± 0.3
Flexural properties	
Strength σ (MPa)	13.7 ± 0.6
Modulus E (GPa)	2.9 ± 0.4
Compressive properties	
Strength σ (MPa)	0.88 ± 0.03
Modulus E (GPa)	0.035 ± 0.002

Table IV-2-1 Physical properties of porous carbon materials by paper making technology (HTT 3000° C)

Heat treatment temperature	1000℃
Bulk density ρ (g/cm^3)	0.521 ± 0.06
Porosity p (%)	72.5 ± 0.3
Flexural properties	
Strength σ (MPa)	13.5 ± 1.3
Modulus E (GPa)	5.6 ± 0.6
Compressive properties	
Strength σ (MPa)	2.69 ± 0.28
Modulus E (GPa)	0.123 ± 0.019

Table IV-2-2 Physical properties of porous carbon materials by paper making technology (HTT 1000° C)

Bulk Density ρ g/cm^3	Porosity P %	Relative Density ρ/ρs	Flexural Properties		Compressive Properties	
			strength σ MPa	modulus E GPa	strength σ MPa	modulus E GPa
0.41	76.2	0.238	8.08	1.67	0.23	0.011
0.41	76.2	0.238	8.43	1.83	0.23	0.011
0.41	76.0	0.240	8.06	1.62	0.23	0.011
0.42	75.9	0.241	8.64	1.64	0.26	0.012
0.42	75.6	0.244	8.89	1.71	0.27	0.010
0.46	73.2	0.268	10.88	2.51	0.58	0.022
0.46	73.1	0.269	11.23	2.74	0.46	0.020
0.46	73.0	0.270	11.43	2.78	0.46	0.022
0.46	73.1	0.269	11.21	2.57	0.53	0.023
0.47	72.6	0.274	9.63	2.41	0.50	0.020
0.49	71.9	0.281	12.08	2.94	0.60	0.029
0.49	71.6	0.284	10.15	3.56	0.72	0.029
0.52	70.0	0.300	13.05	3.24	0.76	0.037
0.52	70.0	0.300	14.69	3.47	0.77	0.041
0.53	69.4	0.306	13.66	3.08	0.86	0.037
0.55	68.0	0.320	15.59	3.77	0.95	0.046
0.55	67.6	0.324	15.80	3.70	0.96	0.047
0.58	66.1	0.339	17.04	4.01	1.25	0.070
0.58	65.9	0.341	16.55	3.98	1.17	0.061
0.58	65.9	0.341	15.47	3.73	1.20	0.064
0.61	64.8	0.352	18.45	5.08	1.40	0.069
0.61	64.5	0.355	20.13	4.56	1.40	0.069
0.61	64.5	0.355	18.86	4.95	1.45	0.070
0.61	64.5	0.355	19.02	4.49	1.41	0.070
0.62	64.8	0.352	20.63	4.46	1.30	0.070

Table IV-2-3 Mechanical properties of porous carbon materials by paper making technology in the density range of 0.41-0.62 g/cm^3 (HTT 2800° C)

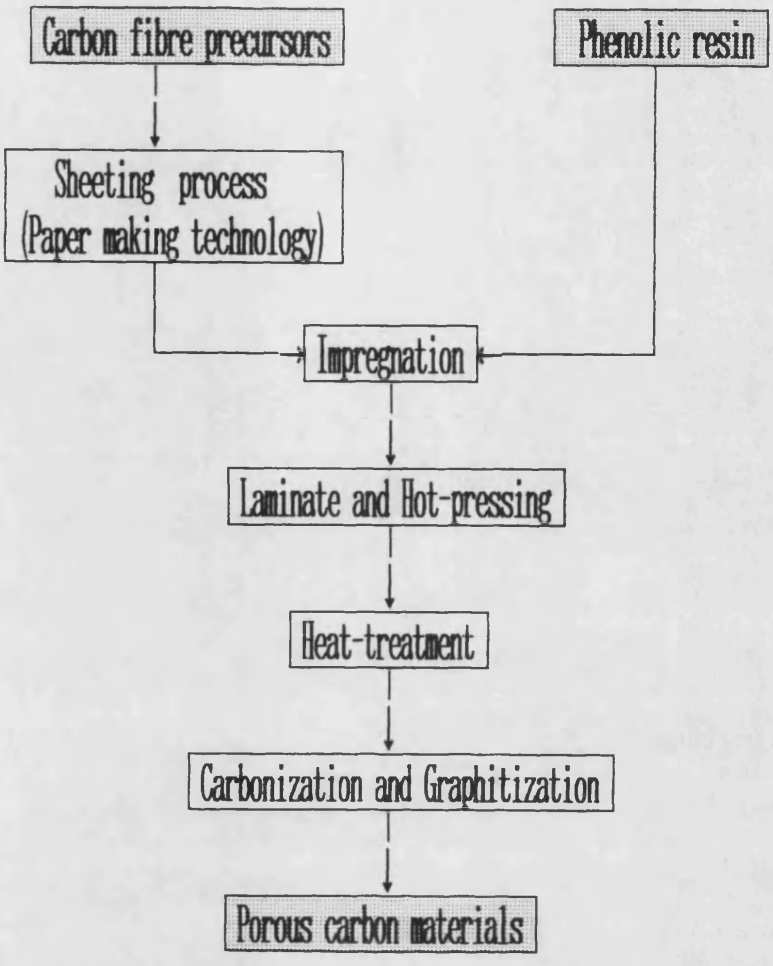

Figure IV-2-1 Manufacturing process of porous carbon materials by paper making technology

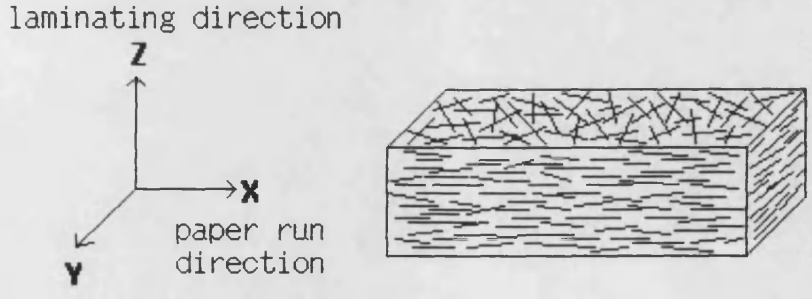

Figure IV-2-2 Schematic microstructure of porous carbon materials by paper making technology

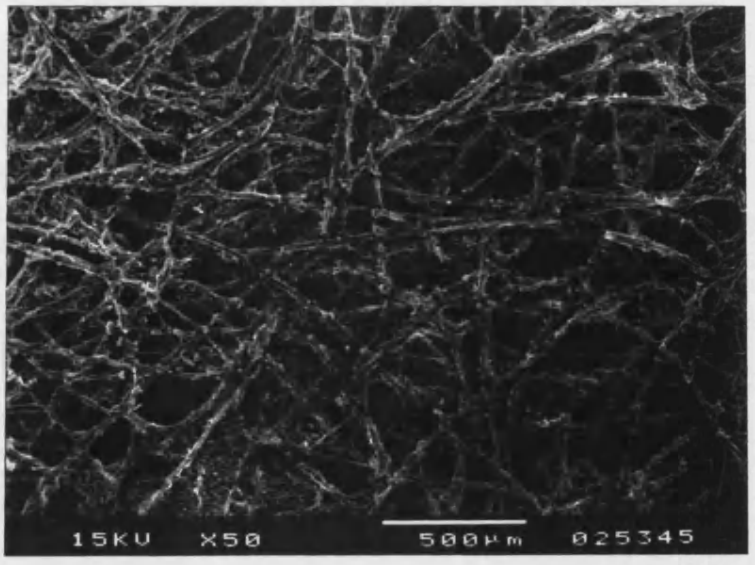

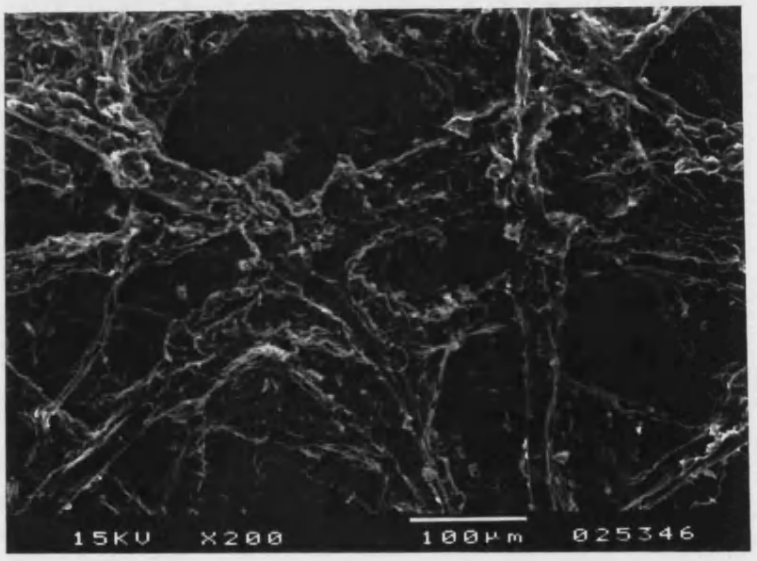

Figure IV-2-3 (a) Scanning electron micrographs of the surface for porous carbon materials by paper making technology (HTT 1000° C)

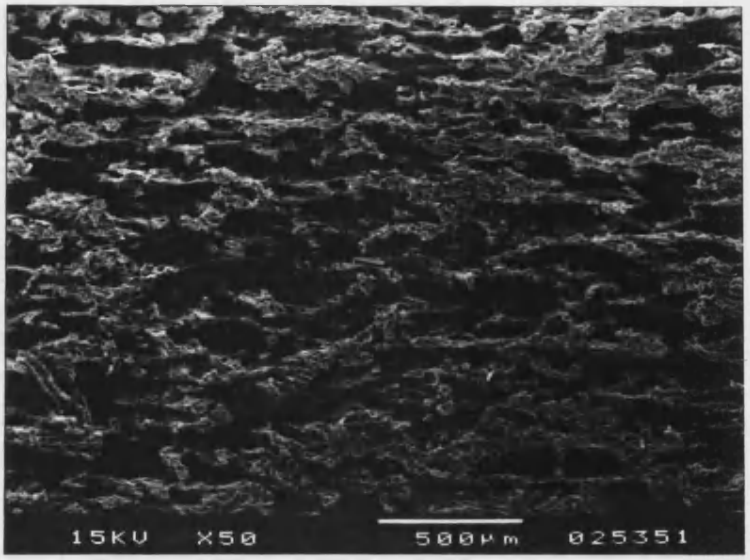

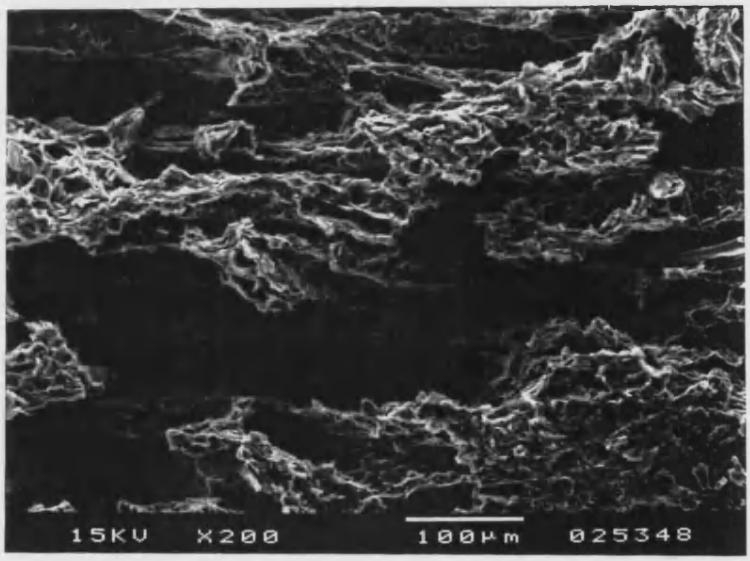

Figure IV-2-3 (b) Scanning electron micrographs of the fracture section for porous carbon materials by paper making technology (HTT 1000° C)

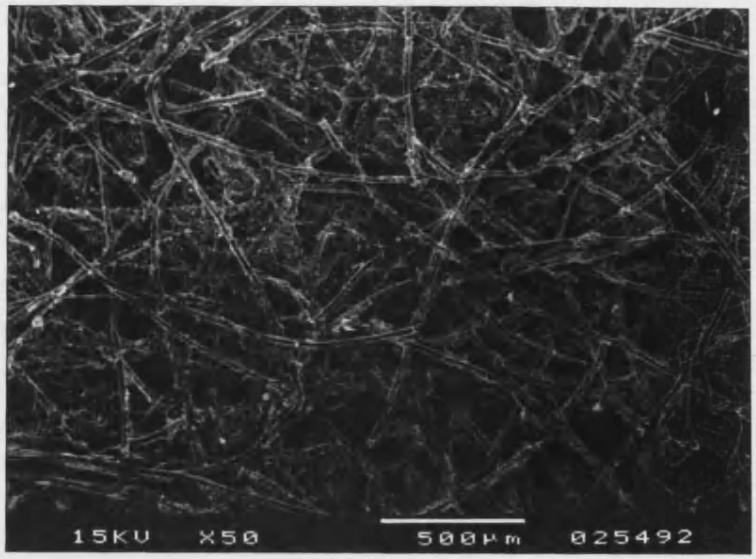

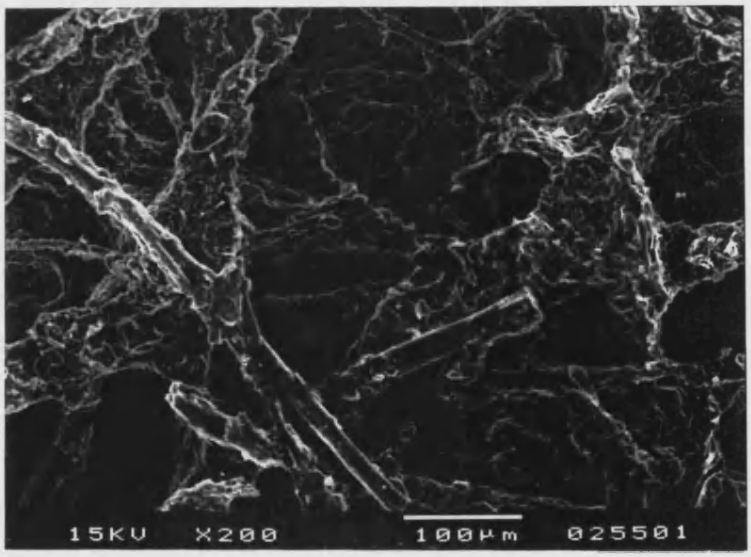

Figure IV-2-4 (a) Scanning electron micrographs of the surface for porous carbon materials by paper making technology (HTT 3000° C)

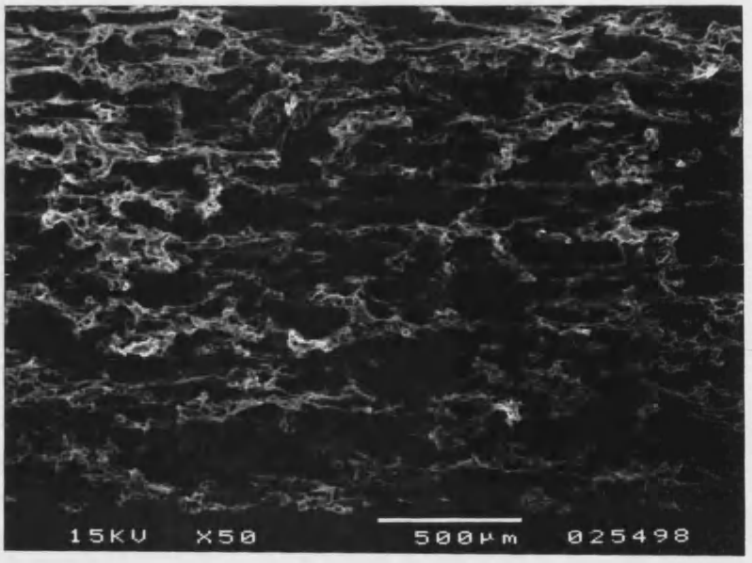

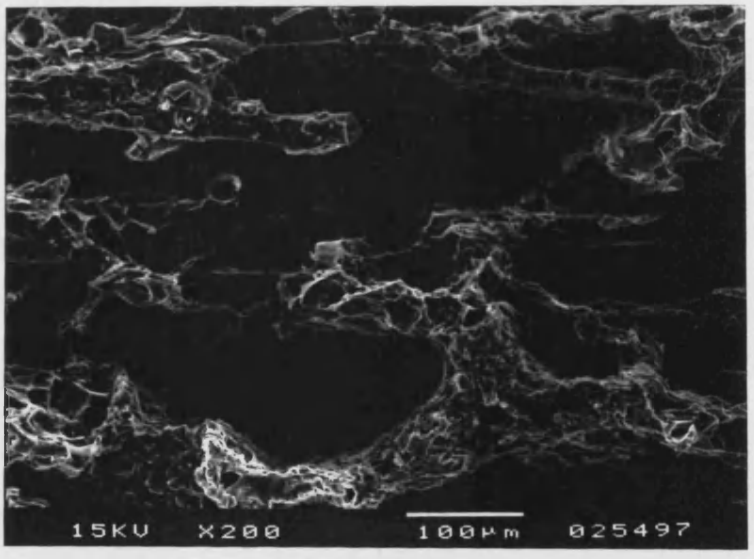

Figure IV-2-4 (b) Scanning electron micrographs of the fracture section for porous carbon materials by paper making technology (HTT 3000° C)

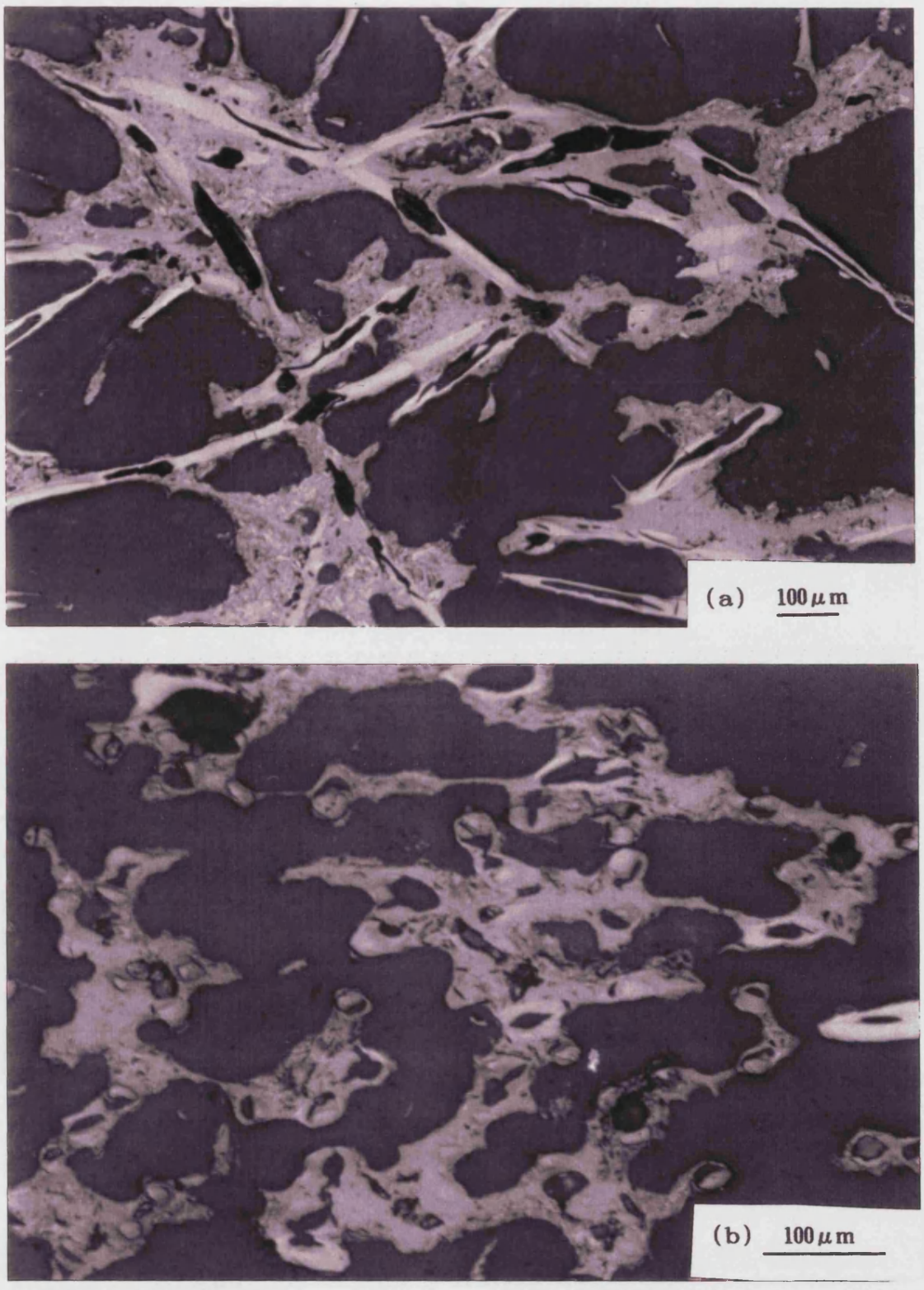

Figure IV-2-5 Polarized micrographs of the polished sections for porous carbon materials by paper making technology (HTT 1000° C) (a) perpendicular and (b) parallel sections in the laminating direction

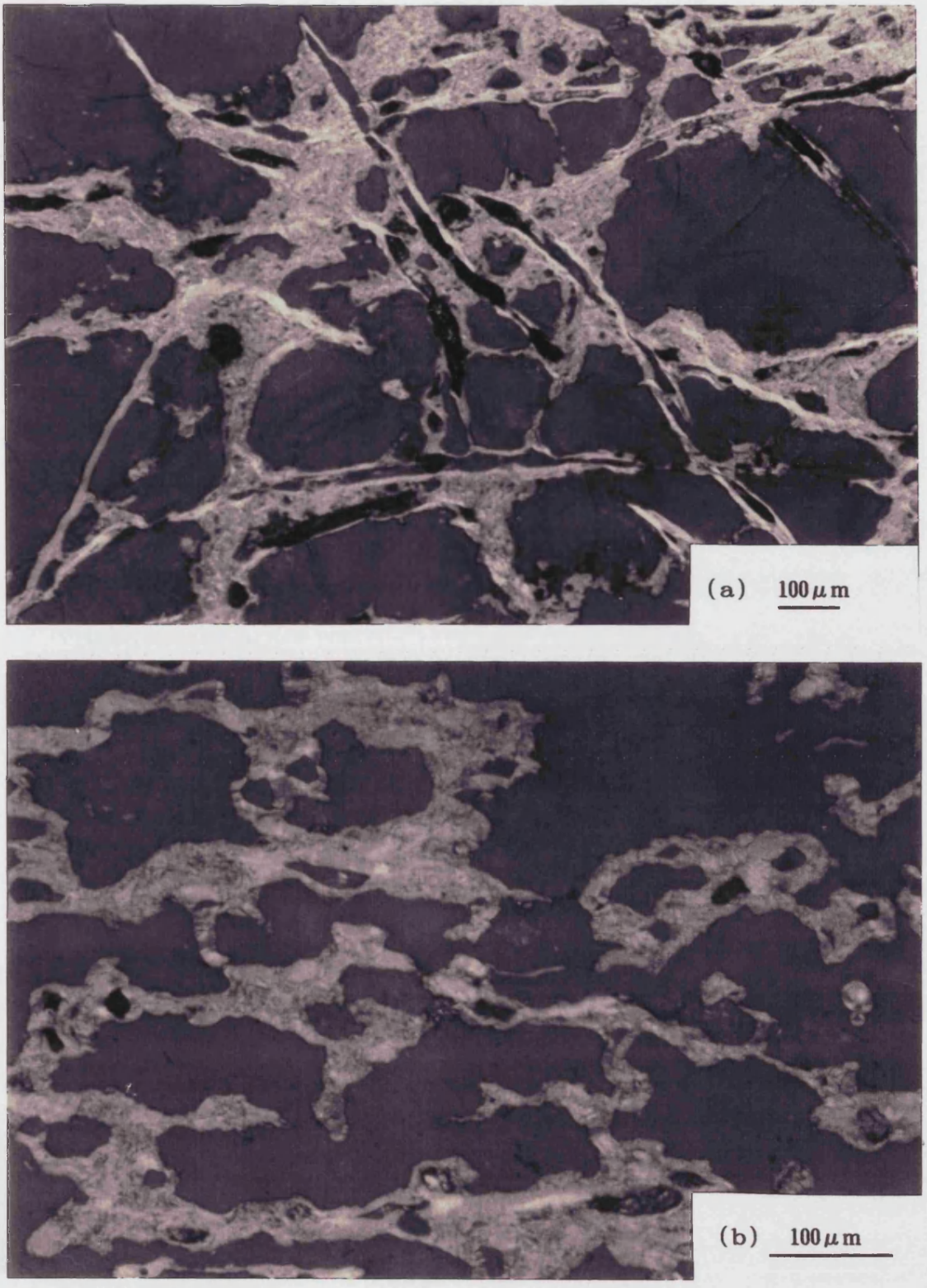

Figure IV-2-6 Polarized micrographs of the polished sections for porous carbon materials by paper making technology (HTT 3000° C) (a) perpendicular and (b) parallel sections in the laminating direction

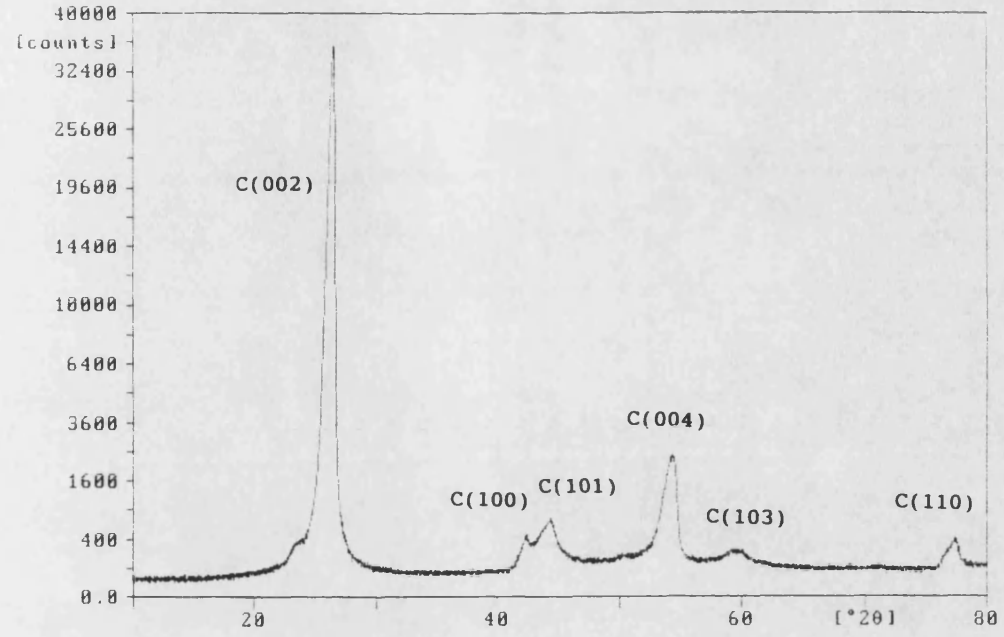

Figure IV-2-7 X-ray diffraction profile for porous carbon materials by paper making technology (HTT 3000° C)

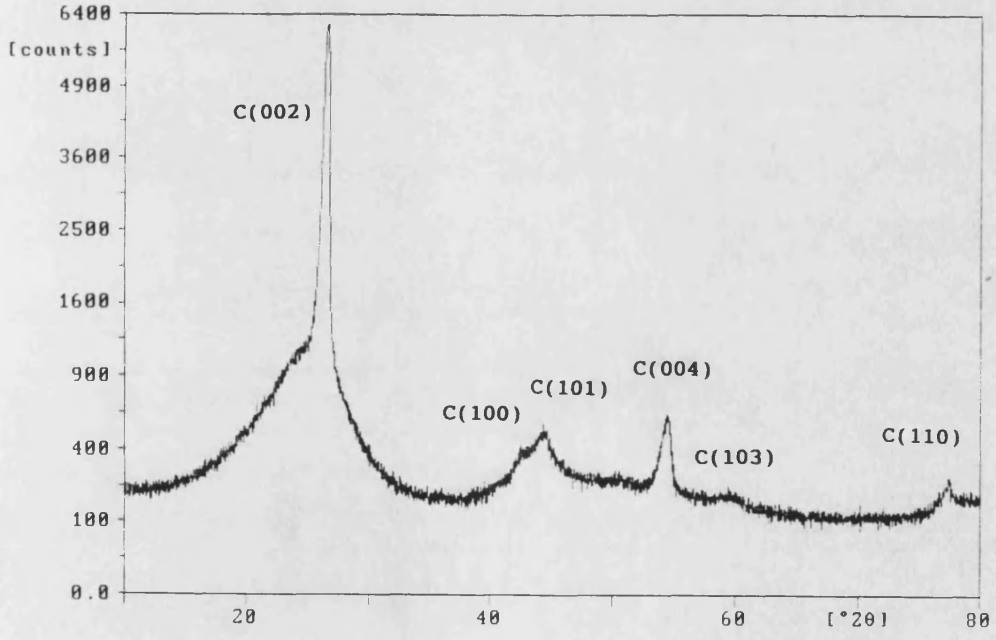

Figure IV-2-8 X-ray diffraction profile for porous carbon materials by paper making technology (HTT 1000° C)

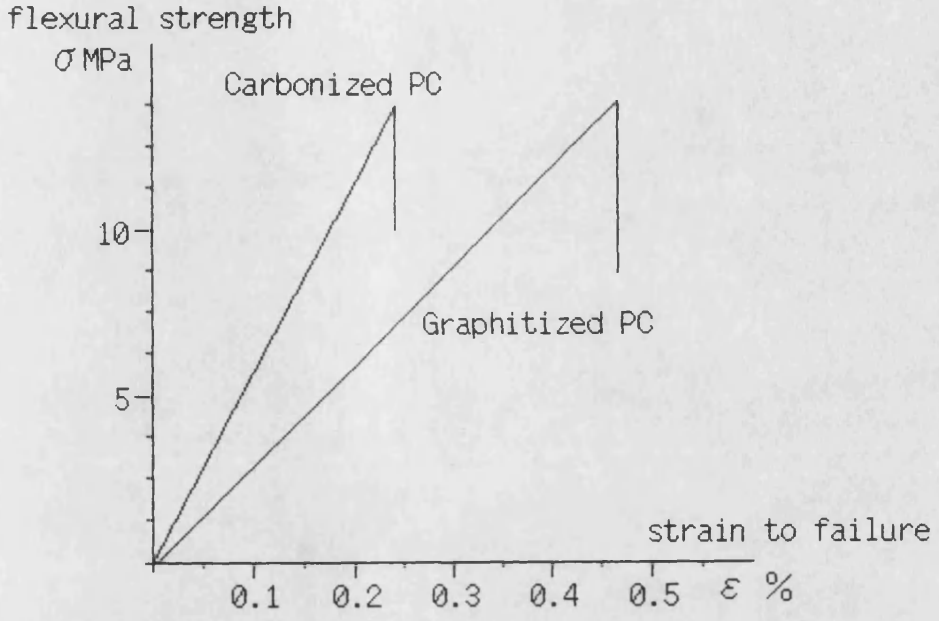

Figure IV-2-9 Schematic flexural stress-strain curves for porous carbon materials by paper making technology

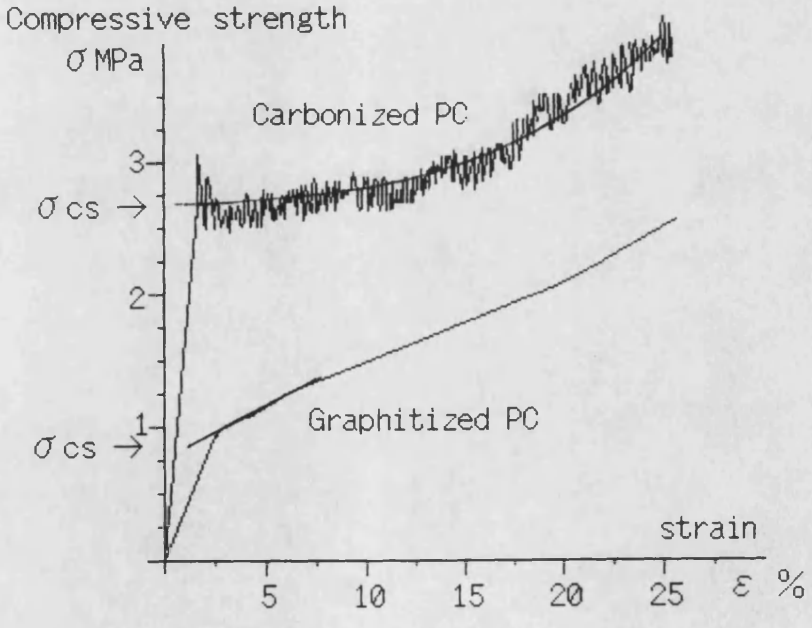

Figure IV-2-10 Schematic compressive stress-strain curves for porous carbon materials by paper making technology

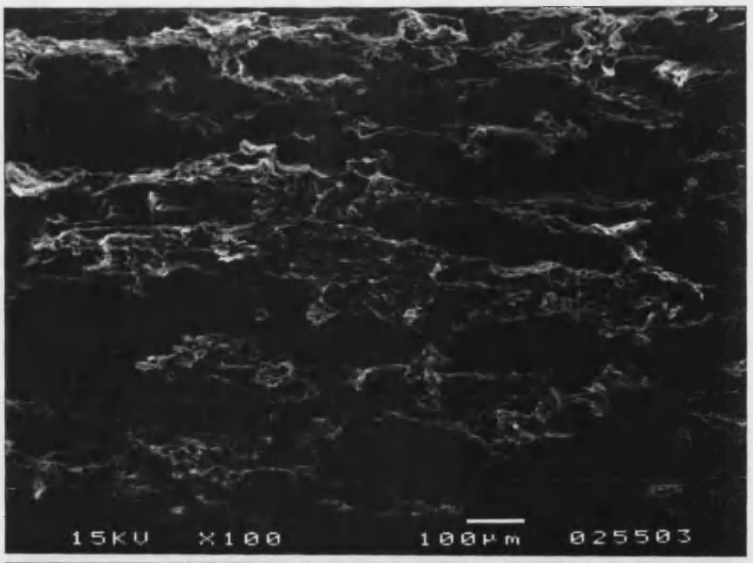

(a)

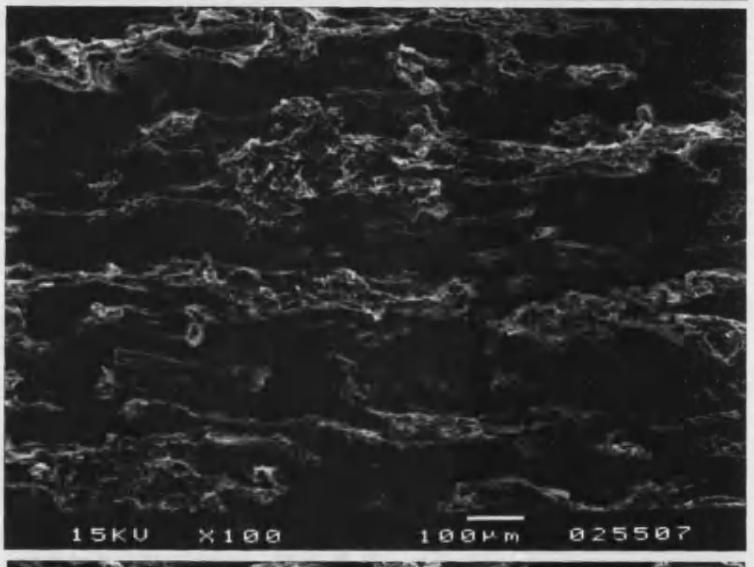

(b)

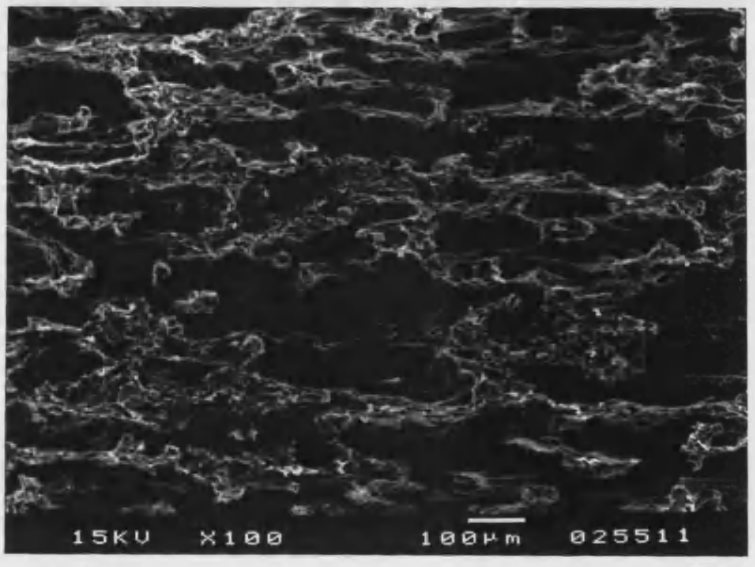

(c)

Figure IV-2-11 Scanning electron micrographs of the fracture sections for porous carbon materials by paper making technology with various densities
(a) 0.41 g/cm^3, (b) 0.52 g/cm^3, (c) 0.62 g/cm^3

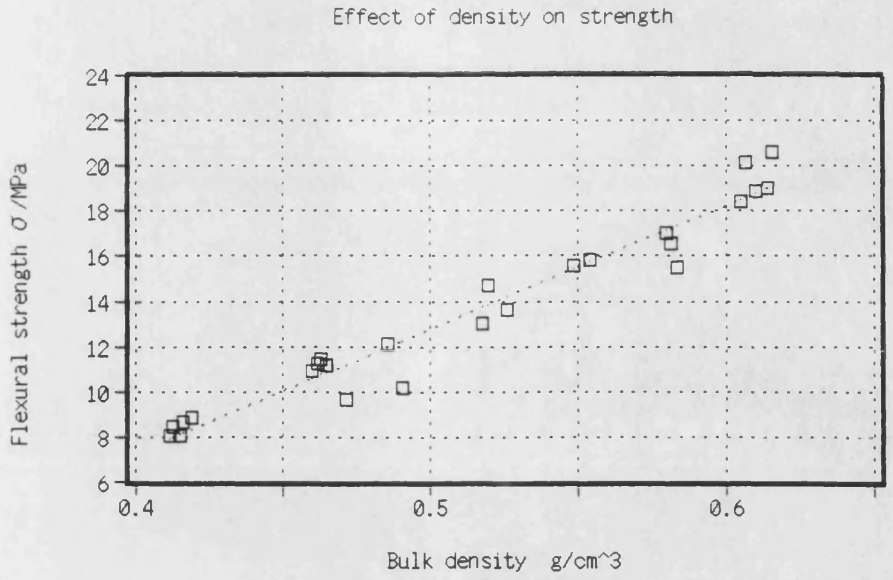

Figure IV-2-12 Flexural strength of porous carbons by paper making technology, plotted against bulk density

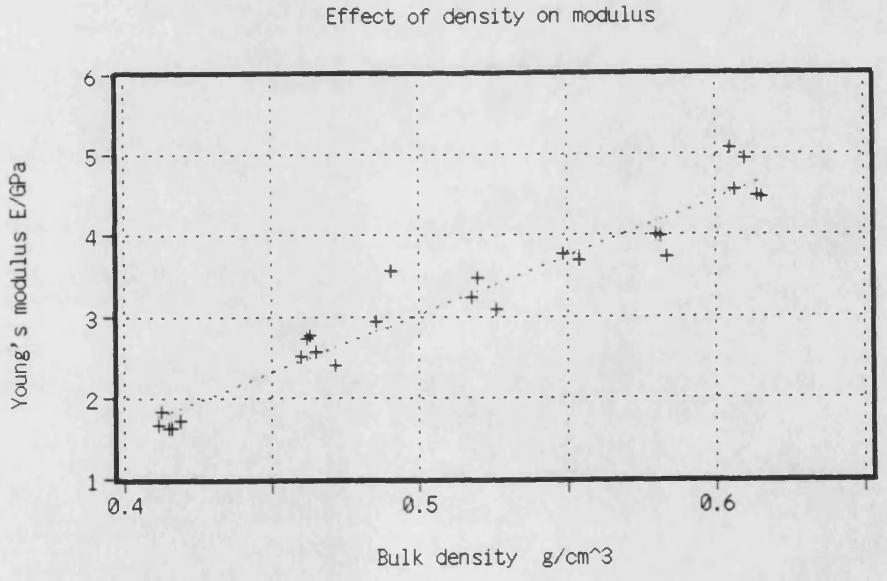

Figure IV-2-13 Flexural modulus of porous carbons by paper making technology, plotted against bulk density

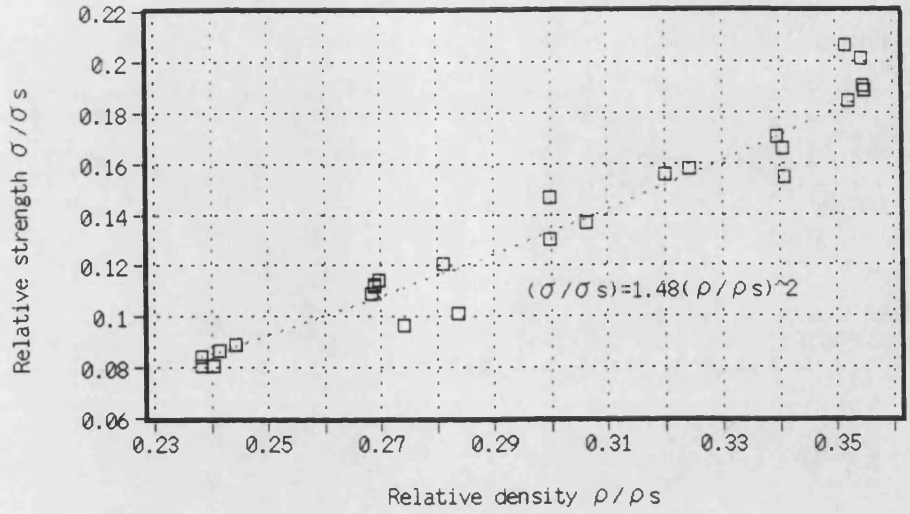

Figure IV-2-14 Relative flexural strength of porous carbons by paper making technology, plotted against relative density

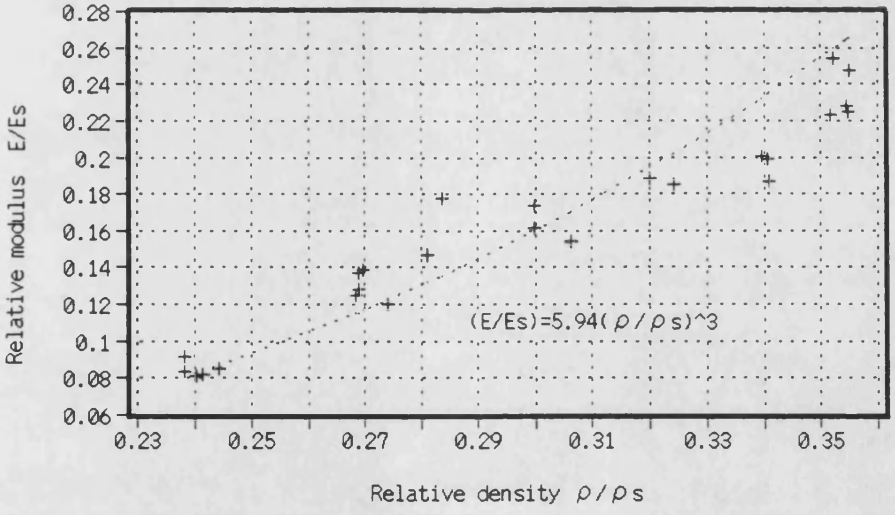

Figure IV-2-15 Relative flexural modulus of porous carbons by paper making technology, plotted against relative density

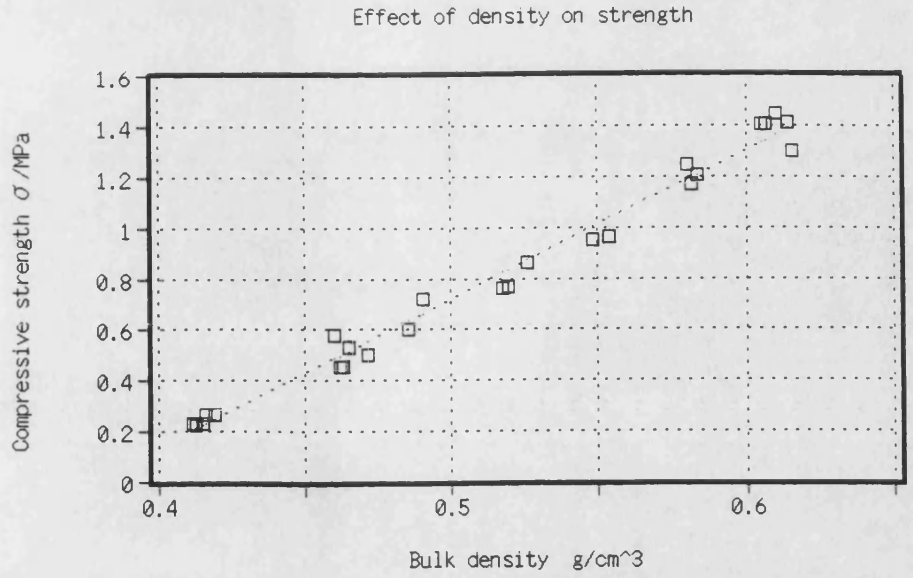

Figure IV-2-16 Compressive strength of porous carbons by paper making technology, plotted against bulk density

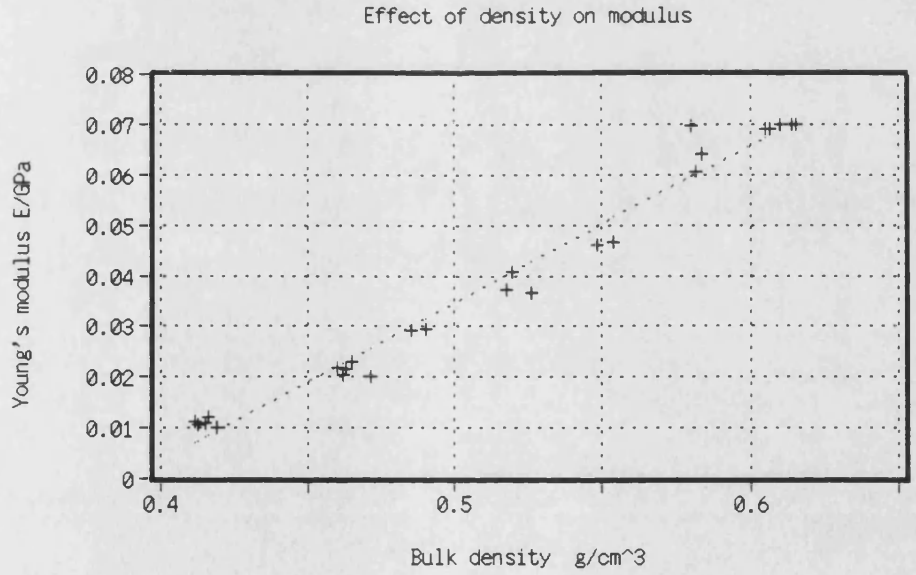

Figure IV-2-17 Compressive modulus of porous carbons by paper making technology, plotted against bulk density

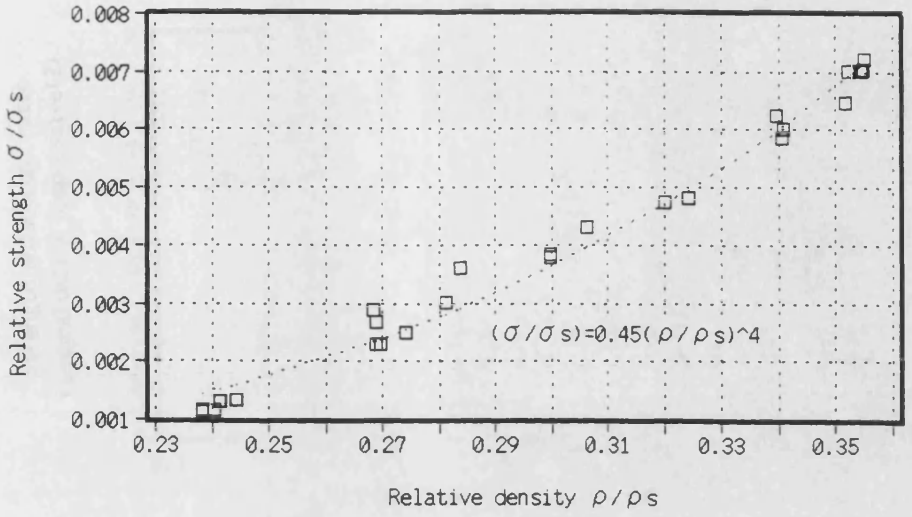

Figure IV-2-18 Relative compressive strength of porous carbons by paper making technology, plotted against relative density

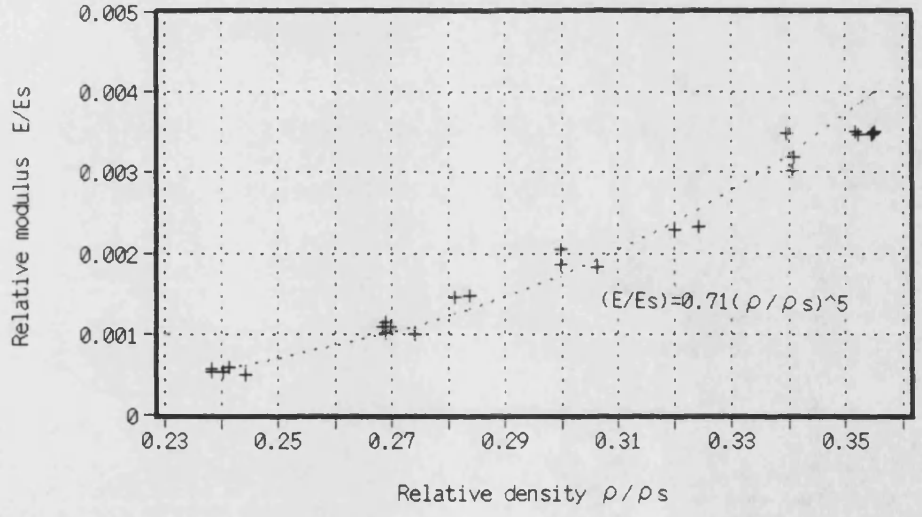

Figure IV-2-19 Relative compressive modulus of porous carbons by paper making technology, plotted against relative density

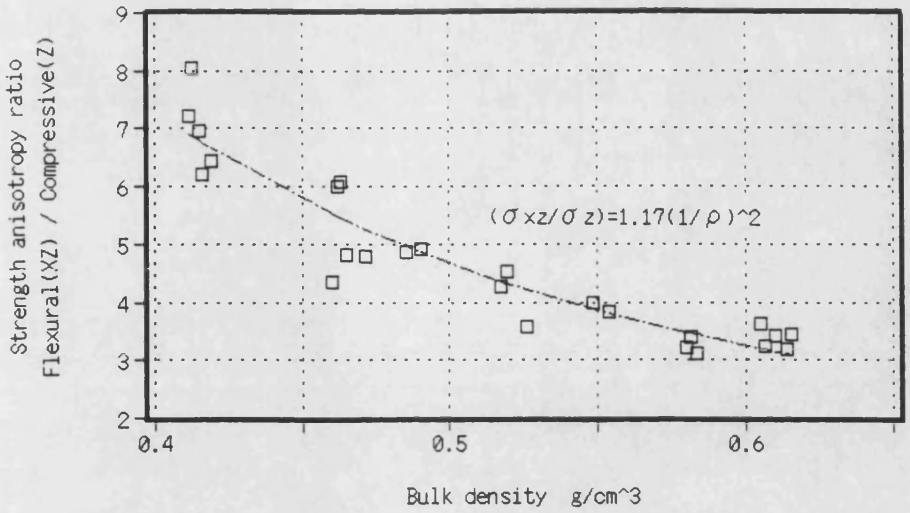

Figure IV-2-20

Strength anisotropy (Flexural(XZ)/Compressive(Z)) of porous carbons by paper making technology, plotted against bulk density

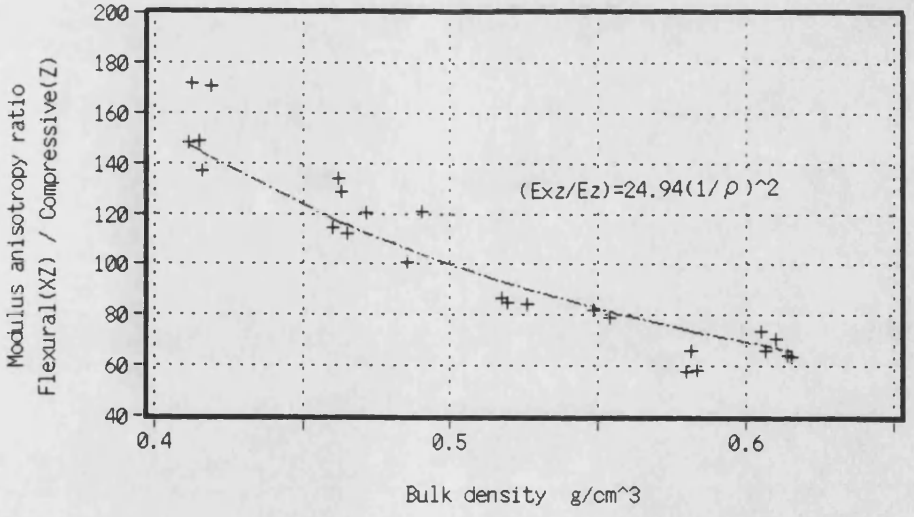

Figure IV-2-21

Modulus anisotropy (Flexural(XZ)/Compressive(Z)) of porous carbons by paper making technology, plotted against bulk density

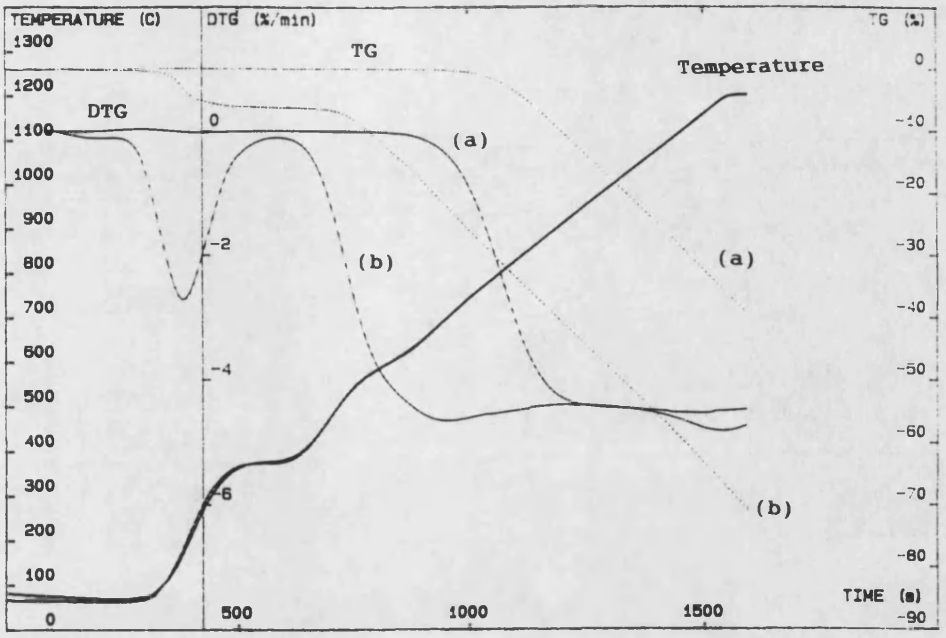

Figure IV-2-22 Thermogravimetric analysis of porous carbons by paper making technology oxidized in air
(a) HTT 3000° C, (b) HTT 1000° C

Bulk density ρ (g/cm^3)	Compressive properties	
	strength σ (MPa)	modulus E (GPa)
0.0245	0.021	0.0034
0.0245	0.021	0.0030
0.0248	0.023	0.0032
0.0251	0.023	0.0033
0.0252	0.025	0.0029
0.0252	0.023	0.0033
0.0252	0.023	0.0031
0.0256	0.025	0.0034
0.0318	0.043	0.0068
0.0341	0.043	0.0071
0.0346	0.041	0.0064
0.0353	0.039	0.0059
0.0357	0.037	0.0057
0.0359	0.039	0.0058
0.0363	0.039	0.0072
0.0376	0.048	0.0081
0.0567	0.102	0.0168
0.0581	0.095	0.0179
0.0604	0.104	0.0187
0.0611	0.101	0.0161
0.0614	0.108	0.0187
0.0666	0.104	0.0181
0.0678	0.110	0.0179
0.0681	0.107	0.0209

Table IV-3-1

Compressive properties of carbon foams in the density range of 0.0245 - 0.0681 g/cm^3

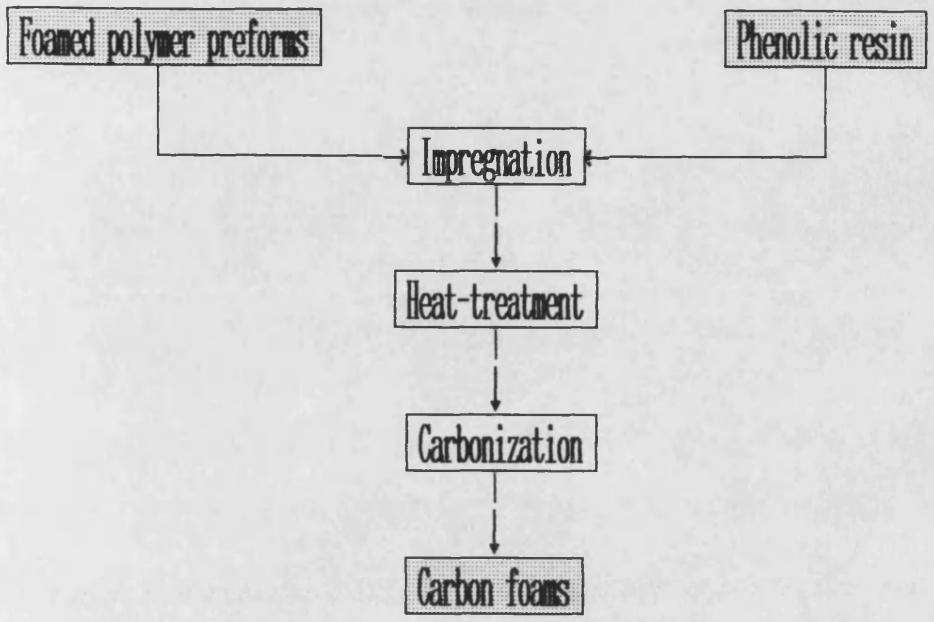

Figure IV-3-1

Manufacturing process for foamed resin based carbons

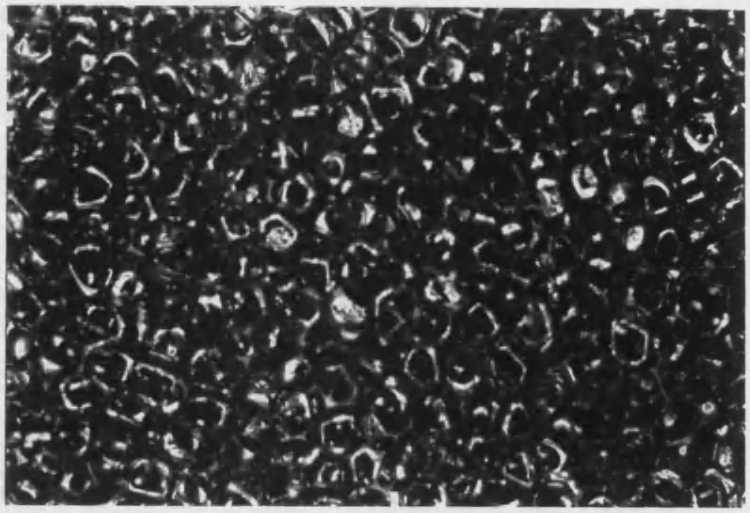

1mm

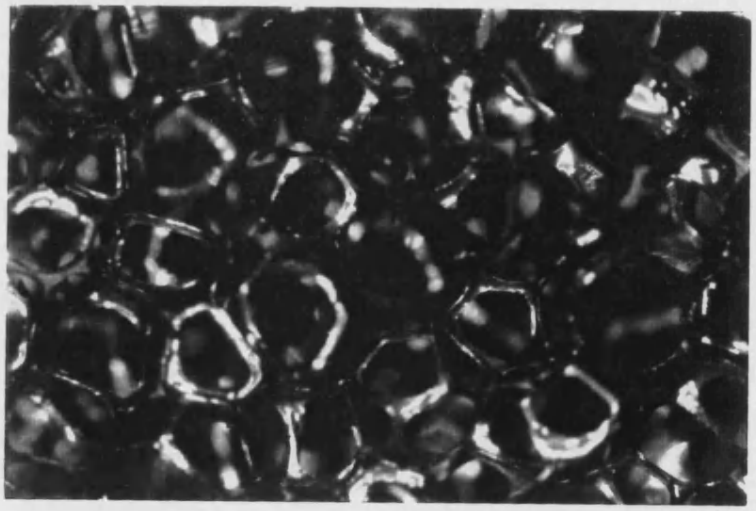

500 μm

Figure IV-3-2 Optical micrographs of carbon foams

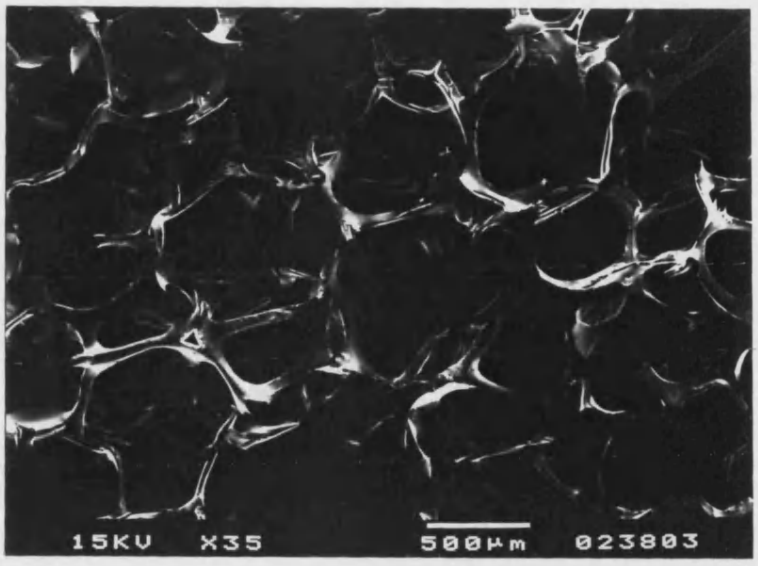

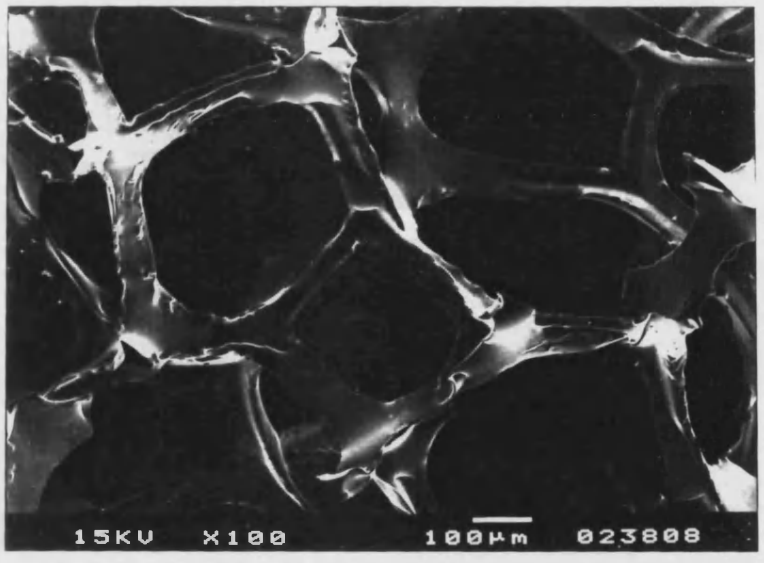

Figure IV-3-3

Scanning electron micrographs of carbon foams

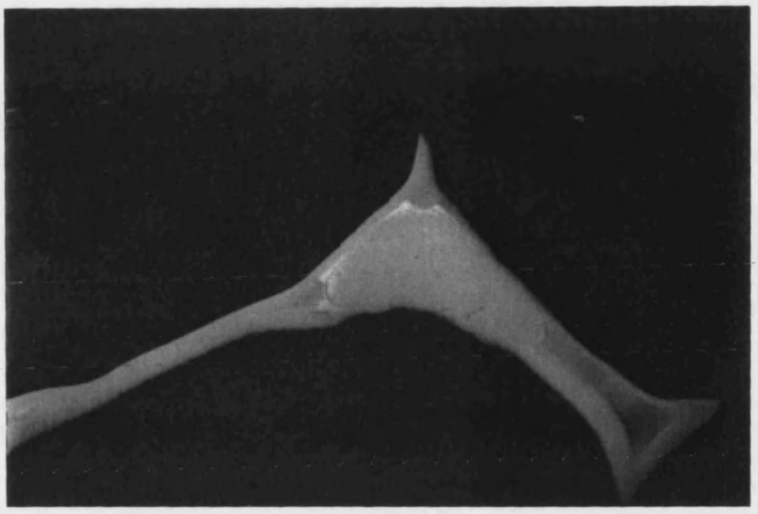

50 μm

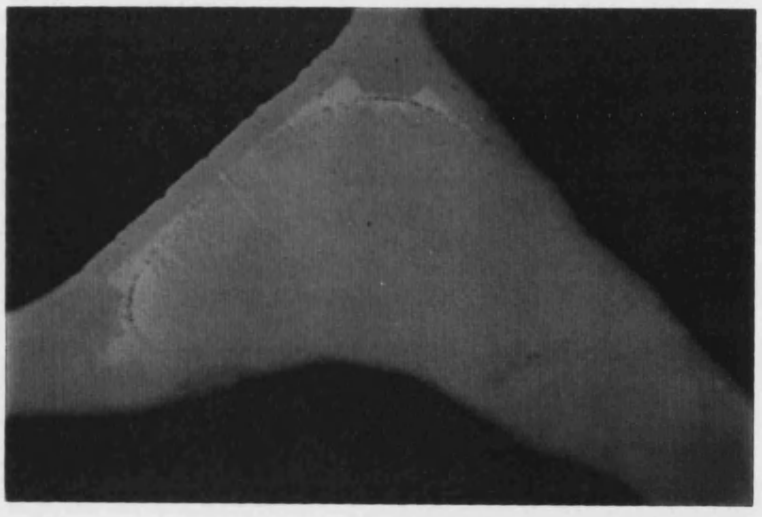

20 μm

Figure IV-3-4

Polished sections of struts for carbon foams

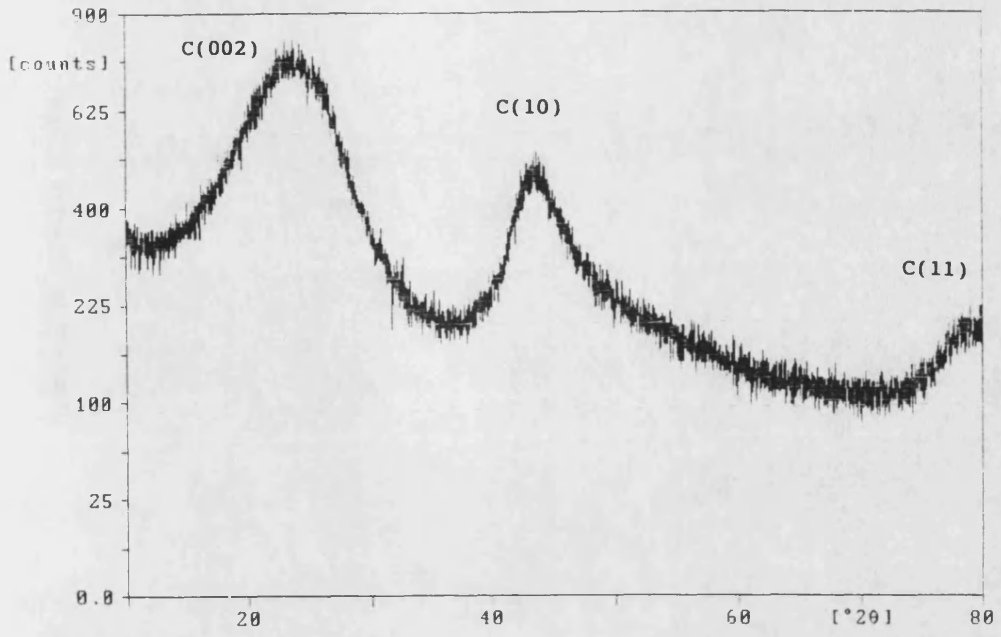

Figure IV-3-5 X-ray diffraction profile of carbon foams

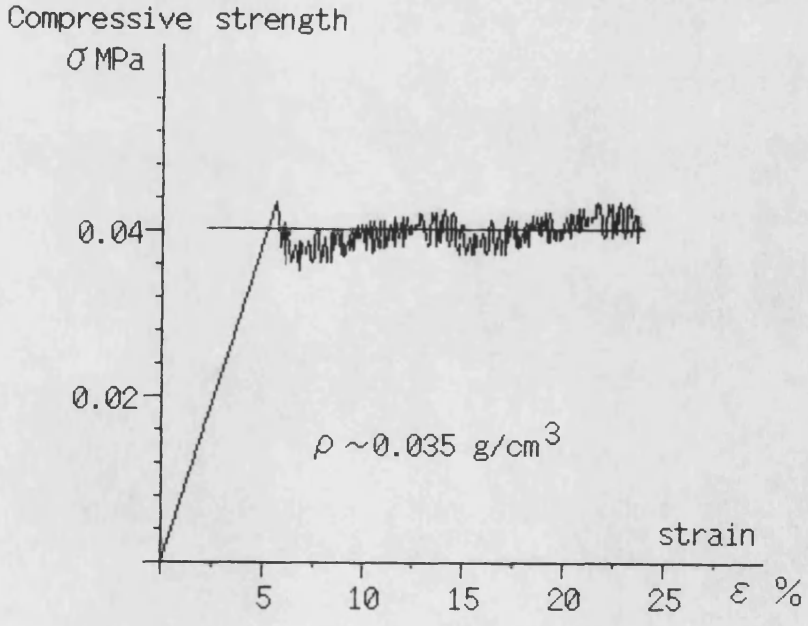

Figure IV-3-6 Schematic illustration of compressive stress-strain curve for carbon foams

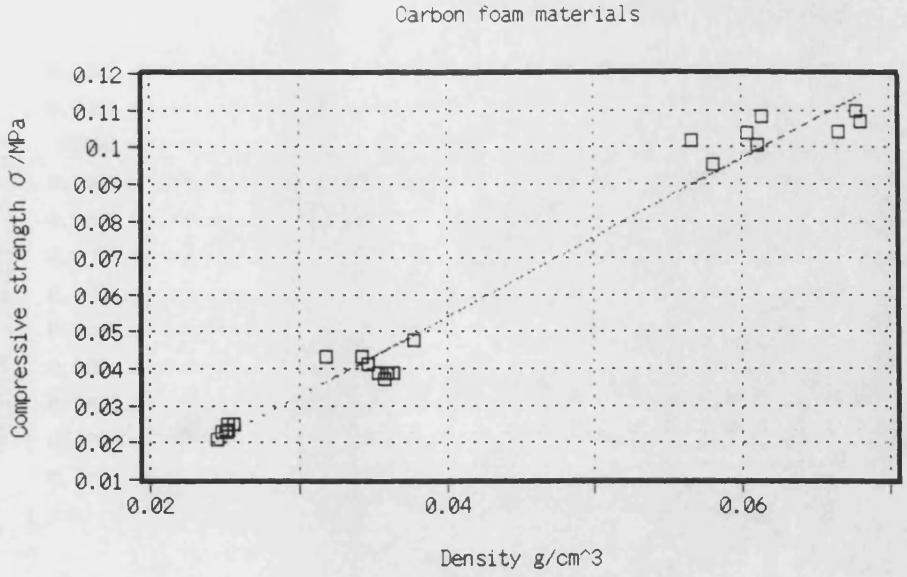

Figure IV-3-7 Compressive strength of carbon foams, plotted against bulk density

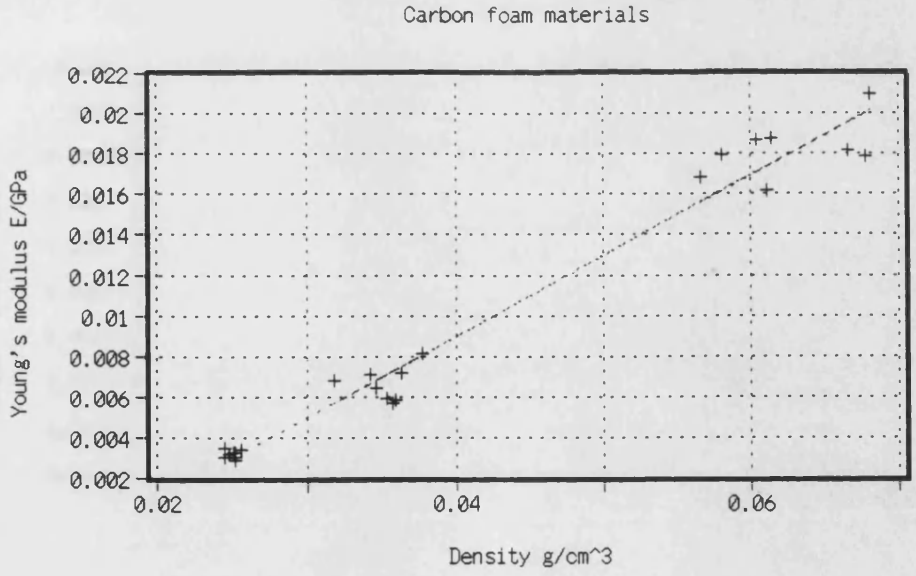

Figure IV-2-9 Compressive modulus of carbon foams, plotted against bulk density

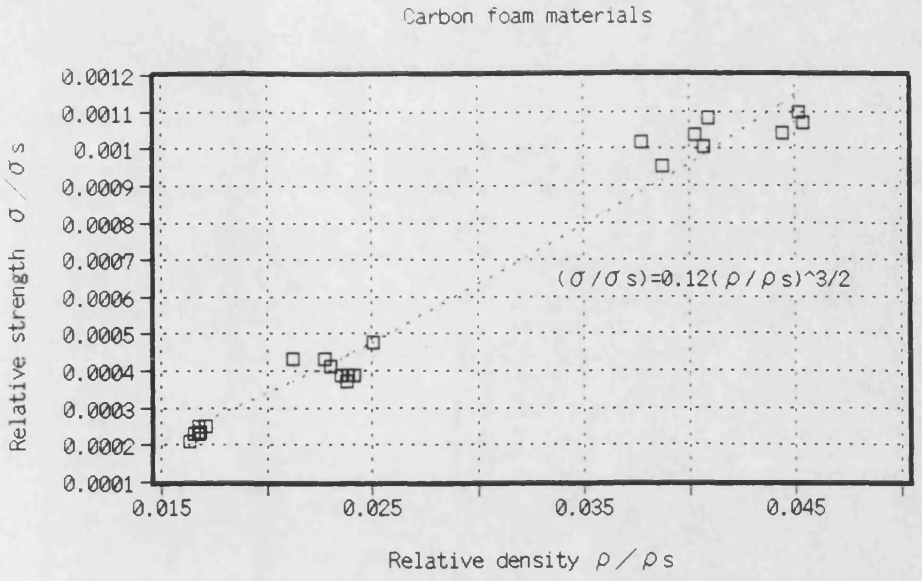

Figure IV-2-8 Relative compressive strength of carbon foams, plotted against relative density

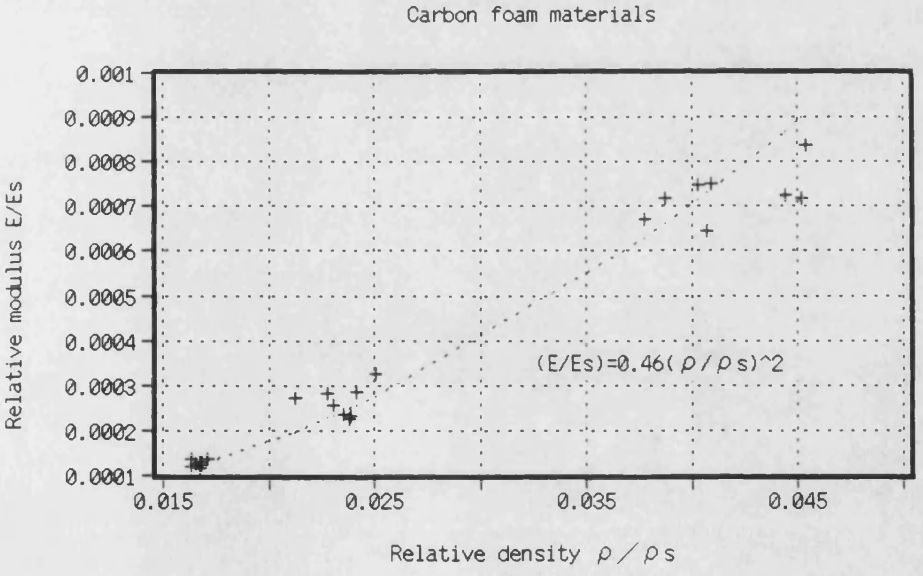

Figure IV-2-10 Relative compressive modulus of carbon foams, plotted against relative density

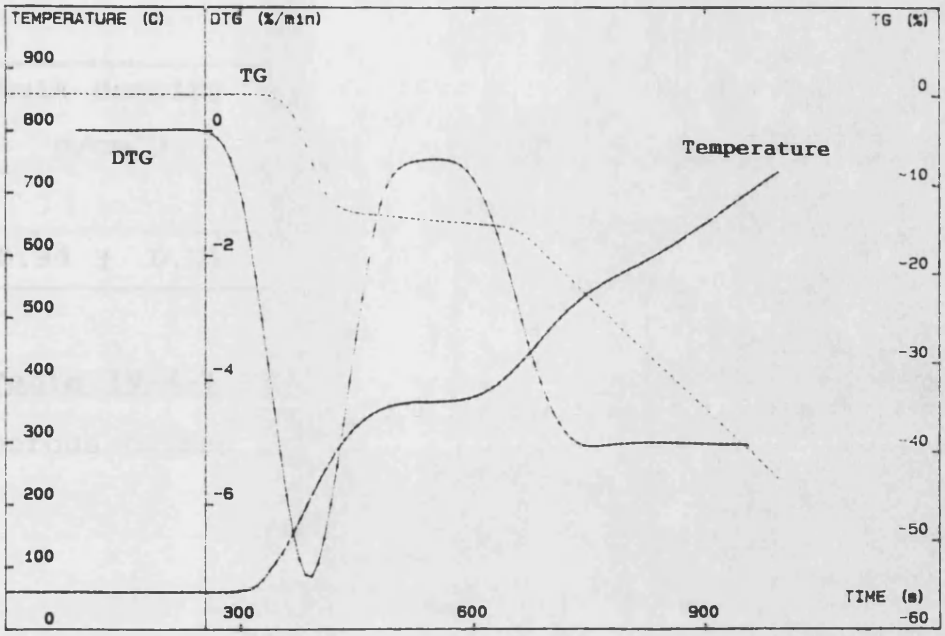

Figure IV-3-11

Thermogravimetric analysis of carbon foam (density 0.068g/cm^3) oxidized in air

Bulk density g/cm^3	Porosity %	Tensile Strength (split cylinder test) MPa
0.94 ± 0.01	44.4 ± 0.8	6.44 ± 0.10

Table IV-4-1 Physical properties of resin powder based porous carbon pellets

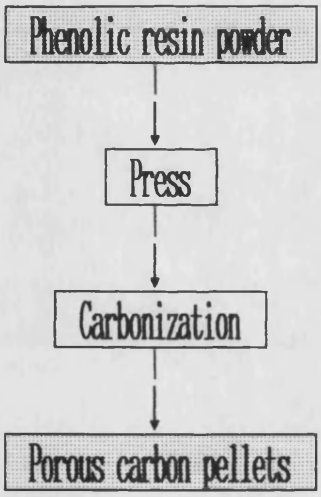

Figure IV-4-1

Manufacturing process for resin powder based porous carbon pellets

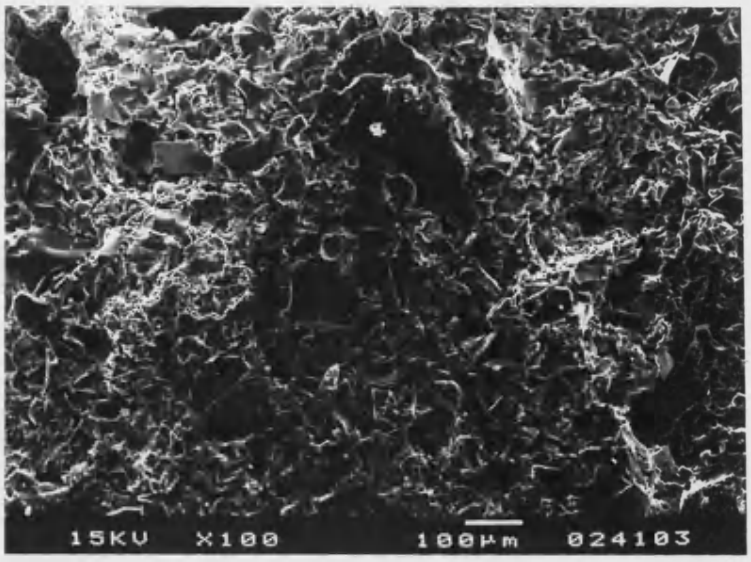

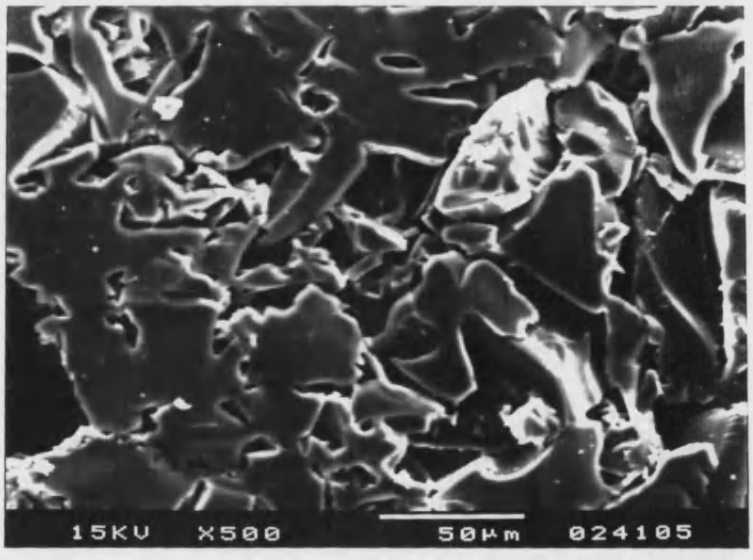

Figure IV-4-2 Scanning electron micrographs of resin powder based porous carbon pellets

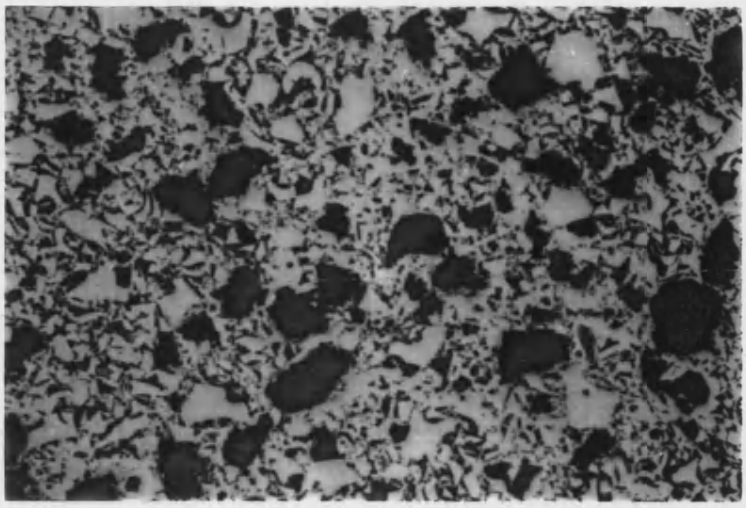

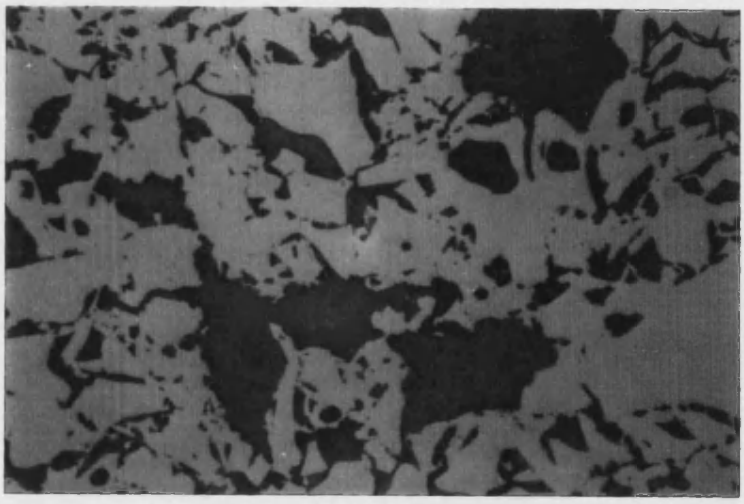

Figure IV-4-3 Optical micrographs of polished sections for resin powder based porous carbon pellets

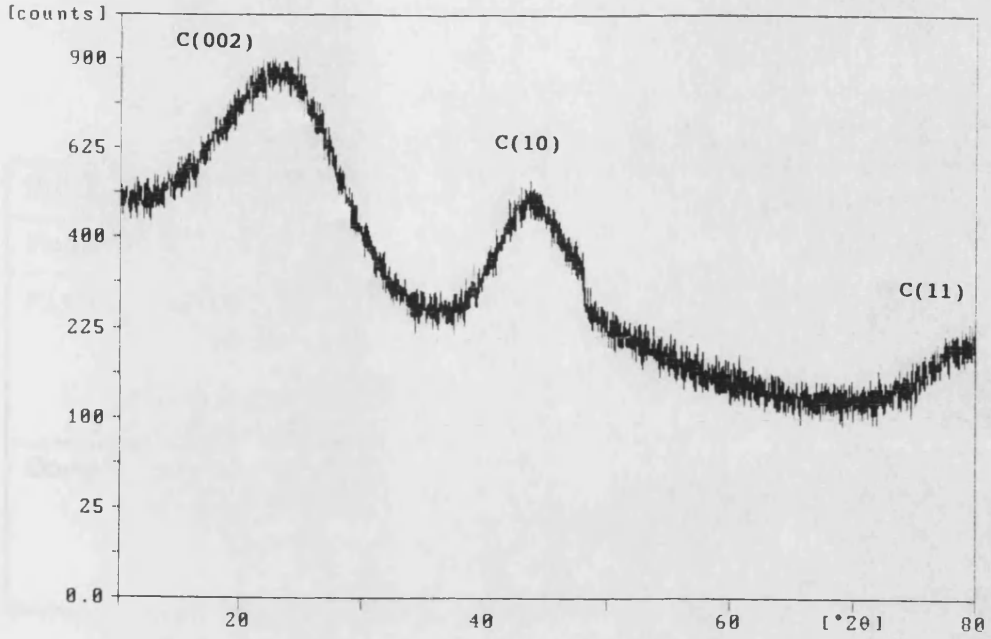

Figure IV-4-4 X-ray diffraction profile of resin powder based porous carbon pellets

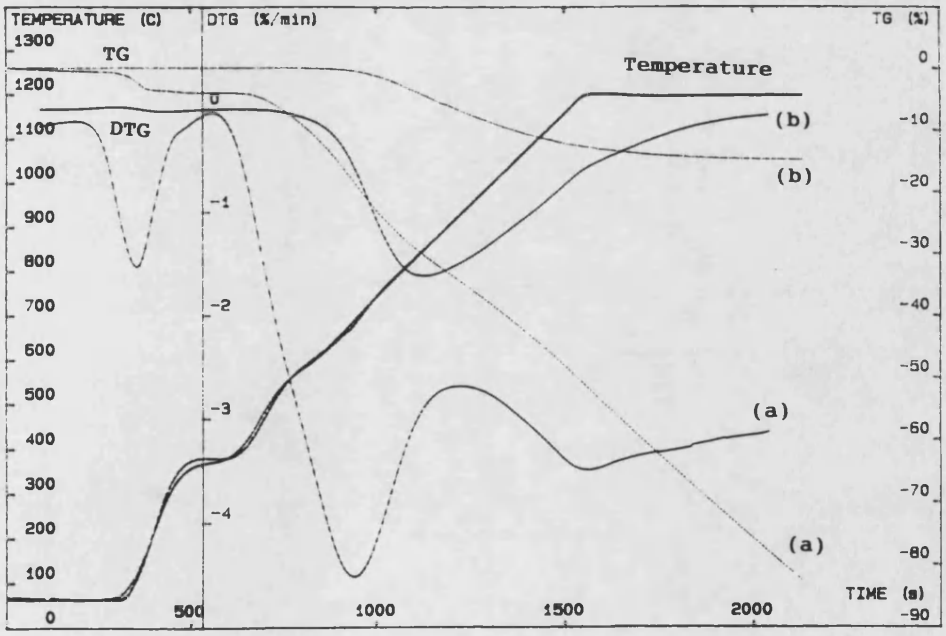

Figure IV-4-5 Thermogravimetric analysis of (a) resin powder based porous carbon pellets and (b) carbon - SiC/Si composites oxidized in air

Bulk density ρ (g/cm^3)	0.347 ± 0.006
Porosity p (%)	76.7 ± 0.4
Flexural properties	
Strength σ (MPa)	4.91 ± 0.36
Modulus E (GPa)	0.76 ± 0.07
Compressive properties	
Strength σ (MPa)	0.68 ± 0.13
Modulus E (GPa)	0.021 ± 0.006

Table IV-5-1 Physical properties of carbon bonded carbon fibre composites

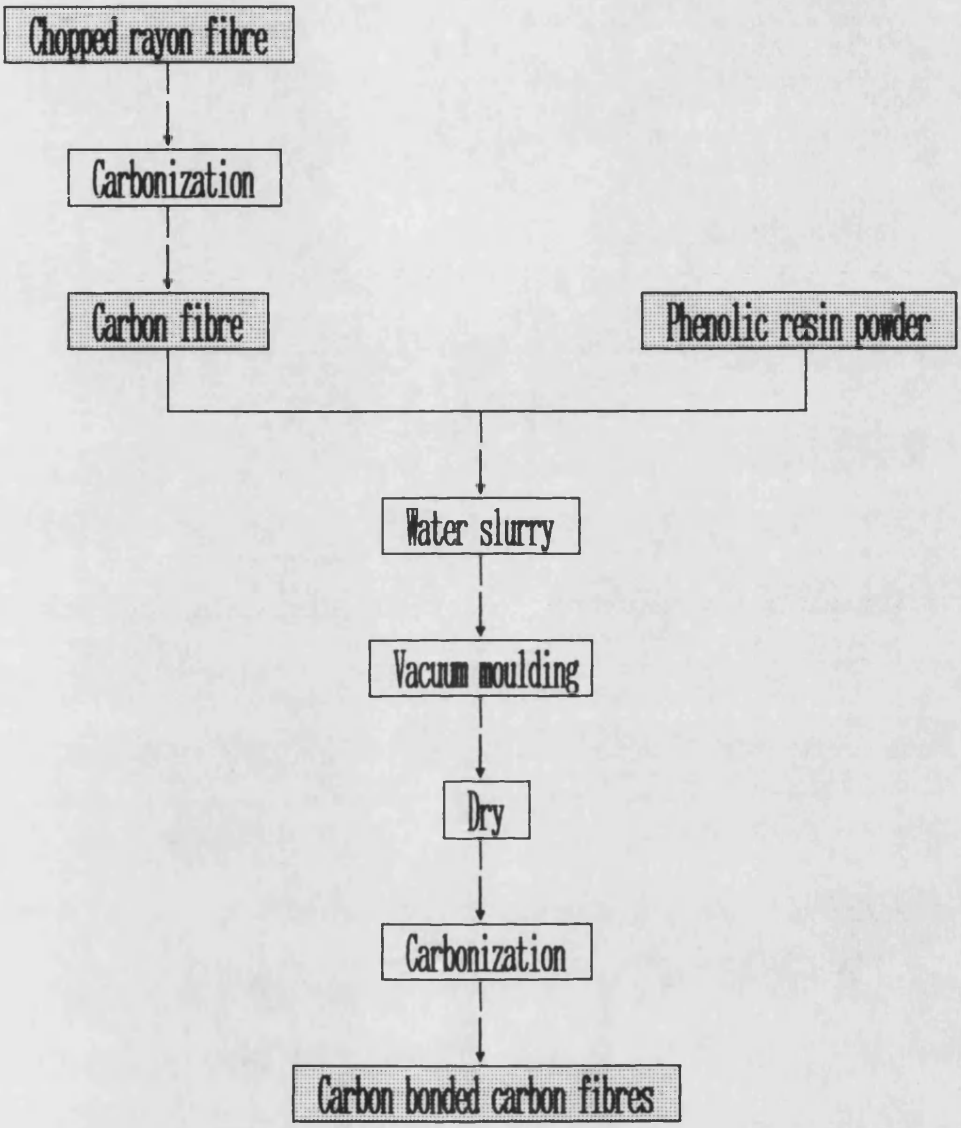

Figure IV-5-1 Manufacturing process of carbon bonded carbon fibre composites

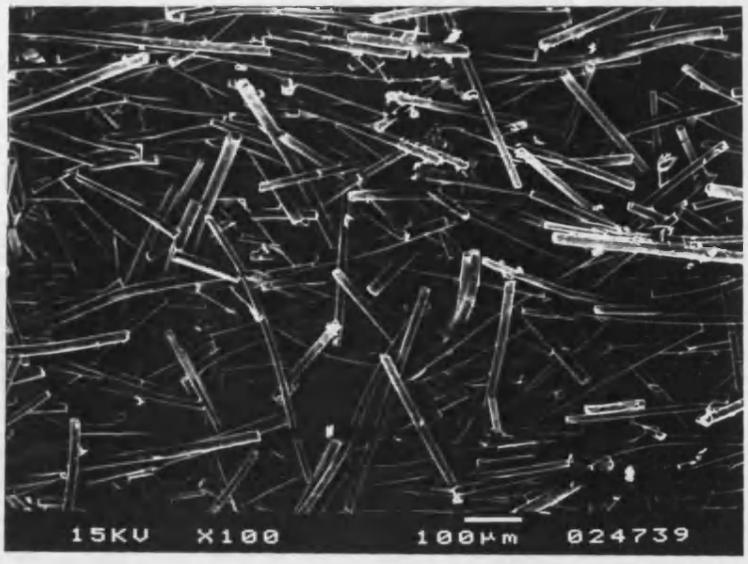

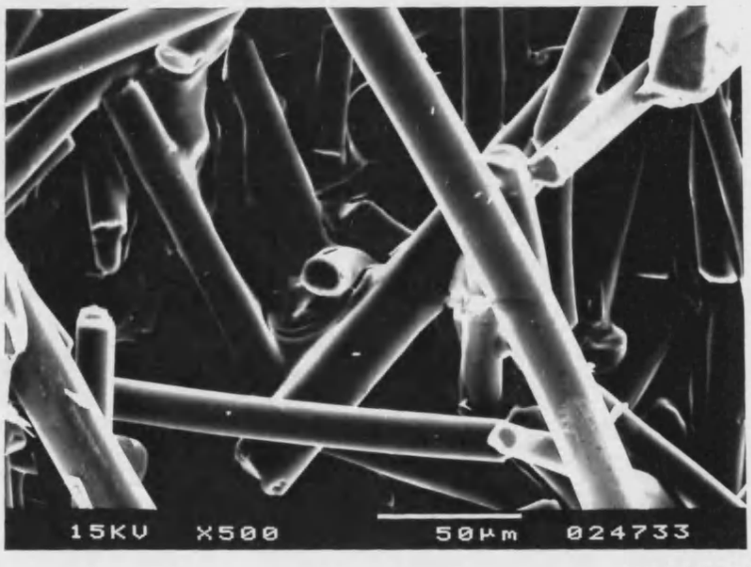

Figure IV-5-2 (a) Scanning electron micrographs of the surfaces for carbon bonded carbon fibre composites (perpendicular sections in the moulding direction)

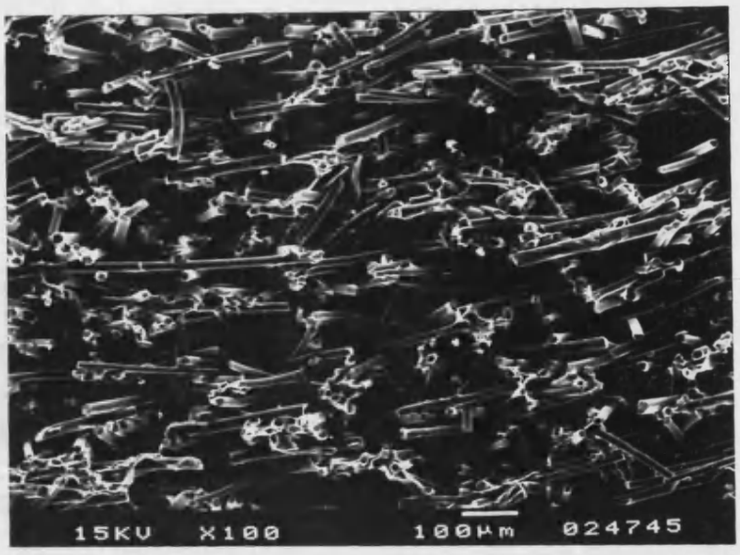

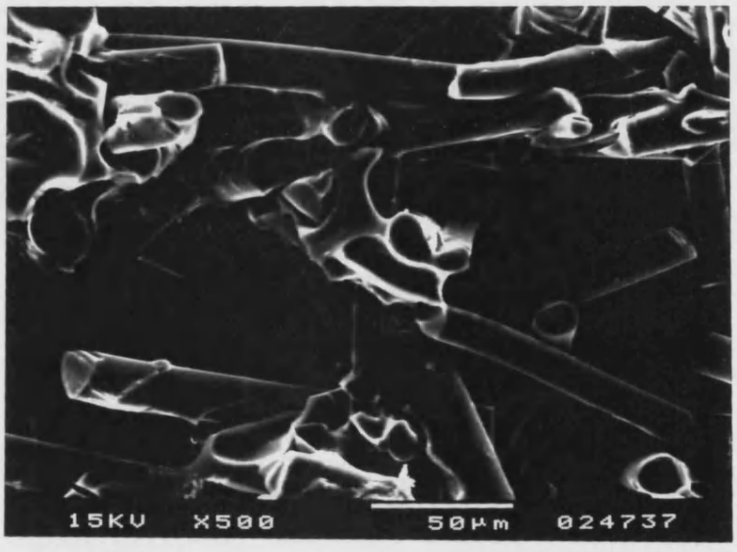

Figure IV-5-2 (b) Scanning electron micrographs of the fracture sections for carbon bonded carbon fibre composites
(parallel sections in the moulding direction)

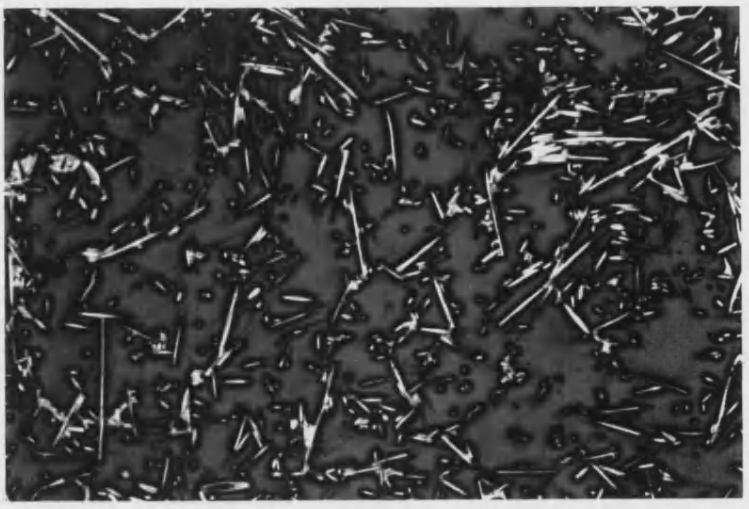

200 μm

50 μm

Figure IV-5-3 (a) Polished sections of carbon bonded carbon fibre composites
(perpendicular sections in the moulding direction)

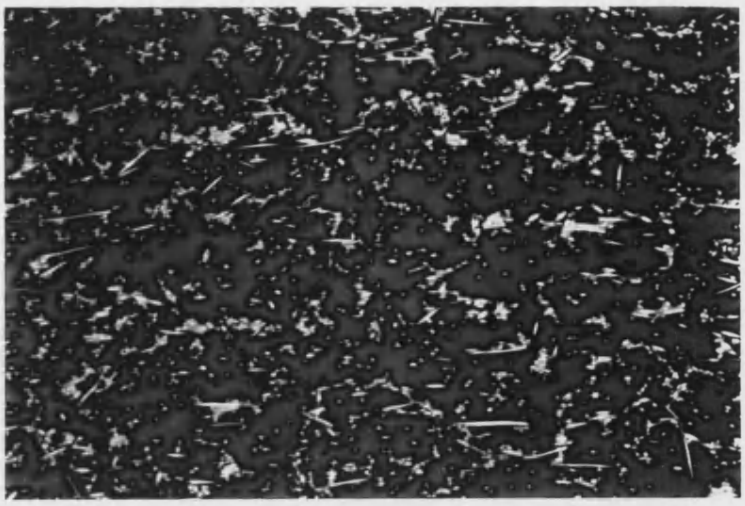

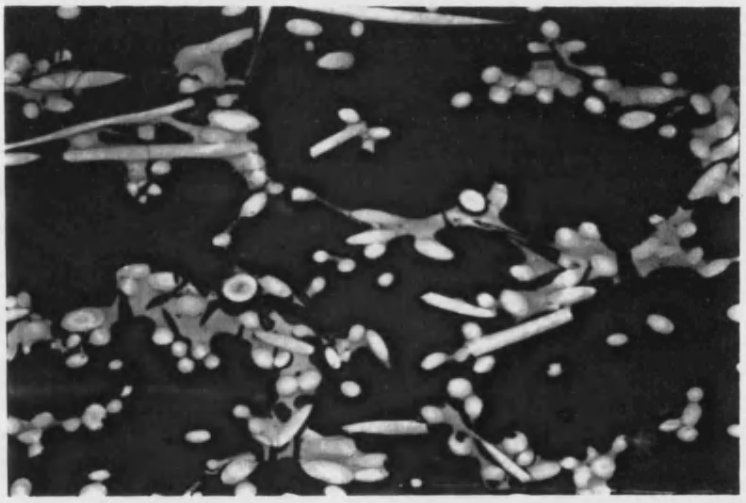

Figure IV-5-3 (b) Polished sections of carbon bonded carbon fibre composites
(parallel sections in the moulding direction)

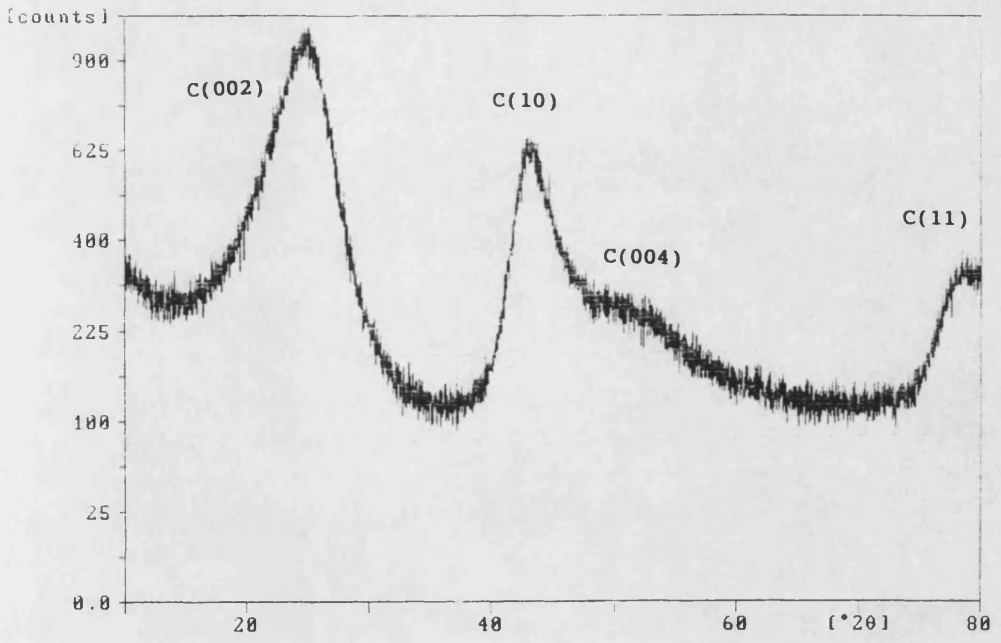

Figure IV-5-4 X-ray diffraction profiles of carbon bonded carbon fibre composites

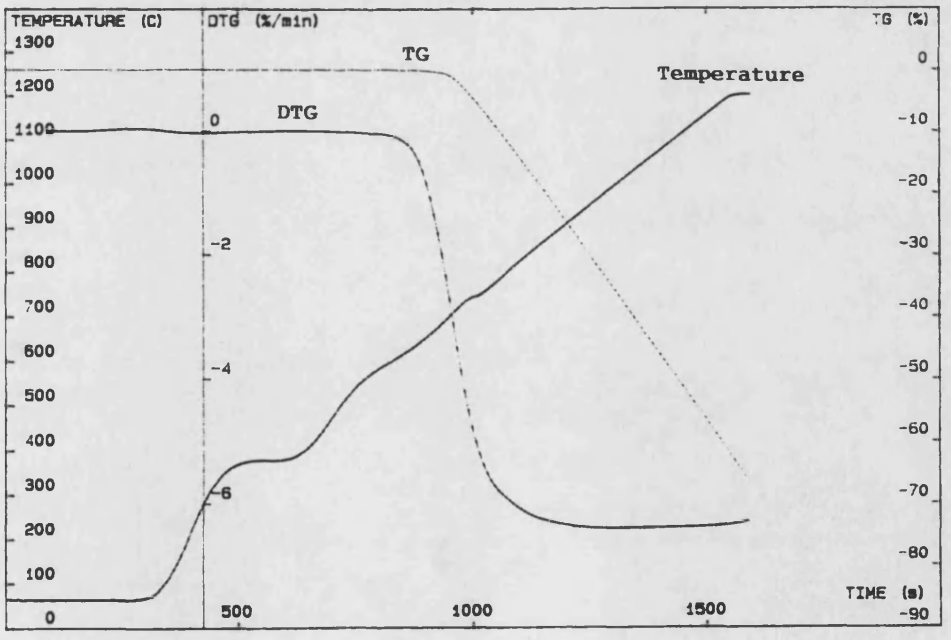

Figure IV-5-5 Thermogravimetric analysis of carbon bonded carbon fibre composites oxidized in air

CHAPTER V POROUS CARBON-CERAMIC COMPOSITES

V-1 Porous carbon - non-oxide silicon ceramic composites

V-1.1 Introduction

Porous carbon-ceramic composites were fabricated starting with infiltration of porous carbon preforms with a mixture of silica sol-gel and resin carbon source. The infiltrated silica-resin mixture was converted into non-oxide silicon ceramics. The synthesis of SiC was carried out by carbothermal reduction of silica with a carbon source in an argon atmosphere. Meanwhile, the synthesis of Si_3N_4 was conducted using the same starting material as that of SiC, but by carbothermal reduction and subsequent nitridation in a nitrogen atmosphere. (Figure V-1-1, p.195) Thus, porous carbons were converted into porous carbon-SiC or carbon-Si_3N_4 composites, via carbothermal reduction or nitridation of infiltrated SiO_2. Multiple infiltration was used until a composite of the required density was achieved. In addition, porous carbon-SiC composites were further impregnated with boron oxide (B_2O_3) in order to improve their oxidation resistance.

V-1.2 Manufacturing process

V-1.2.1 Materials

The following elements were used as starting materials for porous carbon-ceramic composites;

(1) Porous carbon preform: porous carbon materials fabricated by paper manufacturing technology

(2) Silicon ceramic source: a mixture of silica sol-gel, from hydrolysis and polymerization of silicon alkoxide (tetraethyl ortho silicate; TEOS) with acid catalyst (HCl) in acetone, and resol phenolic resin (British Petroleum, Cellobond J2027L) as a carbon source

The molar composition used in the experiments is:

TEOS	Acetone	Water	HCl	Carbon
1	3.2	8	0.03	ca.4

The composition of sol-gel for the non-oxide silicon ceramic precursor applied in this experiment was almost the same as the one that was found to offer the best compatibility of both drying and gelation processes with carbon materials. (Castro - 1991)

(3) Boron oxide source: orthoboric acid (H_3BO_3) in ethanol solution

Orthoboric acid was easily converted into boric oxide by heat treatment over 500° C to protect carbon materials against oxidation. (Ehrburger - 1986)

V-1.2.2 Procedure

Porous carbon preforms, fabricated by using paper making technology, were infiltrated with the mixture of silica sol and carbon source under reduced pressure, followed by treatment in a pressurized vessel at a pressure of 5 MPa. Then, this autoclave was heated at a temperature of 60° C for 24 hours to convert the sol into gel form. The gel-impregnated materials were dried at room temperature for 24 hours and at 60° C for 4 hours. The infiltrated silica gel was subsequently

converted into non-oxide silicon ceramics. Thus, these samples were fired in flowing argon or nitrogen gas (1000 cc/min) at 2 °C/min up to 1350° C in a horizontal tube furnace (Figure V-1-2, p.195), with a soaking time of 8 or 12 hours, to produce porous carbon-SiC or carbon-Si_3N_4 composites, respectively. This infiltration-firing procedure was repeated up to 3 times, to increase the amount of impregnated ceramics.

In addition to the SiC infiltration, porous carbon-SiC composites were impregnated with a solution of boric acid in ethanol (15 wt%), which was evaporated for 2 hours at 60° C. Thereafter, boric acid was converted into boron oxide by pyrolysis at a temperature of 500° C for 1 hour under a nitrogen gaseous atmosphere. Moreover, the composites were annealed at 700° C for 60 hours so that the deposit of boron oxide could spread over the materials.

V-2 Porous carbon-SiC composites

V-2.1 Structural characterization

V-2.1.1 Density and porosity

Typically the bulk density of the porous carbon preform was 0.51 g/cm^3. (Table V-2-1, p.196) After the first impregnation with SiO_2 and carbon source the bulk density was increased to ca. 0.7 g/cm^3. During the course of the carbothermal reduction of the silica to SiC, the bulk density steadily decreased to a value of 0.62 g/cm^3. (Table V-2-1) This transformation to SiC attained nearly saturation after 8 hours at 1350° C.

The composition of each component in the composites was calculated from the weight difference before and after each impregnation-firing process. The composition of the composites was indicated by approximate weights of SiC and B_2O_3 in proportion to the weight of carbon. These figures, in fact, cannot indicate the precise content of each component because the reactants were not completely converted into SiC, however they can be used as a convenient index. Tables V-2-1 and V-2-2 (p.196) summarize some physical properties of the composites.

The bulk densities of composites progressively increased with the infiltration of ceramics, at the same time, their apparent porosities gradually decreased. Nonetheless, their special features, such as high porosity and low density, still remained even after the ceramic impregnations.

V-2.1.2 Microscopic observation

(1) Scanning electron microscopy

The scanning electron micrographs of the porous carbons impregnated with SiC, are shown in Figure V-2-1 (p.197). The surfaces of carbon preforms were covered with plate-like-shaped SiC after the infiltration process. In the case of cross-sections, the pores of carbon preforms were observed to be filled with SiC.

Figure V-2-2 (p.198) shows scanning electron micrographs for carbon-SiC composites impregnated with B_2O_3. It can been seen that the surfaces were covered

with glassy layers of B_2O_3, and the pores inside the composites were further filled with the glass.

(2) Polarized optical microscopy

Figure V-2-3 (p.199) shows polarized light micrographs of polished cross-sections for the porous carbon-SiC composites. The impregnated SiC, which is detected as pale violet under polarized light, filled the pores of carbon materials after the impregnation process. It can be seen that the impregnated SiC is not a homogeneous structure and it may contain some unreacted residue, i.e., SiO_2 and carbon, in it.

Also, the polarized microscopy of carbon-SiC-B_2O_3 composites (Figure V-2-3 (b)) reveals that the glass appears as a black section which mainly fills the pores of carbon or SiC.

V-2.1.3 X-ray diffraction analysis

Figure V-2-4 (p.200) indicates X-ray diffraction profiles for porous carbon-SiC and carbon-SiC-B_2O_3 composites. Compared to the X-ray diffraction profile of the porous carbon preform (Figure IV-2-7, p.150), the carbon-SiC composites exhibited several new X-ray diffraction peaks which indicate the presence of β-SiC; 2θ = 35.6° hkl (111), 60.0° (220), and 71.8° (311). And the broad peaks around 2θ = 20-24° are ascribed to the reaction residue of glassy carbon from the resin. Therefore, the products appeared to consist of a mixture of SiC as a reaction product, and carbon and silica as reaction residues. In addition to those

peaks, the carbon-SiC-B_2O_3 composites show a diffraction peak at 2θ = 27.8° which can be ascribed to hkl (310) of B_2O_3.

V-2.2 Mechanical properties

The flexural properties of porous carbon-SiC and carbon-SiC-B_2O_3 composites with various weight proportions of components are shown in Tables V-2-1 and V-2-2 (p.196).

Porous carbon-ceramic composites exhibited a brittle failure mode under flexural stress. Thus, the stress-strain curves and fracture surfaces of the porous carbon-SiC and carbon-SiC-B_2O_3 composites are almost similar to those formed by the porous carbon preforms.

The flexural strengths of composites improved steadily in proportion to the amount of impregnated SiC. The effect of B_2O_3 glass on improving of flexural strength was also observed as shown in Figure V-2-5 (p.201).

The Young's modulus of composites also increased in proportion to impregnation of SiC. However, the most remarkable phenomenon is that the impregnation with B_2O_3 glass resulted in a radical increase in Young's modulus. (Figure V-2-6, p.201)

With the increase of impregnated SiC, the strain to failure of the composites slightly declined to 4.2 - 4.4% from 4.7%. It is worth noticing that the strain to failure of composites that contain B_2O_3 declined dramatically up to 3.1%. Hence, brittleness was increased in composites with only a slight amount of

B_2O_3 glass.

Thus, SiC infiltration increased the strength of carbon composites, but additions of B_2O_3 resulted in an increase of brittleness as well as strength.

V-2.3 High temperature corrosion resistance

V-2.3.1 Thermogravimetric analysis

The thermogravimetric analysis up to 1000° C for the porous carbon-SiC and carbon-SiC-B_2O_3 composites is shown in Figure V-2-7 (p.202). The threshold temperature of oxidation for carbon-SiC composites decreased ca. 200° C in contrast with porous carbon preforms alone, presumably due to carbon residue from the phenolic resin. The oxidation resistance of the carbon preform was little improved by the SiC impregnation, and this appears to be an inadequate measure for improving the high temperature performance of the materials in air.

The carbon-SiC-B_2O_3 composites exhibited small amounts of weight loss starting around 100° C. This may be dehydration of B_2O_3, because B_2O_3 glass is so hygroscopic that it can easily contain some water in the form of boric acid. However, the main weight decrease began from a slightly higher temperature compared with that of carbon-SiC composites. The inhibition of oxidation up to 800° C was definitely improved with the B_2O_3 glass impregnation. However, above about 1000° C the rate of oxidation increased again. This may be caused by the vaporization of B_2O_3

that starts normally around 1100° C, indicating that the maximum operation temperature of B_2O_3 is below 1000° C. Therefore, thermogravimetric analysis up to 800° C was carried out in order to investigate the oxidation resistance at temperatures below the vaporization temperature of B_2O_3. (Figure V-2-8) It was noted that carbon-SiC-B_2O_3 composites have higher oxidation resistance at 800° C as compared with carbon-SiC composites. Consequently, it was concluded that the SiC-B_2O_3 system may be useful in inhibiting of oxidation of these materials at operating temperatures under 1000° C.

V-2.3.2 Microscopic observation

The carbon-SiC-B_2O_3 composites were oxidized in air at 800° C, and the changes of microstructures during oxidation were observed by using microscopic technique.

The morphology of surfaces began to change on a large scale, after 2 hours' oxidation. It appears that a new phase was formed on the surfaces of composites. From that time on, this new phase grew bigger and spread all over the surfaces in a mosaic formation. At the same time, the pores which may have been produced by oxidation of the carbon component, increased steadily in proportion to oxidation treatment. (Figure V-2-9, p.203) Meanwhile, inside the composites, the pores, formed by oxidation of the carbon component, enlarged with the progress of oxidation, and the morphology of the cross-section finally changed noticeably. (Figure V-2-10, p.204)

Figure V-2-11 (p.205) shows the polarized optical micrographs of the composites after 8 hours' oxidation at 800° C. The protective layer produced by oxidation of SiC-B_2O_3, was formed within mainly about 400 μm on the surface. However, the carbon components in the inside of composites did not benefit from this protective effect. As a result, they oxidized exclusively.

Accordingly, in the case of the oxidation treatment of carbon-SiC-B_2O_3 composites, the protective phase was formed mainly near the surface. However, this phase was hardly observed in the inside of composites, so that the oxidation of the interior of the carbon components proceeded steadily.

V-2.3.3 Fourier transform infra-red analysis

The surface changes of carbon-ceramic composites during oxidation at high temperatures in air, were investigated by utilizing infra-red dispersive reflection spectroscopy, which is a useful method for detecting structural changes and chemical transformations that occur within 0.5 μm of the surface. (Takase - 1985) The composite samples were oxidized in air for various times at 800° C. The oxidized specimens were rapidly cooled down to retain the surface characteristics at the oxidation temperatures, and immediately thereafter infra-red reflection spectroscopy of the surfaces was measured without any special treatment.

Figure V-2-12 (p.206) shows the surface changes of

carbon-SiC composites during oxidation. The band of 800 cm^{-1} may be ascribed to the vibrational mode of SiC. After oxidation treatment, bands around 1100 cm^{-1} and 470 cm^{-1}, which may be assigned to the Si-O stretching mode and the Si-O bending mode, respectively, were observed. This indicates either that the silica residue in the reaction product was exposed to the surface, because the carbon residue was easily oxidized, or SiC was oxidized to silica at this relatively low temperature owing to its high surface area.

Figure V-2-13 (p.207) indicates the surface changes of the carbon-SiC-B_2O_3 composites at various degrees of oxidation at temperatures of 800° C.

In the spectrum of the unoxidized carbon-SiC-B_2O_3 composites (oxidation 0hour), the bands of 3240, 1520, 1200, and 725 cm^{-1} can be ascribed to B_2O_3, which are comparable to those of boron oxide glass as reported previously. (Parsons - 1960) It is well known that B_2O_3 is so hygroscopic that it can easily absorb water from the atmosphere, after which boric acid is formed on the surface of B_2O_3. Therefore, the band of 3240 cm^{-1} can be assigned to the O-H stretching vibrational mode of boric acid. In addition, the band of 800 cm^{-1} may be ascribed to the vibrational mode of SiC.

After oxidation, the band at 1090 cm^{-1}, which can be assigned to the Si-O stretching mode, was formed, and its intensity grew stronger with the oxidation treatment. Meanwhile, the band of 800 cm^{-1}, the vibrational mode of SiC, disappeared.

There were two remarkable changes in spectrum after extended exposures in air at 800° C. One phenomenon is that the band of 1250cm^{-1}, which may be ascribed to boric acid, gradually shifted to higher frequencies, and finally it came to be integrated into the strong broad band around 1400cm^{-1} with the progress of the oxidation treatment. The strong broad band near 1400cm^{-1}, which is characteristic of dried B_2O_3 glass containing no water, can be assigned to the B-O stretching vibrational modes. The shift of frequencies and the formation of the strong broad band can be explained by evolution of stability of the B_2O_3 structure against moisture due to the incorporation of SiO_2 into the B_2O_3 glass.

The other phenomenon is the disappearance of the band assigned to the O-H stretching vibration around 3200 cm^{-1}. It was reported that B_2O_3 glass containing a certain amount of oxides did not exhibit the band caused by the O-H stretching mode. (Konijnendijk - 1975)

Therefore, these observations may suggest that a borosilicate glass was possibly produced during oxidation treatment by the intrusion of SiO_2 into the B_2O_3 glass. It is well known that borosilicate glass can be formed from a mixture of B_2O_3 and SiO_2.

In conclusion, at the early stage of the oxidation treatment, oxidation of the carbon and SiC occurred mainly on the surface where intimate contact with oxygen could be expected. Then, B_2O_3 glass might move

toward the surface of composites to form borosilicate glass. This new glassy phase was effective in protecting carbon from oxidation within about 400 μm of the surface.

V-3 Porous carbon-Si_3N_4 composites

V-3.1 Structural characterization

V-3.1.1 Density and porosity

The carbothermal reduction and nitridation of silica steadily progressed at 1350° C with increase of reaction time, and the density/porosity of the composites after 12 hours' reaction at 1350° C became almost constant. Multiple infiltration procedure up to 3 times was conducted, and Tables V-3-1 (p.208) shows their physical properties which include the weight ratio of components, bulk density, and porosity.

V-3.1.2 Microscopic observation

(1) Scanning electron microscopy

It can be seen in Figure V-3-1 (p.209) that at the early stage of the reaction (4 hours at 1350° C), the morphology of the reaction products had a microporous bulky formation which may consist of a mixture of a small amount of Si_3N_4, and a large amount of unreacted residue of carbon and silica. However, with increasing reaction time (12 hours), the structure of products became much more microporous, as shown in Figure V-3-2 (p.210), because more carbon and silica were converted into Si_3N_4. At the same time, whisker-like Si_3N_4 can be observed partially around the microporous Si_3N_4.

Therefore, two types of Si_3N_4 were formed via different reaction mechanisms. Zhange et al. (1984) proposed that the reaction mechanisms for formation of silicon nitride proceed in two ways: first, there is nucleation of Si_3N_4 which occurs on the carbon or SiO_2 surface, and secondly there is growth via a gas phase reaction between SiO, CO, and N_2 on the growing Si_3N_4 particles, as in the following formulae.

$$3SiO(g) + 3C(s) + 2N_2(g) \longrightarrow Si_3N_4(s) + 3CO(g)$$

$$3SiO(g) + 3CO(g) + 2N_2(g) \longrightarrow Si_3N_4(s) + 3CO_2(g)$$

Hence, at the initial stage of nitridation of SiO, generated via carbothermal reduction of silica, the nucleation of Si_3N_4 occurred in the carbon-silica mixtures and this formation grew with progress of reaction time. This reaction product via solid-gas phase reaction had a microporous structure which consisted of a mixture of formed Si_3N_4 and unreacted residue of carbon and silica. After the nucleation, whisker-like Si_3N_4 also grew partially around the microporous Si_3N_4 via a gas phase reaction.

(2) Polarized optical microscopy

Figure V-3-3 (p.211) shows polarized optical micrographs of the polished cross section of porous carbon-Si_3N_4 composites. The reaction product filled the pores of the carbon preforms. It can be also realized that the reaction products in the specimens had a microporous formation, and they seemed to consist

of a mixture of Si_3N_4 and unreacted residue to some extent, as found by other techniques.

V-3.1.3 X-ray diffraction analysis

The X-ray diffraction profile of porous carbon-Si_3N_4 composites is shown in Figure V-3-4 (p.212). In addition to the peaks of graphite, X-ray diffraction peaks that can be ascribed to Si_3N_4 can be observed. Silicon nitride consisted of a mixture of α- and β-phases. X-ray diffraction peaks of SiO_2 could not be observed during the reaction at all, thus silica may exist as an amorphous structure.

The most noteworthy phenomenon in the X-ray diffraction analysis is that peaks due to SiC or Si_2N_2O, which can exist in the Si-C-O-N system (Siddiqui - 1985), were not observed at all. In particular, Si_2N_2O was considered as one of the intermediates to Si_3N_4, and Wada et al. (1990) reported that Si_2N_2O is the stable phase during the early stage of the reaction. The reason why Si_2N_2O was not observed at all is not clear, however, it is possible reason that the oxygen partial pressure in the experimental system was too low to generate any Si_2N_2O.

V-3.2 Mechanical properties

The infiltration-firing procedure was repeated up to 3 times in order to increase the amount of Si_3N_4 in the composites. Then, mechanical properties of the carbon-Si_3N_4 composites were measured including flexural strength and elastic modulus by using 3-point bending

method. The results of flexural strength and Young's modulus are shown in Table V-3-1 (p.208).

Both the flexural strength and elastic modulus slightly increased with increasing amount of infiltrated Si_3N_4. The infiltrated ceramic did not produce a remarkable improvement of mechanical properties presumably due to its extremely microporous structure as detected by microscopic observation.

V-3.3 High temperature corrosion resistance

The oxidation behaviour of carbon-Si_3N_4 composites at high temperatures in air was investigated.

V-3.3.1 Thermogravimetric analysis

The oxidation resistance of carbon preforms was not improved at all by infiltration of the ceramic. (Figure V-3-5, p.212) The carbon preforms were steadily burned off by oxidation with increasing temperature. As with the SiC infiltration, the composites started their oxidation around 400° C which was about 200° C lower than the unmodified preform presumably due to the carbon residue which had a glassy structure.

V-3.3.2 Fourier transform infra-red analysis

The porous carbon-Si_3N_4 composites were oxidized at 800° C in air for various times. The oxidized samples were subjected to infra-red reflection spectroscopy of the surfaces. Figure V-3-6 (p.213) shows the structural and chemical changes at the surface of carbon-Si_3N_4 composites resulting from oxidation treatment.

After oxidation treatment, bands around 1200 cm^{-1}

which may be assigned to the Si-O stretching mode, were observed. As with the carbon-SiC composites, this may be because the silica residue in the reaction product was exposed to the surface as a result of oxidation of the carbon residue in the early stages of reaction, or Si_3N_4 was oxidized to silica at a relatively low temperature owing to its high surface area.

V-4 Conclusion

The method to produce porous carbon-ceramic composites by infiltration of a silica sol-gel, which was subsequently converted into SiC or Si_3N_4 via carbothermal reduction or nitridation, into porous carbon preforms, was found not to be an effective technique to fabricate high-temperature materials with oxidation resistance in air because:

(1) The infiltrated ceramics did not protect the carbon preforms sufficiently against oxidation.

(2) The ceramic yield of the silica sol-gel with resin carbon was quite low. The reaction products were a mixture of silicon ceramics and a considerable amount of unreacted residue, i.e., carbon and silica.

(3) The physical properties and microstructures of reaction products were greatly influenced by various experimental parameters.

Consequently, a more straightforward and direct technique was investigated for manufacturing of highly porous and low-density ceramic materials which is described in Chapter VI.

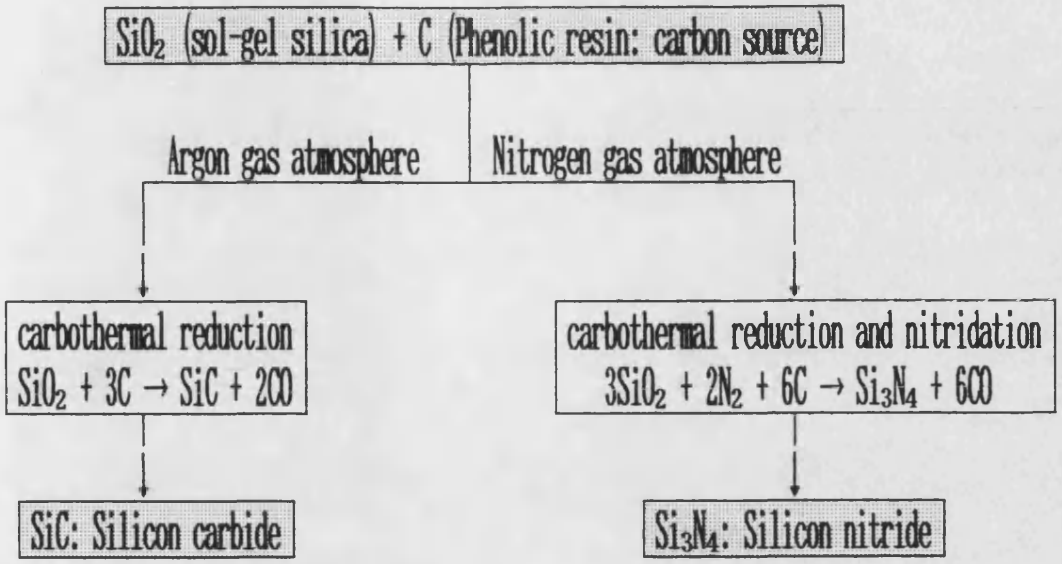

Figure V-1-1 Conversion of sol-gel silica with carbon into non-oxide silicon ceramics by carbothermal reduction and nitridation

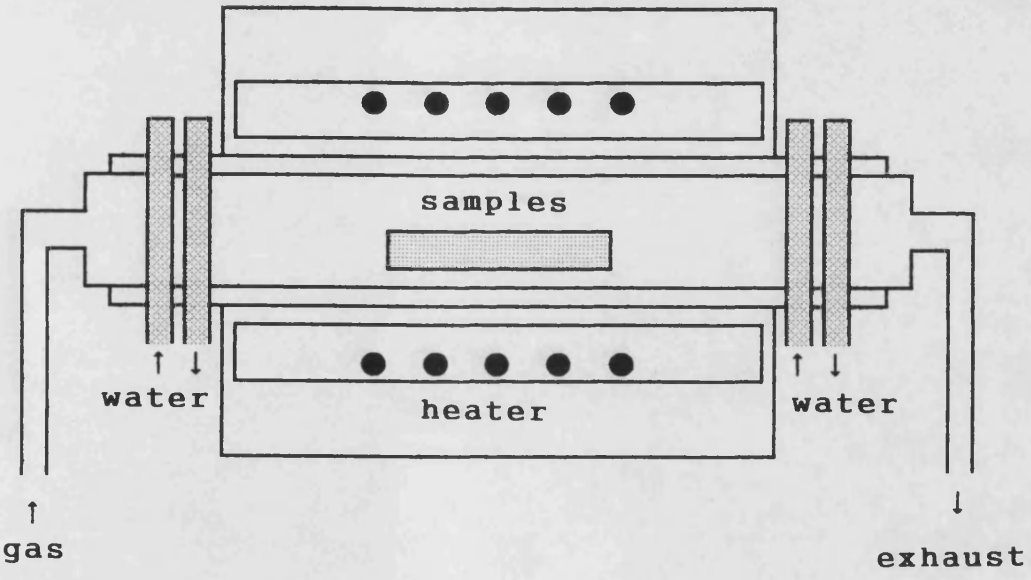

Figure V-1-2 Tube furnace for carbothermal reduction and nitridation of silica infiltrated in porous carbon preforms

Specimen	Weight proportion		Bulk Density [g/cm^3]	Apparent Porosity [%]	Flexural strength [MPa]	Young's modulus [GPa]
	Carbon	SiC				
Porous carbon materials	100	0	0.51	73	13.7	2.92
Porous carbon-SiC composites	100	20	0.62	68	15.1	3.34
	100	40	0.71	63	17.0	4.02
	100	50	0.77	60	20.4	4.65

Table V-2-1

Physical properties of porous carbon-SiC composites

Specimen	Weight proportion			Bulk Density [g/cm^3]	Flexural strength [MPa]	Young's modulus [GPa]
	Carbon	SiC	B2O3			
Porous carbon-SiC-B2O3 composites	100	20	10	0.64	16.4	4.44
	100	20	15	0.65	17.9	4.61
	100	20	25	0.70	19.3	5.15
	100	40	10	0.72	18.0	5.29
	100	40	15	0.75	19.2	5.72
	100	40	25	0.79	20.9	6.00
	100	50	10	0.79	20.6	6.13
	100	50	15	0.81	20.8	6.71
	100	50	25	0.83	21.7	7.06

Table V-2-2

Physical properties of porous carbon-SiC-B_2O_3 composites

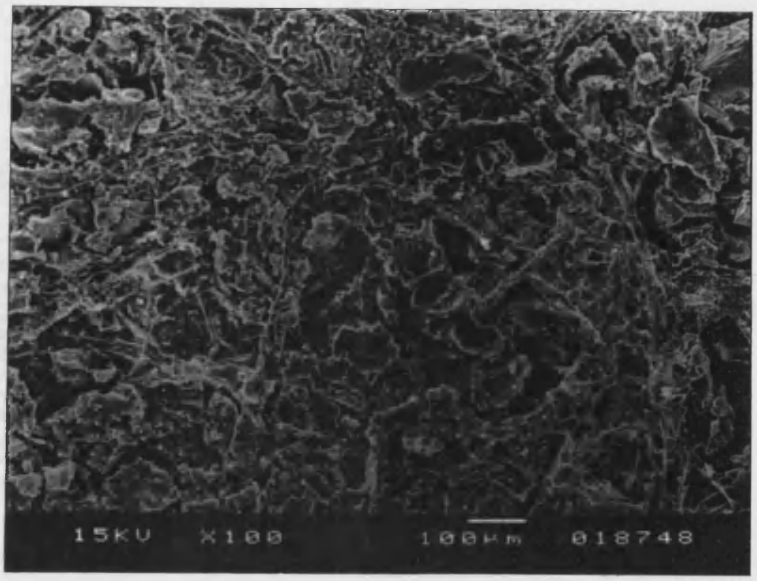

(a)

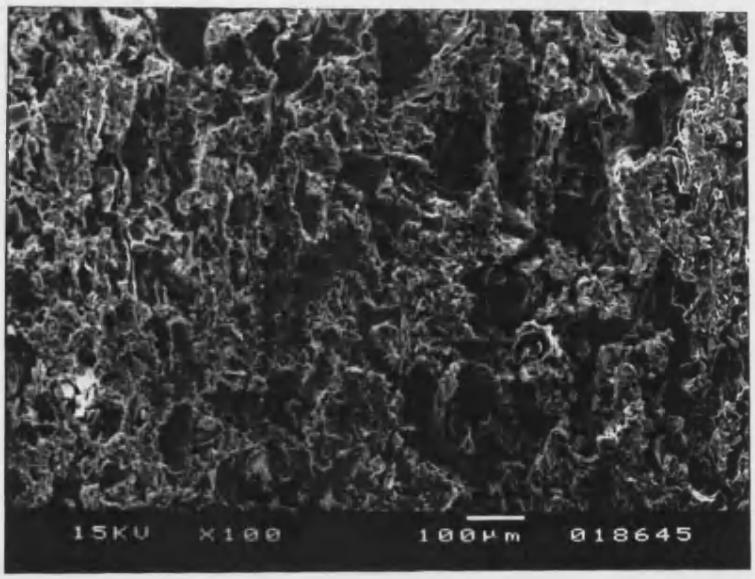

(b)

Figure V-2-1 Scanning electron micrographs of porous carbon-SiC composites (a) surface, (b) fracture section

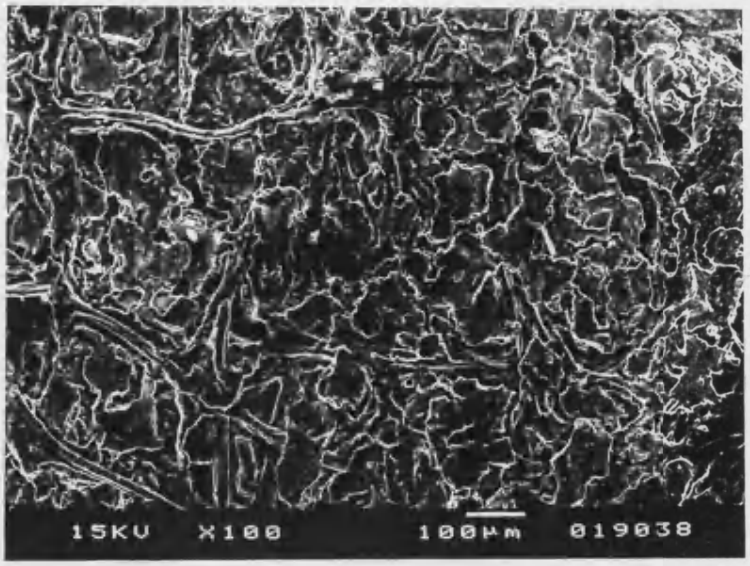

(a)

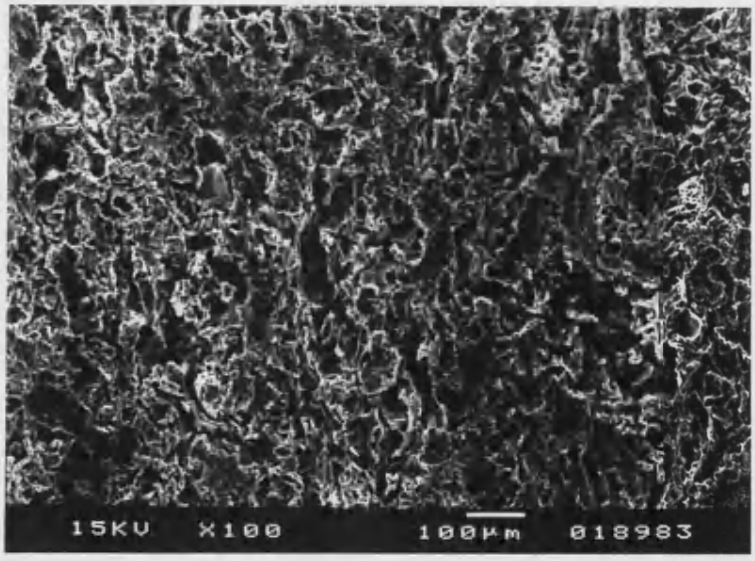

(b)

Figure V-2-2 Scanning electron micrographs of porous carbon-SiC-B_2O_3 composites (a) surface, (b) fracture section

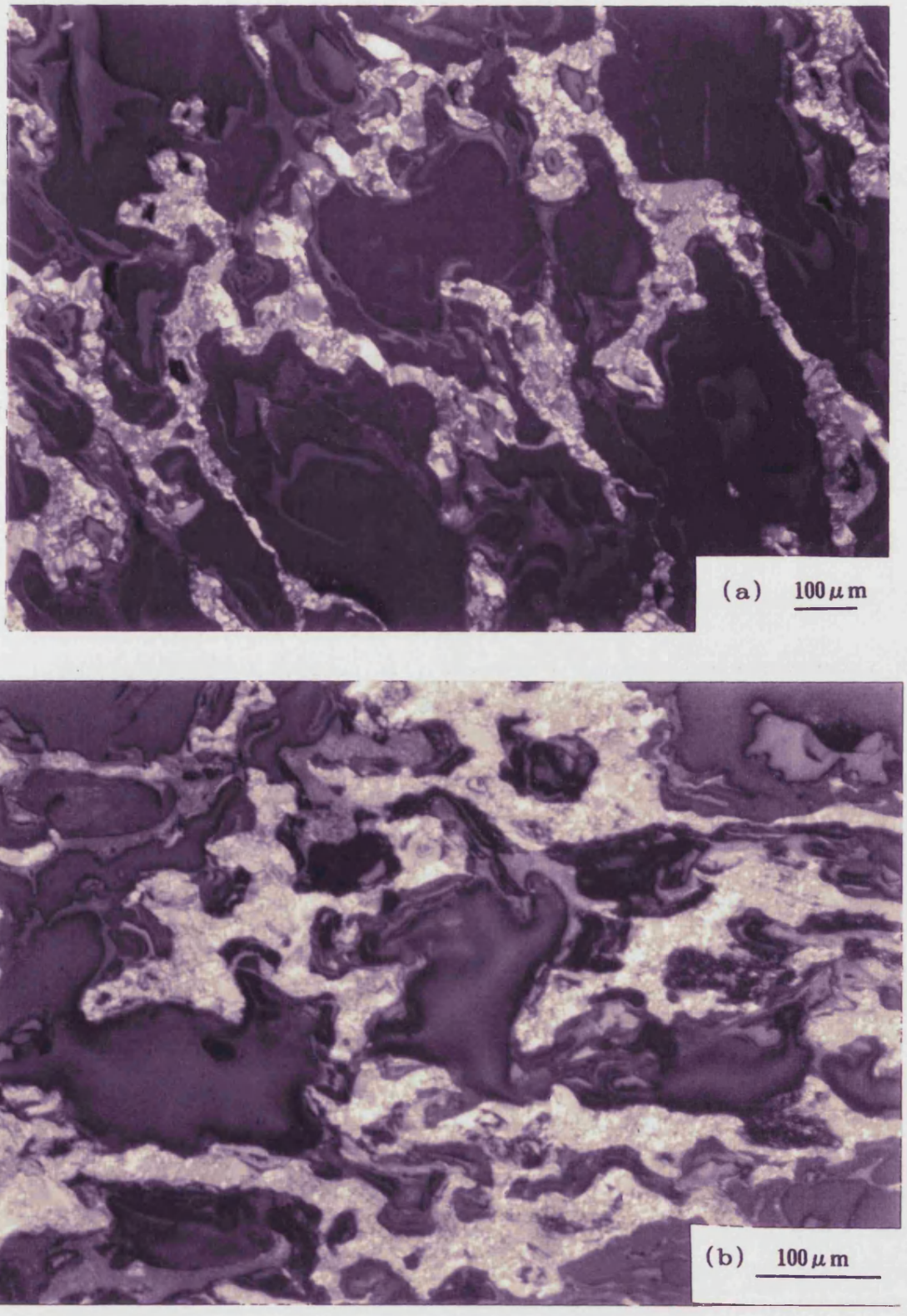

Figure V-2-3 Polarized light micrographs of porous (a) carbon-SiC and (b) carbon-SiC-B_2O_3 composites

(a) carbon-SiC composites

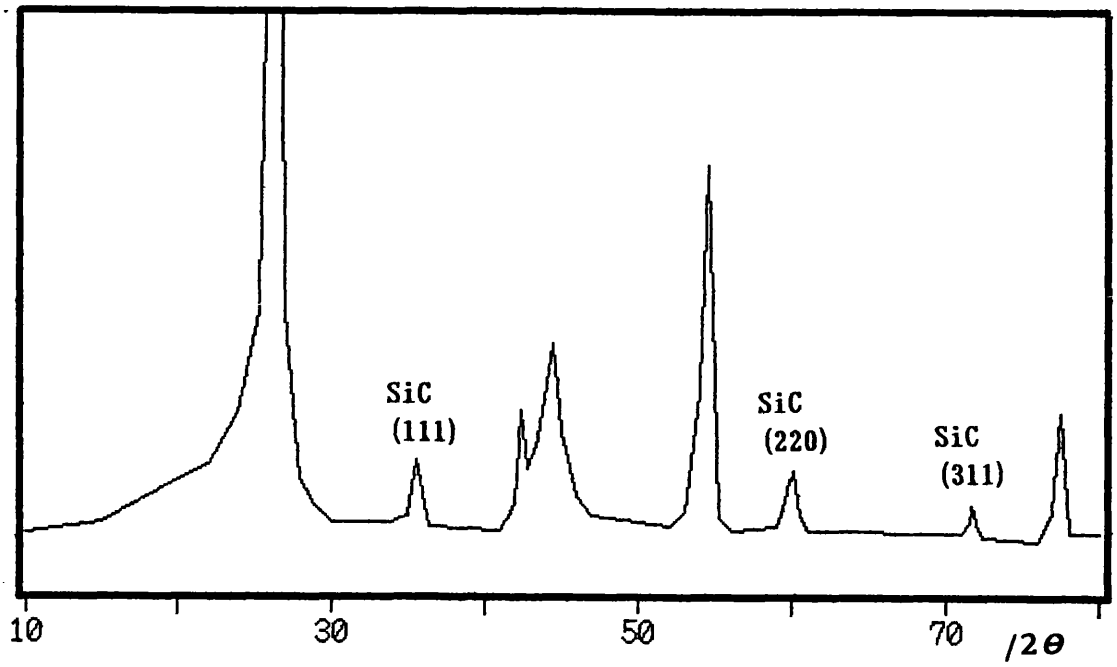

(b) carbon-SiC-B_2O_3 composites

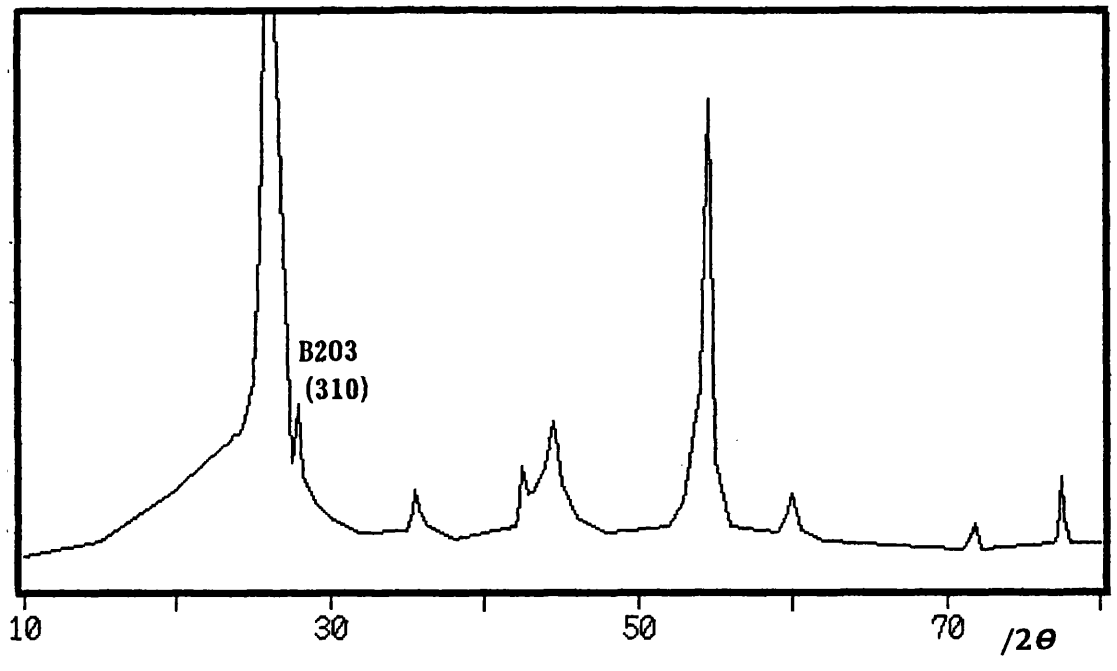

Figure V-2-4 X-ray diffraction profiles of porous (a) carbon-SiC and (b) carbon-SiC-B_2O_3 composites

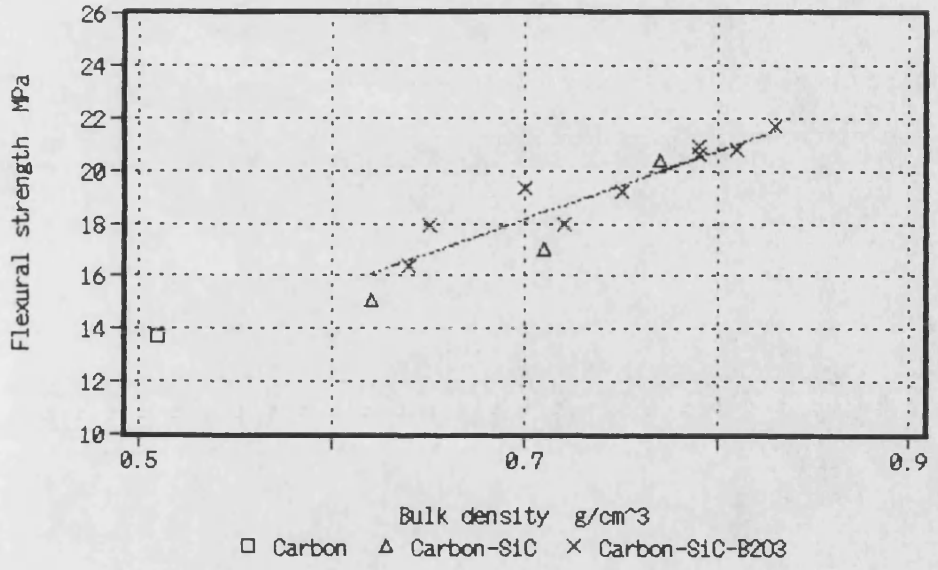

Figure V-2-5 Flexural strength of porous carbon-SiC and carbon-SiC-B_2O_3 composites, plotted against bulk density

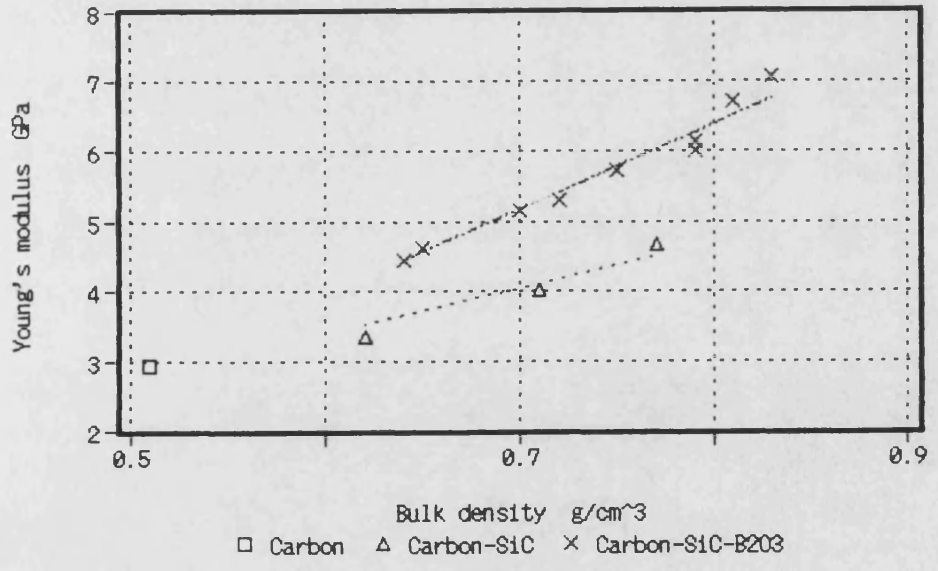

Figure V-2-6 Flexural modulus of porous carbon-SiC and carbon-SiC-B_2O_3 composites, plotted against bulk density

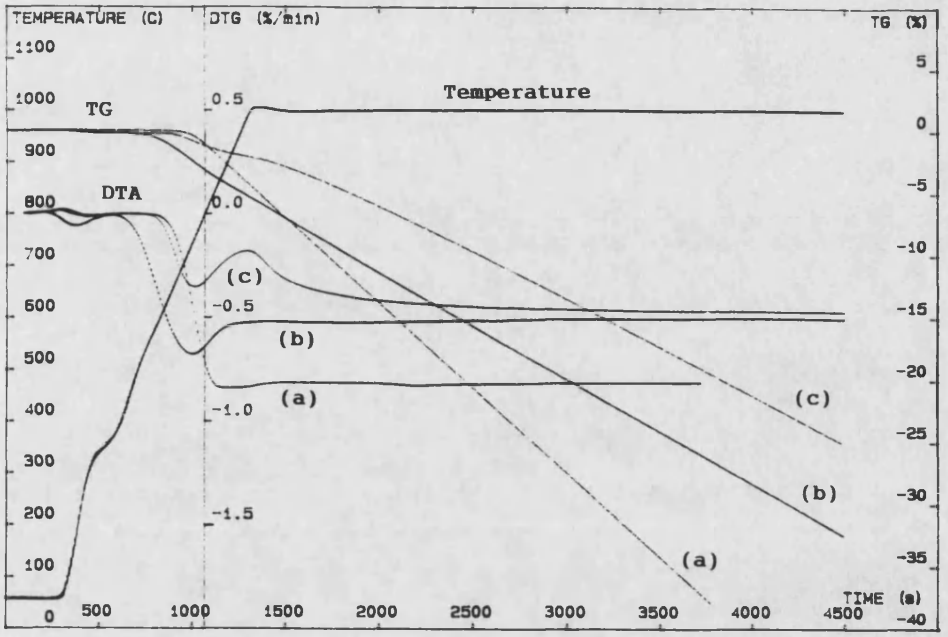

Figure V-2-7 Thermogravimetric analysis up to 1000° C of porous carbon-SiC and carbon-SiC-B_2O_3 composites (a) porous carbon preform, (b) porous carbon-SiC and (c) carbon-SiC-B_2O_3 composites

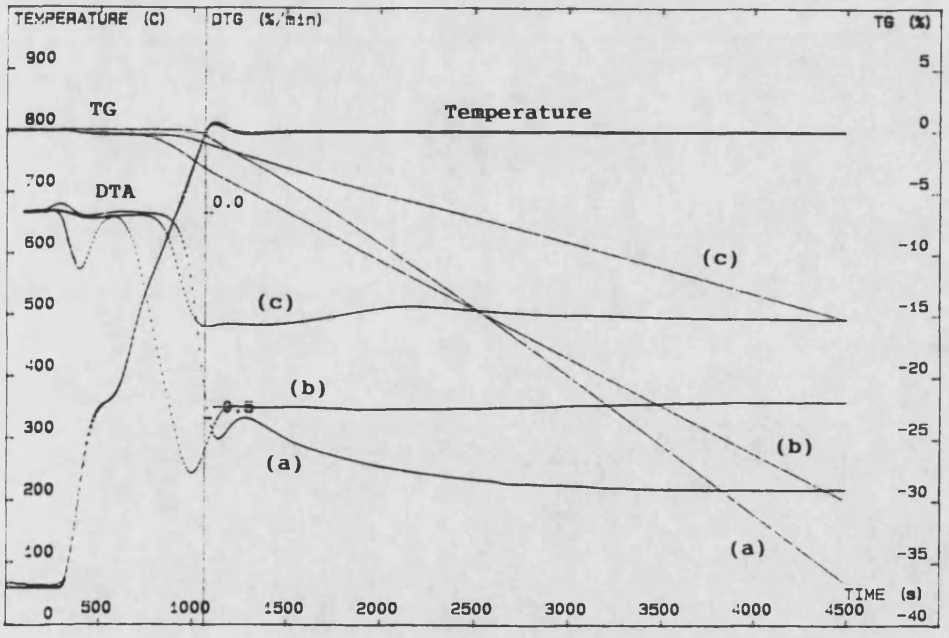

Figure V-2-8 Thermogravimetric analysis up to 800° C of porous carbon-SiC and carbon-SiC-B_2O_3 composites (a) porous carbon preform, (b) porous carbon-SiC and (c) carbon-SiC-B_2O_3 composites

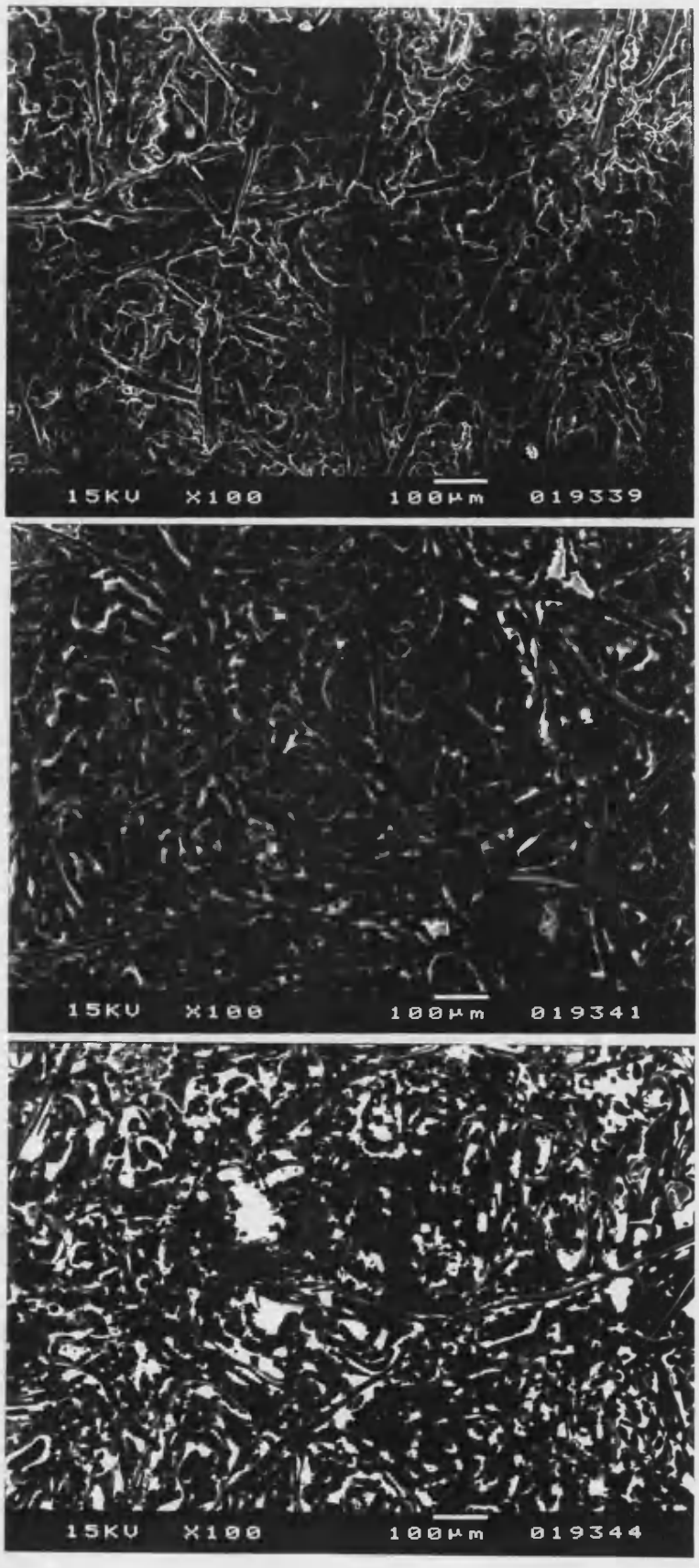

Oxidized for

1hr

2hr

8hr

Figure V-2-9 Microscopic observation of surfaces for oxidized porous carbon-SiC-B_2O_3 composites at 800° C

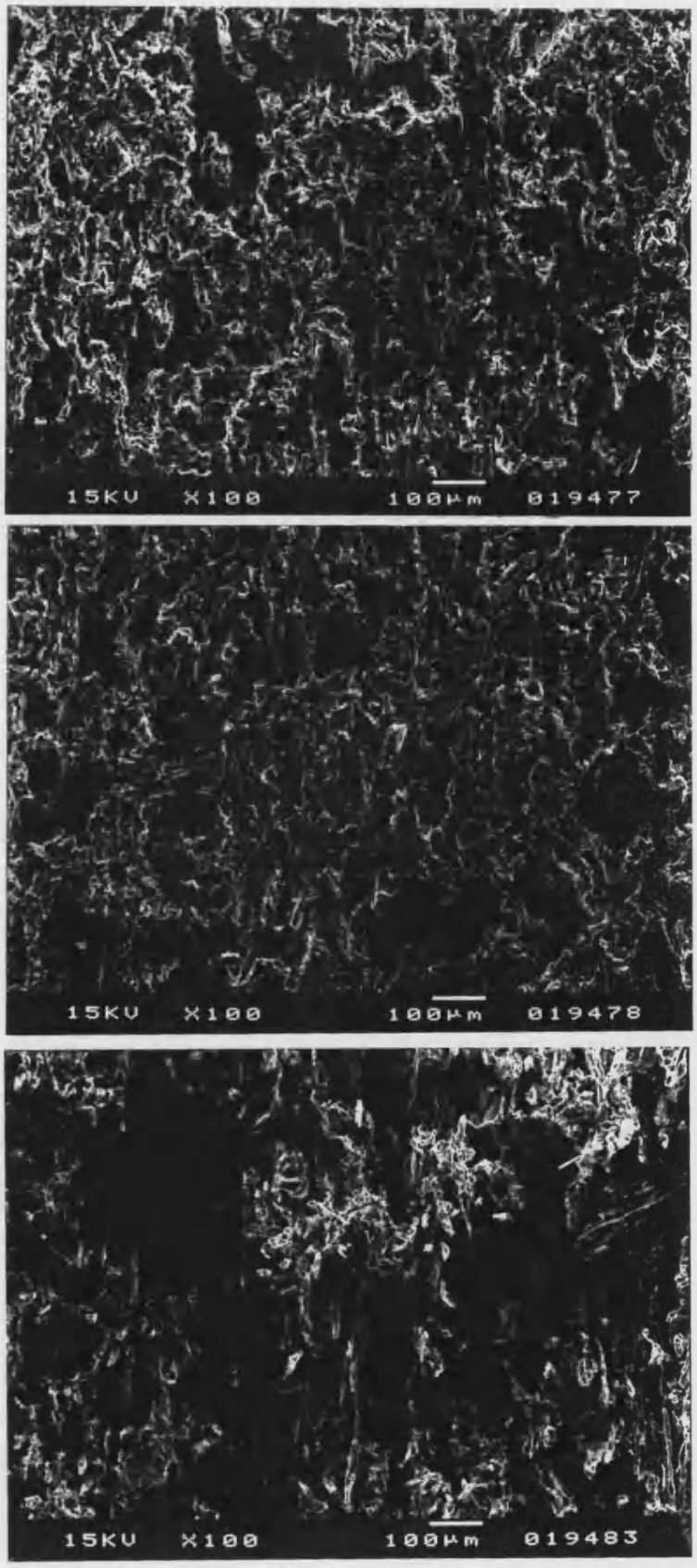

Oxidized for

1hr

2hr

8hr

Figure V-2-10 Microscopic observation of fracture sections for oxidized porous carbon-SiC-B_2O_3 composites at 800° C

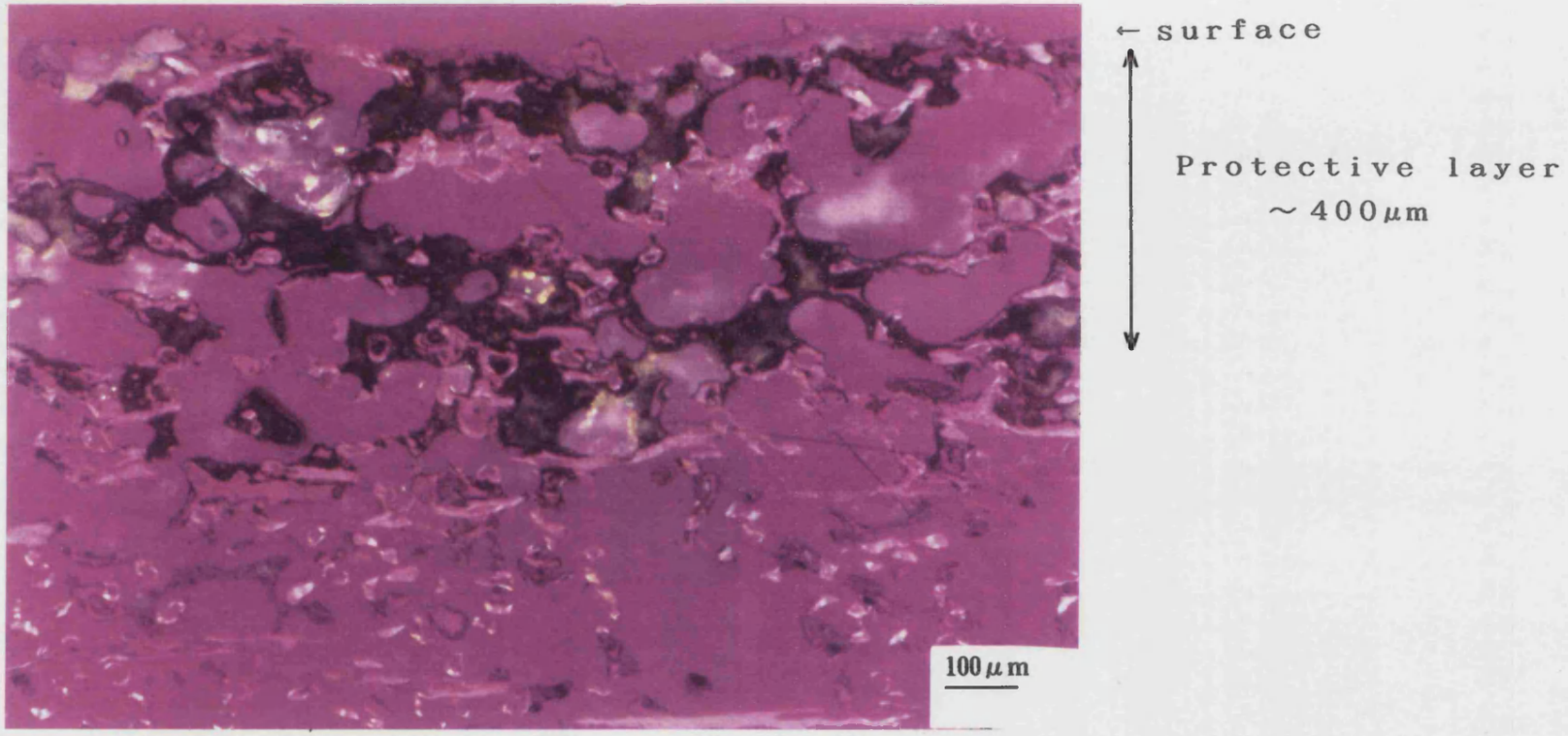

Figure V-2-11 Polished sections of oxidized porous carbon-SiC-B2O3 composites, showing a protective layer within ca. 400 μm on the surface

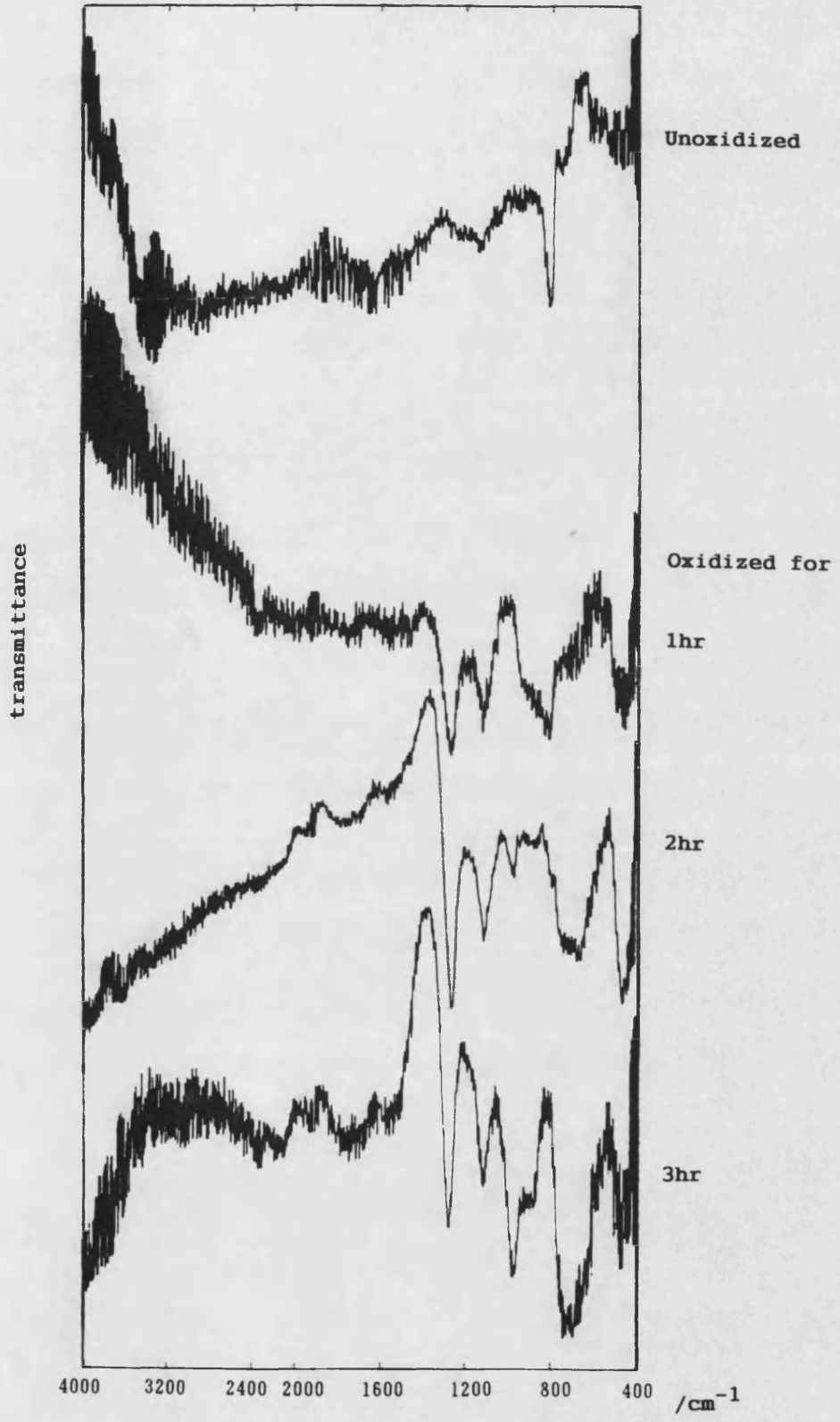

Figure V-2-12 Infra-red reflection spectroscopy of oxidized porous carbon-SiC composites

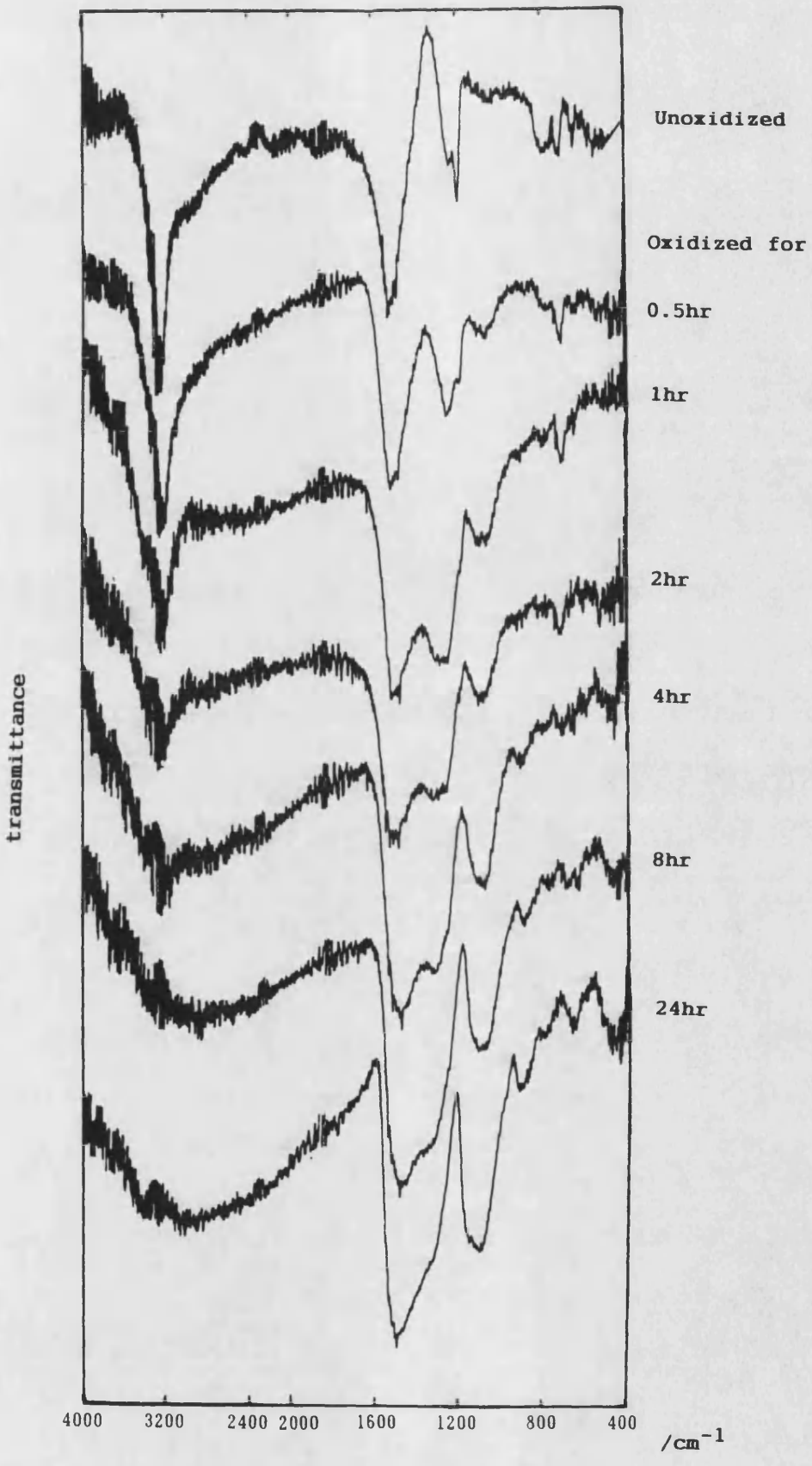

Figure V-2-13 Infra-red reflection spectroscopy of oxidized porous carbon-SiC-B_2O_3 composites

Specimen	Weight proportion		Bulk Density [g/cm^3]	Apparent Porosity [%]	Flexural strength [MPa]	Young's modulus [GPa]
	Carbon	Si3N4				
Porous carbon-Si3N4 composites	100	15	0.59	70	14.1	3.01
	100	25	0.64	68	14.7	3.14
	100	35	0.68	66	15.4	3.25

Table V-3-1

Physical properties of porous carbon-Si_3N_4 composites

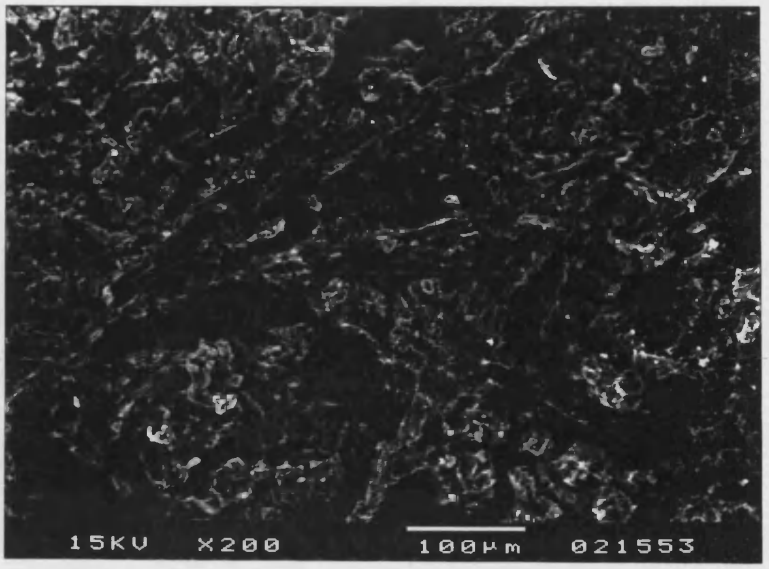

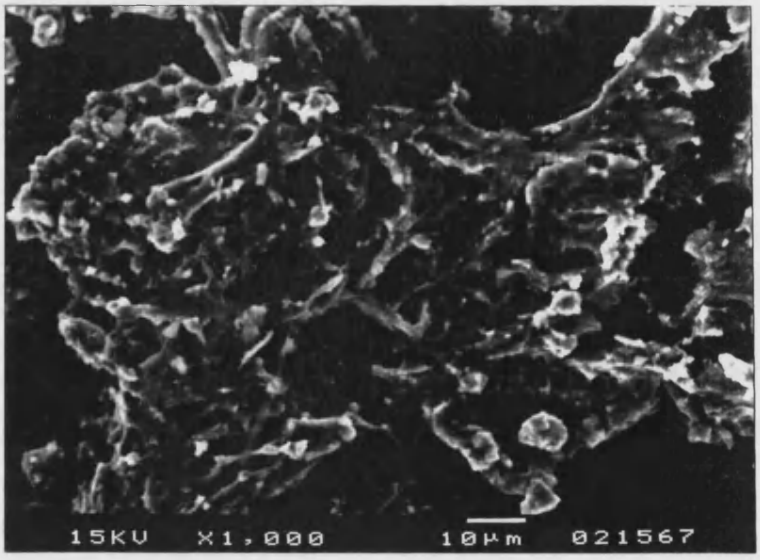

Figure V-3-1 Scanning electron micrographs of reaction product via carbothermal reduction and nitridation of silica on porous carbon preform (1350° C, 4hrs)

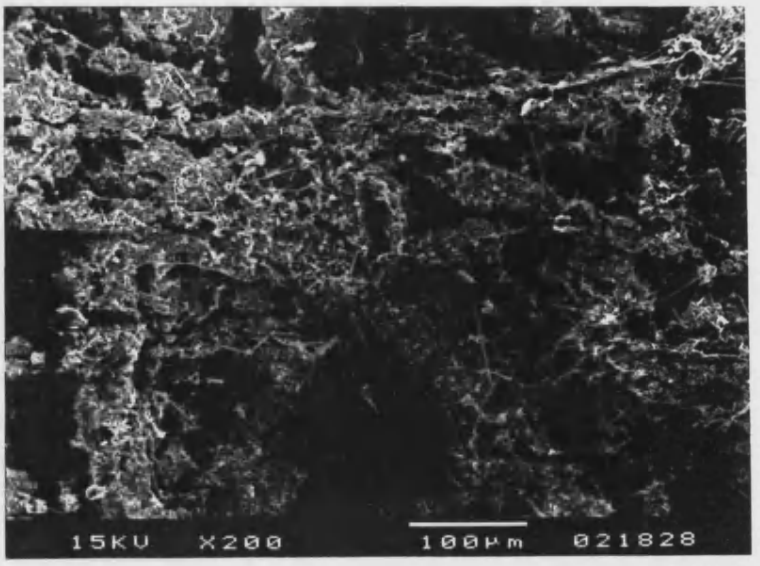

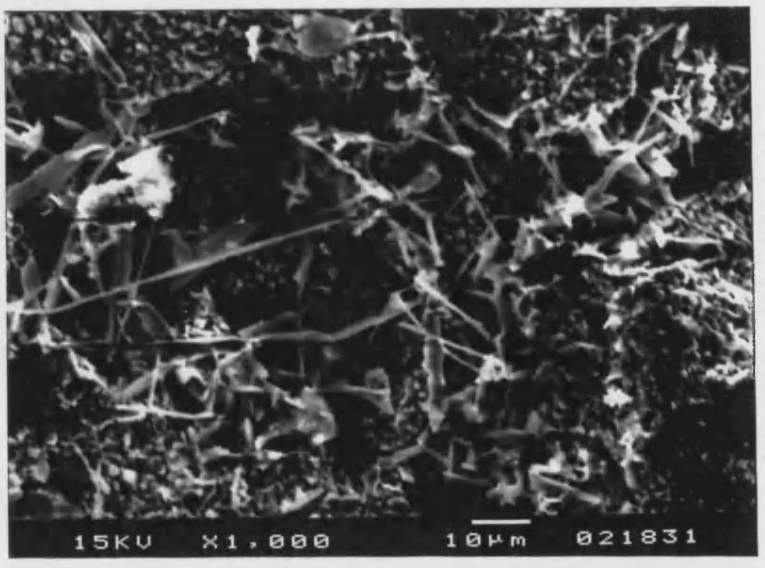

Figure V-3-2 Scanning electron micrographs of reaction product via carbothermal reduction and nitridation of silica on porous carbon preform (1350° C, 12hrs)

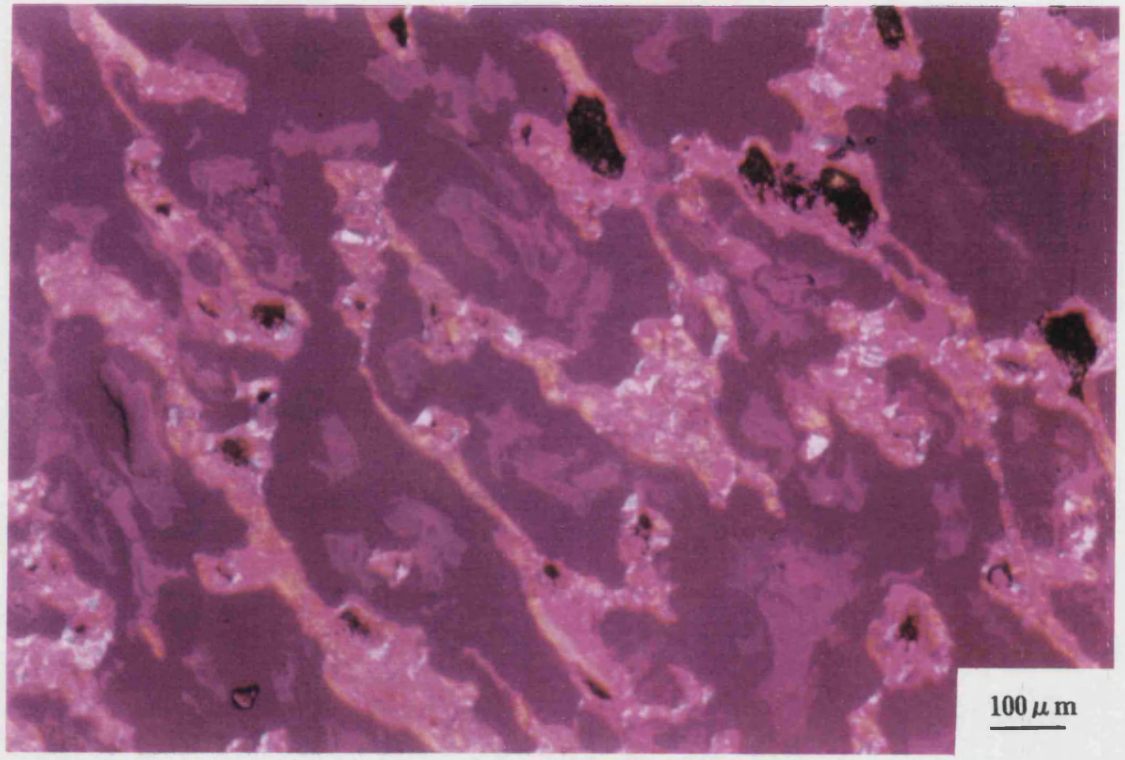

Figure V-3-3 Polarized light micrograph of porous carbon-Si_3N_4 composites

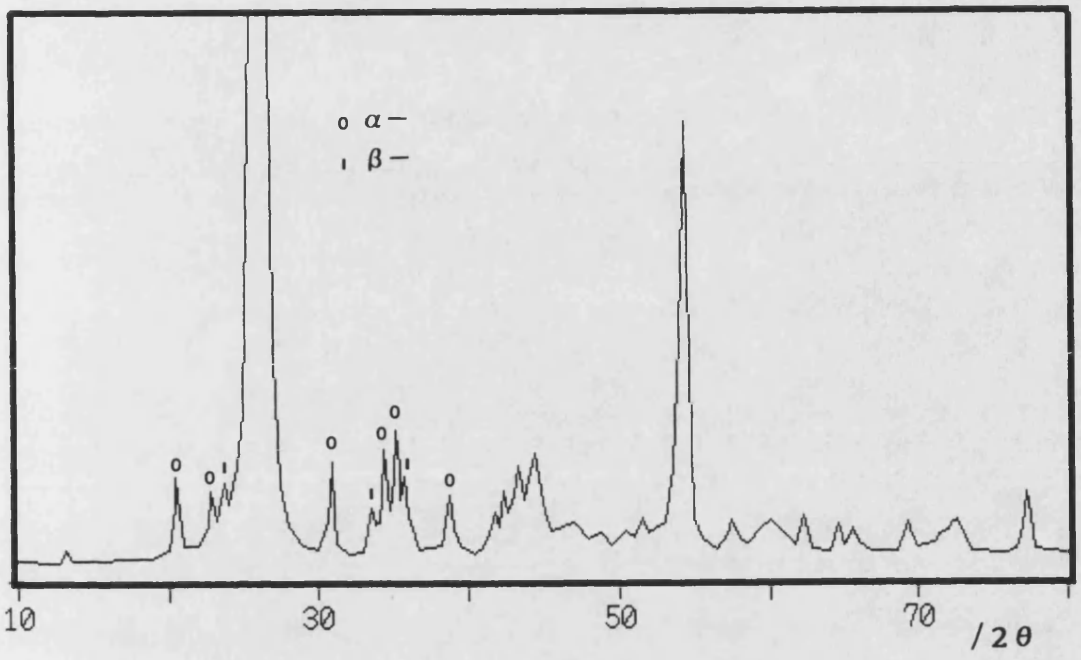

Figure V-3-4 X-ray diffraction profile of porous carbon-Si_3N_4 composites

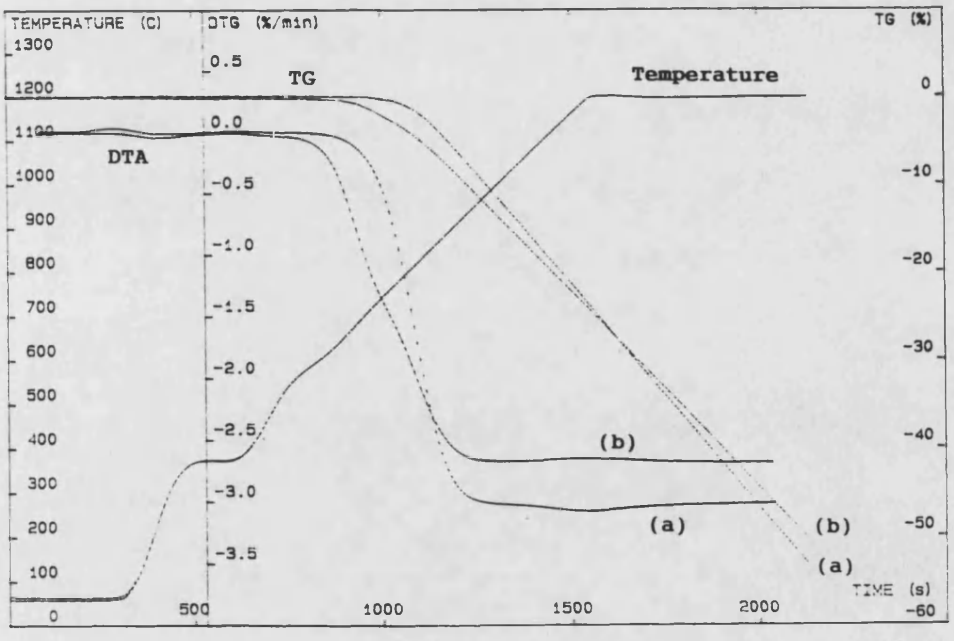

Figure V-3-5 Thermogravimetric analysis up to 1200° C of porous carbon-Si_3N_4 composites (a) porous carbon preform, (b) porous carbon-Si_3N_4 composites

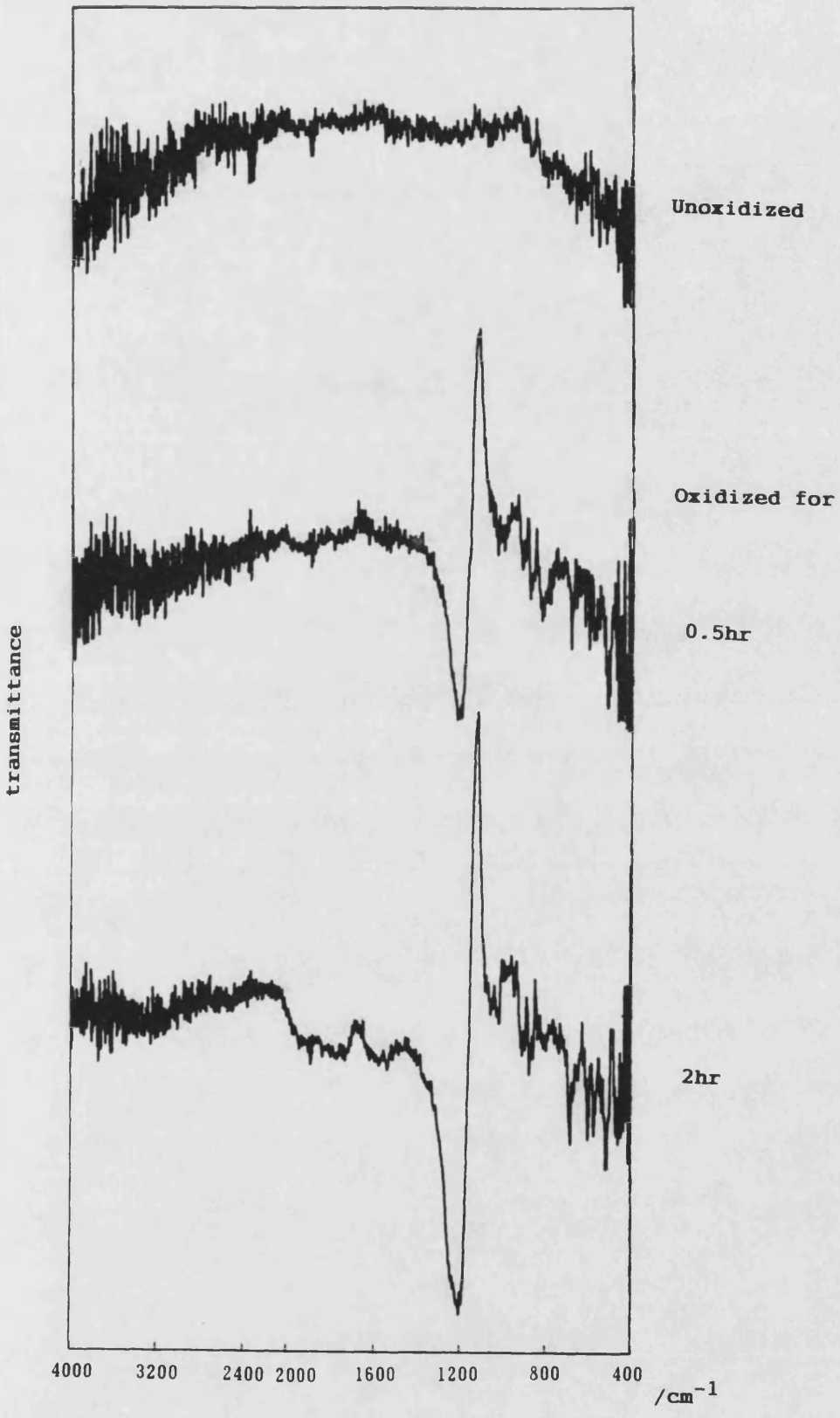

Figure V-3-6 Infra-red reflection spectroscopy of oxidized porous carbon-Si_3N_4 composites

CHAPTER VI POROUS CERAMIC MATERIALS

VI-1 Introduction

Various types of porous carbon materials, fabricated and characterized in Chapter IV, were directly converted, without any special pre-treatment, into porous silicon carbide materials in situ by a reaction bonding process with infiltrated silicon vapour at temperature over 1850° C to 2300° C. (Figure VI-1-1, p.239) The structural features, mechanical and physical properties of the porous silicon carbide materials, developed in this project, were studied.

VI-2 Manufacturing process

The reaction bonding process was performed in a graphite crucible as shown in Figure VI-2-1 (p.239). A silicon source (silicon nitride powder, β-phase, -325 mesh, containing silicon 58% minimum, Aldrich Chemical) was placed in the bottom of the graphite crucible and carbon fibre cloth was placed above it. Both silicon and silicon nitride powders can produce liquid silicon by melting (m.p. 1412° C) and decomposition, respectively, as shown in the following formula (1) and (2). (Greskovich - 1981)

$$Si(s) \longrightarrow Si(l) \qquad (1)$$

$$Si_3N_4(s) \longrightarrow 3Si(l) + 2N_2(g) \qquad (2)$$

Porous carbon materials to be silicided were then located on the carbon cloth. After evacuating the reaction vessel with argon gas, the crucible was raised

to the required temperature at a heating rate of ca. 1000° C/hr and held there for 20 minutes. Excess silicon was consumed by activated carbon placed above porous carbon materials to be silicided.

Two different reaction conditions were used:

(i) Atmospheric pressure at temperatures over 2000° C

(ii) Reduced pressures at temperatures about 1850° C

Reduced pressures (< 0.1 atm) were obtained using a rotary vacuum pump. Infiltration of silicon at atmospheric pressure demanded temperatures in excess of 2000° C. Whereas, under reduced pressures, the reaction could be carried out at temperatures less than 2000° C.

An analysis of the thermodynamics of the experimental reaction bonding system is in Appendix A (p.311). Figure A-1 (p.314) shows that a beneficial effect of operating at low pressures is to increase the partial pressure of Si vapour in the system. Under the experimental conditions used the vapour pressure of Si from decomposition of Si_3N_4 is greater than from liquid Si showing that the nitride is the more important source of Si vapour. Because the vapour pressure of silicon from Si_3N_4 is greater than from liquid silicon in both types of experiments, condensation of silicon vapour to liquid Si is a possibility. This may explain the presence of elementary Si in the reaction bonded porous SiC materials, although the possibility of transport of liquid silicon from the Si/Si_3N_4 source to the porous carbons by capillary action through pores in

the carbon felt cannot be ruled out. (Washburn - 1988)

When the reaction was completed, the crucible was allowed to cool down to room temperature and the silicided porous materials were removed. After siliciding, the unreacted carbon residue was removed by oxidation at 850° C in air.

VI-3 Porous SiC materials from porous carbon preforms fabricated by paper making technology

VI-3.1 Introduction

Porous carbon materials, produced by utilizing a combination of paper making technology (characterized in Chapter IV-2), were converted into porous silicon carbide by the reaction bonding technique at atmospheric pressure and temperatures in the range of 2000-2300° C, and under reduced pressures at ca. 1850° C. Physical and mechanical properties of porous reaction-bonded SiC materials prepared from porous carbon materials (graphitized grade) are presented in Tables VI-3-1 (p.240, at Atmospheric pressure and 2000-2300° C) and VI-3-2 (p.241, under reduced pressure at 1850° C).

IV-3.2 Structural characterization

IV-3.2.1 Density and porosity

The volume expansion caused by the conversion of carbon and silicon into SiC was accommodated within the porosity in the carbon preforms. Therefore, if the siliciding reaction proceeds to completion, the bulk density and apparent porosity of the porous carbon materials may change as follows:

	Porous carbon	+ Si --->	Porous SiC
Molecular weight	12		41
Solid density (g/cm^3)	1.9		3.2
Bulk density (g/cm^3)	0.51		1.74
Porosity (%)	73		46

In fact, as shown in Tables VI-3-1 and VI-3-2, the siliciding reaction of carbon did not proceed to completion. Unreacted carbon residue (about 25-30 wt% at atmospheric pressure, or ca. 35-40 wt% under reduced pressure) was observed after the siliciding reaction. The unreacted carbon residues were subsequently removed by oxidation treatment in air at 850° C. In addition, ca. 25 wt% unreacted free silicon was also infiltrated in both atmospheric and reduced pressure conditions.

(1) Atmospheric pressure at temperatures 2000-2300° C

The apparent porosity of porous SiC produced at atmospheric pressure was almost close to the theoretical porosity. However, the bulk density was somewhat smaller than the theoretical value due to the unreacted infiltrated free silicon ca. 25%.

A significant influence of differences in reaction temperature on density and porosity was not observed, although, there was a slight tendency to increase density and decrease porosity with increasing reaction temperature. Therefore, it can be considered that the siliciding reaction of carbon occurred immediately when carbon contacted with silicon that was impregnated around 2000° C.

(2) Reduced pressures at temperatures at 1850° C

The apparent porosity of porous SiC prepared under reduced pressure was considerably larger than the theoretical porosity due to the large amount (ca. 35-40 wt%) of unreacted carbon residue after the siliciding reaction. The unreacted carbon was subsequently oxidized in air. This larger amount of unreacted carbon is probably because the reactivity between carbon and silicon is lower at the lower reaction temperature.

VI-3.2.2 Microscopic observation

(1) Scanning electron microscopy

Scanning electron micrographs for the surface and fractured cross-section of porous SiC materials produced under reduced pressure at 1850° C are presented in Figures VI-3-1 and VI-3-2 (p.243, 244). The resulting SiC crystals can be clearly seen on the surface of the material. It was revealed from the fractured cross-section that the volume of pores of the material became much smaller due to volume expansion accompanied by the conversion into SiC. Nonetheless, the special features of the carbon preforms such as low-density and high porosity open-cell structure were basically retained after the reaction bonding process.

(2) Optical microscopy

The microstructures of parallel sections in the Z direction (the designation corresponds to that of the carbon preform) for porous SiC materials produced at atmospheric pressure and under reduced pressure are

compared in Figure VI-3-3 (p.245). It can be seen from the micrographs that there is a larger amount of unreacted carbon residue in the porous SiC prepared under reduced pressure, however, its structure more closely resembled that of the original porous structure of the carbon preform in contrast with that produced at atmospheric pressure. The microstructure of porous SiC material produced at atmospheric pressure was altered considerably. This may be the same as the phenomenon reported by Popper et al. (1961) that higher temperature treatment changed the structure of reaction-bonded silicon carbide. This change may be because silicon carbide is not generally stable in contact with liquid silicon. Fitzer et al. reported that grain coarsening and grain disintegration of SiC were found at 1800° C after 1 hour. (Fitzer - 1983)

Figures VI-3-4 and VI-3-5 (p. 246, 247) show the polished sections parallel and perpendicular to the Z direction of the porous SiC materials produced under reduced pressure, after oxidation treatment. Silicon carbide which appears as a grey region can be seen with a small amount of free silicon that shows up as a white region. The majority of the volume of the SiC material consisted of the inter-connected open pores which are the black region in the micrographs. Therefore, it can be said that the material was constituted of random array of bonded fibres in a planar structure.

Consequently, the unique structural features of the

porous carbon preforms summarized in Chapter IV-2.2.4, were, in principal, inherited by the SiC materials even after the reaction bonding process.

Figure VI-3-6 (p.248) shows the electro-chemically etched cross-section of porous SiC material, that reveals the grain boundaries of silicon carbide. The crystal size was in the range of ca. 2-20 μm.

VI-3.2.3 X-ray diffraction analysis

X-ray diffraction profiles of porous SiC materials produced at atmospheric pressure and under reduced pressure, after oxidation treatment, are shown in Figures VI-3-7 and VI-3-8 (p.249). There is no significant difference in their X-ray diffraction profiles. Both profiles consist of the peaks that can be ascribed to β-silicon carbide and silicon.

VI-3.2.4 Summary of manufacturing process and structural features

The silicon vapour infiltration under reduced pressure at lower temperature was adopted for the system for a further conversion of various types of porous carbons into SiC materials. Firstly, the reaction temperature was lower by about 150° C, and, secondly, it has the advantage of retaining the porous structure of the preform more faithfully, due to the higher stability of SiC in liquid silicon.

The unique structural features of the porous carbon preforms were, in principal, inherited by the SiC materials, even after the reaction bonding process. The

majority of the volume of the SiC materials consisted of the inter-connected open pores, and the material was constituted of random array of bonded fibres in a planar structure. However, the volume expansion and considerable amount of unreacted carbon, removed subsequently by oxidation, may have altered their microstructure.

VI-3.3 Mechanical properties

The mechanical behaviour of porous SiC materials, including flexural and compressive properties, were determined at room temperature and 800° C in air. A schematic designation of mechanical test specimens corresponding to that of porous carbon materials fabricated by paper making technology, is given in Figure IV-2-2 (p.143). As with the porous carbons produced by paper making technology, flexural strength was measured in the XZ orientation, and compressive strength was tested in the Z direction.

VI-3.3.1 Effect of reaction pressure and temperature

The microstructures of high-temperature-infiltrated silicon carbide differed considerably from that of reduced-pressure-impregnated material, as shown in the previous section. This difference suggested the need for experiments to examine the effect of infiltration conditions on mechanical properties.

The results of the mechanical tests for porous SiC materials are presented in Tables VI-3-1 and VI-3-2 (p.240, 241), and also Figures VI-3-9 and VI-3-10

(p.250) illustrate the schematic flexural and compressive stress-strain curves.

All porous SiC specimens, regardless of their fabrication conditions, failed in a brittle manner, similar to those of the porous carbon materials (HTT 1000° C), but with much smaller values of strain to failure. This means that nonlinearity was not present in the stress-strain curves up to the point of fracture. Furthermore, this mechanical behaviour was irrespective of applied temperature up to 800° C. Therefore, mechanical properties of the porous SiC materials were independent of temperature at least up to 800° C in air. It has already been shown by many researchers that the strength of reaction-bonded SiC materials is virtually invariant with temperature below 1300-1400° C, where the loss of strength of silicon is appreciable as melting point of 1410° C is approached. (McLaren - 1972, Hillig - 1975)

Mechanical properties of porous reaction-bonded SiC materials were significantly improved, in comparison with those of the carbon preforms. Especially, compressive strength in the Z direction was notably increased, presumably because of reinforcement of interlayer bonds.

Regarding porous SiC materials produced at atmospheric pressure at temperatures of 2000-2300° C, a significant effect of reaction temperature on mechanical strength was not observed. This agreed with

the results of density/porosity.

Porous SiC materials produced at atmospheric pressure exhibited much higher values in both strength and modulus, compared with those prepared under reduced pressure, mainly due to lower porosity. In particular, the flexural modulus of porous SiC prepared at atmospheric pressure was higher, even if its low porosity was taken into consideration.

VI-3.3.2 Effect of density/porosity

Porous SiC materials with various values of density/porosity were prepared by reaction bonding of porous carbon preforms with varied density/porosity, which were analyzed in Chapter IV-2.3.2.

The mechanical properties of porous silicon carbide materials prepared under reduced pressure at 1850° C in the range of 0.98 - 1.36 g/cm^3 for density and 66.7 - 50.8 % for porosity, were determined by flexural test in the XZ orientation and compressive test in the Z direction. Data of mechanical properties of porous SiC with a wide range of density/porosity are presented in Table VI-3-3 (p.242).

(1) Flexural strength

The flexural strength for the porous SiC materials with varied density is plotted in Figure VI-3-11 (p.251). It is clear that the flexural strength value increased with the increase of density; in other words, the strength decreased with increasing porosity.

In the same manner, the flexural modulus versus the

density is plotted in Figure VI-3-12 (p.251). It is apparent that the flexural modulus value also increased with density; that is to say, the modulus increased with decreasing porosity.

These trends correspond with those found for the mechanical behaviour of porous carbon preforms. In consequence, in the same manner as the carbon preforms, the normalized flexural strength (σ/σ_s) and modulus (E/E_s) of porous SiC materials are plotted against relative density (ρ/ρ_s), as presented in Figures VI-3-13 and VI-3-14 (p.252), respectively. The values for σ_s and E_s were selected as 500 MPa and 420 GPa, respectively, which are typical values for dense reaction-bonded silicon carbide.

Because of the scatter in both the flexural strength and modulus data, it may be misleading to apply one specific equation to the relationship between its mechanical behaviour and relative density. However, the following trends drawn from the data are believed to be correct.

The flexural strength of porous reaction-bonded SiC materials varied approximately as the square of the relative density, which is almost identical to the flexural strength behaviour of the carbon preforms. On the other hand, the flexural modulus of porous SiC was nearly proportional to the power of ca. 1.5 of the relative density. This means that the dependence of flexural modulus of porous SiC on the relative density diminished dramatically in comparison with the carbon

preforms.

(2) Compressive properties

The compressive strength of porous SiC materials with varied density/porosity is plotted in Figure VI-3-15 (p.253). Apparently, compressive strength values increased with density; or the strength decreased with increasing porosity.

Likewise, the variation of compressive modulus with density is plotted in Figure VI-3-16 (p.253). The compressive modulus value also increased with density; in other words, the modulus decreased with increasing porosity.

The variation of normalized compressive strength (σ/σ_S) and modulus (E/E_S) with relative density (ρ/ρ_S) are plotted in Figures VI-3-17 and VI-3-18 (p.254), respectively. The values for σ_S and E_S were chosen as 10,000 MPa and 420 GPa, respectively, which are typical values for dense reaction-bonded silicon carbide.

There can be also seen a considerable scatter in compressive strength and modulus data, however, the following general trends can be drawn from the figures. The compressive strength of porous SiC materials varied as nearly the 4th power of the density, which corresponds with the trend for the compressive strength behaviour of the carbon preforms. Meanwhile, the compressive modulus was proportional to the ca. 2.5 power of the density. Again, the dependence of compressive modulus on the relative density declined

drastically, compared with their carbon preforms.

(3) Mechanical anisotropy

As with the porous carbon preforms made by paper making technology, the ratio of the flexural property values in the XZ orientation to the compressive property values in the Z direction can indicate the mechanical anisotropy of the XY plane to the ZX or the ZY plane. As shown in Figures VI-3-19 (p.255) for strength anisotropy and VI-3-20 for elastic modulus anisotropy, with the increase of density, the values of compressive properties increased more rapidly than those of flexural properties. This trend of mechanical anisotropy of porous SiC materials corresponds to the behaviour of the porous carbon preforms. Accordingly, the mechanical anisotropy decreased with increasing density.

It is difficult to determine the specific dependence of mechanical anisotropy on density due to the highly scattered data. However, it may be said that the dependence of strength anisotropy on the bulk density varied in almost the same way as that of the preform, and that the modulus anisotropy shows less dependence on the density in comparison with the carbon preforms.

(4) Conclusions of effect of density/porosity

The flexural and compressive mechanical property values of porous reaction-bonded SiC materials increased with increase of density, which corresponds to the trends for carbon preforms. The dependence of

strength on density was almost the same as that of the preforms, while the dependence of modulus on the relative density declined drastically, compared with the carbon preforms. The mechanical anisotropy of porous SiC decreased with increasing density, which is analogous to the preforms.

VI-3.3.3 Summary of mechanical properties

The following conclusions can be drawn from the investigation on the mechanical behaviour of porous SiC materials from carbon preforms fabricated by paper making technology.

(i) Porous reaction-bonded SiC materials failed in a brittle manner under flexural and compressive stresses.

(ii) The mechanical properties against temperature were independent at least up to 800° C in air.

(iii) Mechanical properties of porous SiC materials were significantly developed in comparison with those of the carbon preforms. Especially, compressive strength was notably increased because of reinforcement of interlayer bonds.

(iv) A significant effect of reaction temperature on mechanical strength was not observed among porous SiC materials produced at atmospheric pressure.

(v) Porous SiC materials produced at atmospheric pressure exhibited much higher values of both strength and modulus, compared with those prepared under reduced pressure, mainly due to lower porosity.

(vi) The flexural and compressive mechanical values of

porous reaction-bonded SiC materials increased with the increase of density, which corresponds to the carbon preforms.

(vii) The dependence of strength on density was almost the same as that of the preforms, while the dependence of modulus on the relative density declined drastically, compared with the carbon preforms.

(viii) The mechanical anisotropy of porous SiC decreased with increasing density, which is analogous to the trends for the preforms.

VI-3.4 High-temperature corrosion behaviour

High-temperature corrosion resistance of porous reaction-bonded SiC materials was monitored by thermogravimetric analysis. (Figure VI-3-21, p.256) The weight of the porous SiC was very stable up to ca. 1000° C, even though a slight fluctuation in the differential thermogravimetric data was observed. Above 1000° C, the weight gradually increased, presumably due to oxidation of SiC or Si to SiO_2. However, the rate of weight increase slowly decreased during oxidation treatment at 1200° C, probably owing to the formation of a protective layer of silica films on the materials.

Consequently, porous reaction-bonded SiC materials have high corrosion resistance against high-temperature air. In particular, they are virtually unaffected by any structural change under 1000° C. Therefore, they are expected to be promising engineering materials for applications in an oxidizing atmosphere.

VI-4 SiC foams from foamed resin based carbons

VI-4.1 Introduction

Foamed resin based carbon materials with densities in the range of 0.0567 - 0.0681 g/cm^3, were converted into silicon carbide foams by the reaction bonding technique under reduced pressure at ca. 1850° C. After siliciding carbon foams, the unreacted carbon residue was removed by oxidation at 850° C in air. Physical and mechanical properties of reaction-bonded SiC foams are presented in Table VI-4-1 (p.257).

IV-4.2 Structural characterization

IV-4.2.1 Density and porosity

The foamed reaction-bonded SiC materials were prepared with various densities in the range of 0.0779 - 0.1243 g/cm^3. A considerable amount (ca. 50wt% or more) of unreacted carbon residue remained after the siliciding reaction at 1850° C, as a result, the densities of SiC foams were much smaller than the theoretical values. Therefore, it can be said that glassy carbon reacts slowly with silicon to form SiC by a reaction bonding process. This may be concerned with the non-graphitic nature of glassy carbon and the absence of micropores.

The porosities of SiC foams are considered to be in the approximate range of 97.5 - 96%, provided that the real density of reaction-bonded SiC, which contains a small amount of free silicon, is about 3 g/cm^3.

Consequently, the density of reaction-bonded SiC foams is extraordinary low and the porosity is high.

VI-4.2.2 Microscopic observation

General microstructures of foamed SiC materials by optical and scanning electron microscopies are presented in Figures VI-4-1 and VI-4-2 (p.258, 259). The following characteristics were inherited from the carbon foam preforms:

- an inter-connected three dimensional network
- open-cell structure

Therefore, the structure of SiC foams is similar to that of the carbon preforms. However, microscopic observation of polished cross-sections reveals that the cell struts were hollow. (Figure VI-4-3, p.260) Only the outer part of cell struts of carbon foams was converted into SiC, but carbon in the centre of struts did not react with silicon and remained after siliciding. The porosity within the cell struts was formed by subsequent oxidation treatment in air at 850° C. Hence, the cell struts of reaction-bonded SiC foams were hollow with a small amount of free silicon.

VI-4.2.3 X-ray diffraction analysis

X-ray diffraction profiles of reaction-bonded SiC foams are presented in Figure VI-4-4 (p.261). The only detectable crystalline phases in the profile are β-silicon carbide and silicon.

VI-4.2.4 Summary of structural features

The structural features of reaction-bonded SiC foams are summarized as followings:

(i) The foamed reaction-bonded SiC materials had

extraordinary low density and high porosity. The densities and porosities were in the range of 0.0779 - 0.1243 g/cm^3, and ca. 97.5 - 96%, respectively.
(ii) The SiC foams had an inter-connected three dimensional network and open-cell structure. The basic characteristics were inherited from the carbon foam preforms.
(iii) The cell struts were hollow.

VI-4.3 Mechanical properties

The mechanical properties of reaction-bonded SiC foams were characterized by measurement of compressive strength at room temperature. The specimens failed in a brittle crushing manner, showing almost similar behaviour to the carbon foam preforms whose schematic illustration of compressive stress-strain curve is given in Figure IV-3-6. Elastic deformation occurred up to typically ca. 9 %, after that a structural deformation by crushing happened. This high fracture strain value was caused by bending of the cell unit. Data of compressive strength and modulus are presented in Table VI-4-1 (p.257).

The variations of compressive strength and modulus with density are plotted in Figures VI-4-5 and VI-4-6 (p.262), respectively. Although a significant scatter was observed in the data, it can be said that both compressive strength and modulus generally increased with the increase of density.

The relative strength and modulus determined as a

function of relative density are shown in Figures VI-4-7 and VI-4-8 (p.263). The values for σ_s, E_s, and ρ_s were chosen as 10,000 MPa, 420GPa, and 3.0 g/cm^3, respectively, values typical for reaction-bonded SiC. Because of the scattered data and the small density range, it is difficult to determine the exact values for a relationship between the relative strength and modulus, and density. However, it may be said that the relative density exponents in both strength and modulus were, more or less, in agreement with those of the carbon foam preforms, although the exponents for strength of the SiC foams may be slightly larger. Nonetheless, a significant disagreement was noticed between the measured values of geometric constants and those suggested theoretically by Gibson and Ashby et al. As proposed previously, it can be anticipated that the mechanical behaviour of foams with hollow struts may differ from foam materials with dense struts. (Hagiwara - 1987)

VI-4.4 High-temperature corrosion resistance

High-temperature corrosion resistance in air of reaction-bonded SiC foams, monitored by thermogravimetric analysis, is shown in Figure VI-4-9 (p.264). Only a slight variation in weight with temperature was detected. This thermogravimetric behaviour is typical to reaction-bonded SiC materials that have high corrosion resistance against high-temperature air.

VI-5 Carbon - SiC/Si composites from resin powder based porous carbon pellets

VI-5.1 Introduction

The resin carbon based porous carbon pellets were converted into carbon - SiC/Si composites by a reaction bonding process under reduced pressure at 1850° C. The resultant materials were not subjected to oxidation treatment after siliciding, and their physical and mechanical properties, are shown in Table VI-5-1 (p.265).

VI-5.2 Structural characterization

VI-5.2.1 Density and porosity

The bulk density and apparent porosity determined by a water absorption method, were 2.44 g/cm^3 and 0.1 %, respectively. A considerable amount of unreacted carbon residue remained after the siliciding reaction, as a result, the density was much smaller than the theoretical values. In addition, the apparent porosity was almost zero because the pores in the materials were filled with free silicon. As a result, this material can be considered as dense carbon - SiC/Si composites, and not a porous material.

VI-5.2.2 Microscopic observation

Scanning electron micrographs and optical micrographs of polished section for carbon - SiC/Si composites are presented in Figures VI-5-1 and VI-5-2 (p.266, 267).

The smaller channel-like pores were converted into SiC with a little free silicon. On the other hand, only the outer parts of the larger pores (ca. 100 μm in

diameter) were turned into SiC, and the majority parts of the larger pores were filled with free silicon.

VI-5.2.3 X-ray diffraction analysis

X-ray diffraction profiles of carbon - SiC/Si composites are presented in Figure VI-5-3 (p.268). The crystalline phases of β-silicon carbide and silicon are detected clearly, in addition the broad peak of carbon is also observed around 25° / 2θ.

VI-5.2.4 Summary of structural features

The structural features of carbon - SiC/Si composites are summarized as followings:

(i) The bulk density and apparent porosity are 2.44 g/cm^3 and 0.1 %, respectively. The composites contained a considerable amount of unreacted carbon and free silicon.

(ii) The smaller channel-like pores were converted into SiC with a little free silicon. On the other hand, only the outer parts of the larger pores (ca. 100 μm in diameter) were turned into SiC, and the major part of the larger pores was filled with free silicon.

VI-5.3 Mechanical properties

The tensile strength of carbon - SiC/Si composites, determined by the split cylinder test, was 78.68 MPa. Thus, the strength of the materials was markedly improved by a reaction bonding process.

VI-5.4 High-temperature corrosion resistance

High-temperature corrosion resistance of carbon -

SiC/Si composites, monitored by thermogravimetric analysis, is shown in Figure IV-4-5 (p.171). The weight of the composites began to decrease above ca. 500° C where the oxidation of carbon started. However, the rate of weight decrease gradually reduced during oxidation treatment at 1200° C, probably owing to the formation of protective layer of silica films which were formed by oxidation of SiC or Si to SiO_2. Accordingly, carbon - SiC/Si composites have high corrosion resistance against high-temperature air.

VI-6 Porous SiC materials from carbon bonded carbon fibre composites

VI-6.1 Introduction

Carbon bonded carbon fibre composites were converted into porous silicon carbide materials by reaction bonding process under reduced pressure at ca. 1850° C. After siliciding CBCF composites, the unreacted carbon residue was removed by oxidation at 850° C in air. Physical and mechanical properties of reaction-bonded porous SiC materials are presented in Table VI-6-1 (p.269).

VI-6.2 Structural characterization

VI-6.2.1 Density and porosity

Unreacted carbon residue remained about 35-40 wt% after siliciding reaction at 1850° C. As a result, the bulk density and apparent porosity of porous SiC materials produced from CBCF composites, were 0.946 g/cm^3 and 67.8 %, respectively, after oxidation

treatment. Therefore, free silicon may also have infiltrated to about 25 wt%.

VI-6.2.2 Microscopic observation

Scanning electron micrographs and optical micrographs of polished sections for porous SiC materials from CBCF composites, showing views perpendicular and parallel to the moulding direction are presented in Figures VI-6-1 and VI-6-2 (p.270 - 273). The structural features of the carbon preforms, that is random in-plane and highly porous open-cell structure, were basically retained after the siliciding, although some transformations in structure were detected.

It was revealed by SEM observation that the resulting SiC crystals were formed mainly at the junctions between the carbon matrix and the fibres. Only the surface of the carbon fibres was slightly affected by the siliciding reaction.

Observations of polished sections show that the carbon fibres were hardly converted into SiC, and only the outer parts of the fibres were turned into SiC. In contrast, the matrix was almost completely converted into SiC with some infiltrated free silicon. Therefore, the reactivity of carbon fibres with silicon may be much less than that of carbon matrix, presumably due to low microporosity on the surface.

VI-6.2.3 X-ray diffraction analysis

X-ray diffraction profiles of porous reaction-bonded SiC materials from CBCF composites are presented in

Figure VI-6-3 (p.274). As with the other reaction-bonded SiC materials, the only detectable crystalline phases in the profile are β-silicon carbide and silicon.

VI-6.2.4 Summary of structural features

The following are conclusions about structural features of porous SiC materials from carbon bonded carbon fibre composites.

(i) The bulk density and apparent porosity of porous SiC materials were 0.946 g/cm^3 and 67.8 %, respectively, after oxidation treatment.

(ii) The porous SiC materials had a random in-plane and highly porous open-cell structure.

(iii) The carbon fibres were hardly converted into SiC, and only the outer parts of the fibres were converted into SiC. In contrast, the matrix was almost completely converted into SiC with the some infiltrated free silicon.

(iv) The reactivity of carbon fibres with silicon is less than that of carbon matrix.

VI-6.3 Mechanical properties

Mechanical properties of porous SiC materials, including flexural and compressive tests, were performed at room temperature in air. A schematic designation of mechanical test specimens corresponds to those used for the carbon preforms. Flexural properties was measured in the XZ direction and compressive properties were tested in the Z direction.

Porous SiC materials from CBCF composites showed a brittle failure manner similar to that found for the porous SiC made from porous carbon preform by paper making technology.

Both flexural and compressive property values increased significantly compared with the carbon preforms. (Table VI-6-1, p.269) In particular, flexural modulus and compressive strength increased dramatically. Mechanical anisotropies (Flexural(XZ) / Compressive(Z)), thus, changed from 7.2 to 1.14 for strength and from 36.1 to 115.7 for modulus in comparison with the carbon preforms. This may be due to dense and strong connection at junctions of fibres and existence of porosity in struts.

Consequently, the mechanical behaviour altered significantly from the carbon preforms by conversion into silicon carbide.

VI-6.4 High temperature corrosion resistance

High-temperature corrosion resistance of porous SiC materials, monitored by thermogravimetric analysis, is shown in Figure VI-6-4 (p.274). The specimen was very stable in flowing hot-air, and its DG/DTG behaviour was similar to those found for the other reaction-bonded SiC materials.

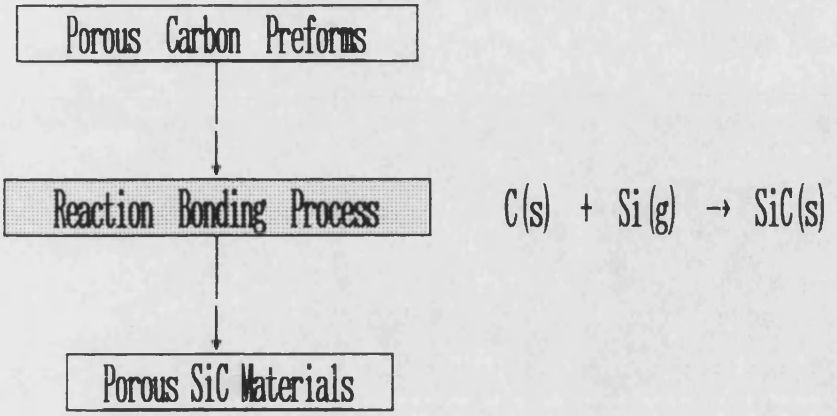

Figure VI-1-1 Manufacturing process of porous SiC materials by reaction bonding technique

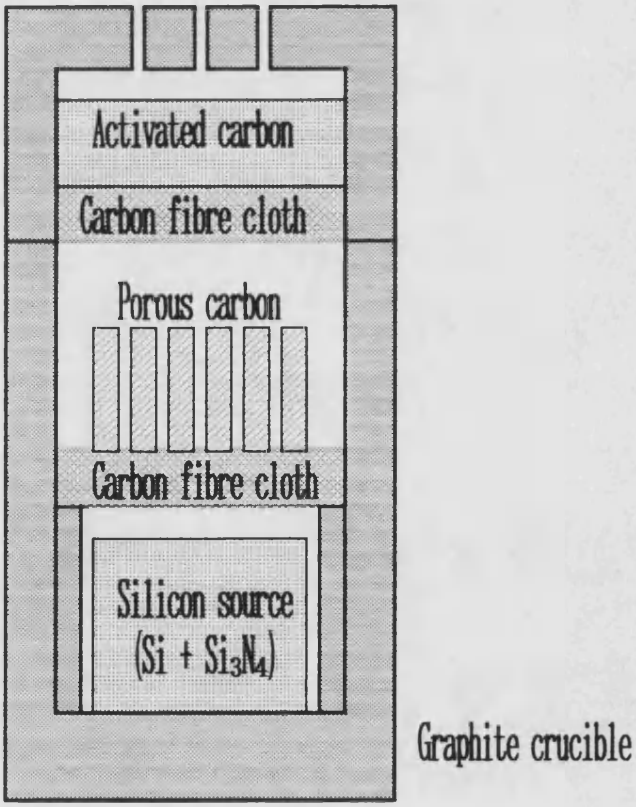

Figure VI-2-1 Graphite crucible system for reaction bonding process

Maximum reaction temperature	2000℃	2150℃	2300℃
Bulk density ρ (g/cm^3)	1.504 ± 0.053	1.521 ± 0.066	1.564 ± 0.046
Porosity p (%)	49.4 ± 1.7	48.7 ± 2.8	47.4 ± 1.4
Flexural properties			
at room temperature			
Strength σ (MPa)	35.9 ± 1.3	36.2 ± 2.7	36.7 ± 2.1
Modulus E (GPa)	47.2 ± 1.3	48.0 ± 0.7	48.7 ± 2.0
at 800℃ in air			
Strength σ (MPa)	36.6 ± 3.2	36.5 ± 1.4	35.8 ± 1.8
Modulus E (GPa)	47.2 ± 1.9	47.9 ± 1.5	48.3 ± 2.3
Compressive properties			
at room temperature			
Strength σ (MPa)	18.5 ± 2.8	18.6 ± 3.1	20.1 ± 1.9
Modulus E (GPa)	0.47 ± 0.03	0.48 ± 0.03	0.50 ± 0.01
at 800℃ in air			
Strength σ (MPa)	19.7 ± 1.7	19.9 ± 3.0	22.2 ± 2.6
Modulus E (GPa)	0.49 ± 0.03	0.49 ± 0.03	0.51 ± 0.02

Table VI-3-1 Physical properties of porous SiC materials reaction-bonded at atmospheric pressure

Maximum reaction temperature	1850℃
Bulk density ρ (g/cm^3)	1.167 ± 0.043
Porosity p (%)	60.5 ± 1.9
Flexural properties	
at room temperature	
Strength σ (MPa)	21.5 ± 2.1
Modulus E (GPa)	22.9 ± 1.0
at 800℃ in air	
Strength σ (MPa)	22.5 ± 2.4
Modulus E (GPa)	22.2 ± 1.0
Compressive properties	
at room temperature	
Strength σ (MPa)	11.2 ± 1.6
Modulus E (GPa)	0.38 ± 0.02
at 800℃ in air	
Strength σ (MPa)	10.7 ± 1.6
Modulus E (GPa)	0.37 ± 0.03

Table VI-3-2 Physical properties of porous SiC materials reaction-bonded under reduced pressure

Bulk Density ρ g/cm^3	Porosity P %	Relative Density ρ/ρs	Flexural Properties strength σ MPa	modulus E GPa	Compressive Properties strength σ MPa	modulus E GPa
0.98	66.7	0.333	18.1	19.0	3.1	0.17
0.98	65.6	0.344	14.2	15.7	2.7	0.15
0.99	65.5	0.345	18.7	20.9	5.7	0.26
1.04	64.5	0.355	19.6	23.7	5.5	0.31
1.04	63.1	0.369	15.6	17.7	4.8	0.26
1.06	63.9	0.361	18.8	23.0	8.6	0.36
1.09	61.7	0.383	22.7	23.3	9.7	0.37
1.10	60.3	0.397	16.6	18.2	4.8	0.23
1.10	60.7	0.393	19.9	25.0	6.1	0.28
1.11	61.4	0.386	24.6	23.0	7.0	0.31
1.11	59.9	0.401	16.3	22.2	4.6	0.22
1.16	59.1	0.409	23.2	20.9	12.5	0.39
1.18	57.8	0.422	22.0	24.3	9.7	0.33
1.22	57.0	0.430	24.8	28.7	8.0	0.35
1.24	56.8	0.432	20.8	23.9	14.3	0.41
1.27	54.2	0.458	26.0	29.5	10.5	0.40
1.27	54.1	0.459	29.1	33.0	11.5	0.39
1.33	52.2	0.478	28.1	27.1	11.8	0.36
1.34	52.5	0.475	31.4	33.4	14.7	0.43
1.36	50.8	0.492	24.8	25.8	9.8	0.37

Table VI-3-3 Mechanical properties of porous SiC materials in the density range of 0.98 - 1.36 g/cm^3

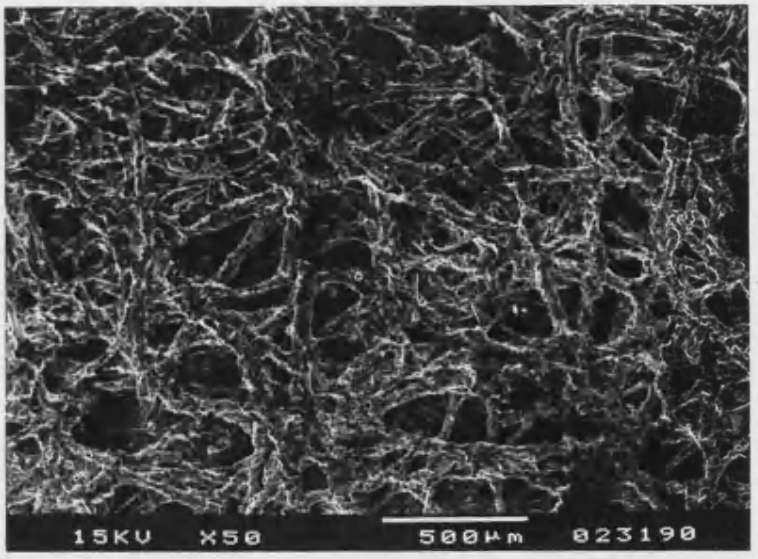

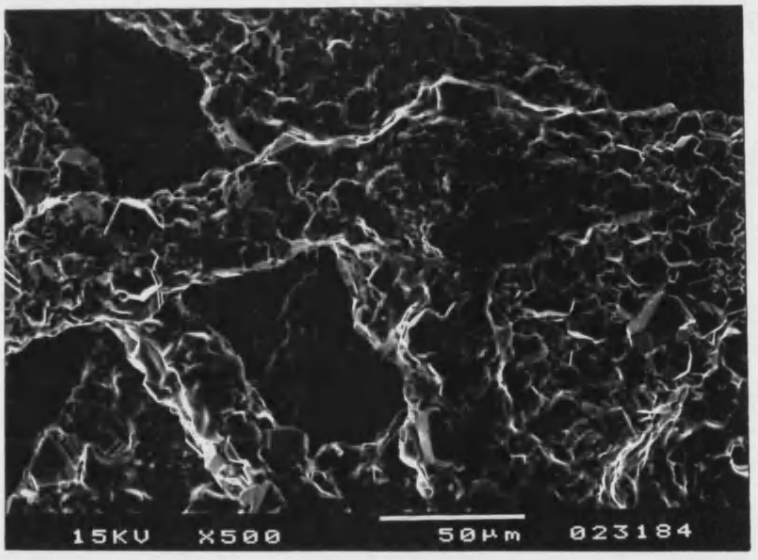

Figure VI-3-1 Scanning electron micrographs of the surfaces for porous SiC materials from carbons by paper making technology

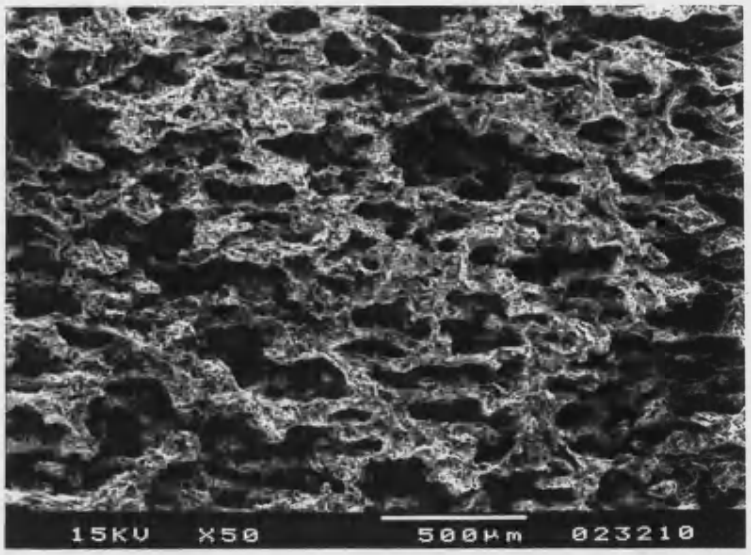

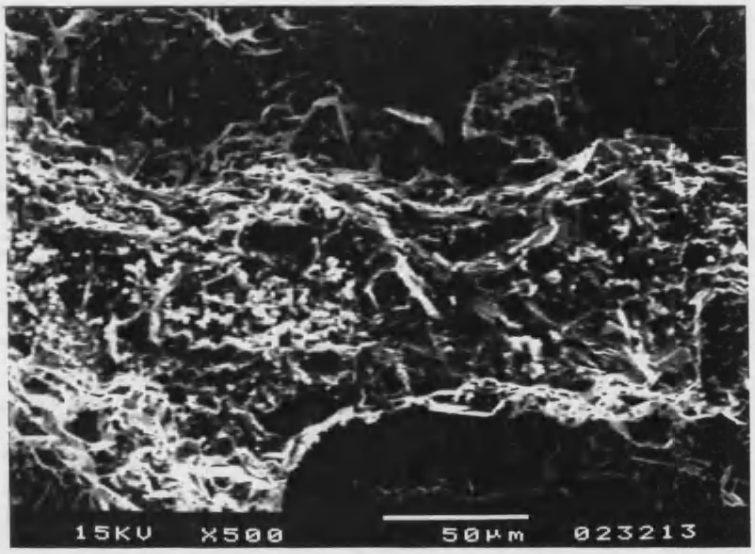

Figure VI-3-2 Scanning electron micrographs of the fracture sections for porous SiC materials from carbons by paper making technology

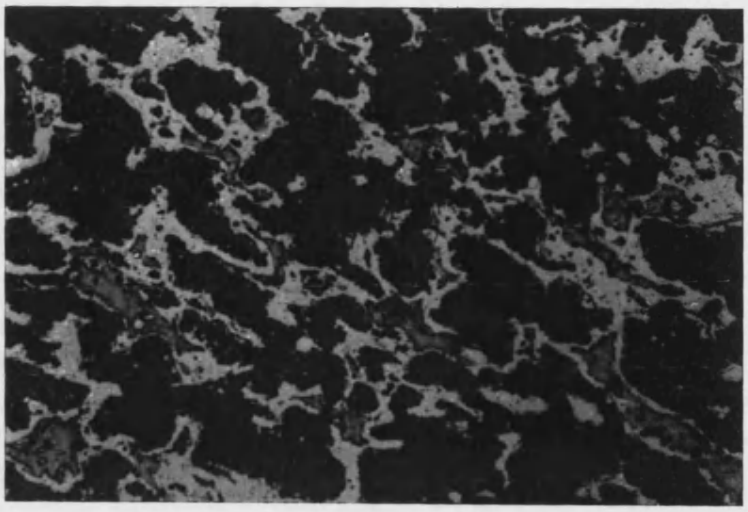

(a)

100 μm

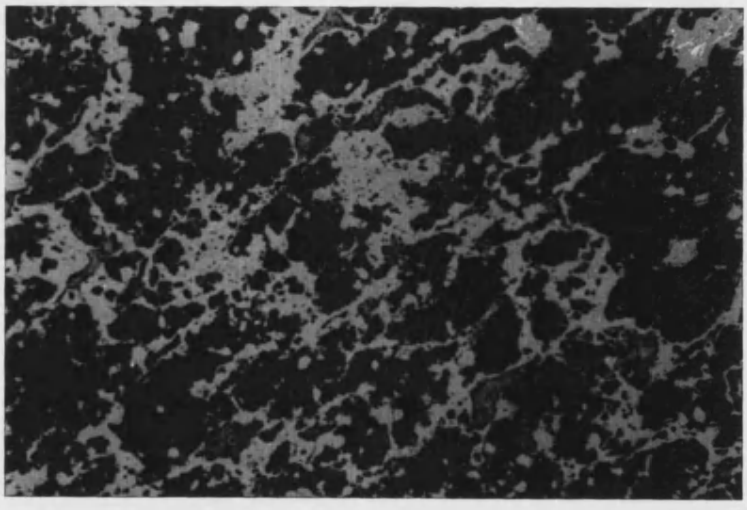

(b)

100 μm

Figure VI-3-3 Microstructures of polished sections for porous SiC materials produced (a) under reduced pressure and (b) at atmospheric pressure

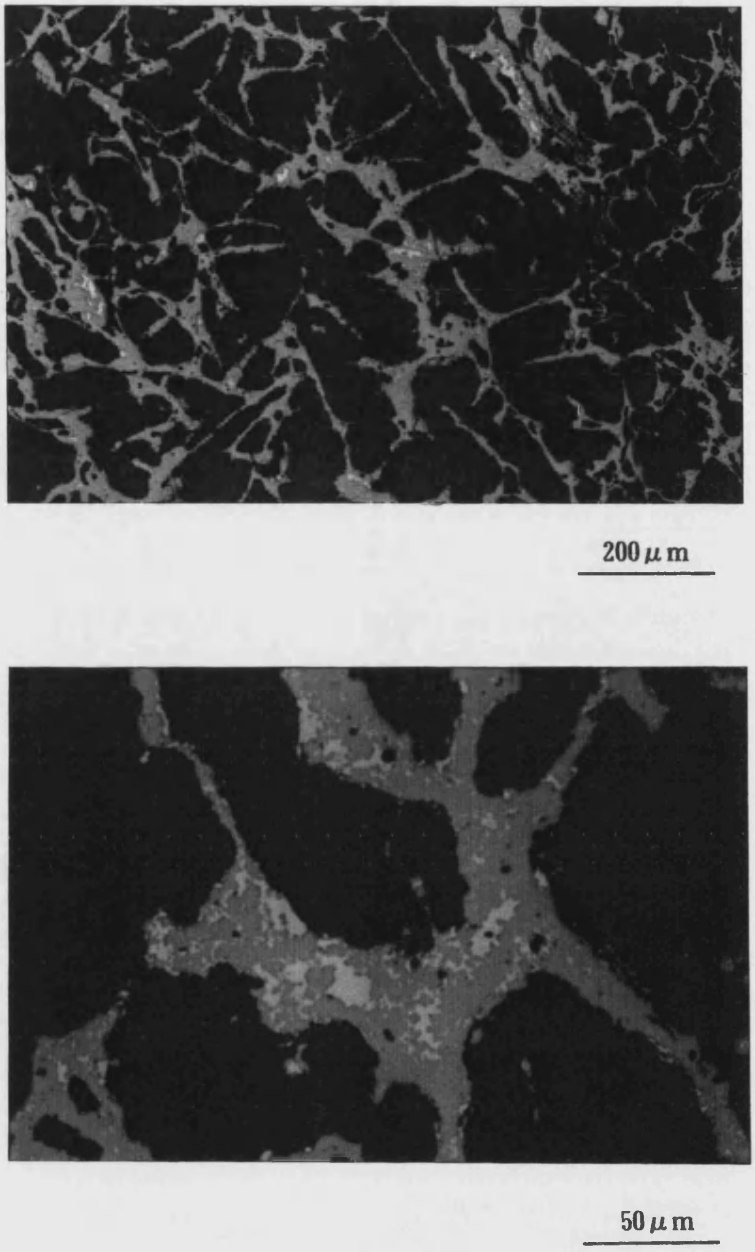

Figure VI-3-4 Optical micrographs of the polished sections (perpendicular to the laminating direction) for porous SiC materials made from carbons by paper making technology

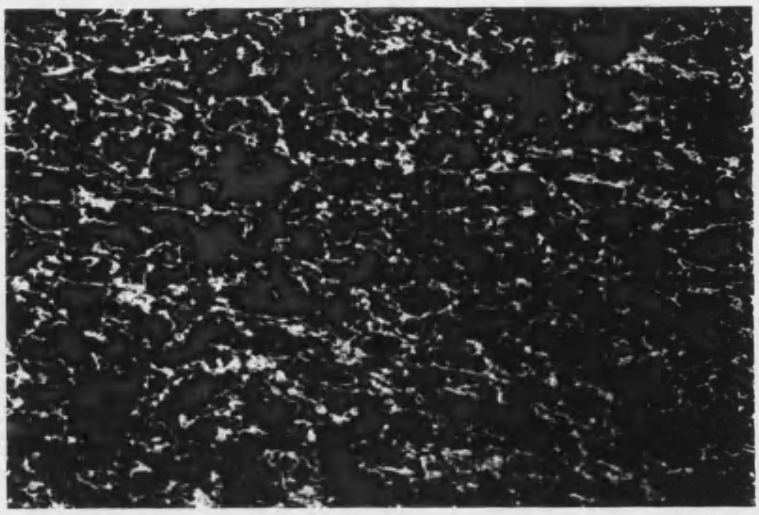

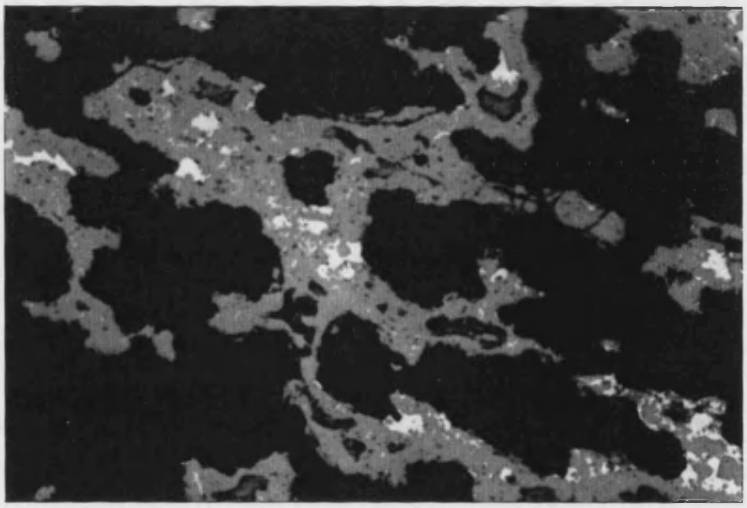

Figure VI-3-5 Optical micrographs of the polished sections (parallel to the laminating direction) for porous SiC materials made from carbons by paper making technology

Figure VI-3-6 Etched cross-section of porous SiC materials, showing grain orientations

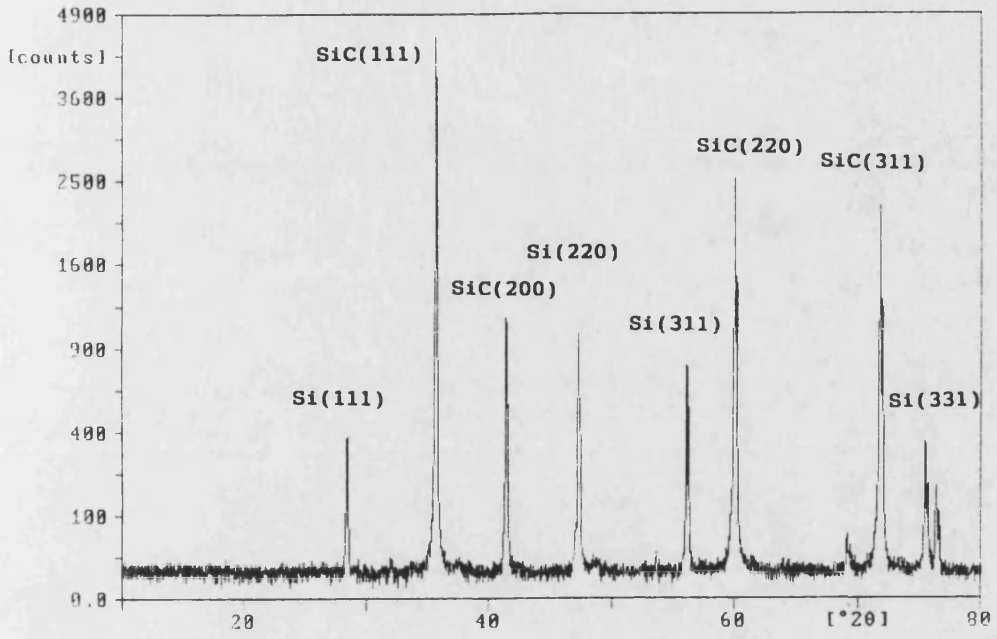

Figure VI-3-7 X-ray diffraction profile of porous SiC materials produced at atmospheric pressure

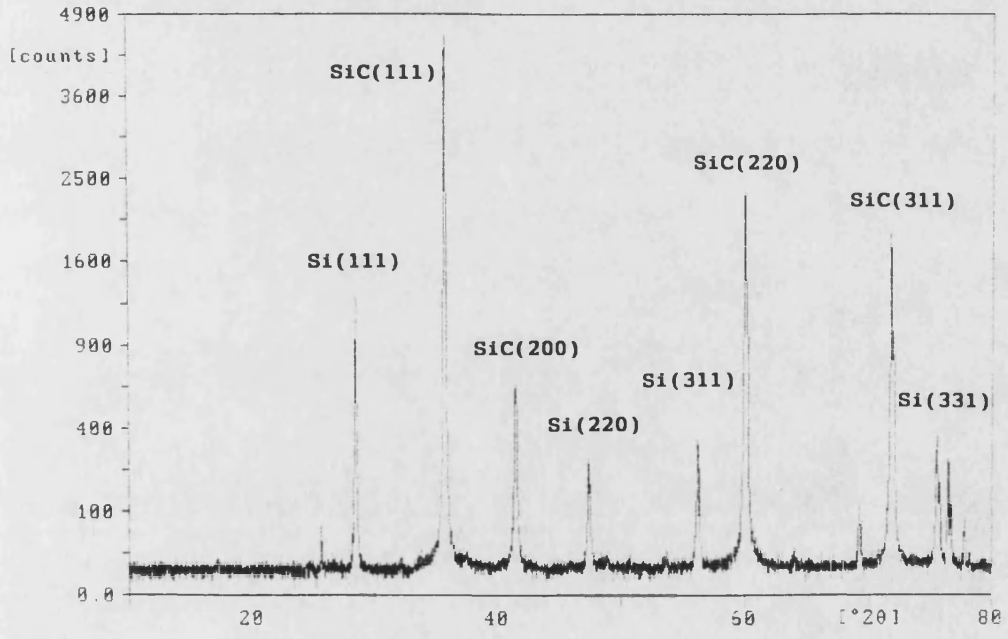

Figure VI-3-8 X-ray diffraction profile of porous SiC materials produced under reduced pressures

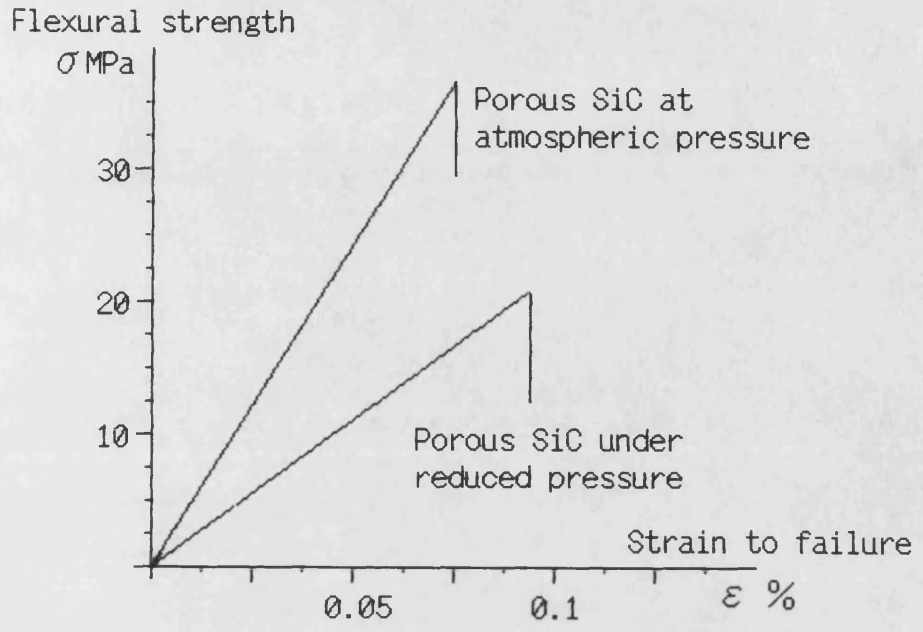

Figure VI-3-9 Schematic flexural stress-strain curves for porous reaction-bonded SiC materials

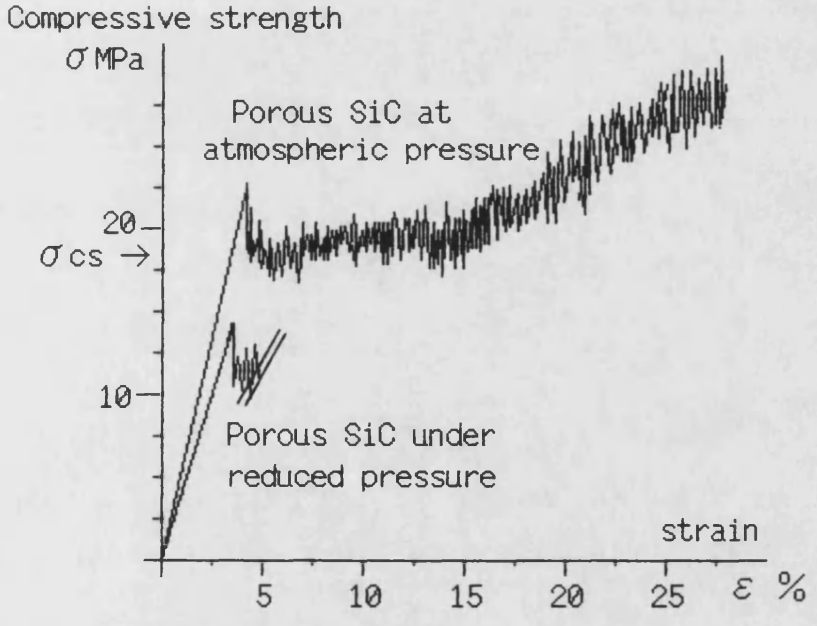

Figure VI-3-10 Schematic compressive stress-strain curves for porous reaction-bonded SiC materials

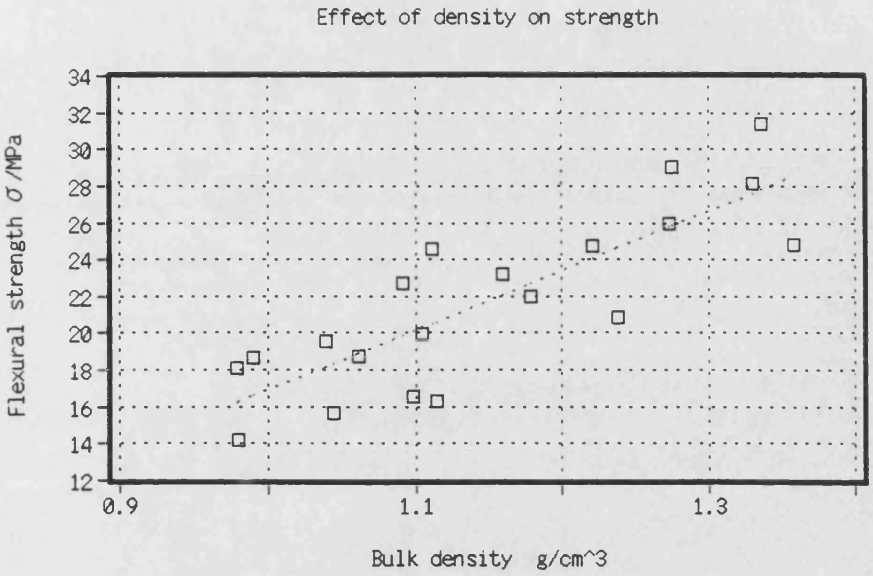

Figure VI-3-11 Flexural strength of porous SiC materials, plotted against bulk density

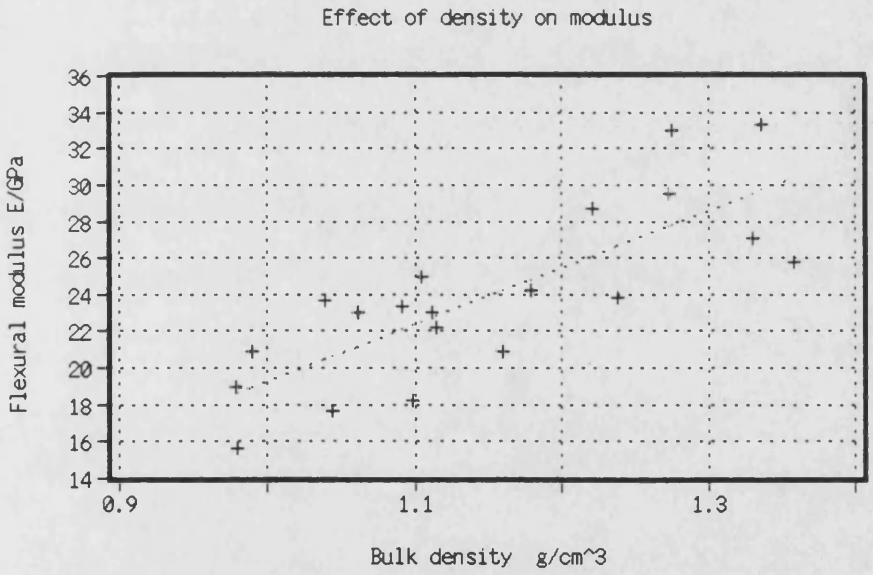

Figure VI-3-12 Flexural modulus of porous SiC materials, plotted against bulk density

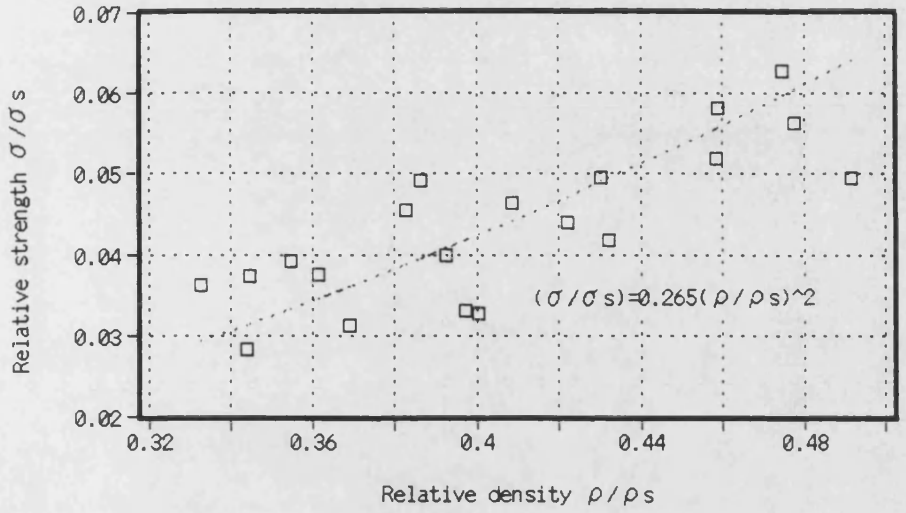

Figure VI-3-13 Relative flexural strength of porous SiC materials, plotted against relative density

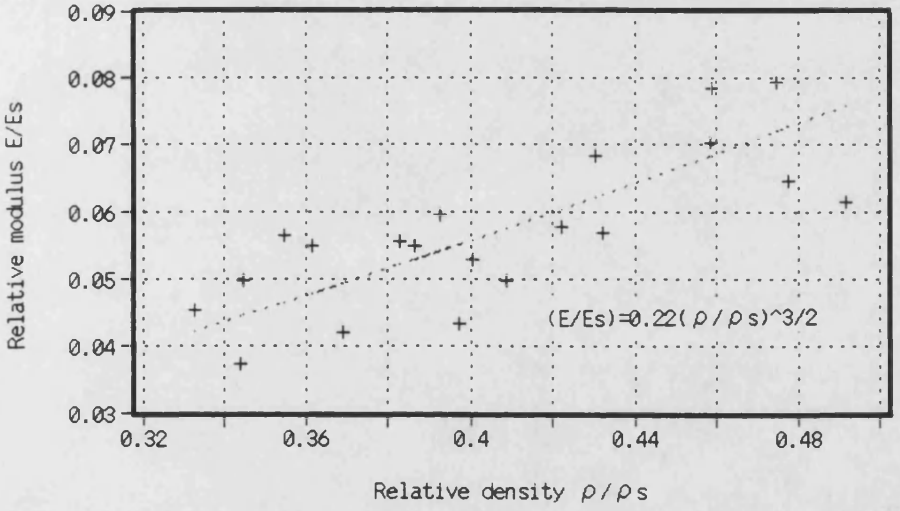

Figure VI-3-14 Relative flexural modulus of porous SiC materials, plotted against relative density

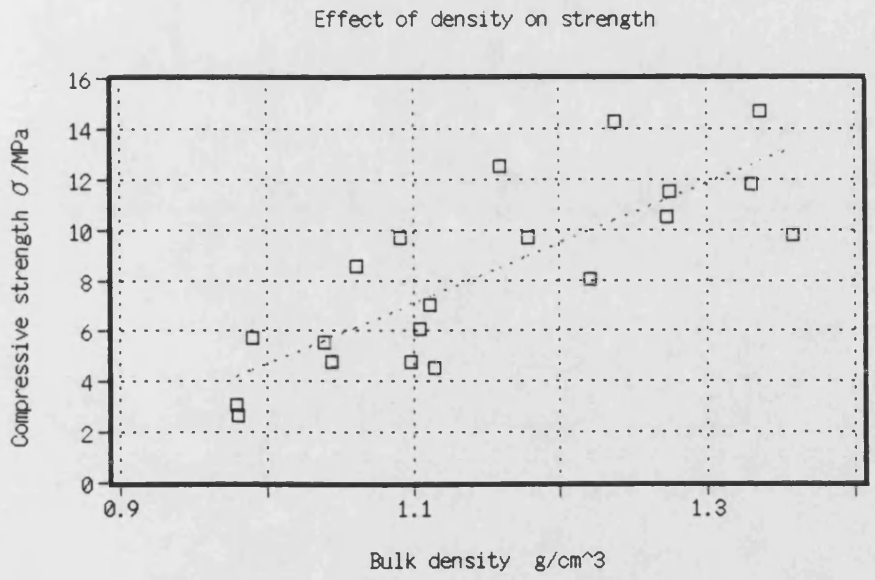

Figure VI-3-15 Compressive strength of porous SiC materials, plotted against bulk density

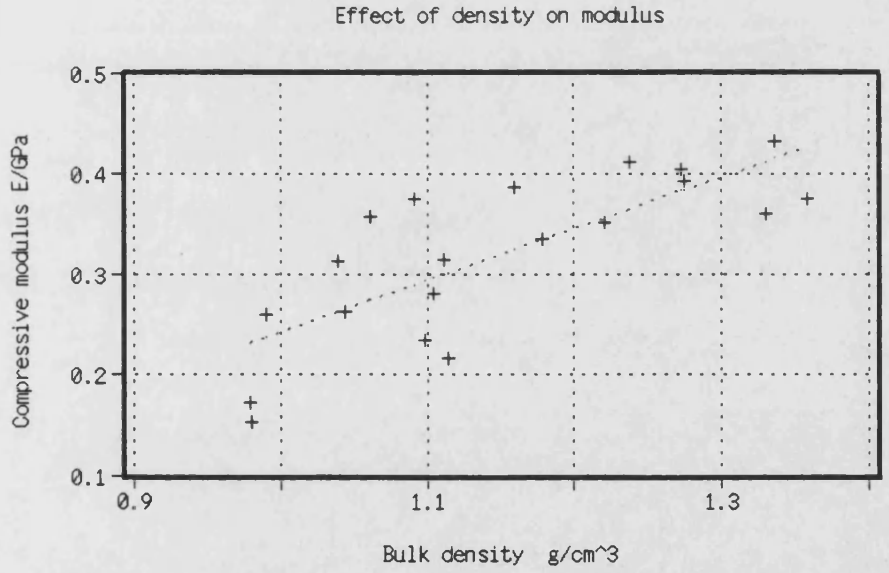

Figure VI-3-16 Compressive modulus of porous SiC materials, plotted against bulk density

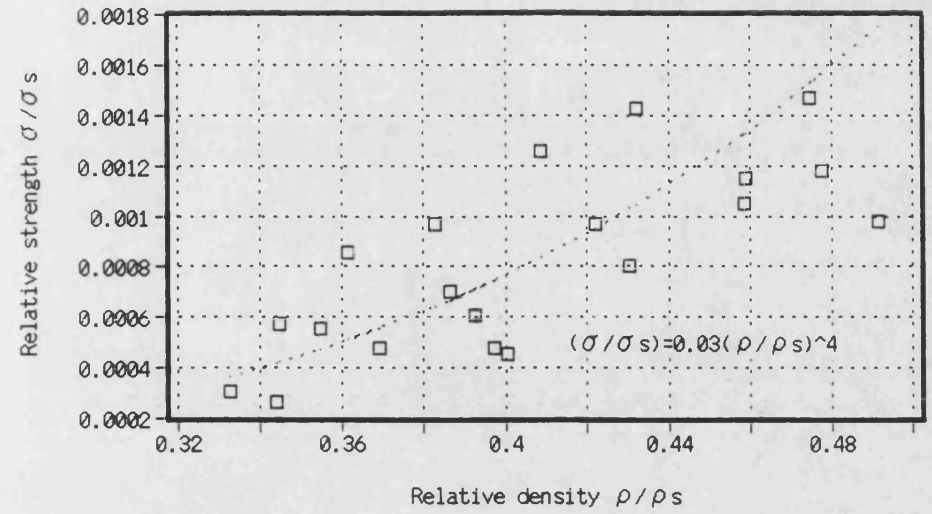

Figure VI-3-17 Relative compressive strength of porous SiC materials, plotted against relative density

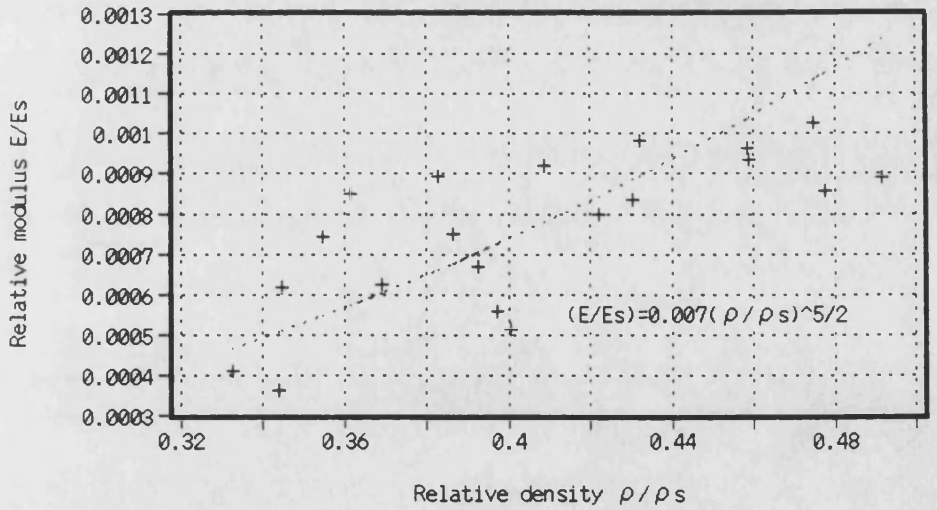

Figure VI-3-18 Relative compressive modulus of porous SiC materials, plotted against relative density

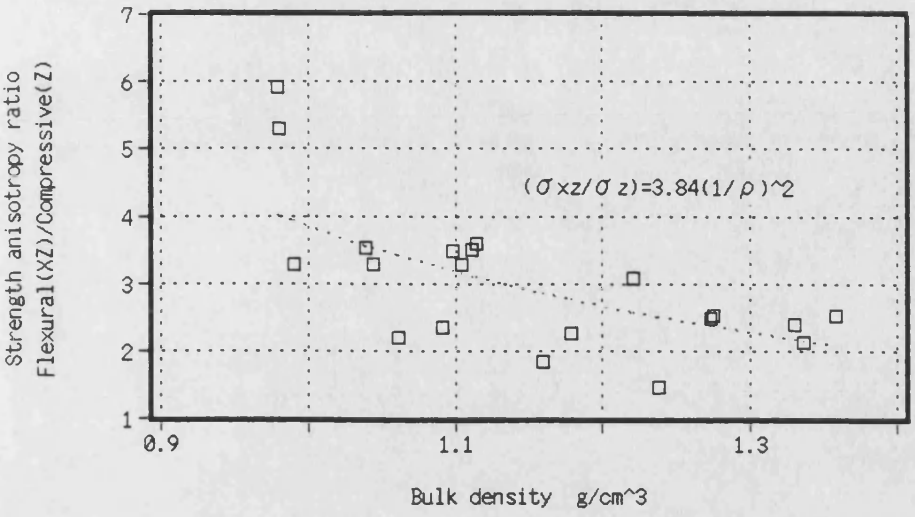

Figure VI-3-19 Strength anisotropy (Flexural(XZ) / Compressive(Z)) of porous SiC materials, plotted against bulk density

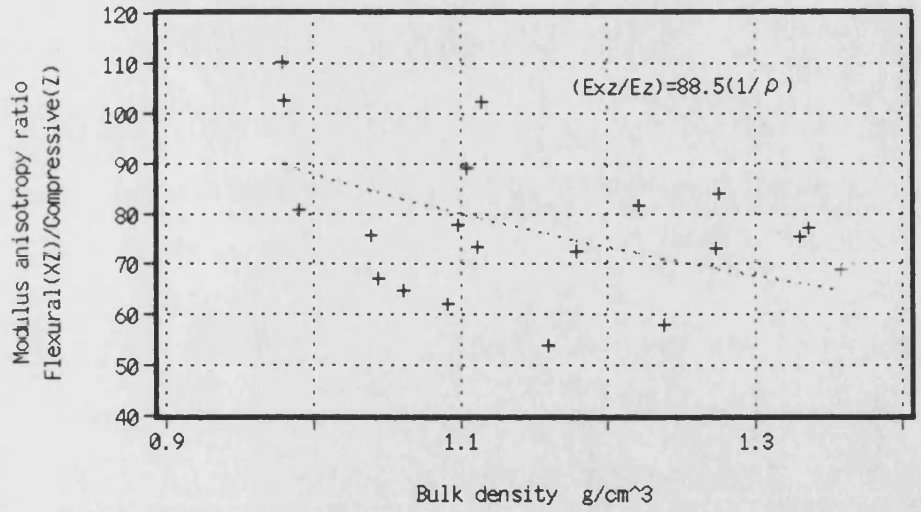

Figure VI-3-20 Modulus anisotropy (Flexural(XZ) / Compressive(Z)) of porous SiC materials, plotted against bulk density

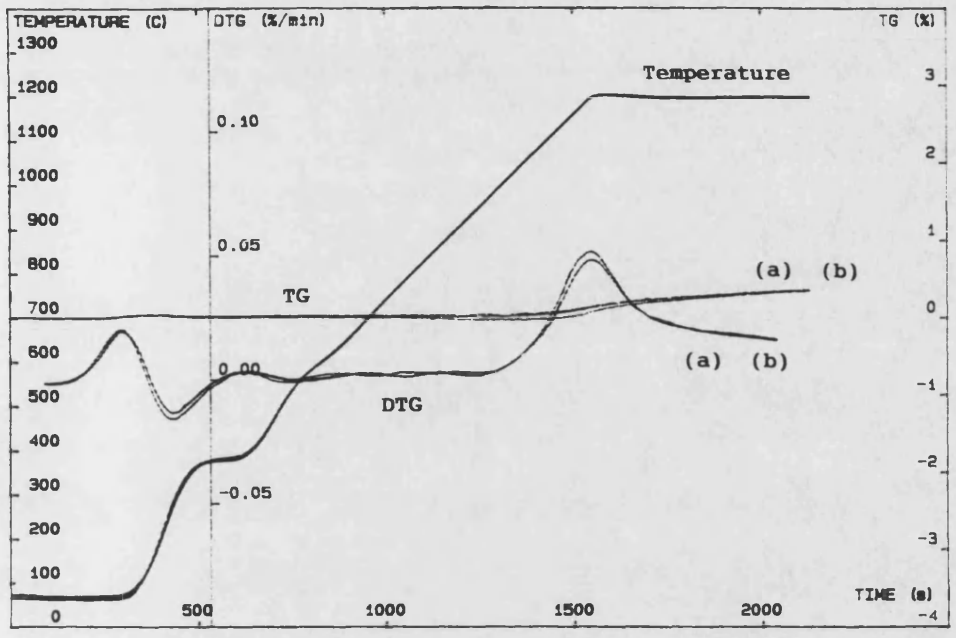

Figure VI-3-21 Thermogravimetric analysis of porous SiC materials produced at (a) at atmospheric pressure and (b) under reduced pressures

Bulk density ρ (g/cm^3)	Compressive properties	
	strength σ (MPa)	modulus E (GPa)
0.0779	0.030	0.0042
0.0811	0.051	0.0048
0.0888	0.052	0.0069
0.0902	0.048	0.0070
0.0928	0.063	0.0080
0.0930	0.045	0.0059
0.0958	0.059	0.0066
0.0965	0.048	0.0056
0.1001	0.057	0.0070
0.1016	0.107	0.0112
0.1098	0.060	0.0067
0.1101	0.080	0.0092
0.1122	0.118	0.0115
0.1136	0.116	0.0080
0.1141	0.135	0.0122
0.1243	0.116	0.0130

Table VI-4-1

Compressive properties of SiC foam materials

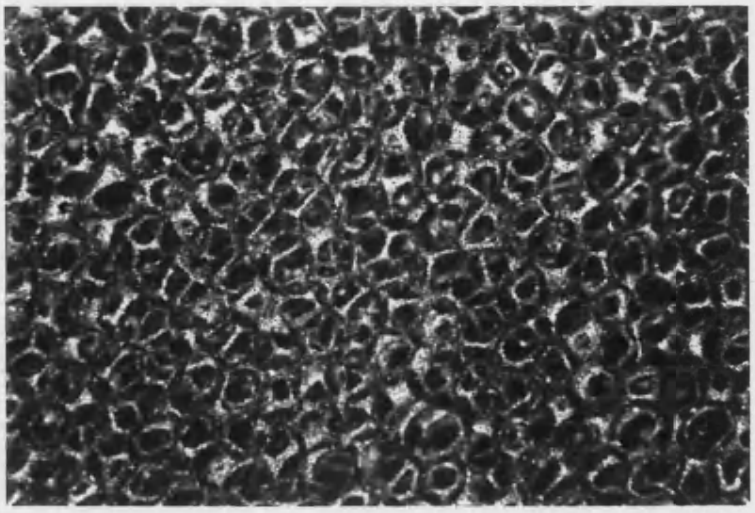

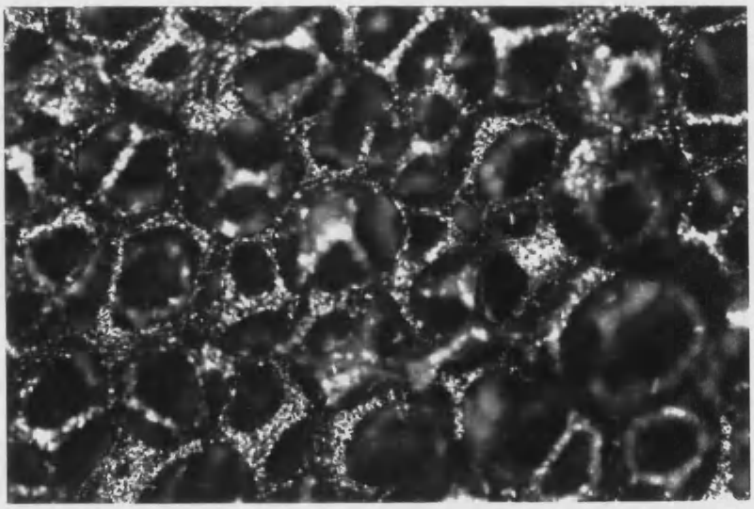

Figure VI-4-1 Optical micrographs of reaction-bonded SiC foams

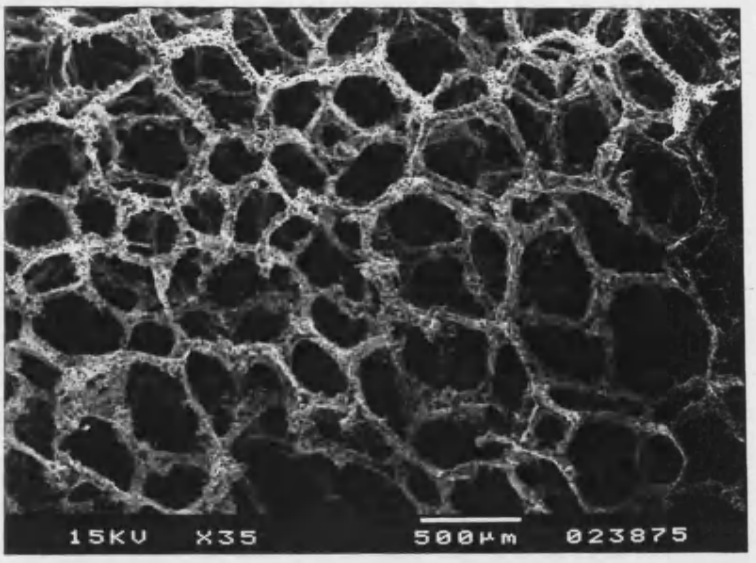

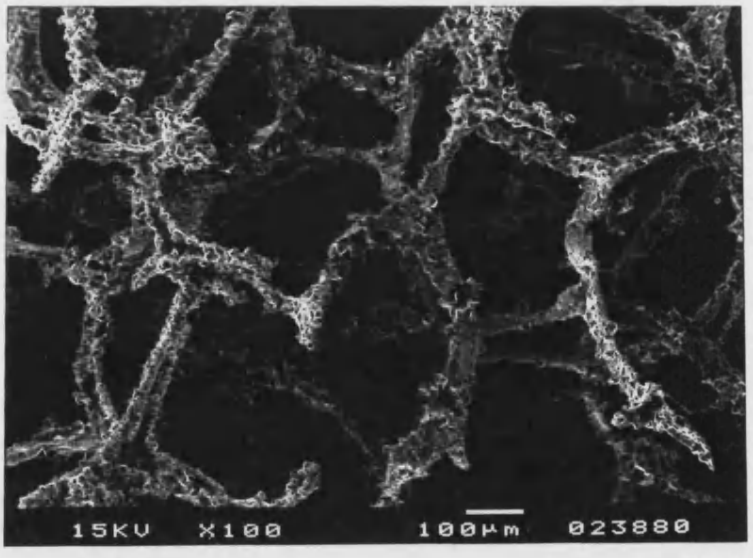

Figure VI-4-2 Scanning electron micrographs of reaction-bonded SiC foams

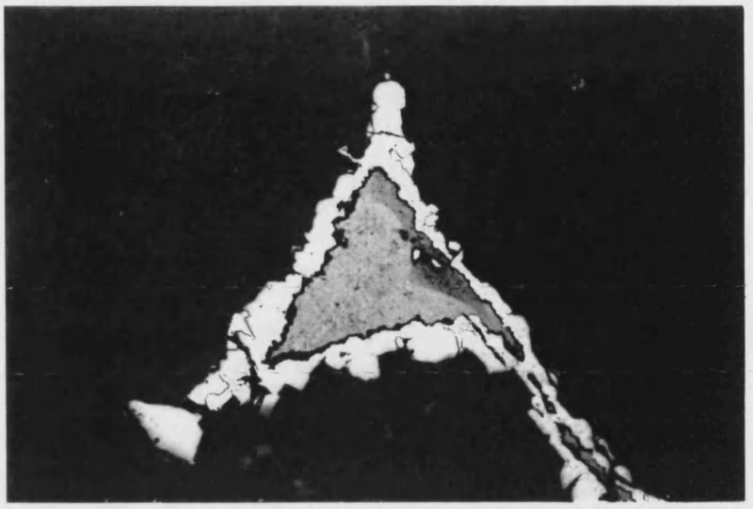

(a)

50 μm

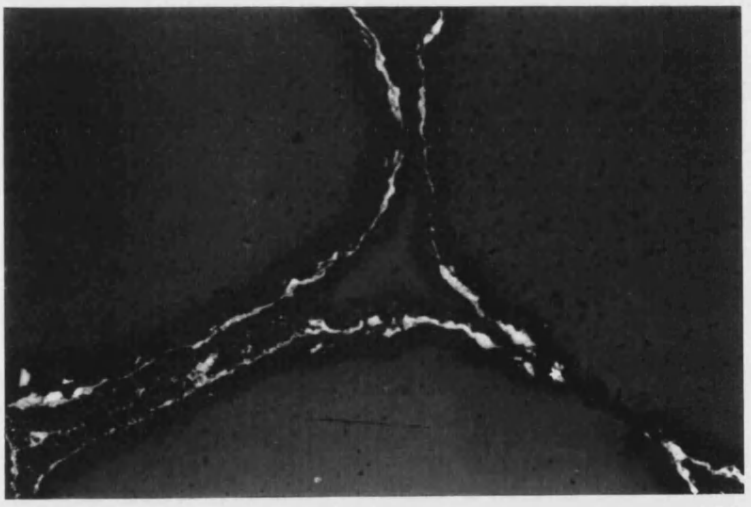

(b)

50 μm

Figure VI-4-3 Polished sections of struts for reaction-bonded SiC foams (a) after siliciding and (b) after oxidation

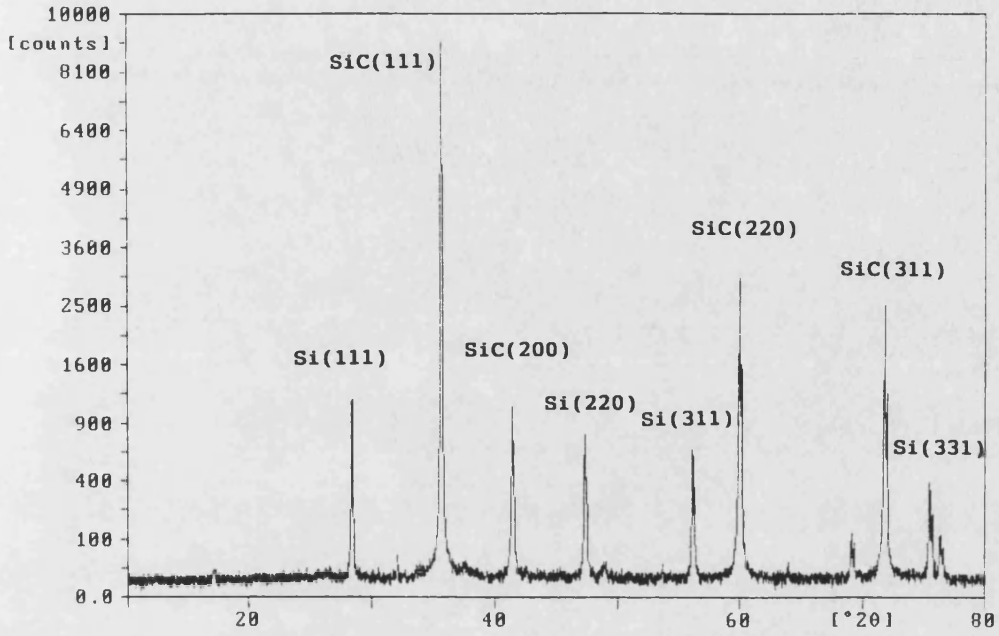

Figure VI-4-4 X-ray diffraction profile of SiC foams

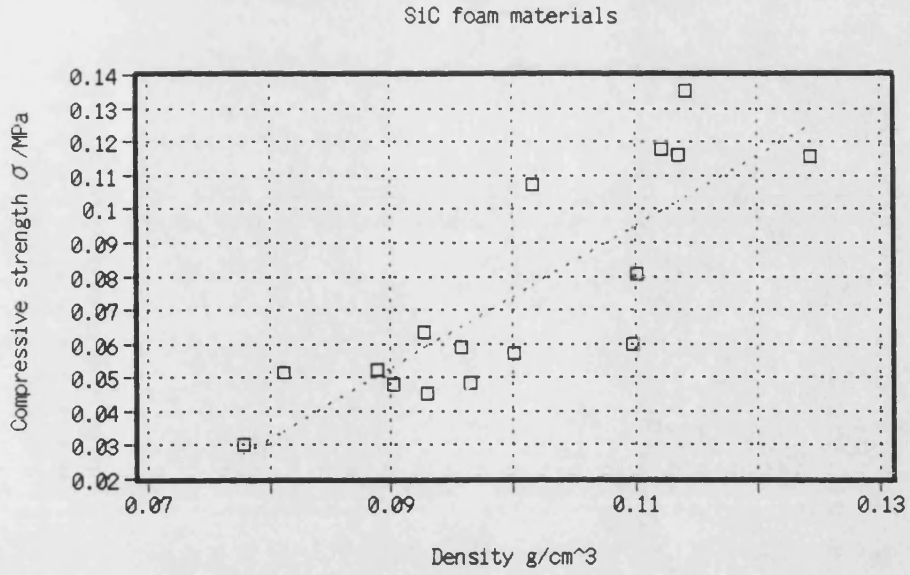

Figure VI-4-5 Compressive strength of SiC foams, plotted against bulk density

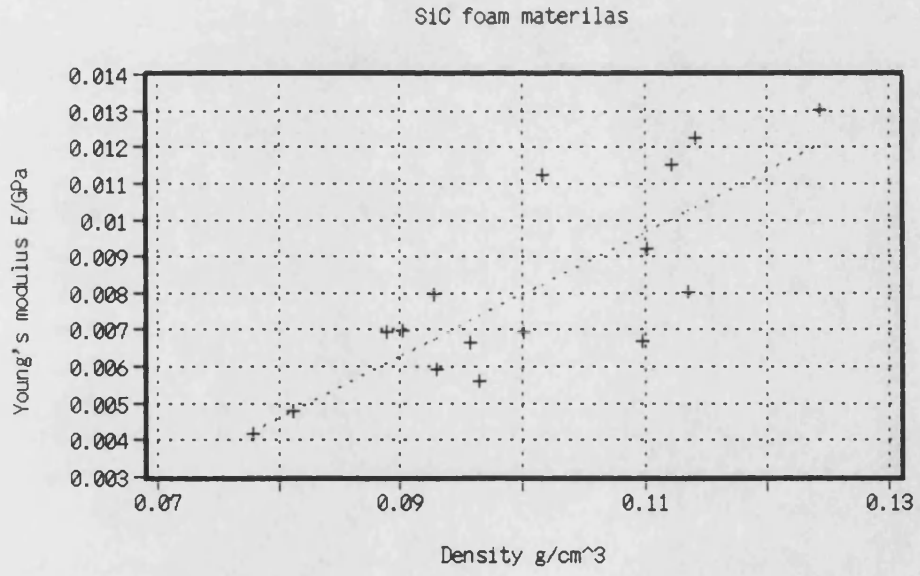

Figure VI-4-6 Compressive modulus of SiC foams, plotted against bulk density

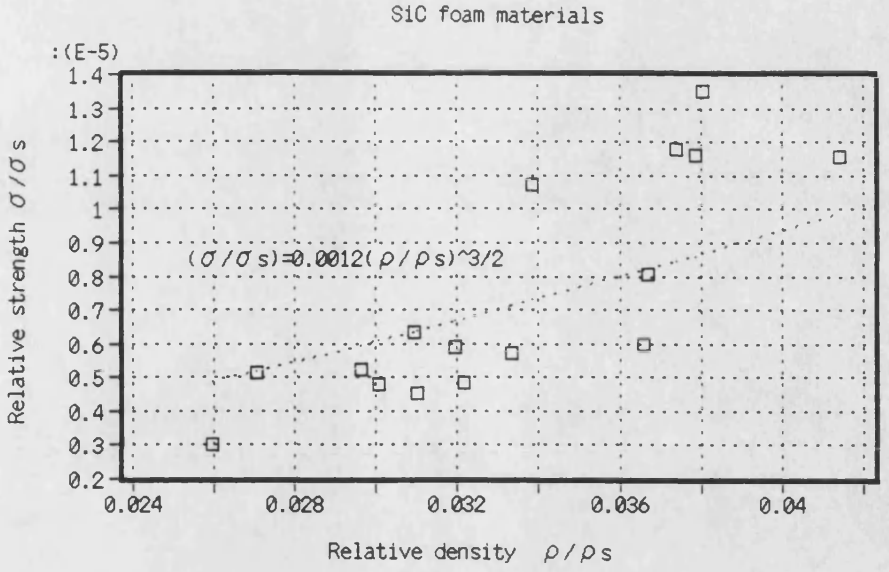

Figure VI-4-7 Relative compressive strength of SiC foams, plotted against relative density

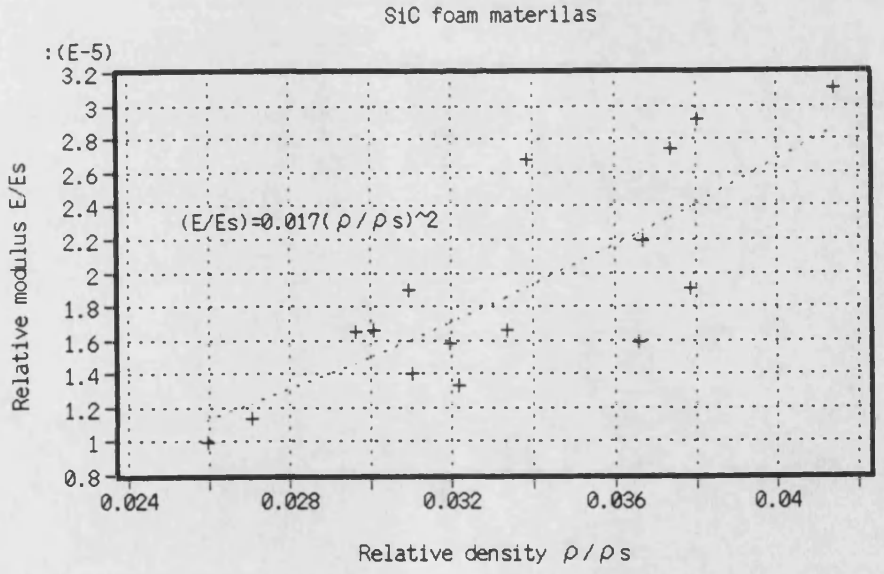

Figure VI-4-8 Relative compressive modulus of SiC foams, plotted against relative density

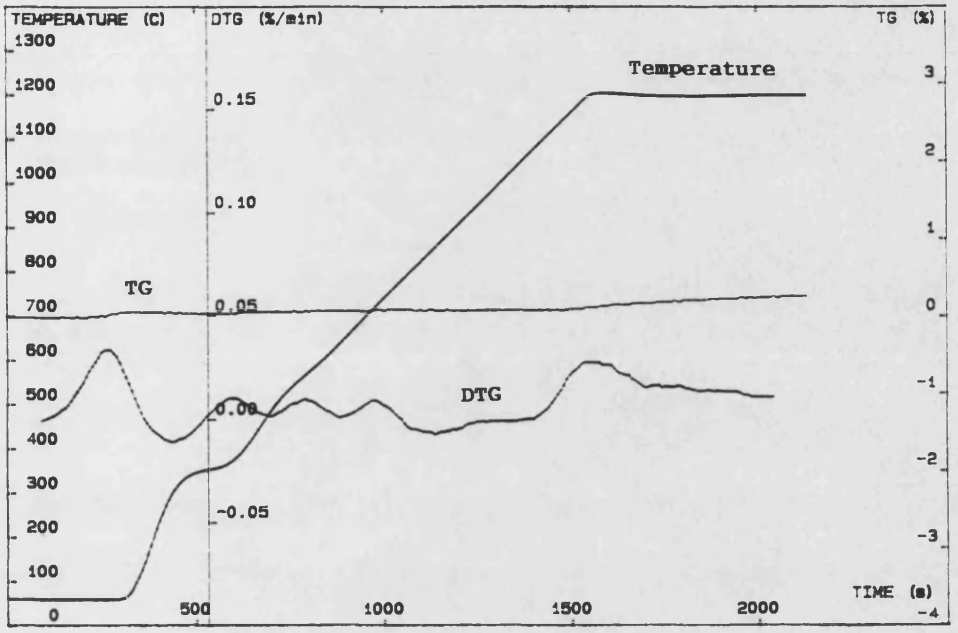

Figure VI-4-9 Thermogravimetric analysis of SiC foams

Bulk density g/cm^3	Porosity %	Tensile Strength (split cylinder test) MPa
2.44 ± 0.05	0.1 ± 0.0	78.68 ± 1.99

Table VI-5-1 Physical properties of reaction-bonded carbon-SiC/Si composites

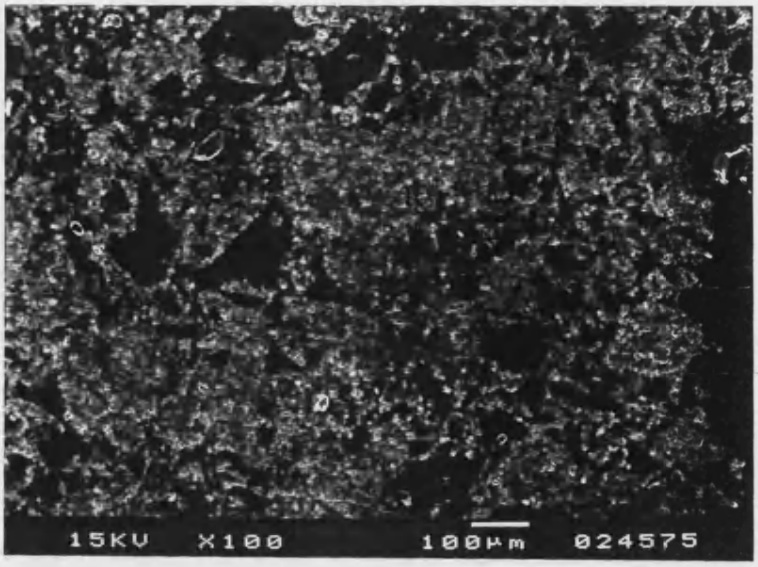

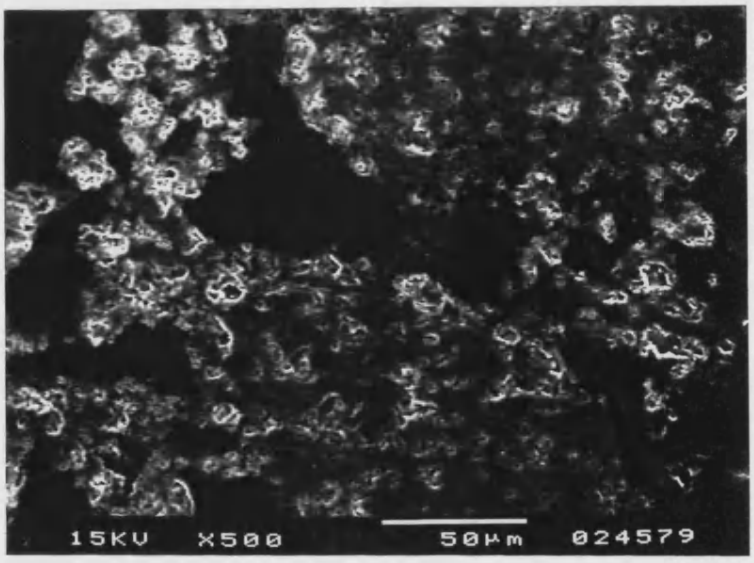

Figure VI-5-1 Scanning electron micrographs of carbon-SiC/Si composites

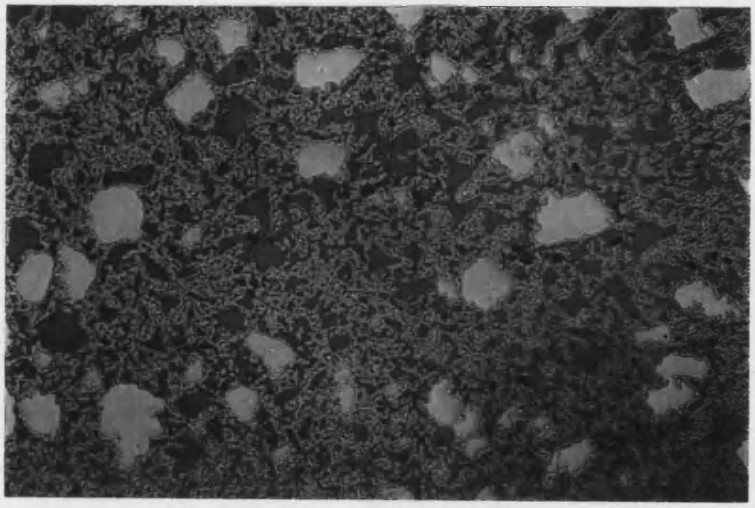

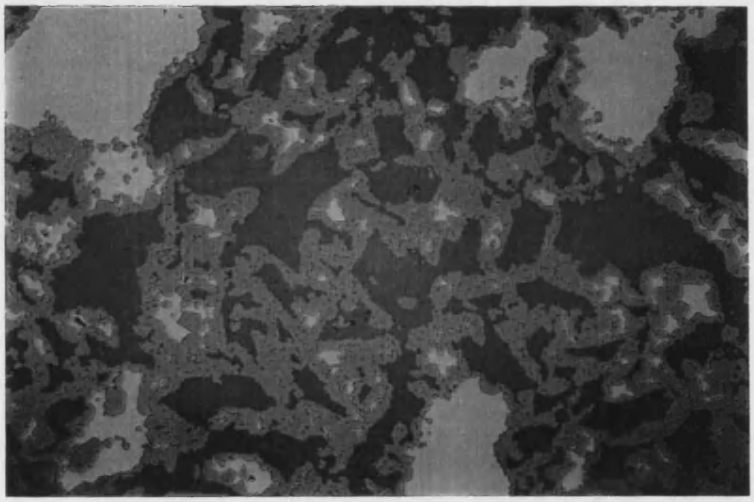

Figure VI-5-2 Optical micrographs of polished sections for carbon-SiC/Si composites

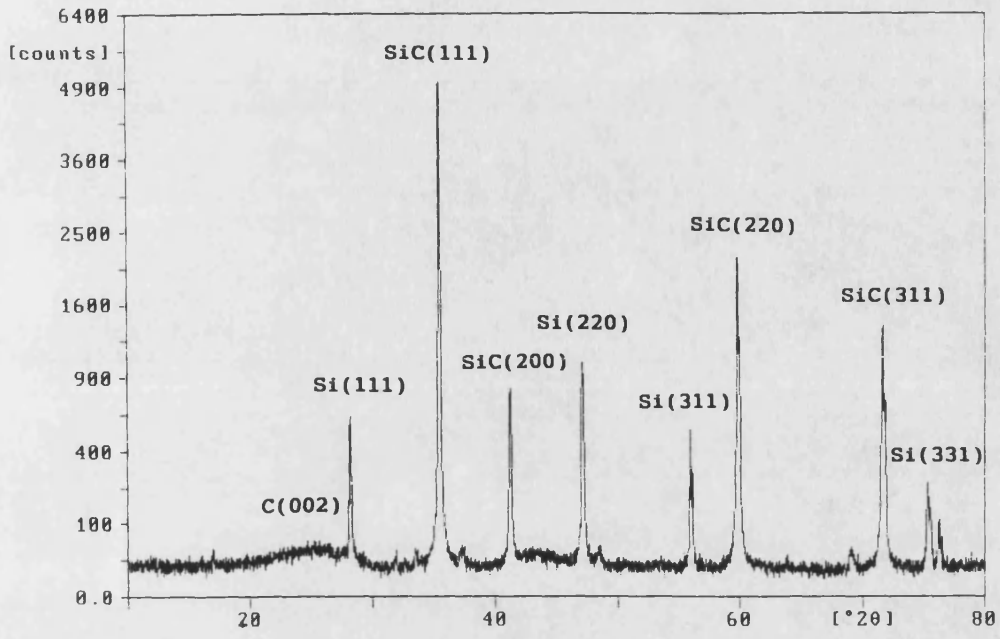

Figure VI-5-3 X-ray diffraction profile of carbon-SiC/Si composites

Bulk density ρ (g/cm^3)	0.946 ± 0.057
Porosity p (%)	67.8 ± 2.2
Flexural properties	
Strength σ (MPa)	12.6 ± 1.2
Modulus E (GPa)	12.5 ± 1.7
Compressive properties	
Strength σ (MPa)	11.05 ± 1.53
Modulus E (GPa)	0.108 ± 0.015

Table VI-6-1 Physical properties of porous SiC materials made from carbon bonded carbon fibre composites

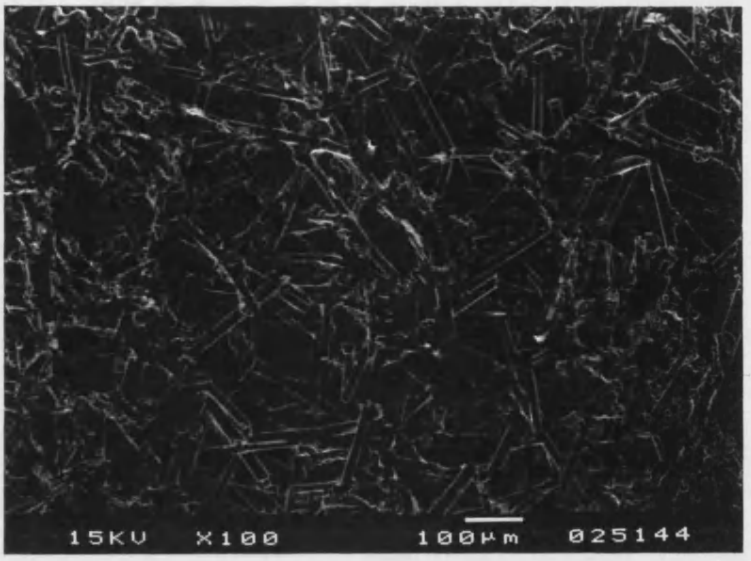

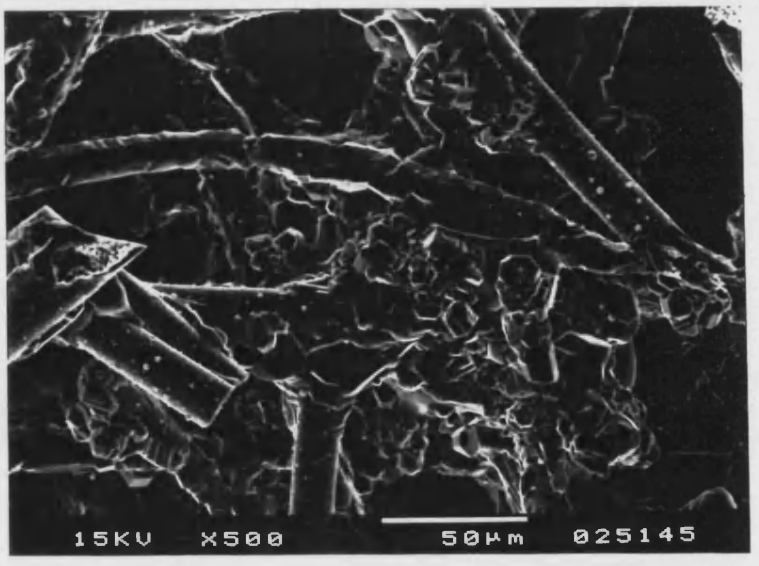

Figure VI-6-1(a) Scanning electron micrographs of the surfaces for porous SiC materials made from CBCF composites (perpendicular section to the moulding direction)

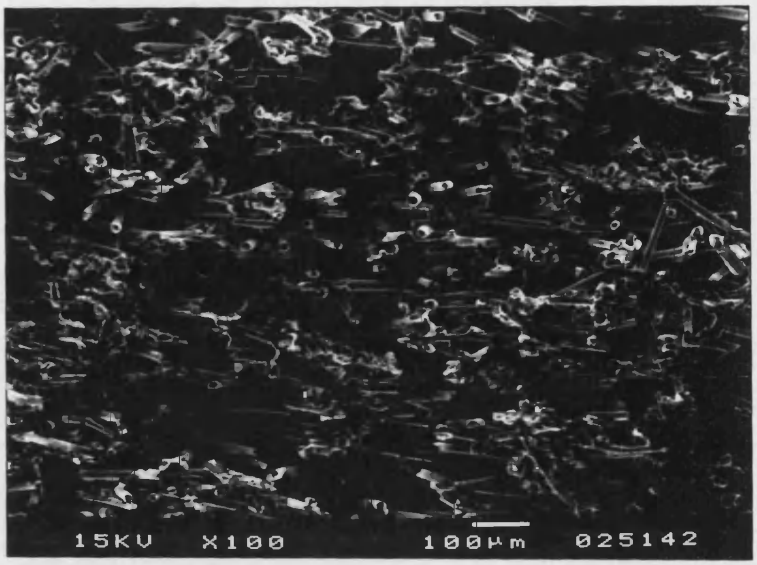

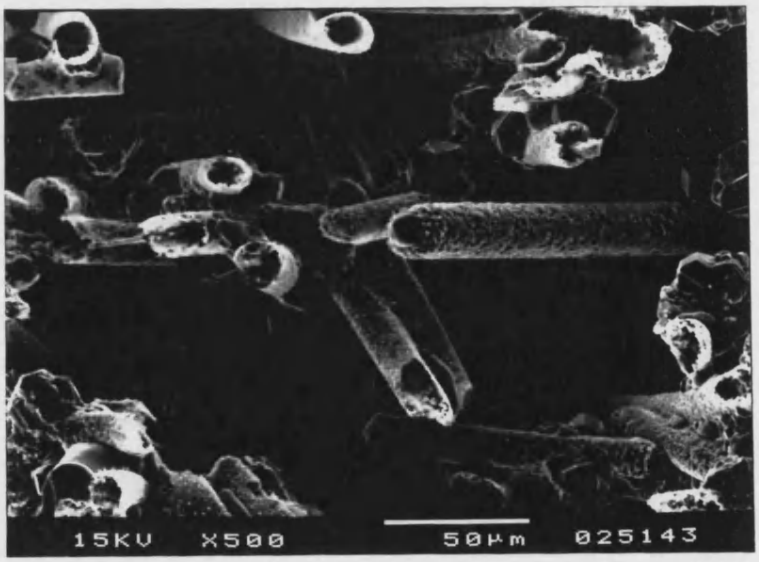

Figure VI-6-1(b) Scanning electron micrographs of the fracture sections for porous SiC materials made from CBCF composites (parallel section to the moulding direction)

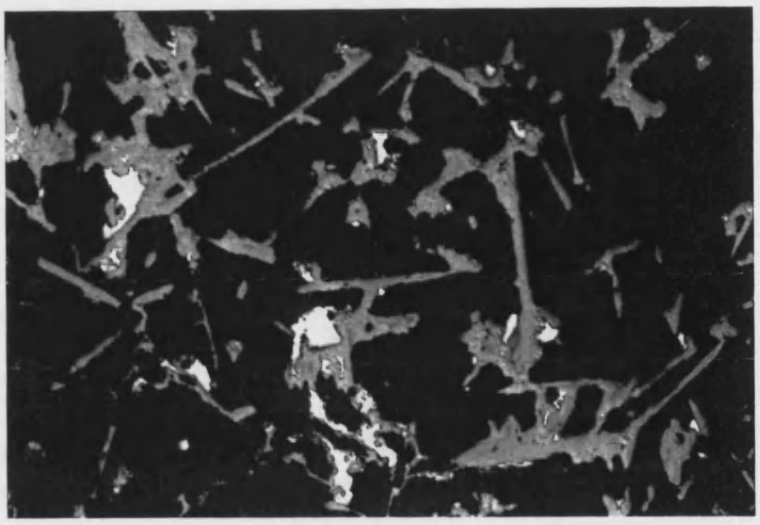

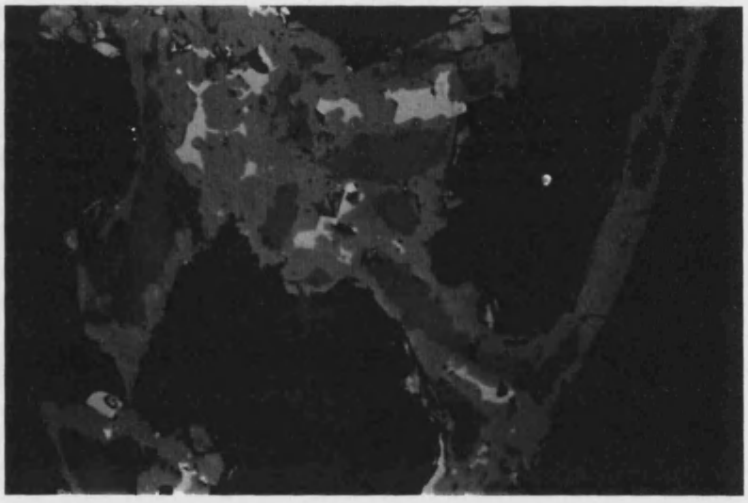

Figure VI-6-2(a) Polished sections of porous SiC materials made from CBCF composites (perpendicular to the moulding direction)

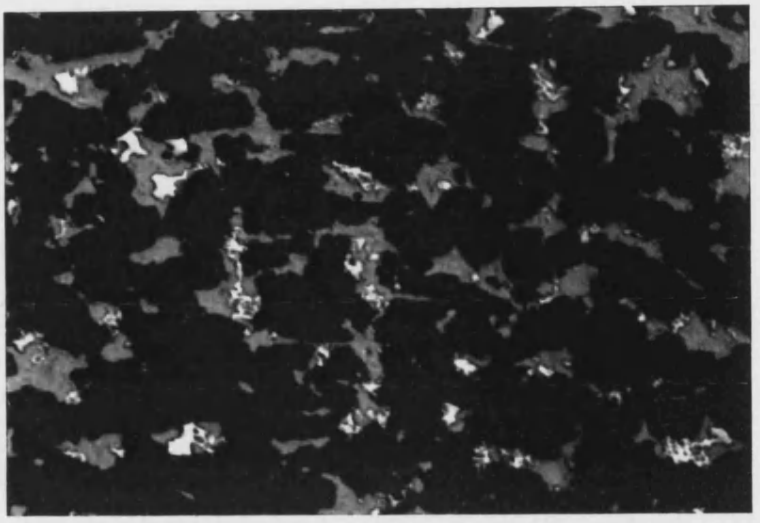

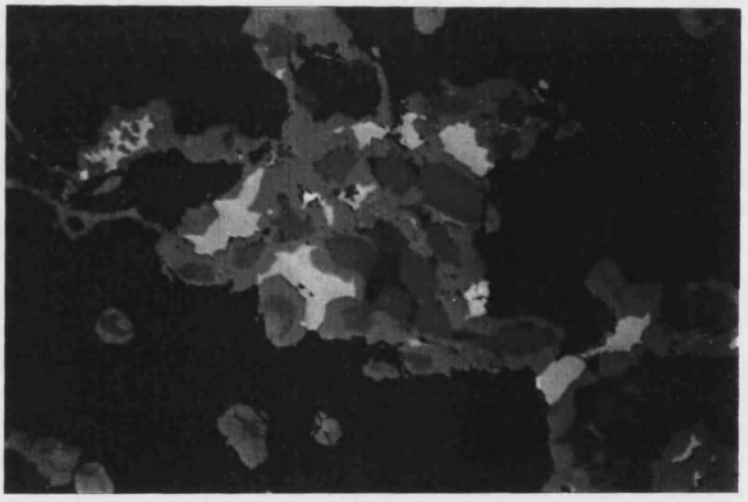

Figure VI-6-2(b) Polished sections of porous SiC materials made from CBCF composites (parallel to the moulding direction)

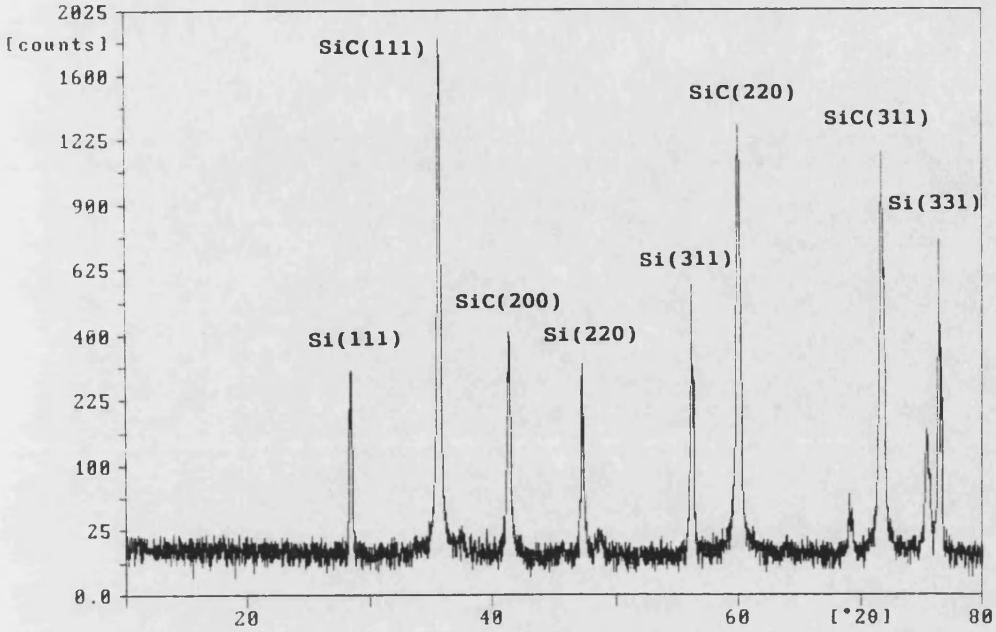

Figure VI-6-3 X-ray diffraction profile of porous SiC materials made from CBCF composites

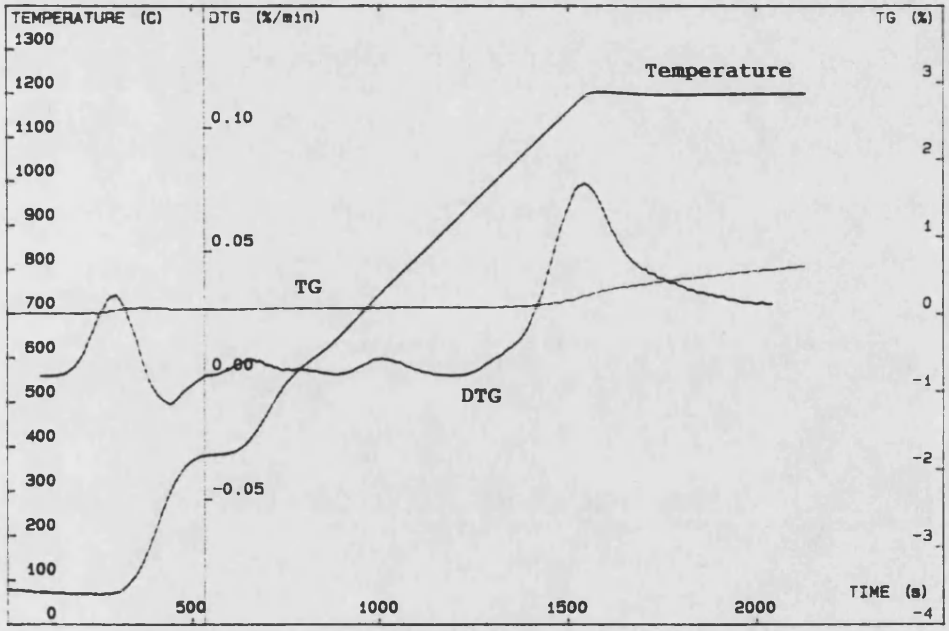

Figure VI-6-4 Thermogravimetric analysis of porous SiC materials made from CBCF composites

CHAPTER VII GENERAL DISCUSSION

VII-1 Introduction

In this work, various different forms of porous carbon and ceramic materials with a wide range of bulk density and porosity were studied. These materials exhibited properties which are related to their geometric structures and the different intrinsic nature of the materials. In this chapter, characteristics and properties of these porous materials are compared. In particular, their mechanical properties are correlated with density/porosity values. In addition, potential application fields which can be suggested from their characteristics are described.

VII-2 Porous carbon materials

The basic characteristics and properties of four different types of porous carbon materials investigated in this work are summarized in Table VII-2-1 (p.282). All of the materials consisted solely of the element carbon, however, their structural characteristics and mechanical properties were very diverse depending upon factors such as raw materials, fabrication process and technique, and thermal history.

Figure VII-2-1 (p.283) shows a relationship between porosity and bulk density (measured by water absorption) of porous carbon materials. The porosity naturally decreases approximately linearly in proportion to the increase of bulk density, because all materials were made of the same element of carbon in

spite of considerable variations in degree of graphitization of carbon.

Flexural strength ranges of these porous carbons plotted against bulk density are presented in Figure VII-2-2 (p.284). The flexural strength in the XZ direction of carbon bonded carbon fibre composites (CBCF) can be regarded as an extrapolation of those of the porous carbon materials made by paper manufacturing technology. This reflects similarities in their structural features, i.e., both materials have random arrays of bonded fibres in the XY plane. The tensile strength of resin powder based porous carbon is relatively low in comparison with the flexural strength values of the fibrous carbons. Brocklehurst (1977) has shown that in general for graphitic materials flexural strength is 1.4 to 2.5 times tensile strength. This goes some way to explain the apparently low value of the tensile strength of the resin powder based carbon. However, the absence of fibre reinforcement is probably also a factor in this case.

Figure VII-2-3 (p.284) presents flexural modulus ranges of fibrous carbons plotted against bulk density. As with flexural strength, the flexural modulus of the CBCF composites can be regarded as an extrapolation of those of the porous carbon materials made by paper manufacturing technology. It is also observed that flexural modulus of porous carbons made by paper manufacturing technology is greatly influenced by heat treatment temperature which causes graphitization.

Figure VII-2-4 (p.285) shows compressive strength ranges of these porous carbons plotted against bulk density. Carbon foams show relatively high strength, taking into a consideration of their extremely low density. This is mainly attributed to their interconnected 3-dimensional network of glassy carbon. Among fibrous carbons, their compressive strength in the Z direction varies significantly, due to degree of graphitization. Compressive modulus values versus bulk density are shown in Figure VII-2-5 (p.285). This trend is almost corresponding to that of compressive strength.

Consequently, mechanical properties of porous forms of carbon materials are greatly influenced by their geometrical structure and degree of graphitization, rather than just depending on density/porosity.

Porous carbon materials fabricated by paper making technology have various analogies in structural and mechanical features to carbon bonded carbon fibre composites. Therefore, the potential application fields of these fibrous carbons may be similar to each other. An important application of these fibrous carbons is electrode materials. In fact, performance of these fibrous carbons as electrodes for phosphoric acid fuel cells has been demonstrated. (Oji - 1990, Kureha - 1990)

Foamed resin based carbons are nearly identical to reticulated vitreous carbon (RVC). (Chapter II-1.4.3)

Hence, their applications are also expected as electrode materials, such as, for flow electrolysis and for heavy metal removal from industrial effluents, because of their high surface area and probable low resistance to fluid flow.

In addition, these fibrous carbons and carbon foams may be useful as high-temperature and corrosion resistant insulators and filters, however their applications are limited to non-oxidizing environments because of the poor oxidation resistance of carbon.

Resin powder based porous carbons may not be suitable for electrodes for flow systems, filters and insulators because their porosity is too low for these applications. There is interest in developing these materials as catalyst supports since it may be possible to tailor the pore structure by careful control of the fabrication process. (McEnaney - 1990)

VII-3 Porous carbon-ceramic composites

Porous carbon-ceramic composites, produced by infiltration of a silica sol-gel which was subsequently converted into SiC or Si_3N_4 into porous carbon preforms, improved their oxidation resistance so little that they cannot practically withstand applications under oxidizing atmosphere at temperatures above 400° C. However, mechanical properties of carbon preforms were slightly improved by the ceramic impregnations.

VII-4 Porous ceramic materials

In this section, mechanical properties of various types of reaction-bonded porous SiC materials are compared in relation to their density/porosity ranges. Carbon-SiC/Si composites from resin powder based porous carbons are excluded because they have a dense body not a porous structure.

Figure VII-4-1 (p.286) shows a relationship between porosity and bulk density of porous reaction-bonded SiC materials. The porosity, as a matter of course, decreases in an approximately linear manner with the increase of bulk density, because all materials consist of silicon carbide with a small amount of free silicon.

Flexural strength ranges of porous SiC materials from fibrous carbon preforms, plotted against bulk density are shown in Figure VII-4-2 (p.287). The flexural strength in the XZ direction of these fibrous carbon based SiC materials is nearly proportional to bulk density, regardless of kind of carbon preforms and pressure condition during the reaction bonding process. The trend of flexural modulus values versus bulk density (Figure VII-4-3, p.287) is almost corresponding to that of flexural strength. Therefore, flexural properties of fibrous carbon based SiC materials are dependent chiefly on bulk density.

Figures VII-4-4 and VII-4-5 (p.288) show compressive strength and modulus ranges of porous SiC materials plotted against bulk density, respectively. The trends of these compressive properties of porous reaction-

bonded materials are, basically, identical to those of carbon preforms, except for some minor changes. SiC foams show low strength and modulus, even if their extremely low density is taken into consideration. This is mainly attributed to the hollow nature of the cell struts.

Consequently, the mechanical properties of porous forms of reaction-bonded SiC materials versus bulk density are virtually corresponding to those of the carbon preforms, because the basic structure of the carbon preforms, in principle, was inherited by the porous ceramics.

The principal potential applications of fibrous carbon based porous SiC materials are high temperature and corrosion resistant insulators and filters. In particular, these materials have potential as highly efficient particulate removal filters which are critical in a wide range of industrial processes. (Chapter II-1.5.2) High temperature gas filters have to withstand extraordinary severe circumstances with the effluent gas stream chemistry. Projected chemical effects on reaction-bonded SiC filters include, e.g., reaction of free silicon, small pore closure and loss of material strength. Thus, fibrous carbon based SiC materials should be assessed for their long-term durability with high particulate collector performance. Also they are expected to be useful as lightweight core materials for sandwich panels where high-temperature

and severe circumstances are applied.

Reaction-bonded SiC foams are also anticipated to be applied as insulators, filters and lightweight core materials. However, their mechanical properties are poor due to the hollow nature of cell struts. Therefore, higher conversion of glassy carbon into SiC should be investigated.

Carbon-SiC/Si composites may be investigated as bio-implant materials, because their mechanical properties are high and both carbon and SiC are known as to have biocompatibility. (Huttinger - 1983)

Porous carbon materials	Structural characterization	Bulk density g/cm^3	Porosity %	Nature of carbon	Mechanical properties			
					flexural properties		compressive properties	
					strength MPa	modulus GPa	strength MPa	modulus GPa
Porous carbons fabricated by paper making technology	-open pores structure -random in plane structure -coherent fibre-matrix	0.41 - 0.62 0.521	76.2 - 64.5 72.5	-highly graphitized -low graphitized	8.06-20.63 13.5	1.62-5.08 5.6	0.23-1.45 2.69	0.011-0.07 0.123
Foamed resin based carbons	-interconnected 3-dimensional network (reticulated) -open pores structure	0.0245 - 0.0681	ca. 98 - 95	-amorphous glassy			0.021-0.110	0.0029-0.0209
Resin powder based porous carbons	-open pores structure -larger pores interconnected 3-dimensionally with small channel-like pores	0.94	44.4	-amorphous	* 6.44			
Carbon bonded carbon fibre composites	-open pores structure -random in planer fibres bonded by discrete matrix	0.347	76.7	-mainly amorphous but marginally graphitized	4.91	0.76	0.68	0.021

* Tensile strength

Table VII-2-1 Basic characteristics and properties of different types of porous carbon materials

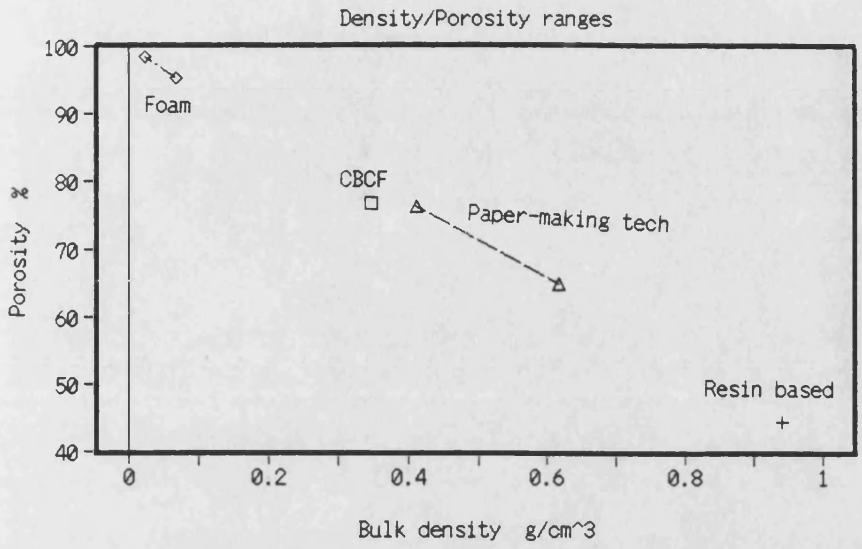

Figure VII-2-1 Relation between porosity and bulk density of porous carbon materials

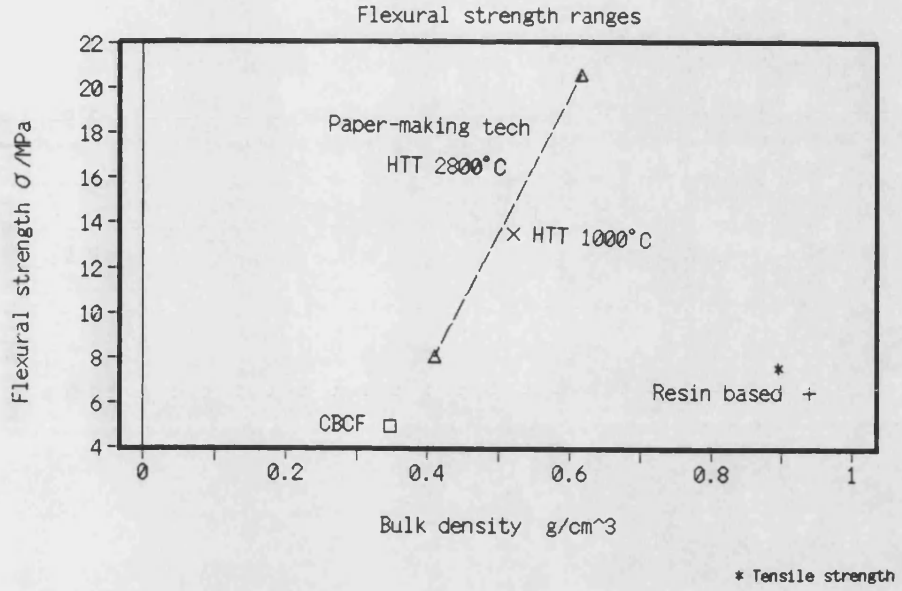

Figure VII-2-2 Flexural strength ranges of porous carbon materials, plotted against bulk density

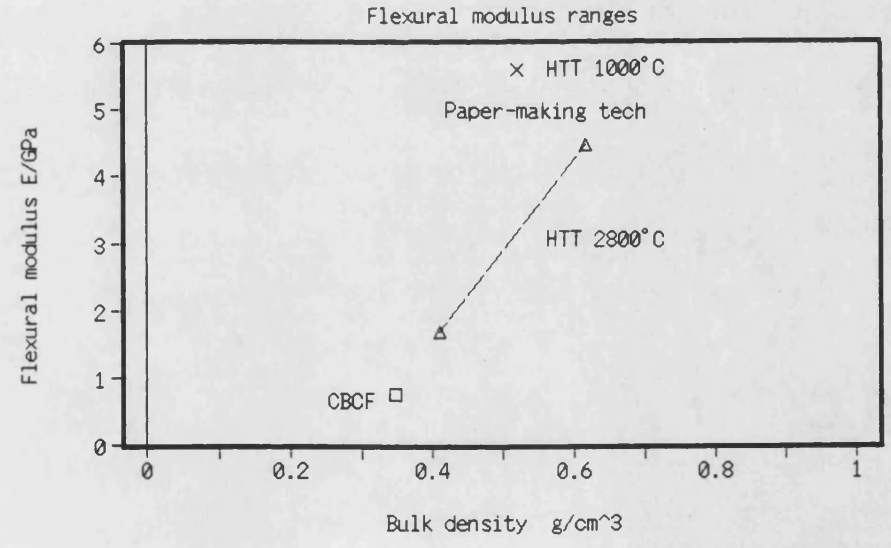

Figure VII-2-3 Flexural modulus ranges of porous carbon materials, plotted against bulk density

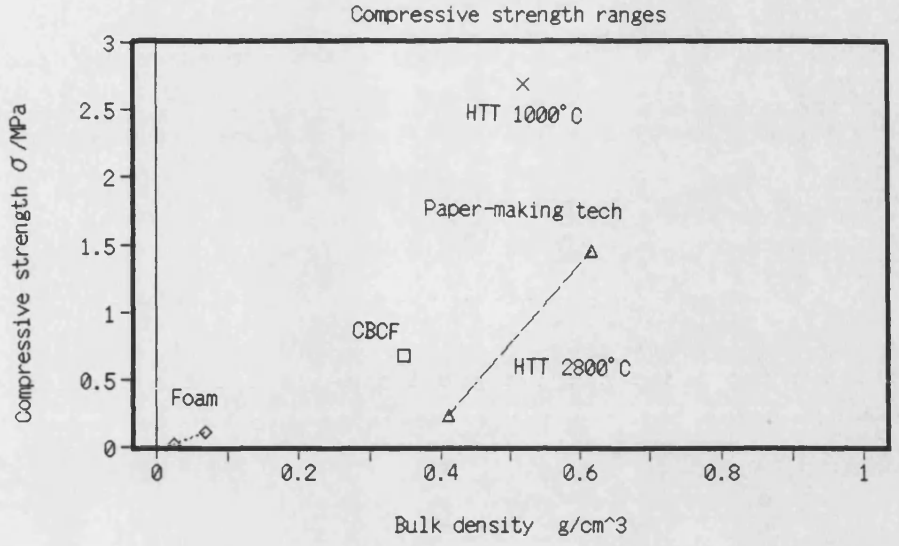

Figure VII-2-4 Compressive strength ranges of porous carbon materials, plotted against bulk density

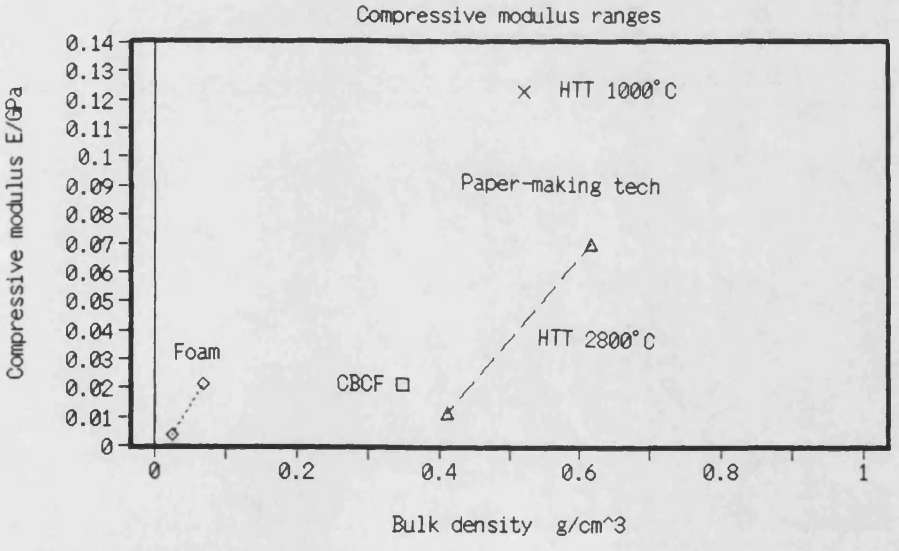

Figure VII-2-5 Compressive modulus ranges of porous carbon materials, plotted against bulk density

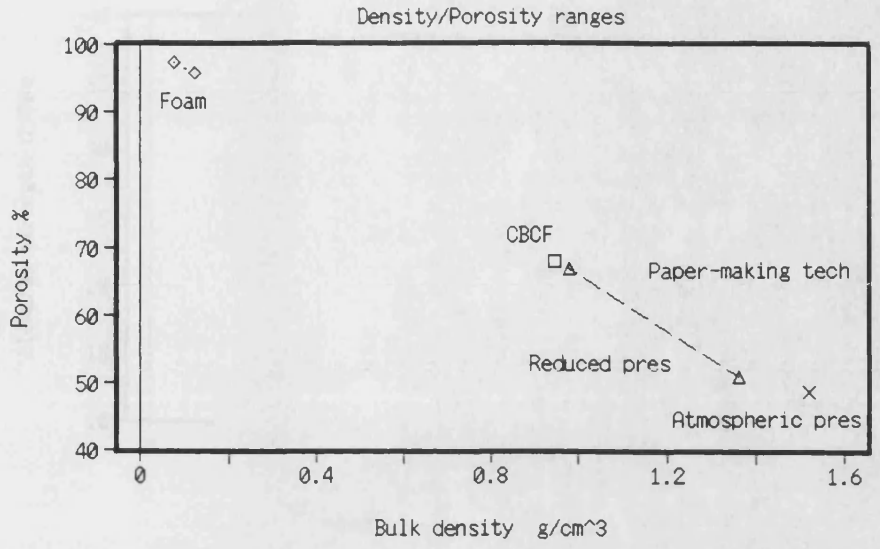

Figure VII-4-1 Relation between porosity and bulk density of porous SiC materials

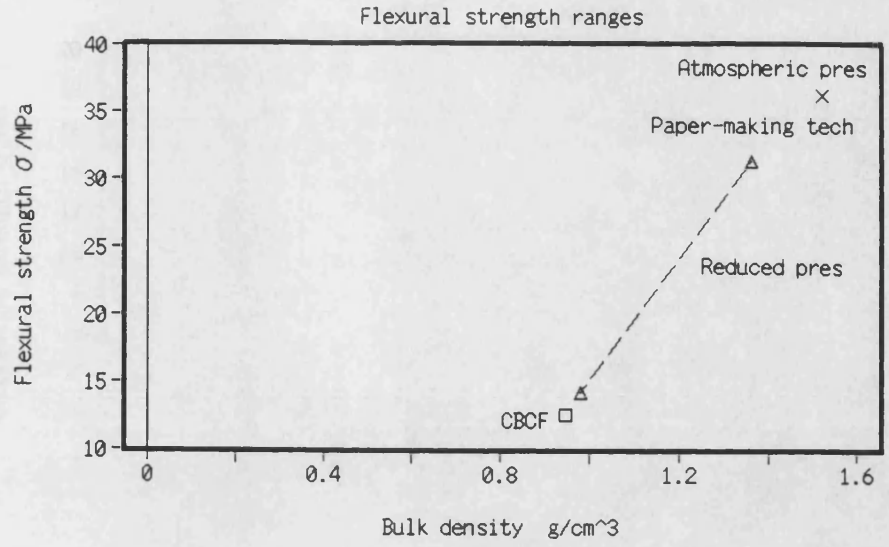

Figure VII-4-2 Flexural strength ranges of porous SiC materials, plotted against bulk density

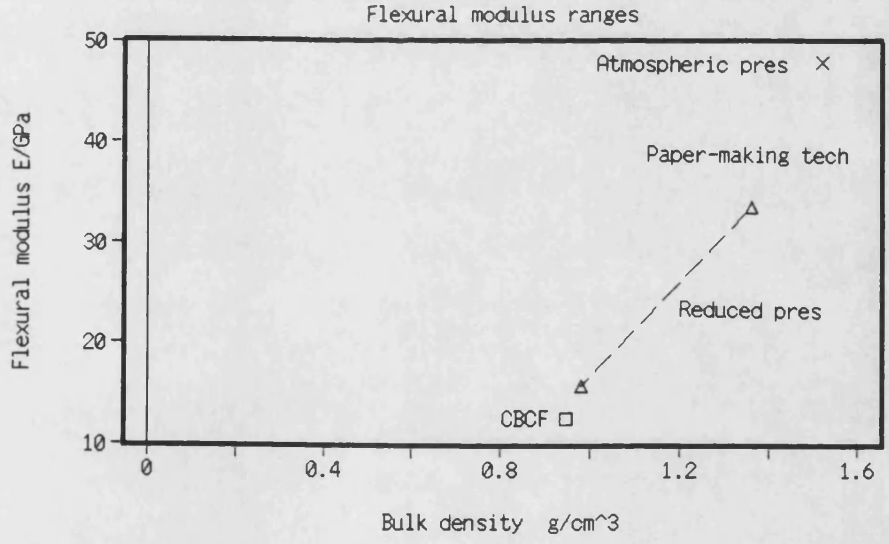

Figure VII-4-3 Flexural modulus ranges of porous SiC materials, plotted against bulk density

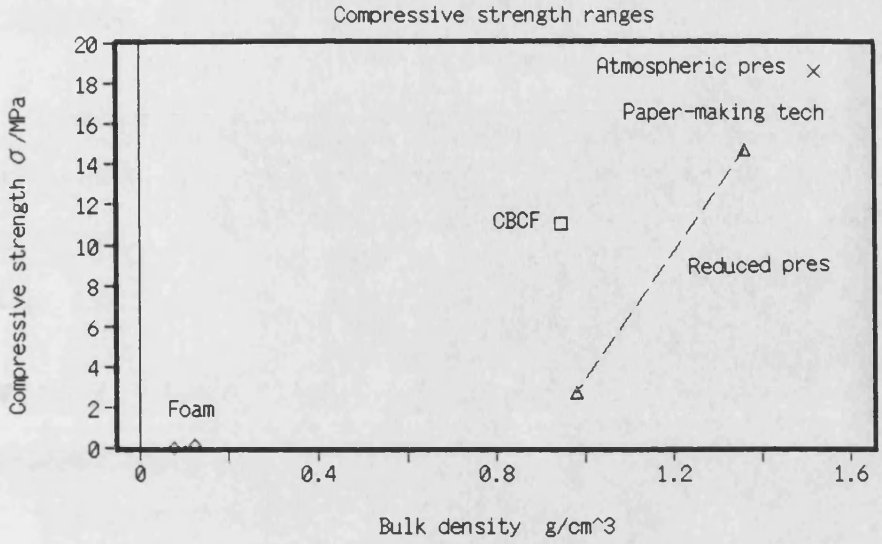

Figure VII-4-4 Compressive strength ranges of porous SiC materials, plotted against bulk density

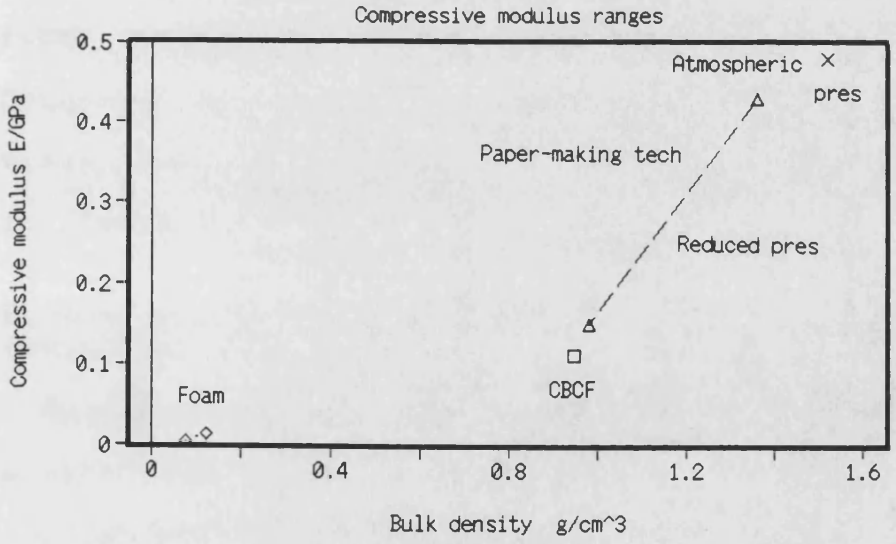

Figure VII-4-5 Compressive modulus ranges of porous SiC materials, plotted against bulk density

CHAPTER VIII CONCLUSIONS AND SUGGESTIONS FOR FURTHER WORK

The principal findings and main conclusions which emerged in this work are summarized in this final chapter, and the thesis concludes with some suggestions for further work.

VIII-1 Conclusions

Porous carbon materials

Various different types of highly porous low-density carbon materials, manufactured by simple techniques using low-cost precursors, were characterized in this work. These materials included (1) porous carbon materials fabricated by paper making technology, (2) foamed resin based carbons, (3) resin powder based porous carbon pellets, and (4) carbon bonded carbon fibre composites. The structural features, mechanical behaviour and high temperature corrosion resistance of these porous carbon materials are summarized in the following paragraphs.

Porous carbon materials fabricated by paper making technology

Randomly-orientated and short carbon fibre precursor sheets, prepared using paper making technology, were impregnated with phenolic resin and laminated by hot-pressing, followed by carbonization and graphitization.

The following are conclusions concerning the structural features:

(1) The density and porosity of the materials were in the ranges of 0.41-0.62 g/cm^3 and 76.2-64.5%,

respectively. The majority of the volume of the materials consisted of the inter-connected open pores.
(2) The materials consisted of layers of random in-planar fibrous carbon sheet, bonded to neighbouring sheets by a relatively small number of connecting points.
(3) Carbonized fibres were bonded to each other by a resin based carbon matrix. However, they fused into each other to form a coherent carbon by a co-carbonization mechanism.
(4) The graphitic structure in the materials developed significantly at heat treatment temperatures between 1000 - 3000° C.

The following conclusions were drawn from the study on the mechanical behaviour of these carbons.
(5) Porous carbons carbonized at 1000° C failed in a brittle manner under flexural and compressive stresses. However, the graphitized carbons heat-treated at 3000° C deformed in a brittle manner under bending stress, but pseudo-plastically in compression.
(6) Heat-treatment over 1000° C did not modify the flexural strength values. However, the flexural modulus decreased significantly due to graphitization. On the other hand, porous carbons heat-treated at 1000° C showed much higher compressive strength with higher elastic modulus than those of graphitized specimens.
(7) Heat treatment temperatures over 1000° C, which resulted in the graphitization of porous carbons, consequently, showed a significant effect on the

mechanical properties.

(8) Both flexural and compressive strength and modulus values were found to increase with density mainly due to denser interlayer bonds.

(9) Flexural strength varied as the square of the density. On the other hand, the modulus was proportional to the cube of the density.

(10) Compressive strength varied as the fourth power of the density, while the modulus was proportional to the fifth power of the density.

(11) There was a sharp decrease in mechanical anisotropy with increasing density. Both strength and modulus anisotropies were almost proportional to the inverse square of the bulk density.

(12) The main oxidation of the carbon heat-treated at 1000° C began around 400° C, after which the weight of carbon was reduced steeply by rapid oxidation. On the other hand, oxidation of the graphitized porous carbon started as high as ca. 650° C, below which graphite was very stable against flowing hot-air. Accordingly, the graphitization has a great effect in enhancing oxidation resistance.

Foamed resin based carbons

Polymer foam preforms were impregnated with phenolic resin, and carbonized in inert environment.

The structural features were summarized as follows:

(1) The densities and porosities were in the range of 0.0245-0.0681 g/cm^3 and ca. 98-95 %, respectively.

(2) The carbon foams had an inter-connected three-dimensional network and an open-celled structure.
(3) The cell struts were made of dense and homogeneous carbon, without any voids.
(4) The cell edge connectivity was typically 4, and face connectivity was 3.
(5) The foamed carbon had an amorphous carbon structure.

The normalized compressive strength and modulus of the carbon foams as a function of relative density, conformed to the following equations.

(6) $$(\sigma/\sigma_s) = 0.12(\rho/\rho_s)^{3/2}$$

(7) $$(E/E_s) = 0.46(\rho/\rho_s)^2$$

The relative density exponents in both equations were in excellent agreement with the theoretical work on open-cell brittle materials. However, there is a significant disagreement between the measured value of the geometric constants and those suggested previously.

(8) The main oxidation reaction started around 450° C, after which temperature carbon was steadily burned out. This low oxidation resistant behaviour is typical for amorphous carbons.

Resin carbon based porous carbon

Phenolic resin powders were pressed with a moderate pressure into pellet form, then carefully carbonized.

Their structural, mechanical and oxidation

characteristics were summarized as follows:

(1) The density (0.94 g/cm^3) was slightly higher and porosity (44.4 %) was less than those of other types of porous carbons.

(2) The majority of pore structure consisted of larger pores (ca. 100 μm in diameter) inter-connected three-dimensionally with smaller channel-like pores. Thus, the material had virtually an open-celled structure.

(3) The carbon consisted of an amorphous structure.

(4) The tensile strength determined by the split cylinder test was 6.44 MPa.

(5) The oxidation resistance was low and the behaviour is typical of amorphous carbons.

Carbon bonded carbon fibre composites

A slurry of short carbon fibres with a phenolic resin binder was cast into a mould, dried, then carbonized.

The structural characteristics, which are similar to the porous carbons fabricated by paper making technology, were as follows:

(1) The density and porosity were 0.347 g/cm^3 and 76.7%, respectively. The vast majority of the volume was dominated by inter-connected open-pores.

(2) The composites consisted of short carbon fibres bonded together at their junctions by discrete, thin regions of the carbon matrix.

(3) The fibres were preferably orientated in planes perpendicular to the thickness direction of the mould form.

(4) The composites can be considered to be constituted

of layers of planar random fibres.

(5) The composites were made mainly of amorphous carbon; however, stress graphitization occurred in small regions during the heat treatment.

(6) The failure of the CBCF composites was analogous to that of the carbonized porous carbon made by paper making technology. The composites thus failed in a brittle manner under both flexural and compressive stresses. Also failure in the Z direction occurred at much lower stress than in the X or Y direction.

(7) The composites showed high oxidation resistance up to about 600° C, below which they did not exhibit any weight decrease. This can be ascribed to a high heat treatment temperature of 1600° C and stress graphitization of the matrix.

Porous carbon-ceramic composites

Porous carbon-ceramic composites were fabricated by infiltration of a silica sol-gel which was subsequently converted into SiC or Si_3N_4 by carbothermal reduction or nitridation, into porous carbon preforms. In addition, porous carbon-SiC composites were impregnated with B_2O_3 glass. The ceramic impregnations hardly improved oxidation resistance of the carbon preforms. Therefore, this poor oxidation resistance restricts applications under oxidizing atmosphere at high temperatures over 400° C. The reaction products were a mixture of non-oxide silicon ceramics and unreacted

residue, i.e., carbon and silica. Thus, the ceramic yield of the silica with resin carbon was quite low. Moreover, carbothermal reduction and nitridation of silica are very complicated systems which are greatly influenced by various experimental parameters, therefore it is difficult to control the reactions.

However, this ceramic impregnation method can be applied to modify mechanical properties, porosity and pore distribution of porous materials to some degree.

Porous ceramic materials

Different types of porous carbon materials were directly converted into porous silicon carbide materials by a reaction-bonding process with infiltrated silicon vapour. The silicon vapour infiltration was conducted mainly under reduced pressures in an argon atmosphere at about 1850° C.

The basic structure of the different forms of carbon preforms, in principle, was inherited by the porous ceramics. Nonetheless, their structural characteristics were changed considerably by a volume expansion which accompanied the conversion, a considerable amount of unreacted carbon, which was removed subsequently by oxidation, and the presence of free silicon. Values of mechanical properties were significantly increased by the conversion into SiC in comparison with porous carbon preforms. At the same time, the mechanical characteristics were altered. Furthermore, porous

reaction-bonded SiC materials exhibited high corrosion resistance against high-temperature air.

Porous SiC materials from porous carbon preforms fabricated by paper making technology

(1) The unique structural features of the porous carbon preforms were, basically, retained in the SiC materials, even after the reaction bonding process. The majority of the volume of the SiC materials consisted of inter-connected open pores, and the material was constituted of a random array of bonded fibres in a planar structure. However, the volume expansion and considerable amount of unreacted carbon, removed subsequently by oxidation, altered the microstructure.

The following are conclusions on mechanical behaviour:

(2) Porous reaction-bonded SiC materials failed in a brittle manner under flexural and compressive stresses.

(3) The mechanical properties against temperature were independent at least up to 800° C in air.

(4) Mechanical properties of porous SiC materials were significantly developed in comparison with those of the carbon preforms. Especially, compressive strength was notably increased because of reinforcement of interlayer bonds.

(5) A significant effect of reaction temperature on mechanical strength was not observed among porous SiC materials produced at atmospheric pressure.

(6) Porous SiC materials produced at atmospheric pressure exhibited much higher values of both strength and modulus, compared with those prepared under reduced

pressure, mainly due to lower porosity.

(7) The flexural and compressive mechanical property values of porous reaction-bonded SiC materials increased with the increase of density.

(8) The dependence of strength on density was almost the same as that of the preforms, while the dependence of modulus on the relative density declined drastically, compared with the carbon preforms.

(9) The mechanical anisotropy of porous SiC decreased with increasing density.

(10) Porous reaction-bonded SiC materials had high corrosion resistance against high-temperature air. In particular, they were virtually unaffected by any structural change under 1000° C.

SiC foams from foamed resin based carbons

The features of reaction-bonded SiC foams are summarized as followings:

(1) The foamed reaction-bonded SiC materials had extraordinary low density and high porosity. The densities and porosities were in the range of 0.0779 - 0.1243 g/cm^3, and approximately 97.5 - 96%, respectively.

(2) The SiC foams had an inter-connected three dimensional network and open-cell structure. The basic structural characteristics were inherited from the carbon foam preforms.

(3) The cell struts were hollow because unreacted carbon was subsequently removed by oxidation.

(4) Because of the scattered data and the small density range, it is difficult to characterize their mechanical behaviour. However, it may be said that the relative density exponents in both strength and modulus were, more or less, in agreement with those of the carbon foam preforms. Nonetheless, a significant disagreement was noticed between the measured values of geometric constants and those theoretically suggested previously, presumably due to the hollow nature of cell struts.
(5) High-temperature corrosion resistance in air of SiC foams, was typical of reaction-bonded SiC that have high oxidation resistance.

Carbon - SiC/Si composites from resin carbon based porous carbon pellets

The structural, mechanical and oxidation characteristics of carbon - SiC/Si composites are summarized as followings:
(1) The bulk density and apparent porosity were 2.44 g/cm^3 and 0.1 %, respectively. The composites contained a considerable amount of unreacted carbon and free silicon.
(2) The smaller channel-like pores were converted into SiC with a little free silicon. On the other hand, only the outer parts of the larger pores (ca. 100 μm in diameter) were turned into SiC, and the major part of the larger pores was filled with free silicon.
(3) The tensile strength of carbon - SiC/Si composites increased markedly to 78.68 MPa.
(4) Regarding high-temperature corrosion, oxidation of

carbon started about 500° C. However, the rate of weight decrease gradually reduced during oxidation treatment at 1200° C, probably owing to the formation of protective layer of silica films which were formed by oxidation of SiC or Si to SiO_2.

Porous SiC materials from carbon bonded carbon fibre composites

(1) The bulk density and apparent porosity of porous SiC materials were 0.946 g/cm^3 and 67.8 %, respectively.

(2) The porous SiC materials had a random in-plane and highly porous open-cell structure.

(3) The carbon fibres were hardly converted into SiC, and only the outer parts of the fibres were converted into SiC. In contrast, the matrix was almost completely converted into SiC with some free silicon.

(4) The reactivity of carbon fibres with silicon was less than that of carbon matrix.

(5) Porous SiC materials from CBCF composites showed a brittle failure manner similar to that found for the porous SiC made from porous carbon preform by paper making technology. Both flexural and compressive property values increased significantly compared with the carbon preforms. In particular, flexural modulus and compressive strength increased dramatically.

(6) Porous SiC from carbon bonded carbon fibre composites was very stable in flowing hot-air, and its thermogravimetric behaviour was similar to those found for the other reaction-bonded SiC materials.

In summary, this thesis is the first comprehensive study of characterization of various types of porous carbon and ceramic materials. Furthermore, this project showed a new method for producing porous carbon-ceramic composites by infiltration of silica sol-gel which was subsequently converted into non-oxide silicon ceramics, and presented a conversion process of various types of porous carbon materials into silicon carbide materials by reaction bonding process.

VIII-2 Future work

Highly porous low-density carbon and ceramic materials, developed in this work, have great potential to be applied into a wide range of industrial fields. Therefore, hereafter, it may be essential to design the materials to modify their specification to meet a specific application by controlling porosity, pore distribution, corrosion resistance which includes not only oxidation by air, but also corrosion by various kinds of chemicals, and mechanical properties, by exploiting the advantages of their porous structure.

In particular, it is anticipated that long-term durability should be proved in order to obtain market penetration in a wide range of engineering fields where high-temperature and corrosion resistance are applied.

REFERENCES

Agarwal, I.C.; Rochon, A.M.; Gesser, H.D.; Sparling, A.B., "Electrodeposition of six heavy metals on reticulated vitreous carbon electrode", Water Res., 18(2), 227-232, (1984)

Alvin, M.A.; Lippert, T.E.; Lane, J.E., "Assessment of porous ceramic materials for hot gas filtration applications", Am. Ceram. Soc. Bull., 70(9), 1491-1498, (1991)

Anderson, D.P.; Gunnison, K.E.; Hager, J.W., "Ligament structure of open-cell carbon foams and the construction of models based on that structure", Mat. Res. Soc. Symp. Proc., vol. 270, Materials Research Society, Pittsburgh, (1992)

Asahi-Dow Ltd., "Silicon carbide", European Patent 52487, (1982)

Asahi Glass Co., Ltd., "Silicon carbide of a high specific surface area", Japanese Patent 58-91026, (1983)

Ashby, M.F., " The mechanical properties of cellular solids", Metall. Trans., 14A, 1755-1769, (1983)

Ashby, M.F.; Palmer, A.C.; Thouless, M.; Goodman, D.J.; Howard, M., Hallam, S.D.; Murrell, S.A.F.; Jones, H.; Sanderson, T.J.O.; Ponter, A.R.S., 18th Annual Offshore Technology Conference, Houston, Texas, 309, (1986)

Bachelard, R.; Joubert, P., "Silicon nitride powders for ceramics obtained by carbothermal reduction, and process for their manufacture", European Patent 240414, (1987)

Blaedel, W.J.; Wang, J., "Rotated porous carbon disk electrode", Anal. Chem., 52, 76-80, (1980)

Blumenthal, J.I.; Santy, M.J.; Burns, F.A., "Kinetic studies of high temperature carbon-silica reactions", AIAA J., 4, 1053-1057, (1966)

Bocker, W.; Hausner, H., Powder Met. Int., 11, 83, (1979)

Brocklehurst, J.E., "Fracture in polycrystalline graphite", Chem. Phys. Carbon, Edited by P. L. Walker Jr., Marcel Dekker, New York, 13, 145-279, (1977)

Buckley, J.D.; Strouhal, G.; Gangler, J.J., "Early development of ceramic fiber insulation for the Space Shuttle", Am. Ceram. Soc. Bull., 60(11), 1196-1200, (1981)

Castro, L.D.; McEnaney, B., "Surface modification of carbon materials to inhibit oxidation - a review", International Symposium on Carbon, Tsukuba, Japan, 336-369, (1990)

Castro, L.D., Ph.D thesis, University of Bath, (1991)

Chan, K.K.; Brownstein, A.M., " Ceramic membranes - growth prospects and opportunities", Am. Ceram. Soc. Bull., 70(4), 703-707, (1991)

Chang, H.W.; Rhee, S.K., "Oxidation of carbon derived from phenolic resin", Carbon, 16, 17-20, (1978)

Christin, F.; Heraud, L.; Choury, J.J.; Naslain, R.; Hagennmuller, R.,"In-depth chemical vapour deposition of SiC within porous carbon-carbon materials", Proc. of 3rd European Conf. on Chemical Vapour Deposition 1980, Neuchatel, Switzerland, 154-161, (1980)

Ehrburger, P.; Baranne, P.; Lahaya, J., "Inhibition of the oxidation of carbon-carbon composite by boron oxide", Carbon, 24(4), 495-499, (1986)

Ehrburger, P., "Protective layers for special types of composites", In "Carbon fibres filaments and composites" Edited by J.L. Figueiredo et al., Kluwer Academic Publishers, Netherlands, 327-336, (1990)

Fischbach, D.B., "The kinetics and mechanism of graphitization", Chem. Phys. Carbon, Edited by P. L. Walker Jr., Marcel Dekker, New York, 7, 1-105, (1971)

Fitzer, E.; Gadow, R., "Investigation of reactivity of different carbons with liquid silicon", Proc. of International Symposium on Ceramic Components for Engine, Japan, 561-572, (1983)

Fitzer, E.; Gadow, R., "Fiber-reinforced silicon carbide", Am. Ceram. Soc. Bull., 65(2), 326-335, (1986)

Forrest, C.W.; Kennedy, P.; Shennan, J.V., "The fabrication and properties of self-bonded silicon carbide bodies", In "Special ceramics 5", British Ceramic Research Association, 99-123, (1972)

Fox, J.R.; White, D.A.; Oleff, S.M.; Boyer, R.D.; Budinger, P.A., "Pyrolysis of organosilicon gels to silicon carbide", Mat. Res. Soc. Sym. Proc., Materials Research Society, 73, 395-400, (1986)

Fox, J.R.; White, D.A., "Manufacture of high-surface-area silicon carbide ceramics, suitable for catalyst supports, from alkoxysilane gels", U.S. Patent 4818732, (1989)

Franklin, R.E., "Crystallite growth in graphitizing and non-graphitizing carbons", Proc. Roy. Soc., A209, 196-218, (1951)

Gibson, L.J.; Ashby, M.F., "The mechanics of three-dimensional cellular materials", Proc. Roy. Soc. Lond., A382, 43-59, (1982)

Gibson, L.J.; Ashby, M.F., "Cellular solids, structure and properties", Pergamon Press, Oxford, (1988)

Green, D.J.; Lange, F.F., "Micromechanical model for fibrous ceramic bodies", J. Am. Ceram. Soc., 65(3), 138-141, (1982)

Greskovich, C; Prochazka, S., "Stability of Si_3N_4 and liquid phases during sintering", J. Am. Ceram. Soc., C96-97, (1981)

Hagiwara, H.; Green, D.J., "Elastic behavior of open-cell alumina", J. Am. Ceram. Soc., 70(11), 811-815, (1987)

Hagiwara, H.; Green, D.J., "The mechanical behavior of lightweight cellular ceramics", In "Advanced ceramics II", Edited by S. Somiya, Elsevier Applied Science, London, 105-120, (1988)

Hampshire, S., "Non-oxide technical and engineering ceramics", Elsevier Applied Science, London, (1986)

Harris, L.A.; Kennedy, C.R.; Wei, G.C.; Jeffers, F.P., "Microscopy of SiC powders synthesized by reacting colloidal silica and pitch", J. Am. Ceram. Soc., 67, C121-124, (1984)

Hase, T.; Suzuki, H., "Properties of submicron β-SiC prepared from siliconization of carbon black", Yogyo Kyokai Shi, 86(11), 541-546, (1978(a))

Hase, T.; Suzuki, H., "Sinterability of submicron β-SiC prepared from siliconization of carbon black", Yogyo Kyokai Shi, 86(12), 606-611, (1978(b))

Hasegawa, Y.; Okamura, K., "SiC-C composite materials synthesized by pyrolysis of polycarbosilane", J. Mater. Sci. Lett., 4, 356-358, (1985)

Hench, L.L.; West, J.K., "The sol-gel process", Chem. Rev., 90, 33-72, (1990)

Hillig, W.B.; Mehan, R.L.; Morelock, C.R.; DeCarlo, V.J.; Laskow, W., "Silicon/silicon carbide composites", Am. Ceram. Soc. Bull., 54(12), 1054-1056, (1975)

Hishiyama, Y.; Inagaki, M.; Kimura, S.; Yamada, S., "Graphitization of carbon fibre/glassy carbon composites", Carbon, 12, 249-258, (1974)

Huttinger, K.J.; Huettner, W., Tanso, 114, 138, (1983)

Inoue, H.; Komeya, K.; Tsuge, A., "Synthesis of silicon nitride powder from silica reduction", J. Am. Ceram. Soc., 65(12), C-205, (1982)

Iseki, T; Arakawa, K.; Matsuzaki, H.; Suzuki, H., "Joining dense silicon carbide by hot-pressing", Yogyo Kyokai Shi, 91(8), 349-354, (1983)

Iseki, T.; Hase, T., "Fabrication and properties of silicon carbide ceramics", In "Fine ceramics" Edited by S. Saito, Elsevier, London, 188-196, (1988)

Ishibashi, T.; Yanagi, H.; Kawato, H.; Sakaguchi, M., Taikabutsu, "Binders and fracture of alumina-carbon nozzles", 35(308), 526-529, (1983)

Ishibashi, T.; Uto, S.; Goto, M., Taikabutsu, "Alumina-zirconia-carbon sliding nozzle plate", 36(316), 300-304, (1984)

Jack, K.H., " The characterization of α'-sialons and the α-β relationships in silalons and silicon nitrides", In "Progress in nitrogen ceramics", Edited by F.L. Riley, Martinus Nijhoff Publishers, The Hague, 45-60, (1983)

Jack, K.H., "Sialons: a study in materials development", In "Non-oxide technological and engineering ceramics", Edited by S. Hampshire, Elsevier Applied Science, London, 1-30, (1986)

Katz, R.N., "Nitrogen ceramics 1976-1981", In "Progress in nitrogen ceramics", Edited by F.L. Riley, Martinus Nijhoff Publishers, The Hague, 3-20, (1983)

Kawamura, K., "SiC/C composite sheet made from PCS/pitch/binder mixture", 20th American Carbon Conference, Santa Barbara, 392-393, (1991)

Kennedy, P.; Shennan, J.V., "An assessment of the performance of Refel silicon carbide under conditions of thermal stress", Proc. of Brit. Ceram. Soc., 22, 67-87, (1973)

Kim, J.; Lee, S.; Park, Y, "Preparation of C-SiC composite by sol-gel method", 20th American Carbon Conference, Santa Barbara, 422-423, (1991)

Kimura, S.; Yasuda, E.; Tanaka, H.; Yamada, S., "Graphitization and microstructure of carbon fibre-glassy carbon composite", Yogyo Kyokai Shi, 83(3), 122-127, (1975)

Kobayashi, K.; Miyazaki, K.; Ogawa, I.; Hagio, T.; Yoshida, H., "Carbon/ceramics composites - preparation and properties", Materials & Design, 9(1), 10-21, (1988)

Komatsu, M.; Nakamizo, M.; Adachi, Y., "Porous SiC ceramics from rice hulls", International Symposium on Carbon, Tsukuba, Japan, 908-911, (1990)

Komeya, K.; Inoue, H., "Synthesis of the form of silicon nitride from silica", J. Mater. Sci., 10(7), 1243-1246, (1975)

Komeya, K., "Fabrication and properties of silicon nitride", In "Fine ceramics", Edited by S. Saito, Elsevier, London, 175-187, (1988)

Konijnendijk, W.L., Philips Res. Rep. Suppl., 1, 135, (1975)

Korb, L.J.; Morant, C.A.; Calland, R.M.; Thatcher, C.S., "The shuttle orbiter thermal protection system", Am. Ceram. Soc. Bull., 60(11), 1188-1193, (1981)

Kuramoto, T.; Ono, H., "Silicon carbide powder containing boron homogeneously distributed", Japanese Patent 58-104011, (1983)

Kureha Chemical Industry Co., Ltd., "Fuel-cell electrode base", Japanese Patent 59-141170, (1984)

Kureha Chemical Industry Co., Ltd., "Development of an advanced ribbed electrode substrate", In "Fuel cell RD & D in Japan", Fuel Cell Development Information Center, Tokyo, 23, (1990)

Ledoux, M.J.; Hantzer, S.; Huu, C.P.; Guille, J.; Desaneaux, M.P., "New synthesis and uses of high-specific-surface SiC as a catalytic support that is chemically inert and has thermal resistance", J. Catal., 114, 176-185, (1988)

Lee, J.G.; Cutler, I.B., "Formation of silicon carbide from rice hulls", Am. Ceram. Soc. Bull., 54(2), 195-198, (1975)

Lee, J.G., Ph.D thesis, University of Utah, (1976)

Lee, J.G.; Cutler, I.B., "Reactions in the SiO_2-C-N_2 system", In "Nitrogen ceramics", Edited by F.L. Riley, Noordhoff International Publishing, Leyden, Netherlands, 175-181, (1977)

Leiser, D.B.; Smith, M.; Goldstein, H.E., "Developments in fibrous refractory composite insulation", Am. Ceram. Soc. Bull., 60(11), 1201-1204, (1981)

Lestrade, C.; Guyomar, P.Y.; Astruc, M., "Electrochemical removal of dilute heavy metals with carbon felt porous electrodes", Environ. Technol. Lett., 2(9), 409-418, (1981)

Maiti, S.K.; Gibson,L.J.; Ashby, M.F., "Deformation and energy absorption diagrams for cellular solids", Acta Metall., 32(11), 1963-1975, (1984(a))

Maiti, S.K.; Ashby, M.F.; Gibson,L.J., " Fracture toughness of brittle cellular solids", Scripta Metallurgica, 18, 213-217, (1984(b))

Markovic, V.; Marsh, H., "Studies of structure in carbonized composites from a phenolic resin and oxidized PAN fibres using chromic acid as an etchant", Carbon, 19, 209-211, (1981)

McEnaney, B.; Pickup, I.M.; Bodsworth, L., "Strength and pore structure of models for carbon catalyst supports", Catalysis Today, 7, 299-308, (1990)

McKee, D.W., "Oxidation protection of carbon materials", Chem. Phys. Carbon, Edited by P.A. Thrower, Marcel Dekker, New York, 23, 173-232, (1991)

McLaren, J.R.; Tappin, G.; Davidge, R.W., "The relationship between temperature and environment, texture and strength of self-bonded silicon carbide", Proc. of the British Ceramic Society, 20, 259-274, (1972)

Mitomo, M., "Fabrication and properties of sialon ceramics", In "Fine ceramics", Edited by S. Saito, Elsevier, London, 197, (1988)

Mori, M.; Inoue, H.; Ochiai, T., "Preparation of silicon nitride powder from silica", In "Progress in nitrogen ceramics", Edited by F.L. Riley, Martinus Nijhoff Publishers, The Hague, 149-156, (1983)

Naslain, R.; Rossignol, J.Y.; Hagenmuller, P.; Christin, F.; Heraud, L.; Choury, J.J., "Synthesis and properties of new composite materials for high temperature applications based on carbon fibers and C-SiC or C-TiC hybrid matrices", Revue de Chimie Minerale, 18(5), 544-564, (1981)

Ogawa, I.; Kobayashi, K.; Nishikawa, S., "Oxidation resistance of carbon-ceramics composite materials sintered from ground powder mixtures of raw coke and ceramics", J. Mater. Sci., 23, 1363-1367, (1988)

Oji Paper Co., Ltd., "Porous carbon plates", European Patent 162976, (1985), "Manufacture of porous carbon plate", Japanese Patent 61-12918, (1986), "Manufacture of porous carbon fiber sheets", Japanese Patent 01-40698, (1989), and "Highly conductive porous carbon fiber sheets", Japanese Patent 03-76821, (1991)

Oji Paper Co., Ltd., "Development of a base plate for electrodes of phosphoric acid FC", In "Fuel cell RD & D in Japan", Fuel Cell Development Information Center, Tokyo, 25, (1990)

Orcel, G.; Hench, L.L.; Artaki, I.; Jones, J.; Zerda, T.W., "Effect of formamide additive on the chemistry of silica sol-gels II. Gel structure", J. Non-Cryst. Solids, 105, 223-231, (1988)

Oren, Y.; Soffer, A., "Graphite felt as an efficient porous electrode for impurity removal and recovery of metals", Electrochim. Acta, 28(11), 1649-1654, (1983)

Papa, A.J.; Proops, W.R., "Phenolic foams", In "Plastic foams vol. II", Edited by K.C. Frish and J.H. Sounders, Marcel Dekker, New York, (1973)

Parsons, J.L.; Milberg, M.E., "Vibrational spectra of vitreous $B_2O_3 \cdot xH_2O$", J. Am. Ceram. Soc., 43(6), 326-330, (1960)

Pickup, H.; Eisele, U.; Gilbart, E.; Brook, R.J., "Analysis of coarsening and densification kinetics during heat treatment of nitrogen ceramics", In "Non-oxide technical and engineering ceramics", Edited by S. Hampshire, Elsevier Applied Science, London, 41-51, (1986)

Popper, P., The preparation of dense self-bonded silicon carbide", In "Special ceramics", Heywood, London, 209-219, (1960)

Popper, P.; Davies, D.G.S., "The preparation and properties of self-bonded silicon carbide", Powder Metallurgy, 8, 113-127, (1961)

Prochazka, S; Charles, R.D., "Strength of boron-doped, hot-pressed silicon carbide", Am. Ceram. Soc. Bull., 52(12), 885-891, (1973)

Prochazka, S., "Ceramics for high-performance applications", Edited by J.J. Burke et al., Brook Hill Pub., Chestnut Hill, Mass., 239, (1974)

Reinoso, F.R.; Romero, F.J.N., "Synthesis of SiC and Si_3N_4 from rice hulls", Anales de Quimica, 87, 788-794, (1991)

Rice, R.W., "Ceramics from polymer pyrolysis, opportunities and needs - a materials perspective", Am. Ceram. Soc. Bull., 62, 889-898, (1983)

Riley, F.L., "Progress in Nitrogen ceramics", Martinus Nijhoff Publishers, The Hague, (1983)

Ritsko, J.E.; Acla, H.L., "High-purity high-surface-area silicon nitride", U.S. Patent 4626422, (1986)

Scherer, G.W., "Aging of gels", In "Sol-gel science and technology", World Scientific, Singapore, 153-179, (1989)

Schmidt, H., "Chemical processing up to gelation", In "Sol-gel science and technology", World Scientific, Singapore, 61-75, (1989)

Schramm, W., "HRSI and LRSI - the early years", Am. Ceram. Soc. Bull., 60(11), 1194-1195, (1981)

Shaffer, P.T.B.; Blackely, K.A.; Jonney, M.A., "Production of fine, high purity beta silicon carbide powder", Adv. Ceram., 21, 257-263, (1987)

Sheehan, J.E., "Oxidation protection for carbon fiber composites", Carbon, 27(5), 709-715, (1989)

Sheppard, L.M., "Corrosion resistant ceramics", Am. Ceram. Soc. Bull., 70(7), 1145-1158, (1991)

Sherman, A.J.; Tuffias, R.H.; Kaplan, R.B., "Refractory ceramic foams: a novel, new high-temperature structure", Am. Ceram. Soc. Bull., 70(6), 1025-1028, (1991)

Shui, X.; Chung, D.D.L.; Hall, F., "Porous carbon made from carbon fibers", 20th American Carbon Conference, Santa Barbara, 376-377, (1991)

Siddiqi, S.A.; Hendry, A., "The influence of iron on the preparation of silicon nitride from silica", J. Mater. Sci., 20, 3230-3238, (1985)

Sioda, R.E.; Keating, K.B., "Flow electrolysis with extended-surface electrodes", In "Electroanalytical chemistry", Edited by A.H. Bard, Marcel Dekker, New York, 12, 1-52, (1982)

Strife, J.R.; Sheehan, J.E., "Ceramic coatings for carbon-carbon composites", Am. Ceram. Soc. Bull., 67(2), 369-374, (1988)

Strohl, A.N.; Curran, D.J., "Controlled potential coulometry with the flow-through reticulated vitreous carbon electrode", Anal. Chem., 51(7), 1050-1053, (1979)

Sun, W.Y.; Walls, P.A.; Thompson, D.P., "Reaction sequences in the preparation of sialon ceramics", In "Non-oxide technological and engineering ceramics", Edited by S. Hampshire, Elsevier Applied Science, London, 105-117, (1986)

Sylwester, A.P.; Auber, J.H.; Rand, P.B.; Arnold, C., Jr.; Clough, R.L., "Low-density microcellular carbonized polyacrylonitrile (PAN) foams", Polym. Mater. Sci. Eng., 57, 113-117, (1987)

Sylwester, A.P.; Clough, R.L., "Electrically conductive reticulated carbon composites", Synth. Met., 29(2-3), F253-258, (1989)

Szweda, A.; Hendry, A.; Jack, K.H., "The preparation of silicon nitride from silica by sol-gel processing", In "Special ceramics, vol. 7", Edited by P. Popper, British Ceramic Research Association, Stoke-on-Trent, England, 107-118, (1981)

Takase, A.; Yoshida, H.; Yamamoto, T., "Investigation of the oxidation of a carbon-ceramic composite with infrared reflection spectroscopy", J. Mater. Sci. Lett., 4, 982-984, (1985)

Thomas, C.R.; Walker, E.J., In "Proc. 1st International Conference on Materials in Aerospace", Royal Aeronautical Society, London, 138, (1986)

Tokai Carbon Co., Ltd. (Sugihara, K.,; Haino, K.; Suzuki, Y.), "Development of porous carbon and its applications", International Symposium on Carbon, Tsukuba, Japan, 558-561, (1990)

Tonen Co., Ltd., "Manufacture of high-strength and oxidation-resistant carbon-ceramic composites", Japanese Patent 03-037159, (1991)

Toray Industry Inc., "Manufacture of conductive porous carbon fiber sheets", Japanese Patent 01-77624, (1988)

Toshiba Corporation, "α-silicon nitride powder", Japanese Patents 57-170807, (1982), and 58-91005, (1983)

Van Der Beck, R.R.; O'Connor, J., "What's new in recrystallized silicon carbide", Ceramic Ind., 68(5), 96-98, (1957)

Wada, H.; Wang, L., "Effect of gas phase composition of SiC and Si_3N_4 formations", Ceram. Eng. Sci. Proc., 11(9-10), 1463-1479, (1990)

Wang, J., "Reticulated vitreous carbon - a new versatile electrode material", Electrochimica Acta, 26(12), 1721-1726, (1981)

Washburn, M.E.; Coblenz, W.S., "Reaction-formed ceramics", Am. Ceram. Soc. Bull., 67(2), 356-363, (1988)

Wei, G.C.; Kennedy, C.R.; Harris, L.A., "Synthesis of sinterable SiC powders by carbothermic reduction of gel-derived precursors and pyrolysis of polycarbosilane", Am. Ceram. Soc. Bull., 63(8), 1054-1061, (1984)

Wei, G.C.; Robbins, J.M., "Carbon-bonded carbon fiber insulation for radioisotope space power systems", Am. Ceram. Soc. Bull., 64(5), 691-699, (1985)

White, D.A.; Oleff, S.M.; Fox, J.R., "Preparation of silicon carbide from organosilicon gels: II, gel pyrolysis and SiC characterization", Adv. Ceram. Mater., 2(1), 53-59, (1987)

Wynne, K.J.; Rice, R.W., "Ceramics via polymer pyrolysis", Ann. Rev. Mater. Sci., 14, 297-334, (1984)

Yamamoto, Y.; Izawa, H., "Carbon and silicon carbide composite (Carbo-SiC)", International Symposium on Carbon, Tsukuba, Japan, 730-733, (1990)

Zaldivar, R.J.; Rellick, G.S., "Some observations on stress graphitization in carbon-carbon composites", Carbon, 29(8), 1155-1163, (1991)

Zhang, S.C.; Cannon, W.R., "Preparation of silicon nitride from silica", J. Am. Ceram. Soc., 67(10), 691-695, (1984)

Zievers, J.F.; Eggerstedt, P.; Zievers, E.C., "Porous ceramics for gas filtration", Am. Ceram. Soc. Bull., 70(1), 108-111, (1991)

Zur, C.; Ariel, M., "The use of graphite cloth electrodes for the recovery and separation of gold", J. Appl. Electrochem., 11, 639, (1981)

Appendix A

Notes for an appendix dealing with the thermodynamics of the SiC reaction bonding system

The decomposition of α-Si_3N_4 in the temperature range 1800-2300° C is

$$Si_3N_4(s) \text{ ---> } 3Si(l) + 2N_2(g) \quad \Delta G^\circ_1 \qquad (1)$$

where ΔG°_1 is the standard free energy of decomposition of α-Si_3N_4.

The vapour pressure of Si can be obtained by adding Equation (2) to Equation (1) to give Equation (3).

$$3Si(l) \text{ ---> } 3Si(g) \qquad 3\Delta G^\circ_2 \qquad (2)$$

where ΔG°_2 is the free energy of vaporization of liquid silicon.

$$Si_3N_4(s) \text{ ---> } 3Si(g) + 2N_2(g) \quad \Delta G^\circ_3 = \Delta G^\circ_1 + 3\Delta G^\circ_2 \qquad (3)$$

$$\Delta G^\circ_3 = -RT\ln K = -RT\ln(pSi')^3(pN_2)^2$$

where pSi' is the vapour pressure of Si in equilibrium with α-Si_3N_4 at temperature T.

Similarly for β-SiC

$$SiC(s) \text{ ---> } Si(l) + C(s) \qquad \Delta G^\circ_4 \qquad (4)$$

$$Si(l) \text{ ---> } Si(g) \qquad \Delta G^\circ_2$$

$$SiC(s) \text{ ---> } Si(g) + C(s) \qquad \Delta G^\circ_5 = \Delta G^\circ_4 + \Delta G^\circ_2 \qquad (5)$$

$$\Delta G^\circ_5 = -RT\ln(pSi")$$

where pSi" is the vapour pressure of Si in equilibrium with SiC at temperature T.

Values of ΔG°_1, ΔG°_2 and ΔG°_4 taken from JANAF tables (Stull - 1971) Table A-1, were used to calculate pSi, pSi' and pSi", where pSi is the vapour pressure of liquid silicon.

Table A-1 Standard free energies (cal mol^{-1})

Temp (K)	ΔG°_1	ΔG°_2	ΔG°_4
1900	-24289	-42753	-12485
2200	+4737	-40067	-9836
2600	+42694	-37388	-6338

The results are in Figure A-1 (p.314). The value of pSi' depends upon the partial pressure of nitrogen in the system. The value of pSi' for pN_2 = 1 atm is shown for reference. In the graphite resistance furnace an atmosphere of argon was used so that the partial pressure of nitrogen was low. This has the effect of increasing pSi' above its value for pN_2 = 1 atm. To illustrate this point for the atmospheric pressure experiments, a value of $pN_2 = 10^{-3}$ atm was assumed (equivalent to 0.1% N_2 in the Ar gas). For the low pressure experiments a value of pAr = 0.1 atm and $pN_2 = 10^{-4}$ atm was assumed. The value of pSi' for these conditions are also included in Figure A-1.

Commentary

1. The vapour pressure of SiC is lower than for Si_3N_4 under all conditions, illustrating the greater thermal stability of SiC.

2. Figure A-1 shows that a beneficial effect of operating at low pressures is to increase the partial pressure of Si vapour in the system.

3. Under the experimental conditions used the vapour pressure of Si from decomposition of Si_3N_4 is greater than from liquid Si showing that the nitride is the more important source of Si vapour. Because the vapour pressure of Si from Si_3N_4 is greater than from liquid Si in both types of experiments, condensation of Si vapour to liquid Si is a possibility. This may explain the presence of elementary Si in the reaction bonded porous SiC materials, although the possibility of transport of liquid Si from the Si/Si_3N_4 source to the porous carbons by capillary action through pores in the carbon felt cannot be ruled out.

Reference

Stull, D.R.; Prophet, H., JANAF Thermochemical Tables, 2nd ed., NSRDS-NBS, 37, U.S. Government Printing Office, Washington, D.C., (1971)

Figure A-1

Vapour pressures for the SiC reaction bonding method